Analysis of Failure Mechanisms of Machine Embroidered Electrical
Contacts and Solutions for Improved Reliability

Analyse van faalmechanismen van machinaal geborduurde elektrische
contacten en oplossingen voor een betere betrouwbaarheid

Torsten Linz

UNIVERSITEIT
GENT

Promoter:

Prof. Dr. Ir. Jan Vanfleteren   (UGent - CMST)

Board of Examiners:

Ir. Johan De Baets   (UGent - CMST)

Dr. Ir. Frederick Bossuyt   (UGent - CMST)

Prof. Dr. Ir. Lieva Van Langenhove   (UGent - Dept. of Textiles)

Dr. Thomas Löher   (Fraunhofer IZM / TU Berlin)

Dr. Andreas Lymberis   (European Commission)

Prof. Danilo De Rossi   (University of Pisa)

Prof. Rik Van de Walle   (UGent - FEA, Academic Secretary)

UNIVERSITEIT GENT

Fraunhofer
IZM

Acknowledgement

Although this was hard work, I have developed this thesis – mostly – with great joy. Nevertheless, this work hardly would have been possible without the friendly support of many wonderful people whom I owe a great debt of gratitude.

I have to start with my wife, Dilek Güngör. We met five years ago, and ever since I have been developing this doctoral thesis parallel to my work as a researcher. Meanwhile, we have married; she has published her first novel and given birth to our two lovely children. I know, she sacrificed countless evenings, weekends and holidays allowing me to finish this dissertation, and I am immensely grateful for this.

I am very glad to have made the acquaintance of Professor Jan Vanfleteren. I like to thank him for his open mindedness towards my research. Embroidering contacts? Pretty unconventional for an electrical engineering dissertation. Nevertheless, when I called him in 2009 to explain my work and to ask whether he would like to be my doctoral promoter, he enthusiastically accepted with the words: *"I would be delighted"*. This single sentence motivated me more than any other event in the years before and ultimately made me finalize this thesis.

I want to thank the *Fraunhofer IZM* for providing me with plenty of resources. In this respect, I like to thank especially my group leader Christine Kallmayer and my department leader Rolf Aschenbrenner. As early as 2003, they recognized that electronics-in-textiles would become a future research topic and created my position providing me with internal funds. Up to that time very little work had been done on integration technologies for electronics-in-textiles. Christine gave me a lot of freedom to develop the field of research together with international partners. In these first years at *IZM*, I also developed the topic of my thesis on my own as there was so little to build upon.

I like to thank all my students who have supported this scientific work with their student projects and diploma theses. Especially the theses of Erik Simon, Malte von Krshiwoblozki and Philipp Foerster have impacted this dissertation fruitfully. Erik and Malte later became colleagues at the *Fraunhofer IZM*, while Philipp is still a student of mine. Often we found ourselves in intense and fertile discussions about contact theory and adhesive bonding mechanisms.

Furthermore, I owe many thanks to my colleagues for inspiring discussions, a lot of help with building test vehicles and providing support with measurement equipment. Among these, Hans Walter deserves a special thank-you for rich discussions about polymer mechanics, and for helping me to use his lab equipment for material characterization. I like to thank my office colleagues Christian Dils and

Contents

Nederlandse Samenvatting / Dutch Summary

In de afgelopen jaren hebben een aantal onderzoeksprojecten en patenten voorgesteld om borduren van geleidend garen te gebruiken om elektrische schakelingen op textielsubstraten te realiseren. Om elektronische modules en componenten met deze circuits te verbinden, werd borduren zelf als contacteermethode gebruikt. Daarbij stikt de borduurnaald doorheen een geleidend contactpad op een elektronicasubstraat en legt de geleidende draad over dit contactpad. Het garen en het contactpad raken elkaar en verwezenlijken zodoende een elektrisch contact.

Echter, tot op heden is deze contacttechnologie, gebaseerd op borduren, niet algemeen aanvaard door de industrie omdat betrouwbaarheidsproblemen onder mechanische stress werden gerapporteerd door verschillende onderzoekers. Aan de andere kant werden de falingsmechanismen nooit grondig onderzocht, evenmin werd er gepoogd hun oorzaak te begrijpen. Dit remde potentiële verbeteringen om deze geborduurde contacten betrouwbaar te maken af. Bovendien hinderde het ontbreken van alternatieve technologieën voor betrouwbare en volumeproduceerbare contacten van geborduurde schakelingen met elektronische componenten of modules, de evolutie van geborduurde circuits naar feitelijke producten.

Daarom, zoals toegelicht in hoofdstuk 1, is de primaire doelstelling van dit proefschrift om het contactmechanisme dat ten grondslag ligt van geborduurde contacten, te begrijpen, en om een theorie te ontwikkelen, die de falingsmechanismen verklaart. De secundaire doelstelling is om deze problemen inzake betrouwbaarheid te overwinnen door het verbeteren van deze contacten, of door het vinden van alternatieven. Omdat het uiteindelijke doel een volumeproduceerbaar contactproces is, worden in dit proefschrift vooral machine geborduurde contacten bestudeerd.

Omdat geborduurde circuits en geborduurde contacten niet-standaard processen zijn, begint hoofdstuk 2 met een analyse van de betrokken processen en materialen, en identificeert gemeenschappelijke mechanismen in implementaties door verschillende onderzoekers en ontwerpers. Een bijzondere nadruk ligt op het begrijpen van de randvoorwaarden van de machine geborduurde contacten. Zo blijkt dat de vereiste van borduren met een machine zeer specifieke eisen stelt aan geleidende borduurgarens en procesparameters. De conclusie is dat van de momenteel beschikbare geleidende garens alleen polymeergarens met metaalcoating geschikt zijn voor borduren van circuits en contacten. Een matuur product werd geselecteerd voor de experimenten in dit proefschrift.

Daarnaast worden in hoofdstuk 2 typische eisen voor geborduurde circuits en contacten vanuit verschillende toepassingsscenario's afgeleid. In het bijzonder worden de eisen voor weerstand tegen verschillende soorten stress besproken. Drie verschillende stresstests werden geselecteerd als exemplarisch voor het analyseren van testvehikels in het kader van dit proefschrift: een temperatuur cyclustest, een wascyclustest en een speciaal ontworpen buigingstest. Daarbij vallen de tests uiteen in twee categorieën met onderscheiden doeleinden. Een korte versie van de temperatuurcyclustest van slechts 25 cycli en de (ook korte) buigingstest dienen om het gedrag van de contacten te begrijpen en om de theorie te verifiëren door vergelijking van de waargenomen defecten met de voorspelde. De wascyclustest van 20 cycli en een lange versie van de temperatuurcyclustest van 1025 cycli hebben als bedoeling om de betrouwbaarheid onder praktisch relevante omgevingsomstandigheden te beoordelen.

Zoals zal blijken in dit proefschrift, spelen de thermo-mechanische en elektrische eigenschappen van de borduurgarens een belangrijke rol voor het gedrag van geborduurde contacten. Daarom worden in hoofdstuk 3 op een grondige manier gemetalliseerde polymeergarens in het algemeen, en specifiek ook het garen, geselecteerd in hoofdstuk 2, onderzocht. Er wordt aangetoond dat de karakteristieke eigenschappen van het geselecteerde garen niet uniek zijn, maar gemeenschappelijke eigenschappen met courante geleidende borduurgarens vertonen.

Hoofdstuk 4 kan worden beschouwd als het belangrijkste hoofdstuk omdat hier de theorie van het contactmechanisme ontwikkeld wordt. Voor dit doel wordt een vereenvoudigd theoretisch model van het contact voorgesteld. Dit model laat zien dat de contactweerstand sterk afhankelijk is van de thermo-mechanische toestand van de lus van het geleidende garen. Zelfs onderbrekingen van het contact kunnen optreden. Bovendien suggereert de theorie dat het geborduurde contact zich op soortgelijke wijze als het vereenvoudigd model gedraagt, maar naast van de thermo-mechanische toestand van het garen ook van zijn elektrische weerstand afhangt.

Op basis van deze theorie en van de analyses van de thermo-mechanische en elektrische eigenschappen van het garen uit hoofdstuk 3, wordt voorspeld dat contactonderbrekingen zullen optreden bij lage temperaturen tijdens temperatuurscycli en dat de contactweerstanden altijd naar goede waarden zullen terugkeren bij hoge temperaturen. Dit geldt evenzeer voor het vereenvoudigde model als voor het geborduurde contact.

Daarnaast suggereert de theorie dat geborduurde contacten gevoelig kunnen zijn voor bepaalde types van buigingen tijdens de buigingstesten.

Om de theorie te verifiëren, werden verschillende experimenten opgezet, deze worden beschreven in hoofdstuk 5. Een experimentele opstelling van het vereenvoudigde model werd gebouwd, en onderworpen aan temperatuurscycli. Ook werden verschillende varianten van geborduurde contacten gefabriceerd en onderworpen aan temperatuurscycli, wascycli en buigingstesten.

De resultaten van deze experimenten worden gepresenteerd in hoofdstuk 6. Deze laten zien dat defecten zich voordoen bij lage temperaturen en tijdens bepaalde verbuigingen. Inderdaad, de resultaten bewijzen dat de theorie het gedrag van zowel het vereenvoudigd model als dat van het geborduurde contact heel goed voorspelt. Bovendien wordt aangetoond dat ook wascycli tot defecten leiden.

Geconcludeerd wordt dat de geborduurde contacten - op zijn minst met de huidig beschikbare geleidende borduurgarens – intrinsiek niet betrouwbaar kunnen zijn onder typische stress. Daarom moet het contactmechanisme worden verbeterd, zodat het niet langer berust op de stabiliteit van de thermo-mechanische toestand van het garen.

Hoofdstuk 7 pakt dit aan door het vasthouden van de goede conditie bij hoge temperatuur door middel van inkapseling. Voor dit doel worden verschillende methodes voor inkapseling in theorie en experimenteel onderzocht. Voor dit laatste werden verschillende testvehikels gebouwd en onderworpen aan de lange versie van de temperatuurscyclustest of de wascyclustest. Het blijkt dat met geschikte inkapseling de geborduurde contacten betrouwbaar zijn onder typische omgevingsstress.

Deze verbetering legt helaas extra processtappen tijdens de fabricage op, hetgeen de technologie minder efficiënt maakt dan aanvankelijk bedoeld. Daarom wordt in hoofdstuk 8 een alternatieve benadering onderzocht voor het contacteren van geborduurde circuits. In dit verlijmingsproces wordt de elektronische module bevestigd op het geborduurde circuit met niet-geleidende lijm (NCA). In tegenstelling tot NCA flip chip bonding is de gebruikte lijm een niet-rigide thermohardende epoxy, maar zacht thermoplastisch polyurethaan. Het voordeel is dat deze lijm gebruikt kan worden als een flexibele en uitrekbare isolator op het geborduurde geleidende garen. Hij kan aangebracht worden voor het contacteringsproces. Tijdens het bevestigen smelt de lijm en wordt hij door de bondingkracht uit het gebied van de contactvlakken geperst, waardoor de contactoppervlakken elkaar kunnen raken. Dit betekent dat geïsoleerde geleiders elkaar kunnen contacteren zonder een bijkomende stripping stap hetgeen deze technologie merkwaardig eenvoudig maakt. Vervolgens zal door afkoelen de lijm stollen. Dan wordt de bondingkracht opgeheven en de lijm houdt de contactoppervlakken in permanent contact. Een tweede voordeel van thermoplastische lijmen t.o.v. thermohardende is dat de contacten te repareren zijn.

Opnieuw werden testvehikels ontwikkeld en getest onder omgevingsomstandigheden. De resultaten tonen aan dat dit een zeer betrouwbare contacttechnologie is voor geborduurde circuits zonder optredende defecten onder deze testomstandigheden.

Translation by Professor Jan Vanfleteren

Summary

In recent years, a number of research projects and patents have proposed to apply embroidery of conductive yarn to build electric circuits on textile substrates. To contact electronic modules or components to these circuits, embroidery itself was applied as contacting method. Thereby, the embroidery needle is stitching through a conductive pad on an electronic substrate and is laying the conductive thread over this pad. The yarn and the pad touch and establish an electrical contact.

However, until today this contacting technology based on embroidery has not been adopted by the industry since reliability issues during stress were reported by different researchers. Yet, neither were these failure phenomena investigated comprehensively, nor was it attempted to understand their cause. This inhibited potential improvements to make these embroidered contacts reliable. Furthermore, the lack of alternative technologies for a reliable and volume producible contacting of embroidered circuits with electronic components or modules kept embroidered circuits from evolving to actual products.

Therefore, as explained in chapter 1, the primary objective of this thesis is to understand the contact mechanism underlying embroidered contacts, and to develop a theory that explains the failure phenomena. The secondary objective is to overcome these reliability issues by improving these contacts or by finding alternatives. As the ultimate goal beyond this thesis is a volume producible contacting process, this thesis looks mainly at machine embroidered contacts.

Since embroidered circuits and embroidered contacts are not standard processes, chapter 2 begins with an analysis of the involved processes and materials, and identifies common mechanisms in implementations of different researchers and designers. A special focus is on understanding the boundary conditions of machine embroidered contacts. As it turns out the machine embroiderability sets very specific conditions on the conductive embroidery yarn and on process parameters. It is concluded that of currently available conductive yarns only metal coated polymer yarns are suited for embroidering circuits and contacts. A mature product is selected for the experiments in this thesis.

In addition, chapter 2 derives typical requirements on embroidered circuits and contacts from different application scenarios. Especially, the requirements on the resistance against different stresses are discussed. Three different stress tests are selected as exemplary tests for analyzing test vehicles within the framework of this thesis: a temperature cycling test, a wash cycling test, and a specially designed bending test. Thereby, the tests fall into two categories with distinguished purposes.

A short version of the temperature cycling test of only 25 cycles and the (also short) bending test serve to *understand the behavior* of the contacts and to *verify the theory* by comparing actual failures with predicted ones. The wash cycling test of 20 cycles and a long version of the temperature cycling test of 1025 cycles intend to *assess the reliability* under practically relevant environmental conditions.

As will be shown in this thesis, the thermo-mechanical and electrical properties of the embroidery yarn play a major role for the contact behavior of embroidered contacts. Therefore, chapter 3 thoroughly investigates metal coated polymer yarns in general and specifically also the yarn selected in chapter 2. It is shown that the characteristic properties of the selected yarn are not unique but common properties of conductive embroidery yarn available today.

Chapter 4 can be considered the main chapter as it develops the theory of the contact mechanism. For this purpose a simplified theoretical model of the contact is developed. This model reveals that contact resistance is strongly dependent on the thermo-mechanical condition of the conductive yarn loop. Even contact disruptions may occur. Furthermore, the theory suggests that the embroidered contact behaves similarly but in addition to the thermo-mechanical condition of the yarn also depends on its electrical resistance.

Based on this theory and on the analyses of the thermo-mechanical and electrical properties of the yarn from chapter 3, it is predicted that contact failures will occur at low temperatures during thermal cycling and that the contact resistances will always return to good values at high temperatures. This applies equally to the simplified model and to the embroidered contact.

Beyond this, the theory suggests that embroidered contacts could be sensitive to certain types of bends during the bending test.

To verify the theory, several experiments are designed which is described in chapter 5. An experimental setup of the simplified model is built which is exposed to temperature cycles. Also different variants of embroidered contacts are built and exposed to temperature cycles, to wash cycles or to the bending test.

The results of these experiments are presented in chapter 6. They reveal that failures do occur at low temperatures and during certain bends. As a matter of fact the results proof that the theory predicts the behavior of both – the simplified model and the embroidered contact – very well. Furthermore, it is shown that also wash cycling leads to failures.

It is concluded that the embroidered contacts – at least with conductive embroidery yarns available today – cannot be reliable intrinsically under typical stress. Therefore, the contact mechanism needs to be enhanced so it no longer relies on the steadiness of the thermo-mechanical condition of the yarn.

Chapter 7 tackles this by fixing the good condition at high temperature with encapsulation. For this purpose different encapsulation methods are investigated in theory and experimentally. For the latter, different test vehicles are built and exposed to the long version of the temperature cycling test or to the wash cycling test. It turns out that with appropriate encapsulation the embroidered contacts are reliable under typical environmental stress.

This improvement unfortunately imposes extra process steps during manufacturing, which makes the technology less efficient than initially intended. Therefore, chapter 8 investigates an alternative approach for contacting embroidered circuits. In this adhesive process, the electronic module is bonded onto the embroidered circuit with non-conductive adhesive (NCA). Unlike in NCA flip chip bonding the adhesive used is not rigid thermosetting epoxy but soft thermoplastic polyurethane. The advantage is that this adhesive can be used as a flexible and stretchable insulator on the embroidered conductive yarn. It can be applied prior to the contacting process. During the bonding it is melted and squeezed out of the contacting area by the bonding force allowing the contact members to touch. This means, insulated conductors can be contacted without an additional stripping step which makes this technology compellingly simple. Subsequent cooling solidifies the adhesive. Then the bonding force is released and the adhesive holds the contact members in touch permanently. A second advantage of thermoplastic adhesives over thermosetting ones is that the contacts are repairable.

Again, test vehicles are developed and tested under environmental conditions. The results show that this is a very reliable contacting technology for embroidered circuits with no failures under these test conditions.

1 Motivation

In the last two decades, industry, academia, artists and to some extent the public likewise were fascinated by the idea of embroidering conductive yarn onto fabrics to achieve drapable[1] conductive circuits. Such textile electronics could make consumer electronics emotionally more tangible than boxed electronics. Technical applications could benefit from textiles with enhanced electronic functions like sensing or light emission.

Such textile electronics are especially useful for solving distributed problems that are mapped over a surface. They solve the wiring between functional elements, e.g.: in a dress with integrated LEDs spread out over the dress [1]; or in a belt conveyor with sewn-in conductive yarn loops for sensing fatigue [2]; or in a textile capacitive touch sensor with embroidered keys [3]. Some further examples are shown in Figure 1.1.

Figure 1.1: From left to right: communication jacket with arm wrist controls for a mobile phone in the pocket [4]; a performance art musical instrument with embroidered touch sensors [5]; a jacket for a bicycle messenger with integrated controls for navigation and managing job tasks [6]; interactive "board" game with embroidered user interface on tablecloth [7].

It was recognized early that contacting electronic components or electronic modules to such drapable circuits is a major issue – especially concerning reliability [8], [9]. The most wide spread approach for contacting embroidered circuits quickly became embroidery itself, i.e. embroidering the conductive yarn through a prepared metallized pad on an electronic module. This is similar to sewing on a button, except that both – the button and the yarn – are conductive. In the do-it-yourself scene this has been largely done by hand embroidery (e.g. [10]). However, also machine embroidery has been applied (e.g. [11], [12]). Figure 1.2 shows some implementations that apply this contacting technique by embroidery.

---

[1] drapable means bendable in two directions without breaking. This often implies also stretchability.

Figure 1.2:   Applications making use of embroidered contacts (from left to right): the *Climate dress* with over hundred LEDs that visualize the CO_2 content of the surrounding air was designed for the climate conference in Copenhagen [12]; an EKG shirt with embroidered electrodes for measuring an electrocardiogram [13]; a do-it-yourself design kit with hand embroidered contacts [14]; shirt with LED display [15]; sensor for measuring an electromyogram [16].

Although some of these examples apply machine embroidery, which is a volume production technology, no products[2] have been released based on these embroidered contacts, until today. The results are merely design studies, prototypes or do-it-yourself arts projects. This is despite market analysts have predicted a prosperous future for such products [17]. The reason is that the reliability of the contacts did not live up to the demands. For end-user satisfaction and market acceptance, reliability of the contacts is vital.

Different publications report of results with particular reliability tests. Contacts created for instance with steel yarn, which can only be processed by hand embroidery, were found to be washable, although the authors admit that more profound tests are required for a final judgment [15]. According to results of [18], which must also be considered to be preliminary results, the resistances of machine embroidered contacts rise critically after a few wash cycles or movement cycles. However, it has never been attempted to find the source of these failures. This impedes a systematic search for qualified materials and adequate methods that could enable reliable products.

Therefore, the primary objective of this thesis is to understand the contact mechanism underlying embroidered contacts and to develop a theory that can explain the failures that may occur during reliability tests.

Naturally, the secondary objective is to improve the contacts or to find alternative approaches to overcome potential reliability issues.

Generally, hereby, the focus is on machine embroidered contacts being a basis for potential products.

---

[2] no products, apart from do-it-yourself design kits

2 State of the Art

Embroidering conductive circuits is not a standard process – at least not yet; even less so is embroidering electrical contacts. Until now, only a small number of researchers and users have investigated these. Therefore, this chapter discusses the principle processes for making embroidered circuits and embroidered contacts. Furthermore, demands on these circuits and contacts are discussed.

2.1 Embroidering Circuits

Before discussing the construction of embroidered electrical contacts, it is helpful to understand the process of embroidery itself as it brings along a number of constraints for the (conductive) embroidery yarns. As the goal of this thesis is an industrializable process, this chapter only explains machine sewing and machine embroidery, rather than hand sewing or hand embroidery.

2.1.1 Introducing Sewing and Embroidery Technology

There are many different types of sewing machines that generate very different seams. They differ in the number of threads (one to four), number of needles (one to three) and in the resulting stitch type. The most popular stitch type is lockstitch. It uses one needle and two threads. Since the top thread goes through the needle it is sometimes called needle thread. The under thread sits in the spool or bobbin which is why it is often called bobbin thread.

The following figure explains the lockstitch sewing process. During the sewing process the needle breaks through the sewing cloth bringing a loop of the top thread to the bottom side of the cloth. The hook pulls this loop around the spool. Finally the needle thread is pulled back to the topside of the cloth which is effected by the take-up lever. The result is an interlacing of the top and bobbin thread.

Depending on the thread tensions applied to top and bobbin thread the interlacing happens more at the top, in the middle or at the bottom of the cloth. Often it is considered optimal when the interlacing is in the middle of the cloth (like in Figure 2.1). [19]

Lockstitch sewing and embroidery are essentially very similar technologies. The difference is that sewing is a joining technology and embroidery is a decorating technology. That means sewing always joins two or more fabrics e.g. when making a garment from different precut pieces of cloth. Embroidery applies the threads only

on one cloth but uses differently colored threads to generate images or patterns on the cloth.

The machines differ in the cloth transportation systems. Sewing machines transport the cloth away from the operator who always leads the cloth with his hands. The embroidery machines (at least the modern ones) operate automatically. The cloth is fixed in an embroidery frame and is moved in x and y direction under the needle.
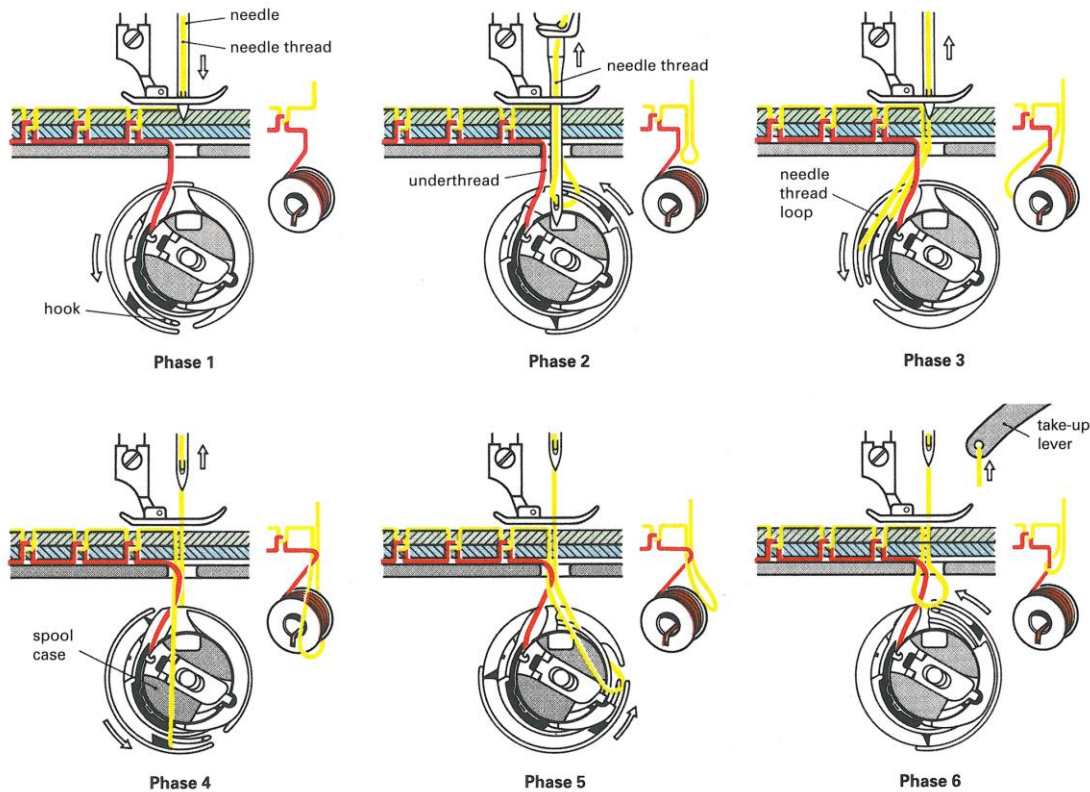

Figure 2.1:   The principle of lockstitch sewing is very similar to the one of embroidery. Source: [19][3]

2.1.2 (Non-Conductive) Embroidery Yarn

In sewing and embroidery the demands on the top thread are much higher than on the bobbin thread. The top thread goes through a pre-tensioning system, through the take-up lever and most critically through the eye of the needle. When the needle breaks through the cloth the top thread is bent sharply. The hook catches and pulls it around the bobbin at high speed. This requires that the thread is strong, very flexible and smooth on the surface to slip over all the different surfaces and sharp edges.

The mechanical demands on the bobbin thread are much lower since it is only rolled off from the spool. However, in mass production it is desirable to use a thin

---

[3] with kind permission of the publisher

bobbin thread. The longer the thread on the spool the less often it has to be replaced. [20]

Unfortunately, the sewability of yarns (top or bobbin) is scientifically not well researched. The knowledge is literally laying in the hands (and fingers) of embroidery experts and is not available in formulas. However, Maggie Orth has made an effort to develop a set of rules for sewability of yarns [21]. Yet, it is not clear how she derived these rules, according to which the top thread should have the following mechanical properties:

> *"...*
>
> - *"High tensile strength or tenacity. Tensile strength of ~580 to 1200 cN, or tenacity of 2.25 to 4.5 cN/dtex[4].*
> - *Moderate % of elongation at breakpoint (between 12-30 %).*
> - *Denier of under ~400.* [equiv. ~440 dtex[5]]
> - *Relatively smooth surface characteristics.*
> - *High flexibility and resistance to shear and permanent deformation under bending.*
>
> *..."*

The upper limit of linear density of 440 dtex seems reasonable although [19] provides a list of sewing yarn types with linear density up to 1000 dtex. Neither [19] nor [21] explain on which machines they have made these tests. After all, sails are being sewn with rather heavy yarns. Of course this requires special sewing machines.

To measure flexibility Maggie Orth developed a curl test which is a scientific approach to the fingernail-test. For the fingernail-test the thread is pinched and pulled through thumbnail and index finger. If the thread curls and stays curled it is an indicator for bad sewability – especially in the needle. Of course, if it does not curl it does not necessarily indicate good sewability since there are other factors as well.

---

[4] note: the exact wording in [21] is *"tenacity of 2.5 to 5"*; the units are missing; I assumed the units are g/denier and converted this into SI units; see also [5]

[5] unlike wires, yarns cannot be defined by their diameter as the diameter is subject to change due to tension; furthermore the diameter is not always constant; therefore the yarn 'numbering' is given in linear density or titre (symbol=Tt): Tt[dtex] = mass[dg] / length[km]; dg = decigram; dtex = dezi-tex; so 1 km of a 440 dtex yarn weighs 44 grams; other less common yarn numbering units are denier (den), metric number (Nm) and English cotton count (Ne_c)

2.1.3 Conductive Embroidery Yarn

In principle there are four ways to attain conductive yarns:

- thinning steel so it becomes fibrous and then spinning yarn from these steel fibers
- spinning carbon yarn from carbon fibers
- spinning non-conductive fibers (typically polymer fibers) together with
  - thin copper wires or
  - steel fibers or
  - carbon fibers
- applying conductive material (Ag, Ni, Cu) to the fiber surfaces of a non-conductive yarn (typically polymer fibers)

Unfortunately, many conductive yarns are not machine sewable due to the high demands on the yarns just explained. In general it may be summarized: the higher the percentage of conductive material, the less likely a yarn is sewable. Thus there is always a tradeoff between conductivity and sewability.

The following is a list of different types of conductive yarns and their sewability according to my own experience and partially also according to other researcher's experience:

- Spun yarn[6] or filament yarn[7], be it twisted or untwisted, of 100% stainless steel fibers cannot be sewn in the needle nor in the bobbin [8]. The same applies for yarn made of 100 % carbon fibers.
- Filament yarns made from polymer fibers (e.g. Nylon) and (silver coated) copper wires (typically ~30 μm diameter) are not sewable in the needle and difficult in the bobbin.
- Metal wires (e.g. Cu, Au or Ag) are not sewable [8], [22].
- Spun stainless steel yarn may be embroiderable as top thread if the percentage of stainless steel fibers is very low (≤20 %) [8]. In the bobbin, spun yarns may be processed even if they have higher steel fiber content (e.g. 70 % stainless steel and 30 % Kevlar [8]).
- Twisted filament yarn of nylon and three continuous strands of stainless steel was not machine sewable in the needle, but machine sewable in the bobbin [8].
- Yarns made from polymer fibers and a low percentage of carbon fibers are sewable in the needle and in the bobbin. Yet, the carbon fibers break easily during processing and use, which further reduces the weak conductivity and

---

[6] spun yarns are spun from many fibers of finite length, so called staple fibers; staple stainless steel yarns contain a mix of steel fibers and non-conductive fibers like polyester [19]
[7] filament yarns are made from endless fibers (also called continuous filament yarns); yarns made of only one fiber are called monofilament yarns as opposed to multi-filament yarns [19]

can be harmful to electronics as broken fibers float around in the air. Inside computers or other high density electronics they can create short circuits.

- Conductive gimped yarns[8] are not top thread sewable as the metal foil wrapping gets jammed in the eye of the needle. Some may be sewable in the bobbin but they are typically quite thick which make them inefficient in the spool.
- Some filament yarns made from metal coated polymer fibers are sewable as top or under thread. Some of these even exhibit good conductivity (down to some tens of Ω/m).

Apparently, those conductive yarns that rely on mixing non-conductive fibers with conductive ones are only embroiderable if the share of conductive fibers is small. This implies a high resistance which is of course unattractive as it limits the applicability of the technology (ref. to 2.3.1). Therefore, this thesis will only consider yarns made of metal coated polymer fibers, as they can offer both good conductivity and machine embroiderability.

When this work was started the number of available products of this kind was very limited. One of the big players was and is to date *Statex*. Their conductive yarns, conductive fabrics and conductive non-wovens were initially mainly aiming for antistatic purposes (e.g. in carpets) and electromagnetic shielding (e.g. for critical electronics). All products are based on Nylon (polyamide 6.6) fibers metallized with silver. Other metal coatings on top of the silver are also available. Their product line of conductive yarns is called *Shieldex*.

Shieldex yarns are available in different yarn counts[9]. The raw polyamide yarns range from 22 dtex monofilaments to 235 dtex 34 filament 2-ply[10] yarns. After metallization their yarn count is 27 dtex[11] and 560 dtex[12] (for both strands) respectively. [23]

Since at the time when this research was started, the prime market of *Statex* had not yet been smart textiles, their yarns had not been optimized for low resistivity. Therefore *TITV*[13] a German textile research institute had started to fill this gap on

---

[8] gimped yarns are yarns wrapped with foil; gimped sewing yarns are wrapped in highly flexible polymer foils; sometimes these are vapor coated with metal to make them shine; however the coatings are so thin that their electrical conductance is negligible; on the other hand there are also gimped yarns with metal foil wrappings with good conductivity; these cannot be sewn

[9] yarn count is a technical term for fineness of yarns; other terms are titre[5] or yarn numbering[5]

[10] 2-ply means twisted from two strands; each strand consists of 34 filaments and has a linear density of 234 dtex; in sum their linear density is slightly larger than double since the length of each strand is slightly larger than the yarn due to the twisting; another word for twisted or 2-ply is twine

[11] source: data sheet of *SHIELDEX® 22/1 dtex DTL* [23]

[12] this is the titre for the twine not of the strands; source: data sheet of *SHIELDEX® 235f34 dtex 2-ply HC* [23]

[13] *TITV* stands for *Textilforschungsinstitut Thüringen-Vogtland e.V.*; the Institute is situated in Greiz, Germany [142]

their own by further metallizing the products of *Statex*. As this was only the beginning of their research the resulting yarns where not very uniform in their characteristics nor were they washable. Therefore, these yarns could not be used for this research.

Today, *TITV* actually produces and sells these yarns. The product line is called *Elitex*. Some of these yarns are sewable and also washable to certain extend, like for instance *Elitex 235/34 PA/Ag 8/22/30* with a resistance of about 20 Ω/m. The lowest resistance reached with these products is 1 Ω/m but this is not sewable anymore. [18]

The following table lists all products from *Statex* and *TITV* available at the beginning of 2010. Furthermore, it contains *Shieldex 117/17 dtex 2-ply* which is not available anymore but was used for the experiments in this work. This does not limit the generality of this work as the results apply equally to other metal-coated polymer yarns as will be explained later.

Table 2.1:   List of silver metallized polyamide yarns. The data are taken from data sheets of the manufacturers [23], [24] and may be incorrect. The data marked with * have been measured by [25] (refer to chapter 3.2 for details). The check green boxes indicate machine embroiderability according to my own experience.

Embroiderability & Product Name	Titer (with Ag) [dtex]	Tenacity (with Ag) [cN/dtex]	Tensile Strength [cN]	Max. Elong. [%]	Resist. [Ω/m]
☒ Shieldex 22/1 dtex DTL	27	5.8	156.6	18-25	<20000
☒ Shieldex 33/10 dtex Z turns	39	3.1	120.9	20±5	<20000
☒ Shieldex 44/12 dtex Z turns	54	3.3	178.2	48±5	<10000
☑ Shieldex 22/1 + 113/32 dtex	145	7.0	1015	~16	<30000
☑ Shieldex 44/12 + 113/32 dtex	170	4.8	816	~16	<30000
☒ Shieldex 78/18 dtex Z turns	88	3.9	343.2	~39	<20000
☑ Shieldex 110/24 dtex ht Z turns	132	4.5	594	45±5	<5000
☑ Shieldex 117/17 dtex 2-ply	280	4.5*	1200*	20*	348*
☑ Elitex 235/34 PA/Ag 8/22/30	~450	~1.7	~750	~10	~20
☒ Shieldex 235f34 dtex 2-ply HC	560	4.6	2576	~15.5	100±10

As can be seen in the table, five products (marked with green check boxes) are sewable in needle and bobbin. This is based on my experience with a professional embroidery machine (*ZSK JCZ 01* [26]). Furthermore, the table reveals that the conditions for sewability defined by Maggie Orth correlate rather well with the actual sewability.

Apart from *TITV* and *Statex* there are other companies that produce metal coated yarn. These are often quite similar. An exception is the product line *AmberStrand* [27]. In 2005 *Syscom Advanced Materials, Inc.* – a US based company – started its production. The yarn is based on fibers of *Zylon*[14]. These are high temperature and high strength fibers. *Syscom* applies rather thick layers of different metals onto each fiber, reaching excellent conductivity values around 1-3 Ω/m. However with so much metal around each fiber the yarn failed the fingernail-test and to my experience could not be sewn in needle or in bobbin. Unfortunately, until today (i.e. 2010) *Syscom* has stuck to the goal of providing ultra low resistance yarns rather than making the yarns sewable and accepting slightly higher resistances (e.g. 20 Ω/m). The cross sections in Figure 2.2 compare an *AmberStrand* filament to a *Shieldex* filament. It becomes obvious that *AmberStrand* will exhibit more the flexibility of a wire than of a thread. Its metal coating has a thickness of roughly 10 µm. The limit for embroiderability may be assumed to be a few 100 nm.
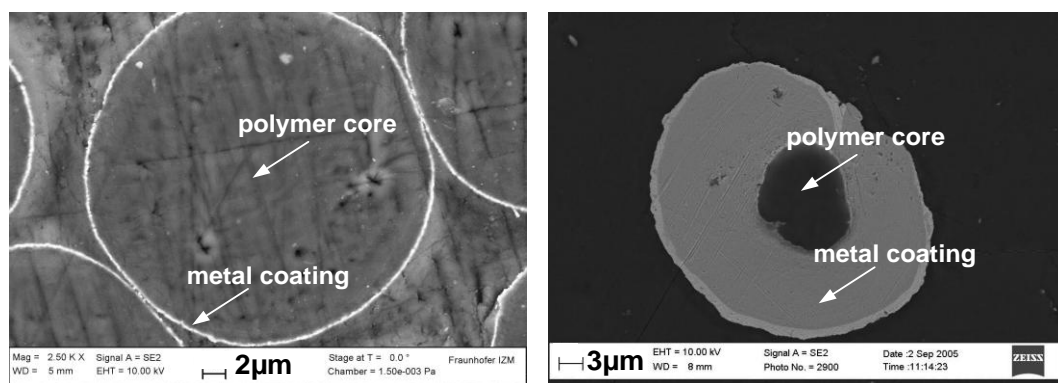

Figure 2.2:   SEM[15] images of cross sections of a fiber of *Shieldex 117/17 2-ply* yarn (left) and of a fiber of *AmberStrand* yarn (right). The ratio between polymer core and metal coating differs strongly between the two fibers.

2.1.4 Special Type of Embroidery: Soutache Embroidery

Soutache embroidery is another embroidery technology that should be mentioned here. It can provide conductive wiring in a different way. Thereby, a conductive thread, a wire or even a cable is laid on the top-side of the cloth and fixed with a zigzag (lock-)stitch.

A simple home sewing machine with braiding foot for this purpose is shown in Figure 2.3 left. In this case, the needle moves from one side to the other to create a zigzag stitch that fixes that laid down yarn. In a professional embroidery machine the needle axis is fixed, therefore the cloth is moved to create the zigzag.

---

[14] IUPAC name: poly(p-phenylene-2,6-benzobisoxazole); short name is PBO
[15] scanning electron microscopy

Furthermore, the embroidery head with the spool for the laying thread can rotate to provide that the laying thread is always oriented the same way as the embroidery direction. The right image in Figure 2.3 shows this special embroidery head called W-head [26], [28]. The latter is actually used to lay the resistance wire to fabricate heating layers for car seats or steering wheels [29].
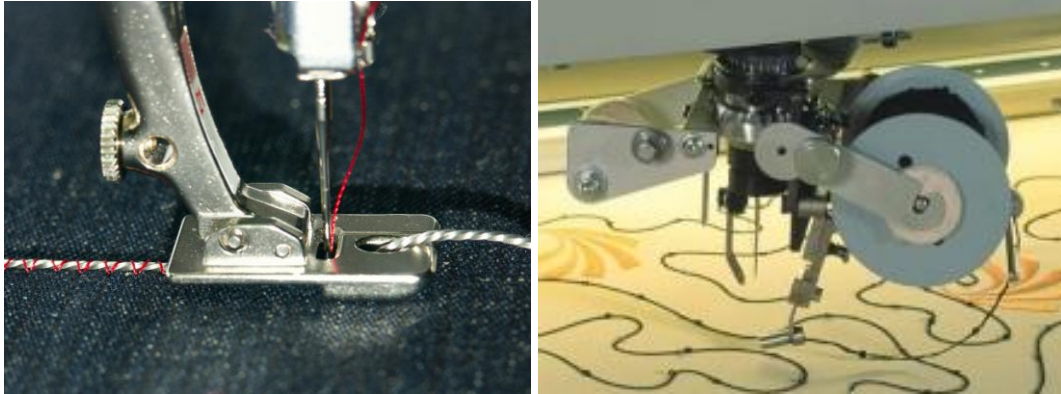

Figure 2.3:   Left: A braiding foot in a home sewing machine. The hole guides the steel cord and the needle fixes it with a zigzag stitch. Right: The rotatable W-head in a professional embroidery machine assures that the direction of the laid yarn is always identical with the direction of the embroidery (Source: [26]).

Though, this technology is not directly suited for embroidering contacts, with some modifications and by using a surface conductive needle thread, it could be used to increase the conductivity of wiring between embroidered contact points.

2.2 Embroidering Contacts

The principle idea of using the wiring thread itself to make the contact to an electronic module has already been present in Maggie Orth's work. She described tying a knot with a conductive thread through the hole of a rigid FR4[16] board. This created a mechanical and electrical connection as shown in Figure 2.4. Since this was handmade she could choose a non-machine sewable *"twine of continuous stainless steel core wrapped with stainless steel and polyester composite thread (BK 50/2)"*. However, she noted that the choice of this particular yarn was crucial to the durability of the knot. Other yarns had broken *under stress*. [8]

---

[16] FR4 is a fiber glass reinforced epoxy laminate used as substrate for making printed circuit boards
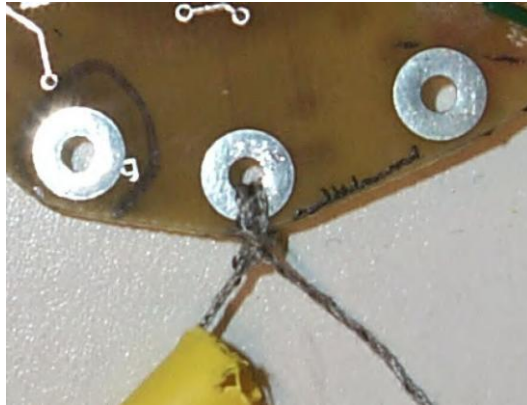
Figure 2.4:   Mechanical and electrical connection with knotted conductive thread. [8]

In 2005, the first machine embroidered contacts were presented by me [30], [31] and Oliver Lindner [32]. On one hand, it was demonstrated how embroidery of conductive yarn could be used to contact a smart textile component like a key pad made from woven conductor lines. See Figure 2.5 on the left. On the other hand, it was demonstrated that an embroidery machine can be used to contact metallized pads on a thin electronic substrate. For this purpose special embroidery pads of different shapes and sizes were foreseen on the electronics substrate. Some were predrilled so that the needle just had to go through the hole. Some were directly pierced by the needle as shown in Figure 2.5 on the right. [31] (Effects of this predrilling or piercing are discussed in chapter 4.2.1.)

In both cases – key-pad and flexible substrate – the embroidered conductive thread served as an electrical contact and mechanical fixation simultaneously, like in Maggie Orth's knot.
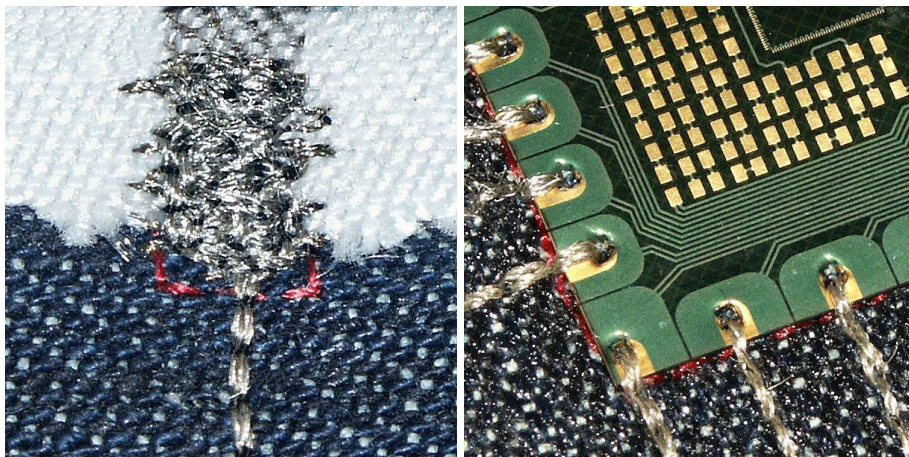

Figure 2.5:   Machine embroidered electrical contacts to woven keypad (left) and to flexible substrate module (right). [30]

Also the hand embroidered *LilyPads* application of Leah Buechley should be mentioned here as an application of these embroidered contacts. In 2006, she

presented a first version of a *"construction kit for electronics in textiles"*. See Figure 2.6 (left). It consists of a microcontroller on a cotton patch with laser cut fabric wiring, which can be contacted to other components like sensors, LED 'sequins' and actuators by stitching conductive yarn through the fabric contacts. [10]

By 2008 this had evolved to an actual product: a kit for children to experiment with electronics-in-textiles shown in Figure 2.6 on the right. The kit consists of seven different rigid substrate based modules with predrilled pads for hand-sewing the electrical contact. [33] Connected to this work and also independently a large number of do-it-yourself projects and design projects were done using hand embroidered contacts: [12], [34], [35], [36], [37], etc.
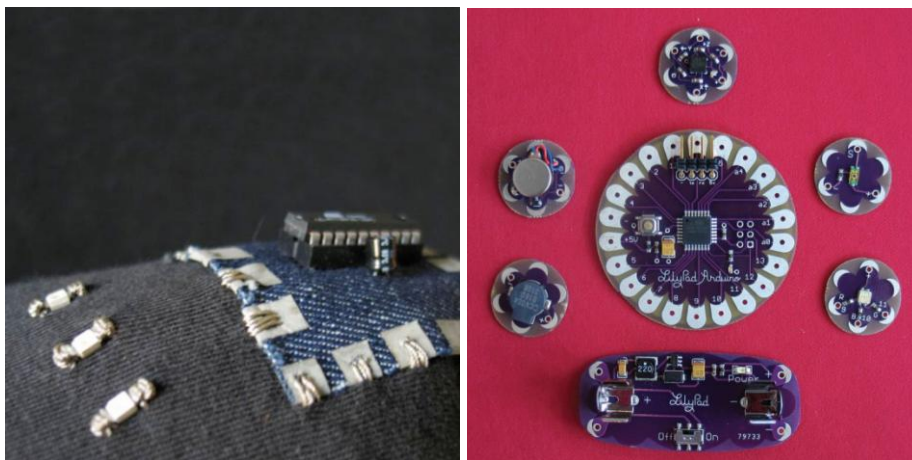

Figure 2.6:   Microcontroller module on a cotton patch which can be contacted to LED 'sequins' via hand embroidered contacts (left) [10]. This ultimately grew to become a kit for children with a set of rigid substrate based modules called LilyPads. [33].

The difference between the examples in the five images above showing embroidered contacts is the substrate material on which the contacts were realized: rigid fiber reinforced substrate with structured metal pads, thin polymer substrate with structured metal pads and structured conductive fabric on fabric. As the coexistence of these three approaches is totally legitimate, the implications of the material choice should be shortly discussed here.

The most natural choice of substrate for electronics-in-textiles seems to be conductive fabric. However this does not solve the prime problem of contacting conductive textile circuitry to electronic components or electronic modules – it is just moving it to a different place. This is why this option will not be considered in this work.

Rigid substrates (i.e. fiber reinforced substrates) require predrilling the embroidery pad. Thin polymer substrates (i.e. without fiber reinforcement) can be pierced by the needle, making predrilling optional. Thin polymer substrates are not drapable or foldable and therefore not washable or wearable without protecting large parts of

the module. Only small parts (e.g. the embroidery pad) may be left without protection. Of course, the rigid substrate is also not drapable, but it might resist most stresses typical to textile applications.

The basic communality of these approaches – and this should apply to all embroidered contacts – is their requirement that both elements – the thread and the pad – are electrically conductive on the surface. The mechanism of tying a knot or attaching by embroidery provides that thread and pad touch and build an electrical contact. Understanding and analyzing the stability of this mechanism is a main objective of this work.

For machine embroidered contacts a second ground rule is that at least the top thread must be conductive. This originates from the fact that modules can only be applied to the top side of the fabric due to the construction of current embroidery machines. This again means that the top thread is the one being laid onto the embroidery pad and as explained, this one has to be conductive on the surface.

Of course, it cannot harm to choose a bobbin thread that is conductive as well. It may help to bring down the overall resistance of the wiring. Since the mechanical demands are lower than on top threads, yarns with thicker metallization can be utilized in the bobbin.

In Orth's and Buechley's work and also in my first experiments the embroidered contact is not only an electrical contact but also a mechanical fixation of the module on the substrate as just discussed. However, according to my experience and also according to [32] leaving the fixation up to the embroidered contact is a reliability hazard. Especially shear forces during washing and mechanical tension created by thermal mismatch can lead to early failures of the electrical contact.

An additional mechanical fixation of the electronic substrate on the embroidery cloth is simple to realize (e.g. with adhesive) and can help to overcome this problem. This is described in detail in 5.2.3.

2.3 Demands on Embroidered Circuits and Contacts

The following discusses demands on embroidered circuits and contacts. This comprises electrical aspects relevant for different applications, comfort aspects during wearing and, reliability aspects. The latter includes an introduction to those reliability tests relevant for this thesis.

2.3.1 Functionalities & Applications

In the sense of this work, the intention of embroidering conductive yarn is to electrically interconnect[17] different entities on a fabric that are located apart from another. These entities may be sensors, amplifiers, computational units, light sources, radio transmitters, actuators or power sources. Special cases are entities that are made of conductive yarn themselves like (body) electrodes, textile keypads or other input devices. Between these entities digital or analog signals or energy may have to be transmitted over the conductive embroidery.

In body monitoring applications the sample rates of sensors are typically linked to body activities and therefore data rates of digital communication are low [38]. Also other wearable applications typically require only low data rates, for instance when displaying the name of a caller in a communication jacket [4]. The same may apply to a majority of technical applications. The input impedances are typically in the MΩ-range.

While digital communication allows smart rerouting of data in case of short or open circuits, analog sensors require permanent interconnection between entities. With analog, typically a voltage is transferred for instance from a sensor or an electrode to an amplifier [13], [16]. Also inversely the voltage may be transferred from an amplifier to electrodes [39], [40].

Power applications comprise everything from powering low power digital sensors to powering high power lighting applications. In power applications a resistive loss in the wiring causes accelerated battery depletion. Also the voltage drop can become a critical factor. This shall be shortly explained at the example of textile displays. Such are likely to become the economic engine for textile integrated electronics. For this case study a 10 x 10 matrix display with white LEDs shall be assumed. The LEDs are arranged at distances of 3 cm from another and each one consumes in average 5 mA at 3.3 V (multiplexed line-by-line). For this scenario the left graph in Figure 2.7 shows the fraction of the resistive loss in the wiring compared to the totally consumed power of the display depending on the yarn resistance in Ω/m of the wiring yarn between the LEDs. The right graph shows the voltage required to power the most distant LED from power source again depending on the yarn resistance in Ω/m. From a power-efficiency point of view, yarn resistances up to 10 Ω/m may be considered acceptable. From a security point of view the required supply voltage reaches a value of 24 V when the yarn resistance is 210 Ω/m. For some applications, e.g. clothing, this may be overcritical which means in these cases a yarn with a lower resistance needs to be chosen.

---

[17] in this thesis interconnection shall refer to the conductive textile wiring between two points; while contact shall refer to the electrical contact between an endpoint of this textile conductor and some electronic component or module
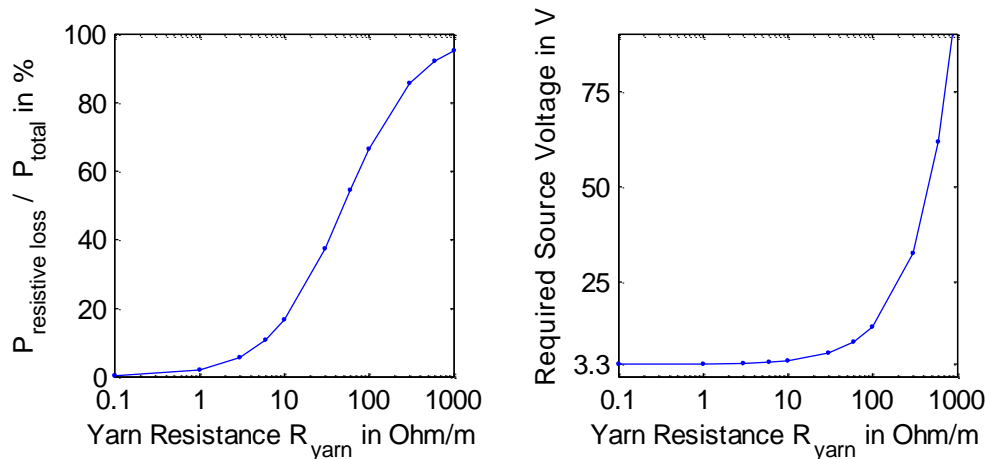
Figure 2.7: 10 x 10 matrix display with LEDs multiplexed 1:10 consuming in average 5 mA at 3.3 V and each at a distance of 3 cm from another. Left: Power efficiency depending on the yarn resistance of the wiring between LEDs. Right: required maximum source voltage for supplying the LED with 3.3 V that is most distant from the controller. This data is based on calculations made with an Excel tool that was developed by Helmar Dittrich at Fraunhofer IZM [41].

It may be summarized that the different applications require that the resistance of the interconnection between two entities is between at maximum some tens of Ω/m for power applications and a few kΩ/m for input devices like touch sensors. As was explained in 2.1.3, the most conductive embroidery yarns reach values of about 20 Ω/m. By applying these yarns as top and as bottom thread, the resistance per stitching track can be halved. A further reduction per stitching track can be achieved by embroidering the track multiple times (or trivially embroidering multiple tracks).

Analog effects like capacitive coupling do not need to be considered for typical applications as frequencies are usually low [15]. Of course, when developing applications, the actual demands have to be set individually by the developers.

The contacts at the end of each embroidered conductive track should not significantly change the overall resistance between the entities. For the LED matrix display example this means, contact resistances should be 30 mΩ[18] or lower. For other applications like a touch sensor even 10 Ω per contact are uncritical. Also for analog sensor connections a high contact resistance may often not be an issue, however, it may be important that the contact is particularly stable and with low noise.

---

[18] it is assumed that the resistance of the yarn is 10 Ω/m; therefore, the resistance between two neighboring LEDs is 300 mΩ plus two times the contact resistance; if the latter is 30 mΩ than this does not significantly change the overall resistance of the connection between the two LEDs

2.3.2 Textile Character

When integrating electronics into textiles for clothing or for technical applications, preserving the textile character of a fabric is an essential demand. According to [42], this textile character *"can be defined in two ways: either by technically measureable properties like drapeability, flexibility, stretchability, weight, water permeability; or by the perception of the user in terms of touch, comfort, optics, etc. For technical textiles typically the technical parameters are predominant. Whereas in clothing the sensation of the user dictates limitations for technical parameters."*

A true textile character will of course only be reached when electronics are integrated directly onto the fiber surface [43]. However, such implementations are still far in the future. For implementations that rely on modules or components attached to textiles, [42] introduced the term *"overall textile character"*. It accounts for the fact that such modules or components *"will always change the textile character locally as they cannot be stretched or draped"*. Depending on the application the required degree of overall textile character may vary strongly. *"For a jacket for instance, blending-in electronic modules into the garment perfectly is not necessary as people are used to carrying wallets, keys and mobile devices in their pockets. Therefore, an integrated device, e.g. a music player, does not need to be smaller, lighter or more flexible than these other things in the pockets. However a T-shirt for permanently monitoring the wearer's health should provide the same comfort as a normal T-shirt does. Of course the wearer's tolerance will increase with the benefits for the wearer – for instance life saving. Other aspects come into consideration when the special clothes are just for temporary use under well defined conditions. An example is a heart rate monitor for running which does not need to be comfortable while sitting or lying down. For technical textiles this concept of preserving the overall textile character applies equally. Locally an electronic module will for instance reduce the air permeability to zero. But on a large panel of fabric this is typically not very critical for the overall air permeability required for the application."* [42]

While technical applications are highly individual concerning these demands, applications in clothing allow generalizing comfort issues. For this purpose different layers of clothing have to be regarded separately. Gimperle at al. have developed design rules for shaping large boxed electronics – like general purpose wearable computers – so they would put the least burden on the body while carrying them [44]. Figure 2.8 gives an impression of this work. For small devices in undergarments like in an EKG sensing shirt such comfort analysis did not exist. So, to know the size limitations for such modules not to be perceived uncomfortable, I initiated and supervised a diploma thesis to analyze this in a user study.
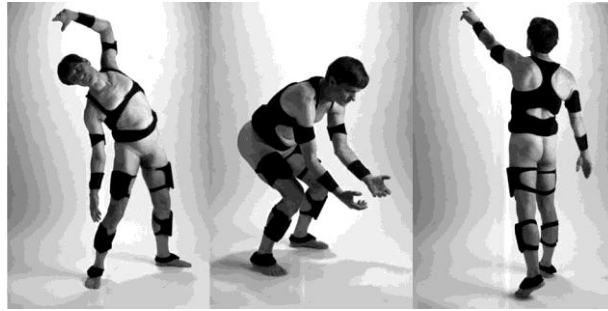
Figure 2.8:   Designs for making boxed electronics more comfortable to carry around the body. Source: [**44**].

In this study Claudia Schuster investigated the comfort of differently sized and differently positioned small modules in a shirt directly worn on the body. For this purpose she developed two types of test shirts – one for male and one for female wearers. These test shirts allowed attaching dummy modules in 27 different positions. These positions are shown in Figure 2.9. She made dummy modules in three different sizes:

- large: 45 x 45 x 4 mm^3 weighing 12g
- medium: 30 x 30 x 3 mm^3 weighing 4g
- small: 20 x 20 x 2 mm^3 weighing 1g

Furthermore, she made bendable rubber variants and rigid variants of each size. The Shore hardness A of the applied rubber was 67.

Then, she had five male and five female test persons who wore the shirts for a number of days for several hours with four to eight modules attached. Afterwards they rated the perceived comfort concerning different aspects like *"overall impression*, *during movement*, *during sitting*, *during sports"* (that includes the aspect of sweating) and the *"impact on optics of garments worn over the test shirt"*.

In the evaluation process she graded each position and weight combination based on the answers of test persons. Hereby, a large variance between test persons or between different aspects of comfort, led to a downgrading of the specific position-weight combination. The possible grades were *"very good*, *good*, *fair and bad"*.

The small and medium sized modules in all positions were considered at least *"good"* but mostly – i.e. in 24 and 19 positions respectively – considered *"very good"*. With the large sized modules, 12 positions were still graded *"very good"*, 10 positions were graded *"good"* and 5 positions were graded *"fair"*.

Surprisingly, the users did not perceive any significant differences between the bendable rubber variant and the rigid variant. Apparently, at this size of modules conformability is not important for electronics integrated into undergarments which is a very important result.

Only sporadically the male group and female group perceived particular positions combinations differently.
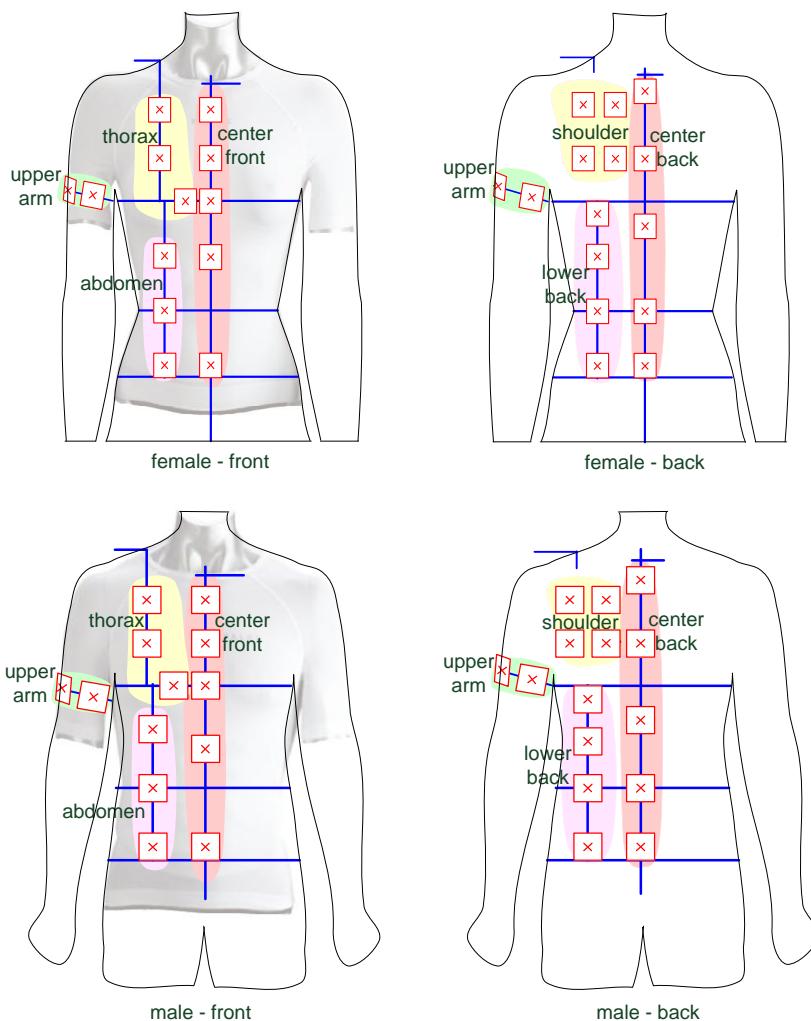

Figure 2.9:   Test positions on the male and female upper body are similar but exact positions differ slightly due to different body shapes. Altered from [45].

For wearable electronics applications, these results are positive. Several demonstrators and prototypes have shown that useful functionalities can be integrated into clothing with modules comparable in size to these dummy modules. Some examples are:

- an EMG module comparable to the small dummy: 16 x 13.5 x 2 mm³ [16];
- an RGB LED module comparable to the small dummy: Ø20 x 1 mm³ [33];
- an EKG module comparable to the medium dummy: 29 x 27 x 2 mm³ [13];
- and a general purpose module comparable to the large dummy: Ø50 x 3 mm³ [33].

With appropriate positioning on the garment the user will not find them uncomfortable.

2.3.3 Reliability

As pointed out by [42], *"another essential concern with electronics-in-textiles is reliability of electronics, textile conductors and contacts while washing, draping, stretching, wearing, etc. The reliability demands are very application dependent. Technical textiles are so versatile that generalization is hardly possible. Therefore an application specific analysis of the requirements has to be done."* However, for consumer applications with permanently integrated electronics in clothing, some requirements were collected by [42]. An elaboration of this list is presented here:

- *Wash Cycling.* Wash cycling is the most wide spread stress test for electronics-in-textiles. For this purpose ISO 6330, a standard test for domestic washing and drying procedures for textiles [46], has become a popular test for electronics-in-textiles as well. It was first applied by [47] for testing clothes with life saving electronic functions for the arctic environment. After that it was used by many others for all kinds of components of electronics-in-textiles, e.g. [48], [18], [42], [49], [50]. The standard offers a variety of water temperature levels for different applications – 30 °C, 40 °C, 50 °C, 60 °C and 92 °C. Most popular for electronics-in-textiles are test conditions 6A (40 °C) and 2A (60 °C). Usually 10 to 20 wash cycles are run. In-between cycles – but not necessarily between every washing cycle – test vehicles are drip dried and their functionality is tested.

- *Temperature Cycling.* In the electronics industry temperature cycling tests are common and were used for electronics-in-textiles as well, e.g. [48], [42], [49], [51]. The standard JESD22 A104 C [52] comprises a number of different temperature ranges for various applications. For consumer electronics the test condition N may be appropriate. It covers a range of -40 °C to +85 °C. Both temperatures are held for 15 minutes each. A typical number of test cycles is 1000. For technical applications higher temperature ranges may be more appropriate, e.g. -55 °C to +125 °C or -65 °C to +150 °C.

- *Humidity Exposure.* Another common test in both worlds – the electronics industry and the textile industry – is exposure to humidity. The electronics test JESD22 A101 B [53] recommends applying 85 % rel. humidity at an elevated temperature of 85 °C for 1000 hours. The following publications have used this test for electronics-in-textiles [48], [31], [49], [51]. Weathering tests combine spray water, elevated temperature and artificial sun light. CMST and Centexbel, partners in the SWEET consortium, have selected the ISO4892-3 [54] standard for this purpose [55].

- *Stretching, Flexing and Crumpling.* Stretching tests were used to test the reliability of stretchable substrates that may be applied onto fabric to create electronics-in-textiles systems [56], [57], [58]. In this context TNO Science

and Industry in Eindhoven proposed to refer to ISO 13934-1 [59] for stretching tests [60]. Furthermore, according to [55], CMST considers performing a flex and crumpling test according to method C of ISO 7854 standard [61]. A similar but proprietary test was performed by [18].

- *Abrasion.* TNO also points out the importance of resistance to abrasion i.e. during wearing. For conductive textiles (but not necessarily also for rigid components attached to it) [60] suggested applying e.g. the Martindale test (ISO 12947-2 [62]).
- *Perspiration.* Furthermore, [47] tested the reliability of electronics versus their resistance to perspiration with ISO 105 – E04 [63] which is originally meant to test the influence of perspiration on color fastness.

As already pointed out in the motivation, the primary objective of this thesis is to develop a theory of the contact mechanism underlying embroidered contacts and to identify failure mechanisms. Therefore, the primary purpose of applying stress tests here is to test occurrence of these failures and thereby validate the theory.

For such fundamental analyses it is particularly instructive to apply single load stress like thermal cycling rather than multi load stress like for instance wash cycling. Therefore, the main stress test in this thesis is a thermal cycling test. It is similar to test condition N defined in JEDEC JESD22 A104 C [52] industry standard for testing consumer electronics. One cycle consists of three isothermal lines at $-40\,°C$, $+20\,°C$ and $+85\,°C$. The dwell times and the transition times are always 15 minutes. The total cycle number is 25 unless otherwise stated. The exact temperature profile is presented in chapter 5.3.1.

Beyond this main stress test, a specially designed bending test was performed to test the contact behavior. During 180 seconds several bends were performed. This helped distinguishing the contact quality of two different implementations as is shown later.

Although a theoretical analysis of the effect of wash cycling is not developed, such tests are performed, since they are considered important in the community of researchers and users. As this is a multi load stress theoretical predictions are difficult. The applied test is in accordance with test condition 6A of ISO 6330 [46]. In total 20 washing cycles were performed.

Carefully note the difference between the first two tests and the third test. The temperature cycling test and the bending test aim at testing the *behavior*. The durations of both tests are too short for assessing the reliability in a practically realistic environment. The wash cycling test however, provides an insight into the actual *reliability* of the contact.

Chapter 7 presents improvements to make embroidered contacts more reliable. To test the *reliability* under realistic conditions, 1025 temperature cycles[19] or 20 wash cycles were applied.

All three stress tests are described in detail in chapter 5.3.

---

[19] 1025 cycles is merely the sum of 25 cycles which were run first and 1000 cycles which were run subsequently; normally one would test for just 1000 cycles.

3 Fundamental Analysis of Conductive Embroidery Yarn

Prior to analyzing the embroidery yarn in-depth, the most important conclusions of the previous chapter on this shall be summarized here:

Machine embroidered contacts require a yarn that
1. is conductive on the surface;
2. is embroiderable in the needle; and
3. reveals a conductivity as high as possible to cover many applications.

Multifilament yarns made of a combination of metal fibers (or wires) and non-conductive fibers are not suited for this purpose, as they are:
- either not embroiderable in the needle if the share of metal is too high or
- are embroiderable but reveal a low conductivity when the metal content is sufficiently low.

Currently, only some yarns made of metal-coated polymer fibers can satisfy all three requirements at once. These yarns have resistances down to some tens of Ω/m, which is sufficient for many applications. However, when this work was started,
- *Shieldex 117/17 Twine*[20] offered the best compromise between embroiderability and conductivity. Yet, its resistance of 348 Ω/m was rather high.
- Anyhow, for understanding the fundamental mechanisms of embroidered contacts which is the goal of this work, even such a high resistant yarn can be used. As will be explained in this thesis the results of course apply equally to other yarns made of conductively coated polymer fibers.
- Therefore, *Shieldex 117/17 Twine* was selected as embroidery yarn for experiments in this thesis.

The objective of this chapter here is to analyze the mechanical *and* electrical properties of such metal-coated polymer embroidery yarns. This is important as these properties have a significant impact on the embroidered contact as will be shown in chapter 4. Hereby, the focus is on the behavior during temperature cycling and during wash cycling as explained in 2.3.3.

The following analyses were carried out on *Shieldex*. However, the deeper understanding of its behavior developed in this chapter suggests that several properties are inherent for yarns of conductively coated polymer fibers and are not

---

[20] in the following this will be referred to as "*Shieldex*"

Shieldex-specific. As it turns out some of these properties are exactly the ones most crucial for the embroidered contact as will be explained in chapter 4.

3.1 Introduction to Metal Coated Polymer Fibers and *Shieldex*

Generally there are three approaches to applying conductive coatings onto polymer fibers:

- physical processes like vacuum deposition (e.g. chemical vapor deposition or physical vapor deposition like evaporation or sputtering) or vacuum spraying [64], [65], [66], [67], [68]
- electroless coating in a bath [65], [68], [69], [70]
- galvanic coating on already conductive fibers [22], [65], [71]

Different materials can be used to coat with: various metals, carbon or conductive polymers. Typical metals are silver, gold, nickel, copper, platinum and zinc [22], [64], [70]. Conductive polymers used for coating fibers are polypyrrol (PPy), polyaniline (Pan) and polythiophene (PTh) [68].

Polymer fibers coated with such materials are reported to be polyamide 6.6 (Nylon), polyaramide, polyester, PBO, polyurethane (Lycra™) and other synthetic fibers[21]. The adhesion of the coating depends very much on this fiber material and on the coating technology. Precursors have been used to improve the adhesion on various fiber surfaces [22], [69].

The thicknesses of coatings range from a few nano-meters for antistatic purposes to a few micro-meters for highly conductive fibers. The application of the fiber coating can be applied at single fiber level, yarn level with many fibers or even at fabric level.

Shieldex yarns are all based on a polyamide 6.6 (also called PA66 or Nylon 66) core with a silver coating. The manufacturer *Statex* and its founder K. Bertuleit claim that adhesion of silver is particularly good on polyamide which has a rough surface structure with nano cavities [23], [72]. However, Statex keeps the coating method secret. In his diploma thesis Erik Simon concluded that the process must be an electroless coating. The reaction does not seem to be autocatalytic which means, silver will only grow on the polymer but not on top of already grown silver. This helps to provide a relatively even coating, even when the fibers are already spun to yarn. The application works also after warp knitting the yarns to fabric as practiced by *Statex*. Conversely this is setting limitations to growing thicker coating layers in the same process. [25]

---

[21] synthetic man-made fibers or synthetic fibers are made by polymerizing monomers

The result is a conductive layer on the polyamide fibers that consists of nano-sized silver particles between 50 and 200 nm in diameter. The surface and the cross section of one fiber taken from a *Shieldex 117/17* yarn are shown in the SEM images in Figure 3.1. The cross section has been cut with a focused ion beam (FIB).

These fibers have a diameter of 30 μm in average (Figure 3.2). 17 of these fibers are twisted with 620 turns per meter to build one strand. Two such strands are combined and twisted with 550 turns per meter in the other direction to make the *Shieldex 117/17 Twine* as shown in Figure 3.3. In the following this yarn is simply called *Shieldex* as it is the only one from the *Shieldex* series used in this work. [73]

The fineness of the raw polyamide yarn is 117 dtex per strand, which means 1 km of yarn weighs 11.7 g. After twisting and metallization the yarn count is 280 dtex for the combined strands. [73]
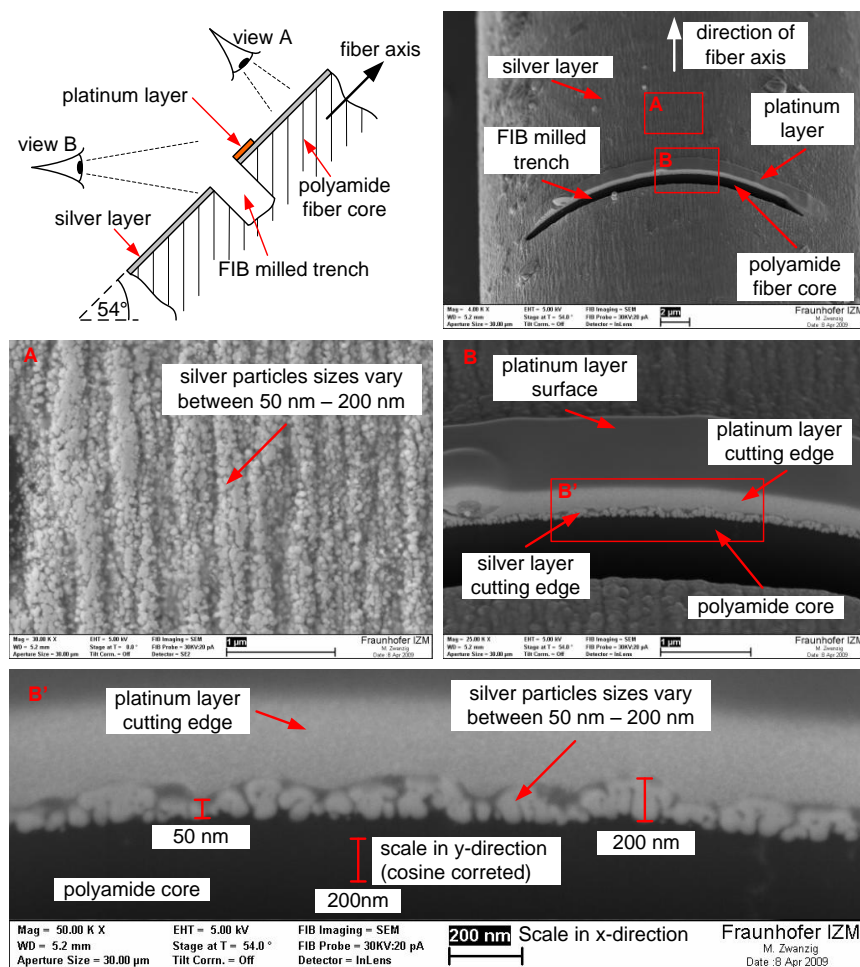
Figure 3.1:   View A shows the fiber surface with an SEM. The views B and B' show a cross section of a fiber of *Shieldex 117/17 Twine*. The cross section has been prepared with a focused ion beam (FIB). A platinum layer has been deposited locally to achieve a sharper cutting edge with the FIB. The lower image shows this cutting edge with an SEM. It reveals nano-sized silver particles on the surface of the polyamide core. The top left sketch explains the two different SEM viewing angles. The top right image shows the global position of view A and B on the fiber. Modified and combined from [74] and [25].
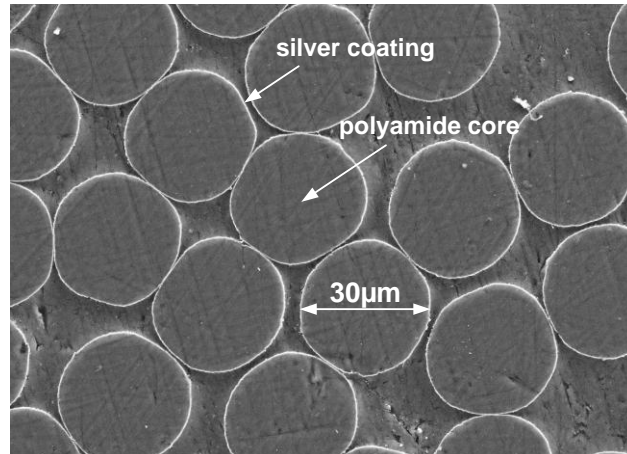
Figure 3.2:   Cross section of *Shieldex 117/17 Twine*. The fibers have a diameter of 30 µm in average.
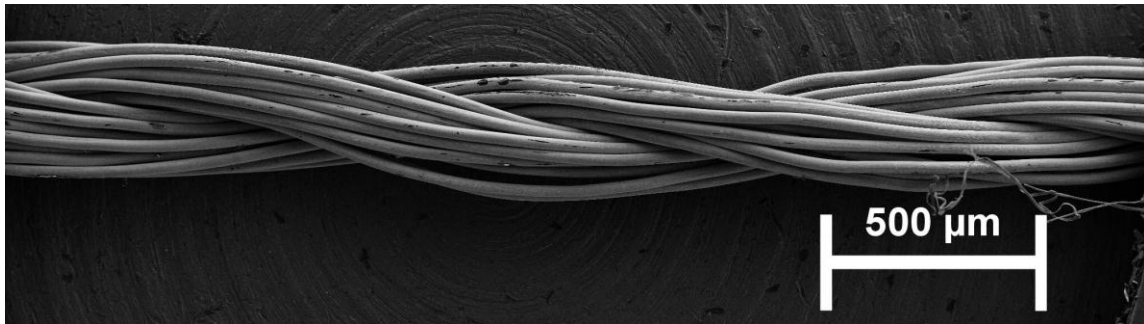
Figure 3.3:   SEM image of *Shieldex 117/17 Twine* with two strands of 17 silver coated PA fibers.

3.2 Electrical Behavior of *Shieldex*

The average resistance of the yarn as received from the manufacturer is 348 mΩ/mm (at RT[22]) with a standard deviation of 16 mΩ/mm [25]. Generally, the silver coating has a positive temperature coefficient (TC) causing the resistance to instantly rise or fall proportionally with temperature.

However, when the yarn is annealed[23] the resistance first falls and after a longer period of annealing rises again. The speed of this process increases with temperature. Philipp Foerster investigated this effect on single *Shieldex* fibers in his student research project [74]. Figure 3.4 shows the resistance change for single *Shieldex* fibers placed in an oven at 200 °C (left plot) and at 85 °C (right plot). All resistance values were measured at the respective oven temperature and are presented relative to the initial value at the respective temperature.

---

[22] RT means room temperature
[23] annealing in this context means exposing to a temperature above room temperature for a certain time
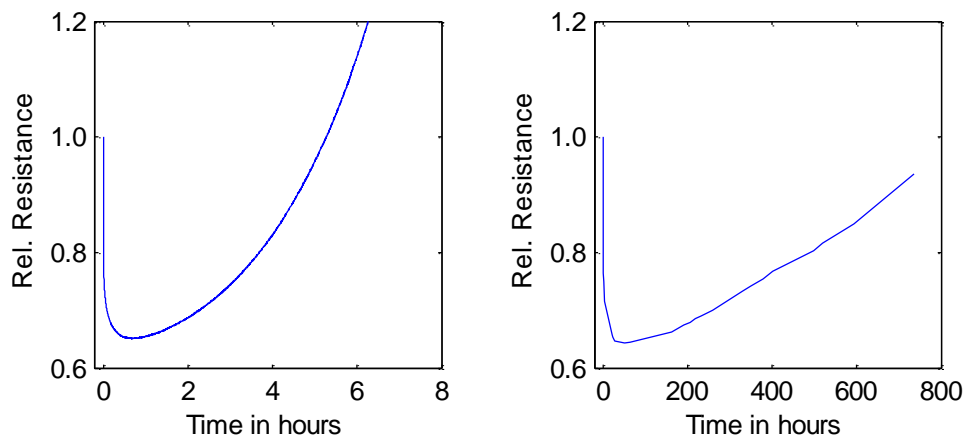
Figure 3.4:   Resistance change of single *Shieldex* fibers over time at 200 °C (left) and 85 °C (right) presented relative to the initial value at the respective temperature. Data from [74].

The effect of *rising* resistances in nano-meter scale silver films was already previously observed at an annealing temperature as high as 635 °C by Sieradzki et al. It was assigned to agglomeration of silver particles. Such thin films contain tiny instabilities, cracks, voids, etc. Above a certain activation energy, surface diffusion sets in, and enables the formation of clusters to reduce surface energy. The activation energy for diffusion to occur in such thin silver films is much lower than in bulk material. As clusters grow, the gaps between them become larger which is causing the resistance to rise. [75], [76]

Sieradzki et al. believe that mechanical stress in thin films may even boost agglomeration. Such mechanical stress can be presumed in silver films on polyamide fibers like in *Shieldex*.

Figure 3.5 shows that agglomeration appears on the surface of *Shieldex* fibers at temperatures as low as 85 °C. The clustering is clearly visible. Yet, this takes much longer than at 230 °C which leads to much larger clusters in short periods of time as also shown in this figure.

The initial *drop* of resistance observed in Figure 3.4 may be explained with different phases of the agglomeration. At the beginning agglomeration may lead to healing of tiny gaps or a reduction of the number of gaps. This may not have been observed in the experiments at 635 °C. This phase of agglomeration in which the resistance drops may have been too short at this temperature to be observable with a slow measurement. Furthermore, it may be that the silver surface on the *Shieldex* fiber is particularly imperfect, leaving room for conductivity improvement while in Sieradzki's experiments the surface may have been more homogeneous.
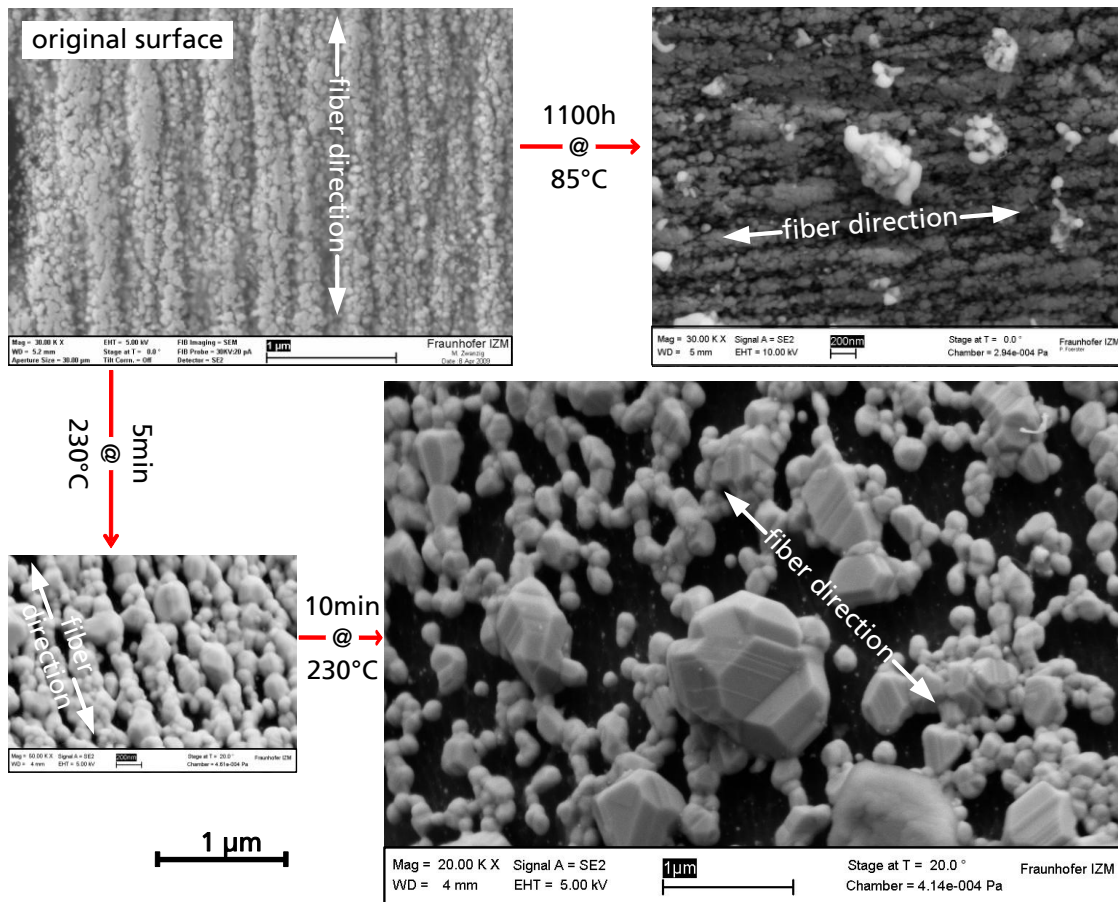
Figure 3.5:   SEM images of *Shieldex* fiber surface after different annealing steps: silver agglomeration becomes stronger with temperature and with time of exposure to this temperature. Note: the images show the fibers in different orientations. The scale on the bottom left is valid for all four images. Images from [**74**].

This thesis will investigate the embroidered contact during *temperature cycling* and *washing*. Furthermore, the contact will be exposed to *heat treatment*. Therefore, the following subchapters present the yarn's behavior under *these* conditions.

3.2.1 Effect of Temperature Cycling on the Resistance of *Shieldex*

Figure 3.6 presents the resistance change of a *Shieldex* yarn during 25 temperature cycles as defined in 5.3.1. Each cycle takes two hours and consists of isothermal lines at -40 °C, +20 °C and +85 °C.

The effect of the positive temperature coefficient is best observed when the resistance is plotted over temperature (Figure 3.6 right plot). The resistance at +85 °C is about 14 % higher than at -40 °C.

The effect of annealing can be observed in the plot over time (left plot). It is the high temperature which causes the resistance *drop* from cycle to cycle. The end resistance is 21 % lower than the starting value. Note, the overall cycling time (at

this temperature) is too short to also show the mentioned resistance *rise* due to annealing.
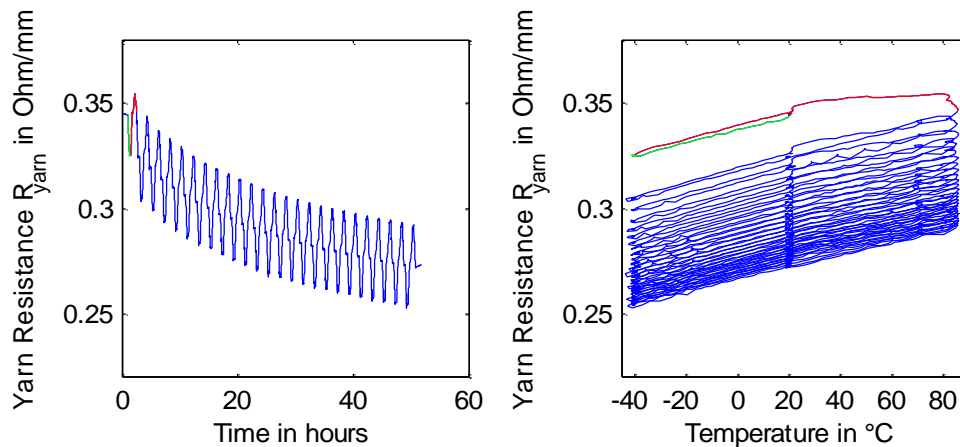
Figure 3.6:   Resistance change of *Shieldex* yarn during 25 temperature cycles at -40/20/85 °C. Sample length was 10 cm. The temperature profile is presented in Figure 5.9. The first cooling phase is represented by the green line and the first heating phase by the red one. [77]

Very similar resistance changes during temperature cycling have been observed in other *Shieldex* yarns by Breckenfelder, Dils and Seliger. [78]

3.2.2 Effect of Annealing on Resistance of *Shieldex*

Above, the effect of annealing was investigated and explained in principle. This subchapter describes results of Philipp Foerster who measured this effect at specific annealing temperatures for a fixed short time of 120 seconds in his student research project [74].

For this purpose *Shieldex* yarn was embroidered onto a meta-aramide fabric as selected in 5.2.1. The yarn was used as needle and as bobbin thread. The length of the embroidered track is 1090 mm and was embroidered three times one over the other. The stitch length was set to 2 mm. Figure 3.7 shows such a test vehicle.

Figure 3.7:   Test vehicle: the embroidered track has been embroidered three times one over the other (the same track) with *Shieldex* in needle and bobbin. The track length is 1090 mm. [74]

Four reference samples were made to test the behavior without heat treatment. Furthermore, for each annealing temperature two test samples were made.

Figure 3.8 shows the result. It plots the relative resistance change after heat treatment compared to before heat treatment. As anticipated the conductivity improves with higher annealing temperatures as the treatment time of 120 seconds is short.
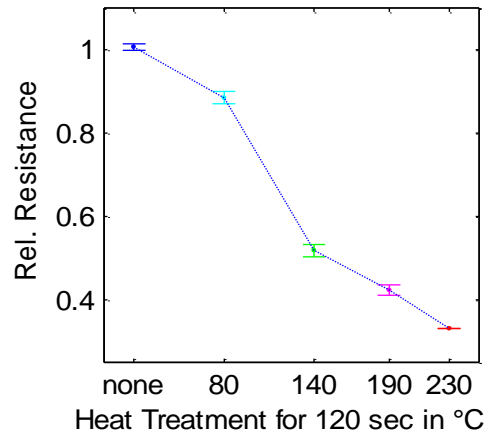
Figure 3.8:   Relative resistance change of embroidered *Shieldex* after heat treatment compared to before heat treatment. Data from [**74**].

3.2.3 Effect of Machine Washing on Resistance of *Shieldex*

All samples described in the previous chapter were washed at 40 °C for twenty washing cycles as described in 5.3.3. Figure 3.9 shows the resistance change of the *reference* samples which were not heat treated.
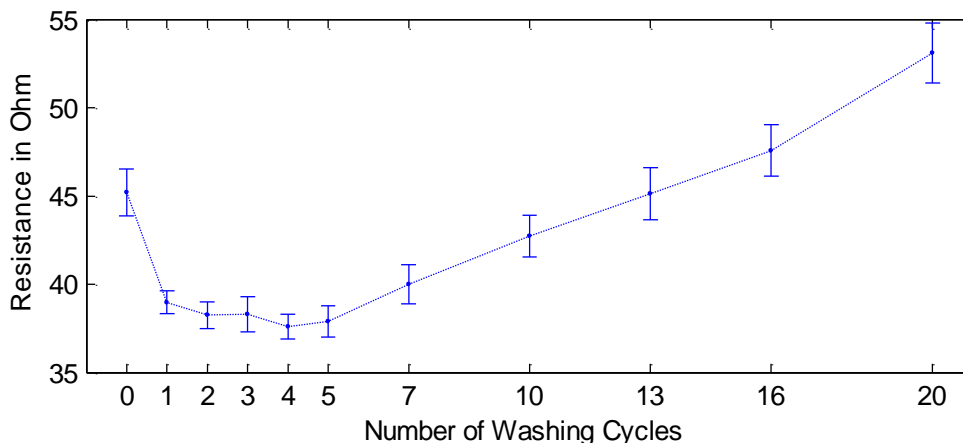
Figure 3.9:   Resistance change of embroidered *Shieldex* (as shown in Figure 3.7) after washing. The plot shows the behavior of the four reference samples that were not heat treated. Data from [**74**].

Apparently, this resistance curve is similar to the resistance curve during annealing discussed above. It may be speculated that the mechanical movement and the water create more stress in the silver film which promotes agglomeration as assumed by Sieradzki et al. This would explain the resistance drop during the first cycles.

Yet Figure 3.10 reveals that after twenty washing cycles the silver film has partially vanished on fibers faced to the outside of the yarn. This must have an effect on the resistance as well.
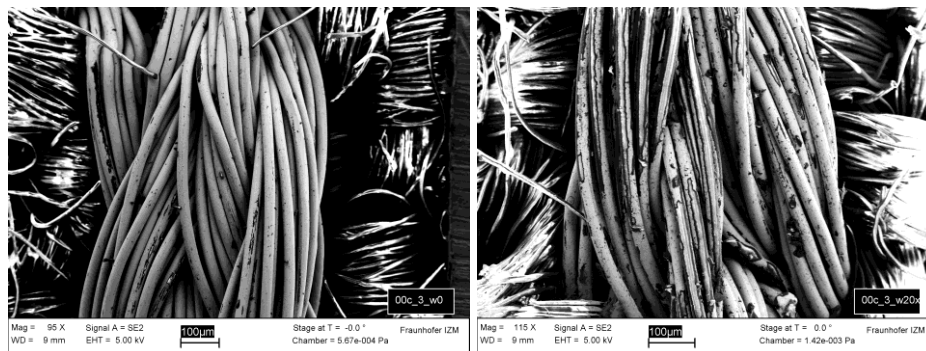
Figure 3.10: Embroidered *Shieldex* before washing (left) and after twenty wash cycles at 40 °C (right). [74]

Heat treatment initially improves conductivity of *Shieldex* as shown above. However, the heat treatment above 140 °C jeopardizes the stability of the conductive coating if followed by washing, as shown in Figure 3.11.
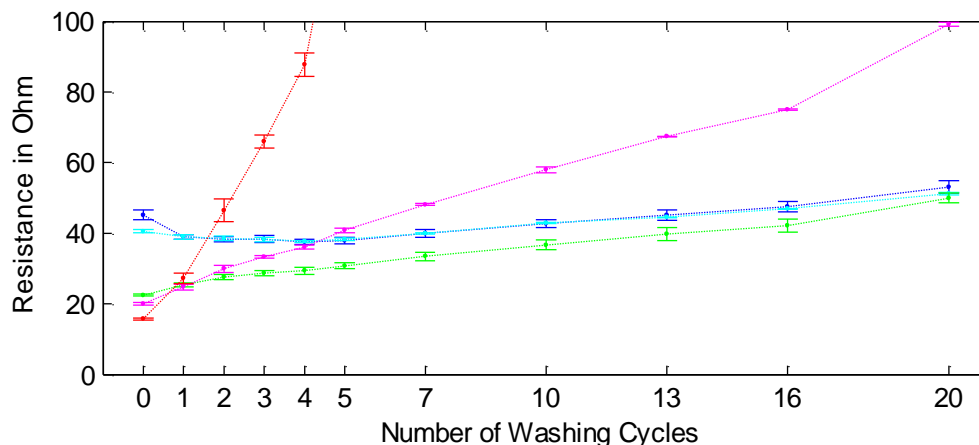
Figure 3.11: Resistance change of heat treated embroidered *Shieldex* (as shown in Figure 5.8) after washing. Blue: not heat treated; cyan: 80 °C; green: 140 °C; magenta: 190 °C; red: 230 °C. Data from [74]

Figure 3.12 proves that after twenty washing cycles silver has almost entirely vanished on all fibers when the sample was heat treated at 230 °C prior to washing.
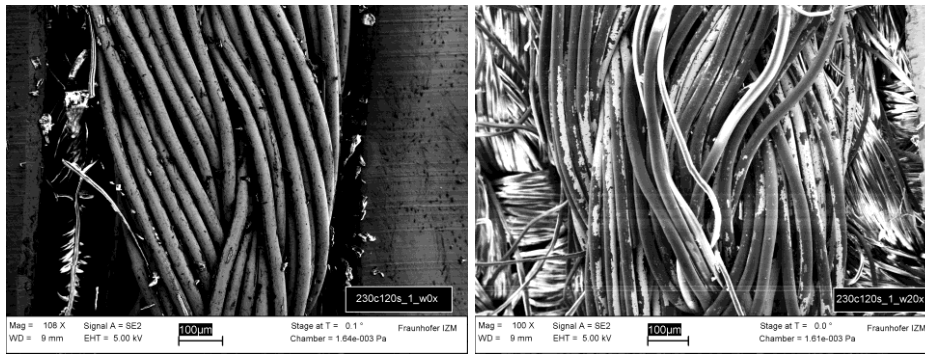
Figure 3.12: Embroidered *Shieldex* heat treated at 230 °C for 120 seconds without any washing (left), and after twenty washing cycles at 40 °C (right). The very shine white areas in the right image are electrostatic charges due to the weak conductivity of the yarn. [74]

3.2.4 Effect of Machine Washing on Polyurethane Protected *Shieldex*

Philipp Foerster discovered that areas on the fiber surface that were looked at by SEM degraded less during annealing than areas that were not looked at. Figure 3.13 demonstrates the effect. [74] Previously, Stahlmecke had similarly observed a reduction of grain growth in nano-sized gold films after exposure to an SEM electron beam [79]. He explained that carbon molecules that remain as pollution in the vacuum chamber of the SEM are atomized by the electron beam and are deposited on the target. He assumed that the carbon interpenetrates the grains and separates them. This would effectively reduce the mobility of gold atoms and thus also reduce the growth of clusters with minimum surface energy.

Stahlmecke's objective was to investigate electromigration. He found that nanostructures of silver and gold that were looked at with SEM exhibited an up to ten times longer life time than those that were not looked at.
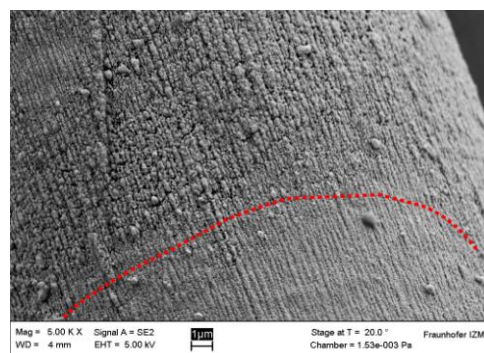
Figure 3.13: *Shieldex* after 5 minutes annealing at 230 °C. Above the red line agglomeration is clearly visible. Below the red line the silver film seems unchanged. This is the area looked at with SEM prior to annealing.[74]

Knowing this, a thermoplastic polyurethane film of 100 µm was laminated onto both sides of two new test vehicles after preparation as described in 3.2.2. The

lamination temperature was set to 190 °C. Pressure was not applied. The lamination time was 120 seconds. Figure 3.14 shows the test vehicles.
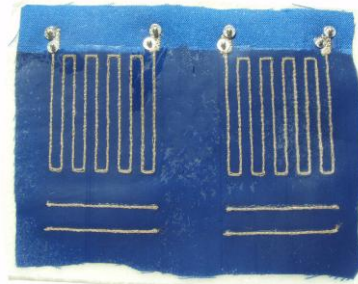

Figure 3.14: Test vehicles with embroidered *Shieldex*, afterwards protected by a laminated polyurethane film [74].

With these test vehicles washing tests were performed. Figure 3.15 shows the result and compares it to the reference test vehicles from Figure 3.9.
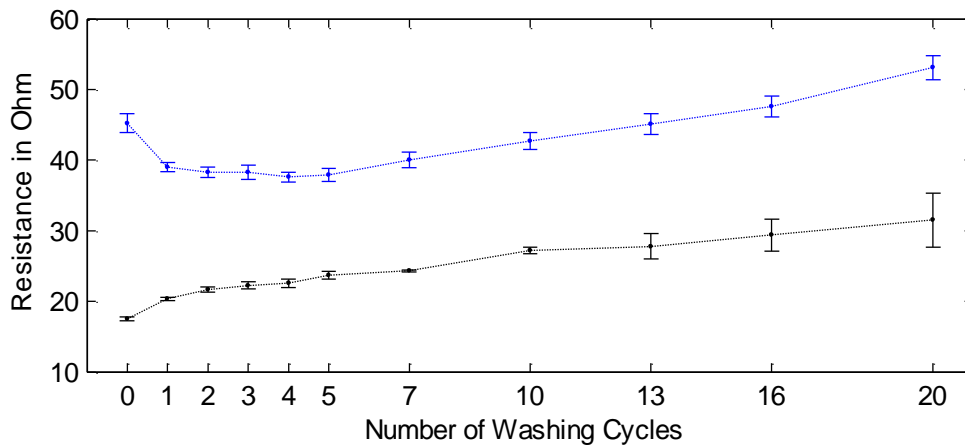

Figure 3.15: Resistance change of reference test vehicles (blue) and polyurethane protected test vehicles (black) during 40 °C washing cycles. Data from [74]

The lamination process lets the resistance drop by the same factor as in the 190 °C samples in Figure 3.11. Apparently, the high temperature still leads to a healing of gaps in the silver coating before the polyurethane stops the cluster building. During subsequent washing the polyurethane film seems to reduce cluster building and mechanical abrasion as the resistance does not rise as much as in those 190°C samples without protection. In fact the samples with polyurethane performed better than any other sample.

With these results it may not surprise that recently Statex and TITV started selling their conductive yarns (Shieldex and Elitex) also with a thermoplastic polyurethane coating. However, these yarns cannot be embroidered in the needle or in the bobbin. Yet, they may be laid with soutache embroidery as explained in 2.1.4.

3.2.5 Generalization

The previous subchapters analyzed the electrical behavior of *Shieldex* in particular. This is important for this thesis as it influences the contact resistance of the embroidered contact. However, it is also important to understand that *Shieldex* is not special in its behavior. It can be anticipated that nano layers of silver on other polymer fibers will also have a positive temperature coefficient and will also tend to agglomerate when annealed.

Yet, if the silver films are thicker than a few hundred nanometers, like it is the case on *Elitex* or even more so on *AmberStrand*, agglomeration will probably not occur or at least will not have a measurable effect on the overall resistance. Also with other metals, agglomeration may be less strong.

Generally, it should be investigated whether it is possible to apply a thin carbon film onto the nano silver with a mass manufacturing technology that is as effective as the carbon deposition with the SEM (perhaps there is one of the many CVD or PVD variants which is applicable).

Rising resistances during washing are often a problem with conductive yarns of all sorts, and are often related to mechanical abrasion. The acceptable percentage of the rise depends on the application.

3.3 Thermo-Mechanical Behavior of Polymer Yarns in General and of *Shieldex* in Particular

Also the mechanical and thermo-mechanical behavior of the conductive embroidery yarn influences the behavior of the embroidered contact significantly as later chapters will prove. Understanding this behavior of such yarns in general, and related to *Shieldex* in particular, is the objective of this subchapter.

The previous chapter showed that only conductively coated synthetic yarns can be used for embroidering contacts. Among these only those with conductive coatings made of metals are practically interesting until now. Furthermore, these yarns can only be embroidered as long as their metal coating is very thin (a few 100 nm at maximum). Such thinly metallized fibers and yarns are mechanically very similar to un-metallized ones. The only significant difference is their surface smoothness which is typically reduced by the metallization. The effect of this on embroiderability was already discussed in chapter 2. This subchapter analyzes un-metallized synthetic yarns in general before discussing *Shieldex* which reveals a similar mechanical behavior.

3.3.1 Introduction to Polymer Mechanics

Mechanical properties of polymers like elongation under stress are time dependent, temperature dependent and dependent on the stress level. This subchapter provides a short and simplified introduction to the mechanisms – as much as needed to understand the effects treated in this thesis.

3.3.1.1 Glass Transition and Crystallization

When cooling a melt it solidifies at a certain temperature point. If the melt does not crystallize the material becomes glassy or in other words it becomes an amorphous solid. A glass is an under-cooled melt which means that the molecules are not in equilibrium. Under this condition the solidification temperature is called glass transition temperature T_g. [80]

Some polymers solidify above the T_g which is due to their tendency to crystallize partly when they are cooled from a melt. This temperature is called crystallization temperature or melting temperature T_m. Yet, in such partly crystallized polymers the T_g still has an influence on the amorphous phases of the material and can be observed as a slight change in modulus, volume, heat transfer, etc. [80]

The molten phase of the polymer is characterized by viscous flow. In amorphous polymers this is above T_g. In semi-crystalline polymers this is above T_m.

Both T_g and T_m are not sharp points but temperature ranges in which the polymer transforms from one phase to another. Furthermore, the cooling speed slightly changes T_g and may significantly influence the level of crystallization (near T_m). In literature, however, mean values are often used to denote T_g or T_m.

Above a certain temperature the polymer chains start to decompose. This temperature is called decomposition temperature. In some materials decomposition comes before melting which practically means that the material never reaches the molten phase.

3.3.1.2 Polymer Classification

Polymers may be classified by the temperature behavior of their modulus and by their tension set[24]. Four groups are defined in EN 7724 [81]:

- elastomers
- thermoplastic elastomers
- thermoplastics
- duromers (also called thermosets)

---

[24] tension set is the result of an elongation test; according to EN 7724 [81] the material is elongated by 100 % for one minute; then the material is left without tension for one minute; the remaining elongation is the tension set; this test cannot be carried out with materials that break at elongations smaller than 100 %

Elastomers are loosely meshed network polymers that show rubber-elasticity within the service temperature region. They are typically made of vulcanized rubber and cannot be melted nor dissolved to shape the material permanently.

Exceptions are multiphase materials consisting of a soft phase with rubber-elastic character in the service temperature and a network building hard phase that can be melted at a higher temperature for processing (i.e. for shaping the material). Alternatively they may be dissolved for processing. The melting or dissolving process is repeatable. These materials are called *thermoplastic elastomers* (e.g. thermoplastic polyurethane).

Elastomers and thermoplastic elastomers show a strong restoring force with a tension set below 50 %. Their glass transition Temperature T_g is below 0 °C. Figure 3.16 shows the modulus of a thermoplastic elastomer.
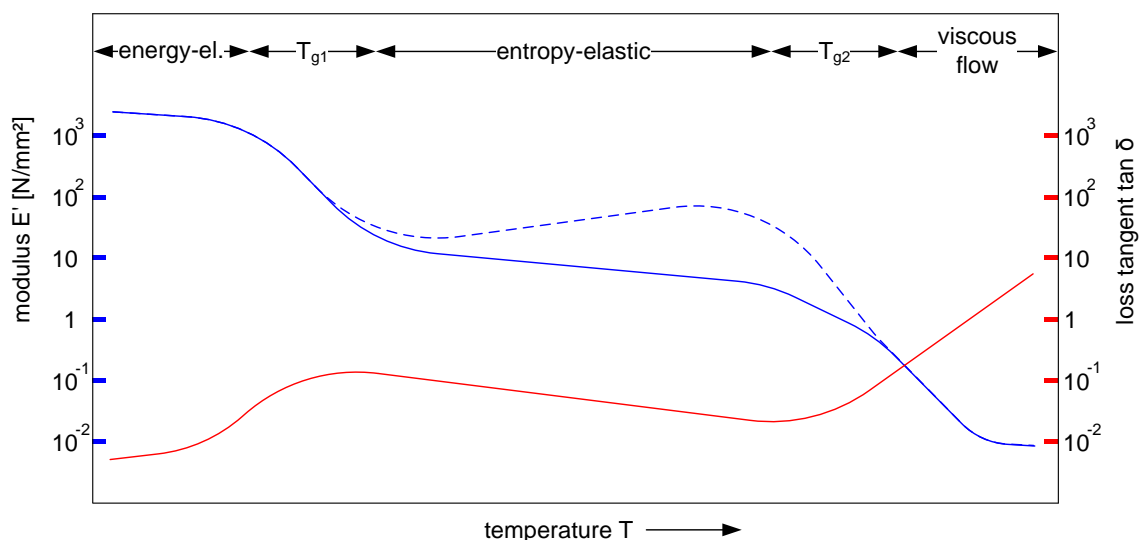
Figure 3.16: Typical plot for thermoplastic elastomers of real part of modulus and loss tangent. Thermoplastic elastomers show entropy elastic behavior within the serving temperature region. Frozen tensions may lead to rising modulus in the entropy-elastic zone (dotted line). The glass transition of the low melting phase T_{g1} is well below 0 °C. In the flow region above the glass transition of the high melting phase T_{g2} the material can be shaped. Combined information from [82], [81], [83].

Thermoplastics are built of long chain linear polymers linked by strong covalent bonds along the chain and, by weaker hydrogen and van der Waals bonds between chains. Besides chemical bonds, a mechanical entanglement of these long molecules takes place. Their structure may be amorphous or semi-crystalline as shown in Figure 3.17. Amorphous thermoplastics become viscous at their glass transition temperature or slightly above. Semi-crystalline thermoplastics show a slightly lower modulus above their glass transition than below their glass transition, which is due to the melting of the amorphous phase. At the crystal-melting point T_m the material becomes viscous. In this state thermoplastics can be shaped. This

form can be fixed by cooling below the solidification temperature which is T_g for amorphous thermoplastics or the T_m for semi-crystalline thermoplastics. This process is repeatable. The service temperature of thermoplastics is below the solidification temperature. [80]
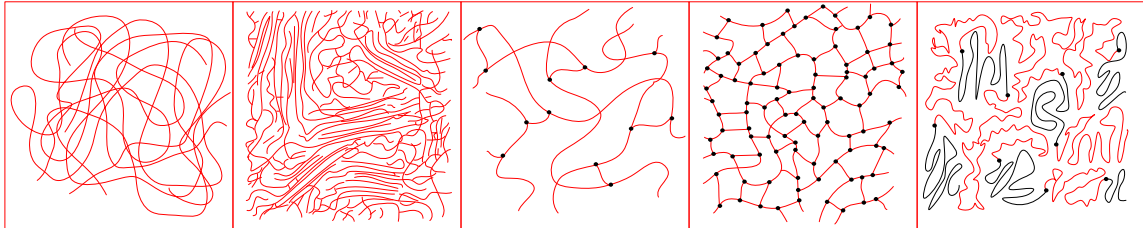

Figure 3.17: Structure of amorphous thermoplastics, semi-crystalline thermoplastics, elastomers, duromers and thermoplastic elastomers (from left to right according to [84], [85], [84], [84], [82]). Valency bonds are represented by black dots. The black and red lines in the thermoplastic elastomer represent high melting polymers and low melting polymers, respectively.

Polyamide 6.6 – the basis of *Shieldex* – is such a semi-crystalline thermoplastic. Its crystal-melting point is at 265 °C and it starts decomposing at 350 °C [86]. Its level of crystallization is between 40 % and 50 % [87].

Thermoplastics do not exhibit strong restoring forces. Their tension set is either above 50 % or cannot be measured as the material breaks at elongations smaller than 100 %. The modulus curves for amorphous and semi-crystalline thermoplastics are given in Figure 3.18 and Figure 3.19 respectively.
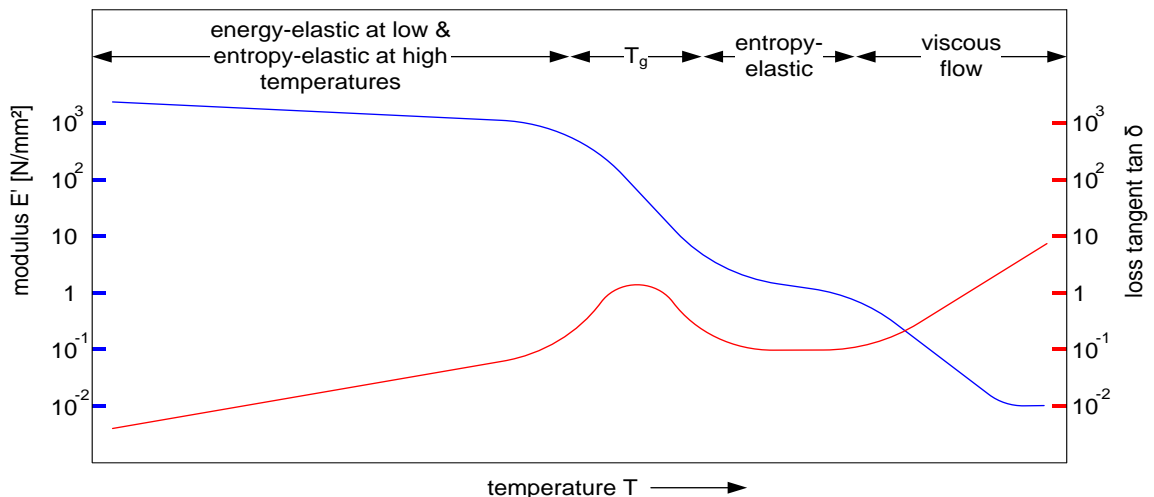
Figure 3.18: Typical plot for amorphous thermoplastic of real part of modulus and loss tangent. The application range is below T_g. In the flow region the material can be shaped. Combined information from [83], [82], [88], [84].
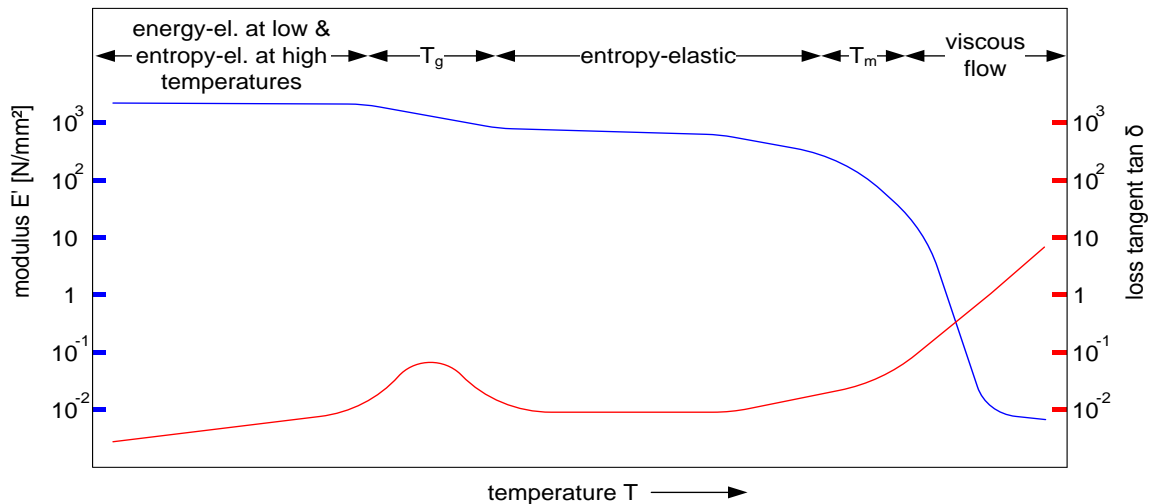
Figure 3.19: Typical plot for semi-crystalline thermoplastic of real part of modulus and loss tangent. The application range is below T_m. In the flow region the material can be shaped. Combined information from [83], [82].

Duromers are polymers with strong covalent bonds building a three dimensional network that is narrowly meshed. These materials are rigid and cannot be melted or dissolved. Their decomposition temperature is below the theoretical melting point. After cross-linking they can only be shaped by machining. The tension set cannot be measured as the extendibility is very small. Figure 3.20 presents the modulus curve. [80][81]

Elastomers, thermoplastic elastomers and duromers have an amorphous network structure as shown in Figure 3.17.
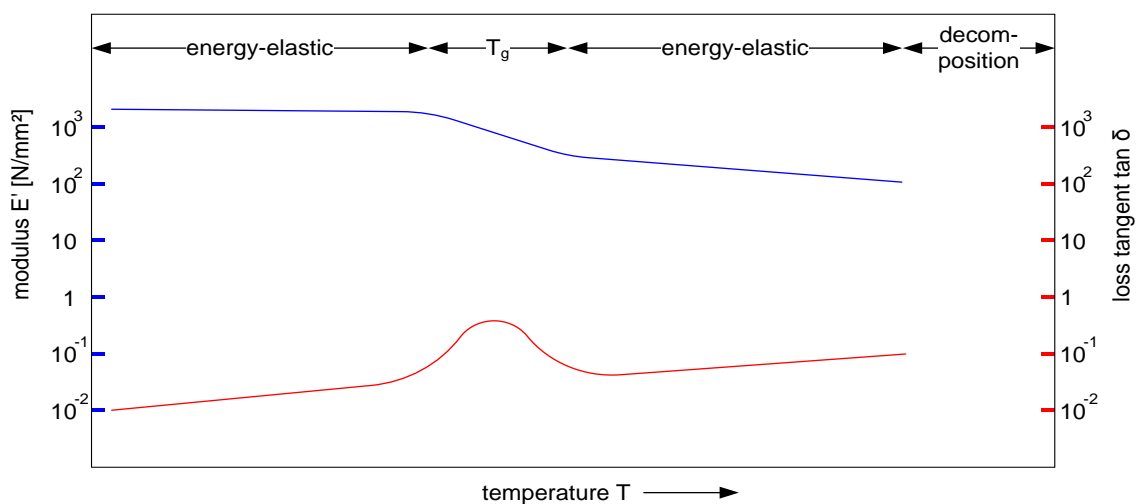
Figure 3.20: Typical plot for duromer of real part of modulus and loss tangent. The application range is below the decomposition range. Duromers can only be shaped by machining. Combined information from [82], [83].

3.3.1.3 Elasticity

Besides on the type of polymer, the mechanical stress response depends on temperature, time and stress level. At the extreme ends of the spectrum the behaviors can be characterized as elastic or viscous. However, in most situations polymers exhibit a material character that is a combination of both. This is called viscoelasticity.

Elasticity is characterized by a mechanically and thermodynamically entirely reversible process with a bijective relationship between stress and strain. The response is instantaneous and therefore time independent. Two types of elasticity are distinguished: energy-elasticity and entropy-elasticity. [88]

Energy-elasticity results from restoring forces in atomic bonds. When a force acts on a material the distances and angles of atomic bonds are deformed. Upon release of the deforming force the bonds spring back to their thermodynamic equilibrium. Energy-elasticity follows *Hook's law*:

$$\sigma = E\varepsilon \qquad \left[\frac{N}{mm^2}\right] \qquad\qquad 3.1$$

The stress σ is in a linear relation with the strain ε. The strain is the ratio of change of length over initial length. *E* is the material dependent modulus in *N/mm²*. Pure energy-elasticity exists only at small strains up to 0.5 %. [82]

Entropy-elasticity appears in macromolecular materials. The restoring force is driven by the systems desire to reach maximum entropy. The state with the highest number of different possible molecular conformations and thus the highest entropy is the coiled state. Straining the material orients the molecules. This ordering process requires energy which is returned upon release of the deforming force. Figure 3.21 illustrates this.
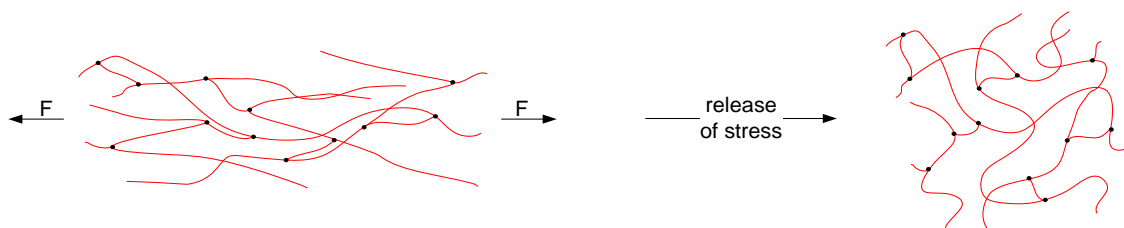
Figure 3.21: Entropy-elasticity acts in the direction of highest entropy. [84].

Other than energy-elasticity, entropy-elasticity may be effective over up to several hundred percent of strain. The relationship between stress and strain is

$$\sigma = \frac{E}{3}(\lambda - \lambda^{-2}) \qquad \left[\frac{N}{mm^2}\right] \qquad\qquad 3.2$$

with the draw ratio

$$\lambda = \frac{L}{L_0} = 1 + \varepsilon \qquad\qquad 3.3$$

Hereby the modulus *E* rises with crosslink density *N* and with temperature *T*. *k* is the *Boltzmann* constant:

$$E = 3NkT \qquad \left[\frac{N}{mm^2}\right] \qquad\qquad 3.4$$

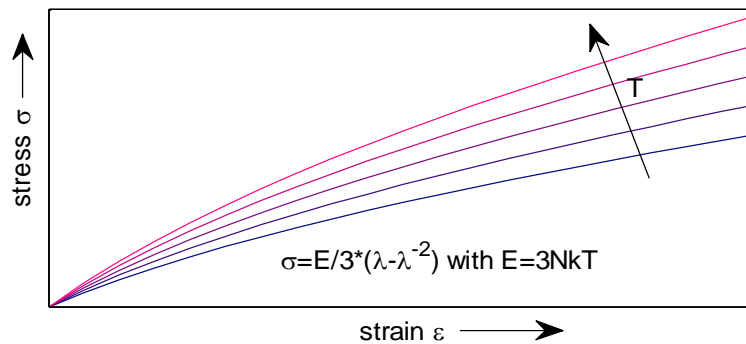The plot in Figure 3.22 demonstrates the effect of temperature dependence of *E* on the stress-strain diagram. [88]

Figure 3.22: Stress-strain diagram of entropy-elasticity depending on temperature.

Entropy-elasticity is found in elastomers which is why it is also known as rubber-elasticity. However, also amorphous and semi-crystalline thermoplastics exhibit entropy-elastic characteristics. The common mechanism is that the molecules can move to a certain extent but their mobility is also limited by crosslinks to keep the material from flowing.

In normal elastomers and in thermoplastic elastomers this crosslinking is effected by covalent bonds. In thermoplastics, molecular entanglements and (in semi-crystalline thermoplastics also) crystals act as crosslinks. In all these materials entropy-elasticity becomes dominant above the glass transition temperature where the mobility of molecules is higher than below the glass transition.

For amorphous thermoplastics this means that the temperature range in which entropy-elasticity is observed is very small and lies between the glass transition and the flow region.

Energy-elasticity is found in all polymers. In thermoplastics and elastomers it dominates below the glass transition temperature while in duromers it dominates the whole temperature range up to decomposition. Figure 3.16 to Figure 3.20 illustrate the active ranges of both types of elasticity.

3.3.1.4 Viscosity

Viscosity describes a mechanically and thermodynamically irreversible process. Applied stress leads to an instantaneous displacement of molecules and thus a deformation of the material. After release of stress any deformation stops and the shape remains as it is. This form of deformation is called flow or also viscous flow. Viscous flow is observed in melts of thermoplastics and in melts of thermoplastic elastomers. [88]

In the viscous state all mechanical energy applied to the material is dissipated due to intermolecular friction. The frictional forces are deformation velocity dependent. If strain-velocity and stress are in a linear relation the viscosity is *Newtonian*:

$$\sigma = \eta^T \frac{d\varepsilon}{dt} = \eta^T \dot{\varepsilon} \qquad \left[\frac{N}{mm^2}\right]$$

3.5

η^T being the elongation viscosity or *Trouton* viscosity[25]. [88] After integration over time t on each side of the equation and reforming this becomes:

$$\sigma = \frac{\eta^T}{t} \varepsilon$$

3.6

3.3.1.5 Viscoelasticity

Low-molecular materials[26] are elastic in the solid phase and viscous in the fluid phase (e.g. water). High-molecular materials often feature a blend of both of these material characteristics. This is called viscoelasticity. It combines reversible and irreversible processes [88].

While in elasticity and in viscosity the mechanical response is instantaneous. The response in viscoelasticity is delayed. This means that the modulus *E* becomes a function of time *t*. The effect of this is demonstrated in Figure 3.23.

---

[25] the T in elongation viscosity η^T is there to distinguish it from the 'normal' η which is the shear viscosity; in the case of shear, eq. 3.5 would become τ=η·(dγ/dt) with τ being shear stress and γ being shear strain [88]; in the elasticity chapter stress and strain were referred to elongation rather than shear; therefore to keep this chapter on viscosity analogous, presenting elongation viscosity was given the preference over presenting shear viscosity

[26] low-molecular material means consisting of small molecules; the opposite is high-molecular material
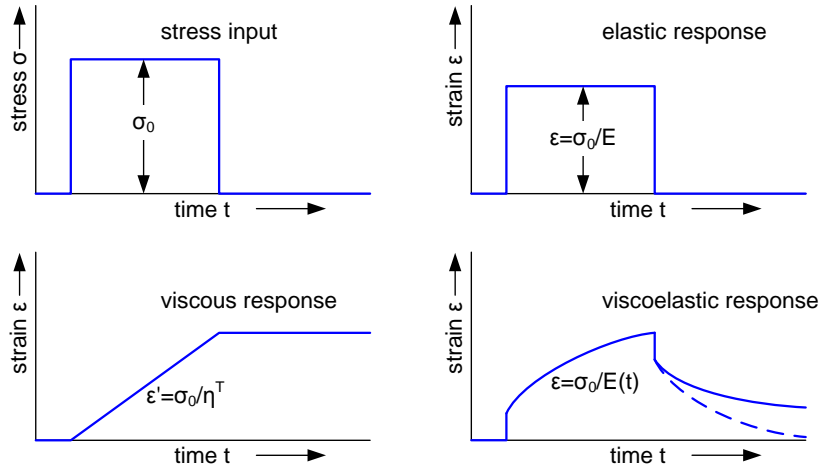
Figure 3.23: Comparing creep and recovery curves of elastic, viscous and viscoelastic materials. The elastic response is entirely reversible while the viscous response is entirely irreversible. The viscoelastic response may contain an irreversible strain (continuous line) or be fully recoverable (dotted line). In viscoelasticity the modulus *E* becomes time dependent. Modified from [83].

Viscoelastic behavior is especially dominant during glass transition and melting. [89],[83], [88]

In a certain range of strains viscoelastic behavior can be described with a linear differential equation. In the glassy state this range is around 1 % elongation. However, in polymer melts or in the entropy-elastic range of elastomers it can be up to 100 % elongation. Above such strains load-dependence sets in. In this case the differential equation becomes non-linear and cannot be solved without simplifications and approximations. [88], [83]

Linear viscoelasticity is based on the validity of the Boltzmann superposition principle which says that a sum of individual causes leads to the sum of their individual effects. For the relationship between stress and deformations this can be expressed mathematically in the following manner:

$$\left. \begin{array}{ll} If & \varepsilon_1(t) \rightarrow \sigma_1(t) \\ and & \varepsilon_2(t) \rightarrow \sigma_2(t) \end{array} \right\} \quad then \quad \varepsilon_1(t) + \varepsilon_2(t) \rightarrow \sigma_1(t) + \sigma_2(t) \qquad 3.7$$

This implies that the stress at time *t* depends on the prehistory of all past deformations *ε(τ)* defined from *-∞<τ<t* is relevant. This stress can be calculated by segmenting *ε(τ)* into step functions starting at *τ* of step height *ε'(τ)·Δτ* and summing up the stresses *E(t-τ)·ε'(τ)·Δτ* created by each of these strains from *-∞* to *t*. [83]

$$\sigma(t) = \int_{\tau=-\infty}^{t} E(t-\tau)\frac{d\varepsilon(\tau)}{d\tau} d\tau \qquad 3.8$$

This means that stress and deformation at -∞ must be known. In practice this may be achievable by heating the polymer to the flow region. Then stress and deformation can be assumed to become zero. However, often materials are supplied in a form which would be destroyed by heating it to this region e.g. silver coated yarns. In this case it is difficult to calculate the stress at time t.

Furthermore, the time dependent modulus $E(t)$ must be known which in the viscoelastic case is complex as a consequence of phase shift between stress and strain:

$$E^* = E' + iE'' \qquad \left[\frac{N}{mm^2}\right] \qquad\qquad 3.9$$

With E' representing the storage modulus and E'' the loss modulus, the ratio of these two becomes the loss tangent which was also plotted in Figure 3.16 to Figure 3.20:

$$\tan \delta = \frac{E''}{E'} \qquad\qquad 3.10$$

Figure 3.24 shows an example of such a time dependent modulus (at different temperatures).
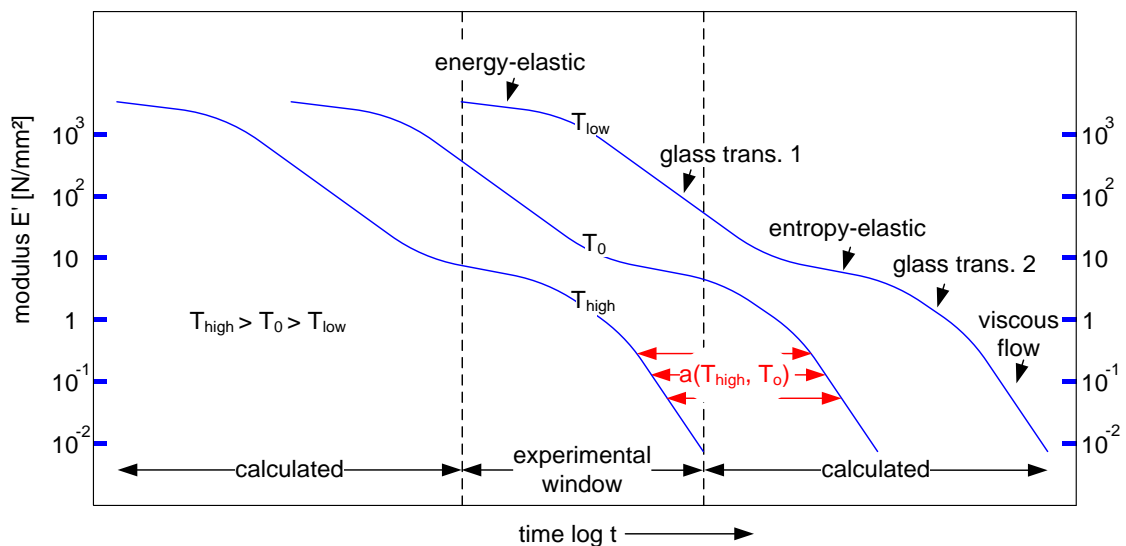
Figure 3.24: Typical course of real part of time dependent modulus E'(t) of a thermoplastic elastomer at different temperatures. The time-temperature shift function a(T, T₀) allows shifting a known modulus function at a reference temperature T₀ to different other temperatures T.

E' and *tan δ* can be found with a dynamical mechanical analyzer (DMA). A sinusoidal force is applied to the probe which changes its length. Both length and applied force

are measured and used to calculate the real part of modulus and loss-tangent. A phase shift of $\delta = 0°$ indicates pure elasticity while a phase shift of $\delta = 90°$ indicates pure viscosity. Viscoelasticity exhibits a phase shift between those extremes.

To obtain modulus and phase shift for different time durations the frequency of the sinusoidal force can be tuned. The result is then a frequency dependent E' and $tan\,\delta$ which can be transformed into a time dependent $E'(t)$ and $tan\,\delta(t)$. The dotted lines in Figure 3.24 indicate that the experimental window for such testing frequencies is limited and that the modulus outside this window must be calculated as described in the next subchapter.

Looking back, it should be noted that Figure 3.16 to Figure 3.20 represent the temperature dependence of modulus E' and $tan\,\delta$ only at one particular frequency. In data sheets the frequency used for making such plots is often 1 Hz.

From the plot in Figure 3.24 it also becomes clear why it is true to say that viscoelastic behavior is especially dominant during glass-transitions and during melting (the latter is not shown in this figure). In these regions the slope $dE(t)/dt$ in a double logarithmic plot is somewhere in the middle between zero and minus one. This means that the modulus is very time dependent which is the character of viscoelasticity. In the elastic regions this slope is nearly zero which means it is time independent. In the flow region the slope reaches minus one in double logarithmic plot which describes the *Newtonian* viscosity presented by equation 3.6. So the term η^T/t in this equation could be interpreted as a time dependent modulus $E(t)$. This means, with the knowledge of $E(t)$, the entire mechanical character of a polymer can be described for a certain temperature – as long as the deformations are within the linearity limit. [83]

3.3.1.6 Time and Temperature Dependence of Viscoelastic behavior

Figure 3.24 also shows that the modulus E is not only time dependent but also temperature dependent. However, empirically it has been found that an increase in temperature shifts the modulus curve $E(t)$ to shorter times (or higher frequencies). Hereby, the shape of the modulus curve changes only very slightly which for practical applications can be neglected. This makes the representation of the time and temperature dependent modulus $E(t, T)$ much simpler. It can be presented by two functions that depend only on one variable: a time dependent so called master curve $E_0(t)$ at a reference temperature T_0 and a temperature dependent shift function $a(T, T_0)$. [83]

Furthermore, this allows calculating the modulus outside of the experimental frequency window of the DMA. To do so, the DMA is carried out at different temperatures. The obtained curves can be shifted to lower or higher frequencies

outside the experimental window. Figure 3.24 illustrates this for the plot at T_{high} using the time-temperature shift function $a(T_{high}, T_0)$.

3.3.1.7 Thermal Expansion

When materials are exposed to temperature changes they often undergo dimensional changes. This can be described by the coefficient of linear thermal expansion (CTE) α, defined as the relative change of length L over the change of temperature T.

$$\alpha = \frac{1}{L}\frac{dL}{dT} \qquad \left[\frac{1}{K}\right] \qquad\qquad 3.11$$

The CTE is temperature dependent; however, it can often be linearly approximated within the different physical phases or around particular temperature points.

Most materials possess a positive CTE i.e. dimensions increase with temperature. This is due to the expansion of interatomic bonds with temperature. Polymer materials in their entropy-elastic phase, however, may reveal a negative CTE when they are loaded with a force. This can be explained graphically with Figure 3.22. If a stress σ_0 is applied to the material at low temperature (blue curve), this leads to an elongation ε_{T-Low}. As the temperature is increased (towards the red curve) and σ_0 is held constant, the material shrinks to ε_{T-High}.

Molecularly, this phenomenon can be explained with the probability distribution of conformations of the carbon chain. If the C-C bonds in a C-chain were entirely free to move, a large number of possible positions would lead to a compact molecule and only a few positions would lead to a fully extended chain. So in average such a molecule would have a compact form. However, the free movement of neighboring C-C bonds is limited by side groups (e.g. hydrogen). This leads to a potential energy of a C-C bond which depends on its angle to neighboring C-C bonds. In a simple molecule with only CH_2 chain links the potential energy is lowest when the C-C bond finds itself in plane with its neighbors. Further relative minima are at $\pm120°$ out of plane.

This means at a low temperature a C-chain would take up a more extended form than at high temperatures. At higher temperature the kinetic energy of the molecule is higher, and can therefore provide the higher energy required to overcome the energy thresholds to move the C-C bonds in the more compact conformations. The average dimensions of such molecules chains will be smaller. If such a molecule finds itself totally disordered between many other molecules, like a noodle in a plate of spaghetti, this desire to shrink at higher temperatures is limited by these other molecules and counteracted by their desire to shrink.

However, if many of these molecules are oriented the same way (e.g. due to stress) these shrinkage forces act jointly and cause the material to shrink at rising temperatures and extend again at lower temperatures. At temperatures well below the T_g this effect stops as the chains mobility dramatically drops. At temperatures above T_g (and even more so in the viscous phase) the mobility can be so high that pre-oriented molecules can permanently change their position by sliding past another. This part of the shrinkage cannot be recovered with cooling. [83], [84]

This is particularly interesting as this phenomenon applies equally to externally applied stress as well as to stress that exists internally in the material. Such stress can be found in drawn polymers and in super cooled amorphous or semi-crystalline polymers. The tensions in these materials can be understood as frozen tensions. Especially drawing (i.e. creating a permanent stretch, as with fibers) leads to an orientation of macromolecules which creates a thermo-entropic force opposed to the draw direction along the fiber. As the mobility of the chain is limited at temperatures well below the viscous phase this stress cannot relax (at least not entirely) in reasonable amount of time.

Beyond this, it is important to realize that materials with frozen tensions are not in thermo-mechanical equilibrium. This means, that their behavior depends on their thermo-mechanical prehistory. Heating often results in permanent release of parts of the frozen stress which leads to a permanent shrinkage. For the CTE measurement this means, the first heating cycle shows more contraction than following heating cycles at the same temperature lift. Increasing the maximum temperature in a follow-up heating cycle will often lead to additional permanent shrinkage. [90]

3.3.1.8 Chemical Effects on Polymer Mechanics

All the above presented theoretical considerations on elastic, viscous and viscoelastic properties, as well as on DMA analysis and thermal expansion, do not take into account chemical aging. Heat and time for instance may lead to post-polymerization or post-poly-condensation. Similarly heating and time may lead to degradation reactions, self-oxidization or cyclization[27]. Over time softening agents may diffuse out. All these factors may change dimensions, modulus, CTE, strength, etc. [91]

3.3.2 Manufacturing and Molecular Models of Fibers and Yarns

Fibers and yarns (natural or synthetic ones) differ substantially from bulk material in inner structure as well as in properties that result from this inner structure. In the bulk, material properties like modulus or elongation to break are usually more or

---

[27] cyclization: chemical reaction that leads to carbon ring-molecules like benzene

less isotropic. In fibers the longitudinal properties are largely different from transversal properties. This is a result of molecular orientation along the fiber. In natural fibers like cotton or wool this molecular orientation is a result of the biological growing process. In synthetic fibers, orientation is achieved by drawing, which is the last of the six main production steps: [19], [87]

- *synthesis* of reactive monomers
- *polymerizing* of thousands of monomers to long polymer chains; if monomers of one type are used the polymers are called homopolymers examples are polypropylene, polyvinyl chloride and polyacrylics; two or more monomer types lead to copolymers like polyester and polyamide; a polymerization of different types of homopolymers leads to block copolymers like polyurethane
- *liquefying* these polymers by dissolving or melting; this implies that only thermoplastics and thermoplastic elastomers can be used for making fibers
- *extrusion* through a spinning nozzle called spinneret; a single opening builds a monofilament while a number of openings creates a multifilament
- *solidification*: removing solvents in a bath or removing solvents by drying in warm air; or cooling the melted polymer in cold air; extrusion and solidification bring a first molecular orientation that depends on the spinning speed; at this point in the production chain, LOY (low oriented yarn) and POY (partially oriented yarn) are being distinguished
- *drawing*: stretching the fiber in length by factors of 3 to 5 will give the fiber its final properties; such yarn is called FDY (fully drawn yarn).

Drawing orients linear molecules longitudinally along the fiber axis as Figure 3.25 illustrates. This increases the strength in fiber direction since bonds along the polymer chains are valence bonds and these are strong bonds. On top of that, as molecules are oriented parallel to one another, the level of crystallization rises and further increases the strength. Transversally only weak van der Waals forces or medium strong hydrogen bonds are active. However, these transversal forces play an important role in preserving this structure generated by drawing. Without these forces the aligned molecules would return to a disordered arrangement. [92][28]

---

[28] chapter 1.3
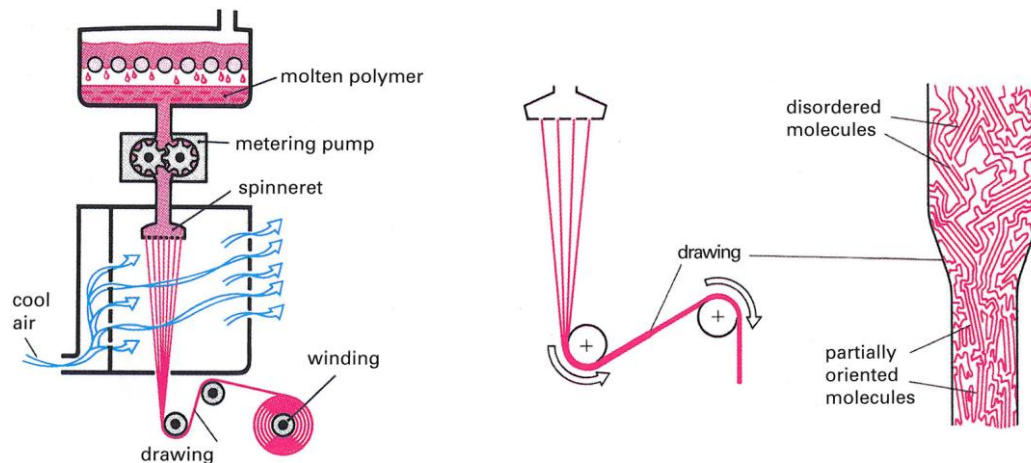
Figure 3.25: Polymer fiber manufacturing process: An important element is the drawing process which leads to a molecular orientation along the fiber axis. Source: [19][29]

All technically useful fibers are drawn [93]. Beyond this molecular orientation in the single fibers, also the twisting of fibers within a yarn increases the longitudinal strength of the yarn. This explains why fibers are twisted to yarn. Therefore, examples of treatments on the way to the final yarn are: [92][30]

- *twisting* the fibers to fiber strands to increase the transversal compression, and thus to increase the friction between adjacent fibers; this again increases longitudinal strength
- *twisting* the fiber strands to 2-ply or to multi-ply yarns to further increase transversal binding and longitudinal strength

3.3.3 Free Shrinkage in Drawn Yarns and *Shieldex*

The alignment of molecules by drawing, significantly influences the mechanical and thermo-mechanical behavior of yarns. Most importantly for this thesis, it leads to the inherent character of all fibers to shrink or to generate a shrinking force with rising temperatures [94]. While chapter 3.3.1.7 discussed negative temperature coefficients on the basis of theoretical polymer mechanics, this and the following subchapter are devoted to analyzing some typical fibers and *Shieldex* in particular.

Figure 3.26 demonstrates this for acrylic fibers as a representative of textile fibers, and for PBO fibers as a representative of high-tech technical fibers. The absolute length changes are generally less with high-tech fibers but still with a negative temperature coefficient.

---

[29] with kind permission of the publisher
[30] chapter 1.3
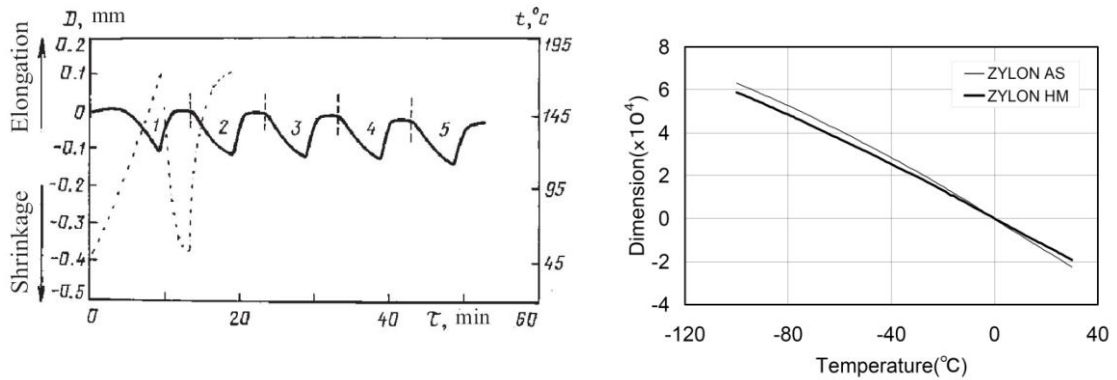
Figure 3.26: Left plot: free reversible shrinkage in PAN-I fiber as a result of thermoelastic effect [95]. The full line is the fiber length change and the dotted line is the first temperature cycle. Heating results in shrinkage, cooling in elongation. The sample length being 15 mm, the diagram reveals a CTE of approximately -50 ppm/K. Right plot: free reversible shrinkage in high-tech PBO fibers with a CTE of approximately -6 ppm/K [96].

Forward and Palmer have done substantial analyses on free length changes in Nylon 66 and found differences in reversible and irreversible shrinkage on heating as shown in Figure 3.27. When a yarn is heated for the first time above a certain temperature T_1 to a higher temperature T_2 it experiences an irreversible shrinkage that will remain when cooled back to T_1. After that any temperature cycle below T_2 will result mainly in reversible length changes – with a negative temperature coefficient of course. The yarn is then considered to be set with respect to temperature T_2. If the yarn is heated above T_2 new irreversible shrinkage occurs.
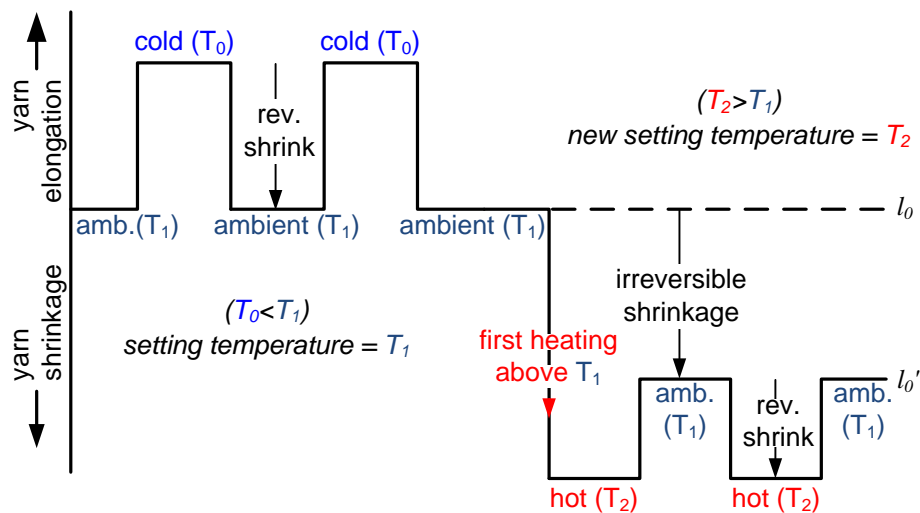
Figure 3.27: Reversible and irreversible free length changes with temperature in drawn Nylon 66 yarn. Modified from [97].

Figure 3.28 presents their free shrinkage measurements of technically relevant *drawn* Nylon 66 monofilaments. Furthermore, Forward and Palmer found that the

behavior of undrawn Nylon is inverse but less pronounced with a maximum of 4% irreversible extension during heating.
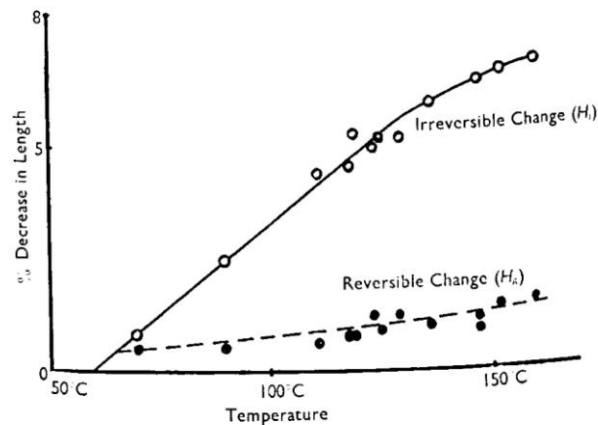
Figure 3.28: Irreversible and reversible free shrinkage in *drawn* Nylon 66 monofilament of 16.7 dtex after heating the yarn for the first time above 25 °C and cooling back to 25 °C. For each measurement a new sample was used. [97]

Forward and Palmer explain the irreversible shrinkage in the following manner. With rising temperature entropy rises and secondary bonds between chains weaken. The weakest chain links break and allow a reformation of chain segments. Some of the broken bonds build new bonds which gives a new set structure. [97]

Beyond this, Dismore and Statton observed that molecular orientation changes only marginally. They conclude that this reformation of chain segments is predominantly a folding mechanism. Aside from explaining irreversible shrinkage this also explains how entropy can rise and yet orientation changes only little.

While this folding appears in the amorphous phase, it leads partly also to an enlargement of crystals and to a formation of new crystals. This way, especially at very high temperatures (above 160 °C) crystal perfection and crystal density rise. The right plot in Figure 3.29 shows such high temperature shrinkage in Nylon. [98]

Similarly, in other fibers irreversible shrinkage occurs although the explanation may differ. Kalashnik et al. for instance found for acrylic fibers that, above 150 °C, cyclization[31] leads to permanent shrinkage as shown in Figure 3.29 in the left plot [95]. Fouda et al. believe that in Nylon 6 (not 66) shrinkage due to annealing originates from molecular disorientation [99].

---

[31] forming of rings in a chemical substance
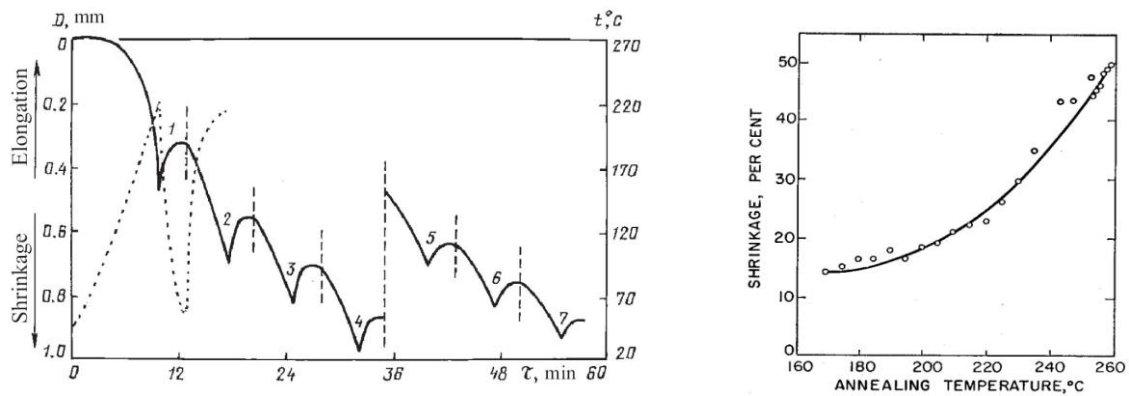
Figure 3.29: Left plot: irreversible free shrinkage in PAN-I at high temperatures as a result of cyclization [95]. The full line is the fiber length change and the dotted line is the first temperature cycle. Right plot: irreversible free shrinkage due to chain folding during one minute annealing at high temperatures of Nylon 66 [98].

Also *Shieldex* has a negative temperature coefficient, and shrinks irreversibly when first heated to a particular temperature as the measurement in Figure 3.30 proves. This free shrinkage analysis was made on a 10 mm sample with a thermo-mechanical analyzer TMA/SDTA841e. Like in other experiments cited above, the yarn sample was left to relax for 48 h at 20 °C in dry atmosphere prior to the measurement. The pre-tension that is required to carry out the length measurement was set to 0.005 N. This is – normalized on the yarn count – similar to the pre-tension used by [97] who have shown that such a little force does not affect the free length change.

The applied temperature profile is identical to the temperature cycling profile used for the other experiments in this thesis except that only four cycles were run rather than 25 (ref. to Figure 5.9).

The yarn behaves almost as predicted by Forward and Palmer. It extends when cooled below room temperature and shrinks partly irreversibly during the first heating. However, its length changes in the second and third cycle are not perfectly reversible. There is a slight extension in the third cycle compared to the second cycle. Yet, the fourth cycle is very similar to the third and allows assuming that from that cycle on changes are indeed reversible. Unfortunately, this experiment could not be run for more cycles as it requires liquid nitrogen for controlled cooling which is limited by the size of the nitrogen containment.
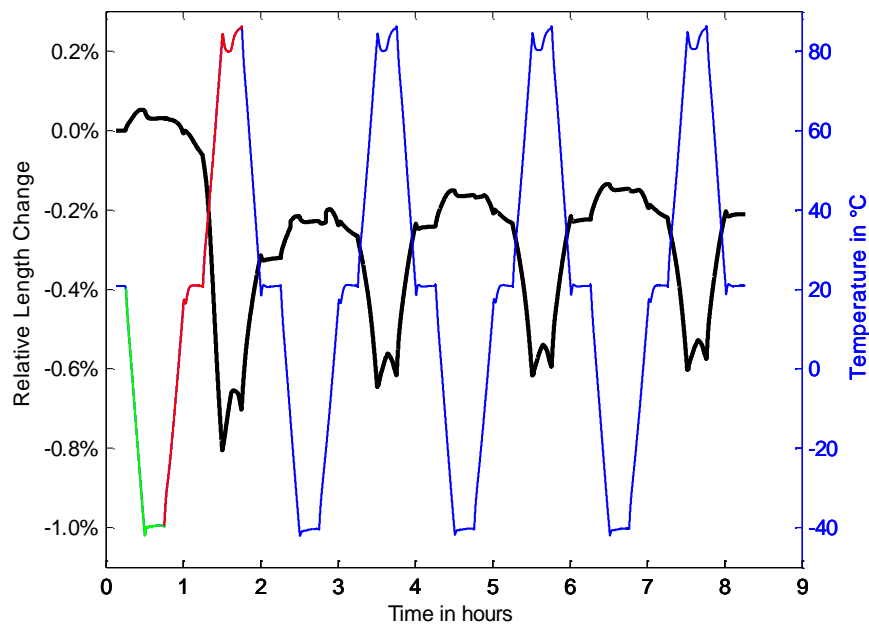
Figure 3.30: Free length change of *Shieldex 117/17 twine*. The black curve is the relative length change in percent. The other curve is the temperature profile. The green colored part of this curve is the first cooling phase and the red colored part of this curve is the first heating phase. This temperature profile (see Figure 5.9) was also used for all other experiments in this thesis but with 25 cycles. [77]

Calculating the CTE in the temperature ranges shown in Table 3.1 demonstrates that the yarn goes through a transition from entropy elasticity at high temperatures to energy elasticity at low temperatures. This is not surprising and in line with Engelter and Müller who observed that at room temperature undrawn (unoriented) polyamide behaves mainly energy elastic while drawn (oriented) polyamide behaves mainly entropy elastic [100]. (Note: According to [101] Nylon 6.6 bulk material i.e. unoriented has a positive CTE of $81 \cdot 10^{-6}$/K.)

Table 3.1:   CTE of *Shieldex* calculated from Figure 3.30

Temperature Range	CTE [10^{-6}/K]
+20 °C; +85 °C	-58
-10 °C; +20 °C	-23
-40 °C; -10 °C	-3

3.3.4 Shrinkage Force in Drawn Yarn and *Shieldex*

The previous subchapters have considered *free* length changes of yarn. Free in this context means the yarn is not constrained in any way. The results give the impression that after a few temperature changes yarn must always be shorter than

before – due to irreversible shrinkage. Yet, it is very instructive for this thesis to also investigate what happens when the yarn is constrained. For this purpose the shrinkage forces are regarded that yarns generate when fixed at both ends and exposed to temperature changes. Only little work has been done on shrinkage forces of Nylon or other fibers that would be of general use for this thesis. Most analyses, like [102], [103], [104], [105], are only concerned with shrinkage forces upon heating but do not consider what happens when cooling back to ambient or even to temperatures below 0° C. Only Mukhopadhyay and Hearle did look at force changes when cooling back to ambient temperature [106]. However, their analysis is too short in time to be relevant for this thesis – furthermore, it does not investigate subzero temperatures.

Therefore, a test was carried out with *Shieldex* yarn during four temperature cycles with the profile presented in 5.3.1. This is the same temperature cycle as for all experiments in this thesis (ref. to Figure 5.9). The yarn was strained by a pre-tension of 0.2 N within two seconds. Then the yarn was fixed at both ends for the rest of the experiment, and its tension was measured during temperature cycling. In principle this is a stress-relaxation experiment with temperature cycling. The result is plotted in Figure 3.31 over time and in Figure 3.32 over temperature. Also here, the yarn was kept at 20 °C in dry atmosphere lying slack for at least 48 h prior to the measurement.

As anticipated with the results of the free length change, the shrinkage force rises and falls with temperature. Yet, on cooling the yarn tension drops to zero. In the first cycle the force becomes zero only below -20 °C. While in the subsequent cooling phases it reaches zero already at +40 °C. At 85 °C the tension is always 0.5 N and therefore higher than the pre-tension. After the first cycle the tension changes are repeatable with temperature cycles.

The experiment was repeated with fresh pieces of yarn with pre-tensions of 0.5 N and 1.1 N. Yet, only one cooling cycle was done. In the sample pre-tensioned with 0.5 N the tension had dropped to zero at -25 °C. While in the 1.1 N-sample the tension had dropped to 0.3 N at -40°C. Upon return to room temperature the initial 1.1 N had dropped to 0.6 N, suggesting that also this sample would drop to zero tension if more cycles were carried out.

Maybe at higher pre-tensions the tension in the yarn does not drop to zero. Though, perhaps it just takes more cycles for it to drop to zero. Still, higher pre-tensions have not been investigated. Chapter 4 will explain why this is not necessary for this work.
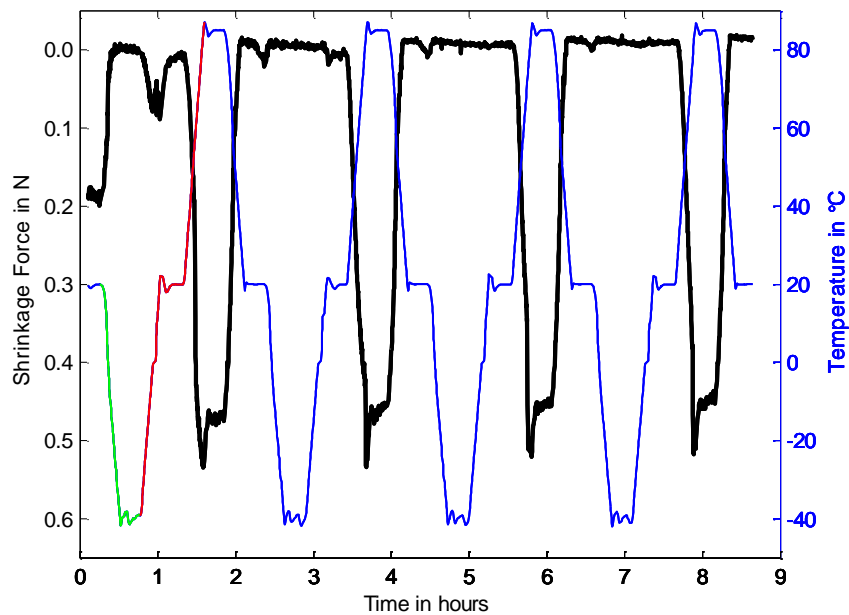
Figure 3.31: Shrinkage force of *Shieldex* yarn during temperature cycles. At the start of the experiment a pre-tension of *0.2 N* was applied. The black curve is the tension in Newton. The other curve is the temperature profile. The green colored part of this curve is the first cooling phase and the red colored part of this curve is the first heating phase. This temperature profile (see Figure 5.9) was also used for all other experiments in this thesis but with 25 cycles. The measurement was effected with a *GABO Eplexor 100N* dynamical mechanical analyzer in stress-relaxation mode.
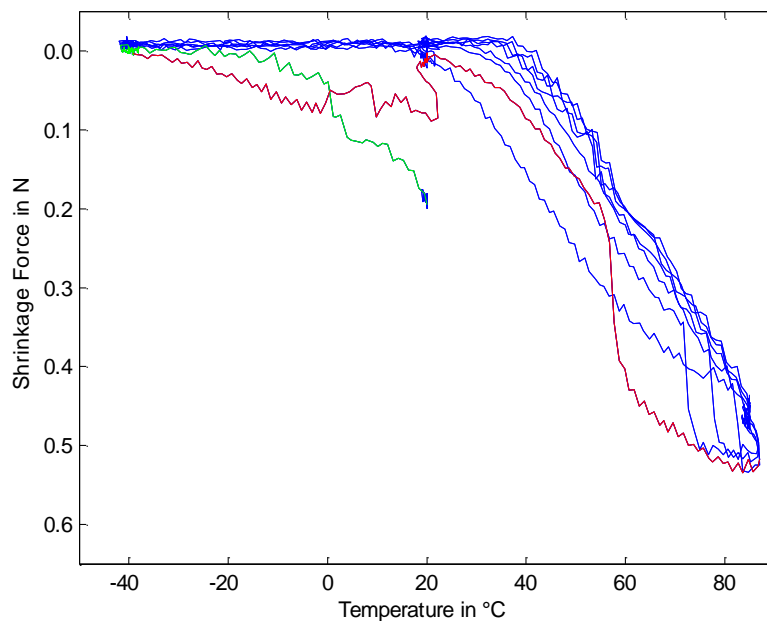
Figure 3.32: Shrinkage force of *Shieldex* yarn as measured in Figure 3.31 (where it was plotted in black) but plotted versus temperature. The green colored part of this curve is the tension during the first cooling phase and the red colored part is the tension during the first heating phase.

3.3.5 Effect of Yarn Sagging during Temperature Cycling in Shieldex

Beyond this drop of shrinkage force to zero, a remarkable yarn sagging was observed during temperature cycling. For this experiment the yarn was pre-tensioned with 0.2 N and then fixed at both ends like in the previous experiment. Then the same temperature cycles (see Figure 5.9) were applied – yet instead of four cycles, 1000 cycles were applied. In the first cycles the yarn was not sagging. Yet, after about 60 cycles a yarn sagging was observed at temperatures below around 30 °C. It can be assumed that this is a continuous process that starts already after the first temperature cycle but at the beginning it is too feeble to be noticeable. This effect was only observed visually and not further quantified. Note: at the high temperatures the yarn seemed taut even after 1000 cycles.

Despite there was no notion of this effect in literature, I learned in a discussion with fiber and textile experts from TITV Greiz and Sefar, that this is also observed with other yarns. During setting at elevated temperatures, yarns or fabrics are sometimes fixed in a frame. Upon return to room temperature the yarn or fabric sags in this fixation frame. [107] The cause of this effect can only be speculated. At the high temperature, the high tension may break bonds allowing the yarn to extend permanently. Yet, this implies that after many cycles the tension at the high temperature should be lowered – at least slightly.

The fact that yarn sagging was witnessed in other yarns too, means that the drop of the shrinkage force to zero observed above is not specific to *Shieldex*. Yet, it is not clear whether this is the case in all yarns. Technical fibers like PBO or aramide fibers may not sag or entirely lose tension during temperature cycling.

3.3.6 Modulus of Nylon Yarn

Chapter 3.3.1.5 explained the value of a master curve and its time-temperature shift function. With such the response of material on stress or strain applied to it can be calculated. Although theoretically feasible, in practice it becomes very difficult when trying to apply this to yarns during temperature cycles. Due to the frozen tensions, the yarns change in length or generate tensions during temperature changes. Parallel the modulus changes according to the master curve.

For this reason the previous three subchapters investigated the actual response of the yarn based on literature and own measurements. After all, the focus of this work is not on the yarn itself but on the embroidered contact. Though, for completeness, this subchapter quickly considers the modulus of Nylon being the core material of *Shieldex*.

Murayama et al. have developed a master curve and shift function for Nylon 66 yarn. Figure 3.33 shows the modulus plot over time at different temperatures. It

reveals that at elevated temperatures (e.g. 85°C) the modulus drops quickly with time. Yoshitomi et al. found the same for Nylon 6 yarn. With their master curve shifted to 85 °C one finds that a tension applied to the yarn drops to 10 % within 2.8 h. [108], [109]
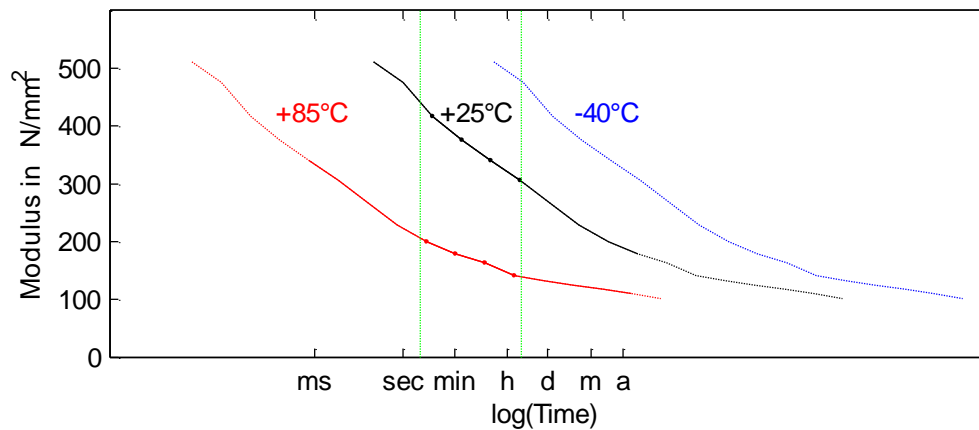
Figure 3.33: Modulus of polyamide 6.6 at 25 °C as analyzed by [108] (color: black). They also provided a time-temperature shift function for temperatures from 25 °C to 145 °C. This function was applied here to plot the modulus curve at +85 °C. To plot the modulus also at -40 °C, the shift function provided in their publication was extrapolated. The green dotted lines denote the limits of the experimental window.

3.3.7 Generalization

It was found that all technically useful polymer yarns consist of drawn fibers. The consequences of this drawing are that they all have negative temperature coefficients and generate a shrinkage force upon heating. Upon cooling this force drops.

At least in some yarns and at least with limited pre-tensions this force drops to zero; even yarn sagging is observed. Exceptions could be technical fibers. Yet until now, there are no such yarns available that would be conductively coated and are embroiderable at the same time.

Steel filaments, copper wires and potentially other non-polymer based yarns despite being drawn do not have a negative temperature coefficient. Yet, as is known from the previous chapter, these are not applicable for embroidery anyway. Therefore, they are not relevant for this research.

4 Theoretical Analysis of the Contact Mechanism in Embroidered Contacts

The previous two chapters introduced embroidered contacts and investigated which types of yarn can be used for making such contacts. Furthermore, the yarn was analyzed mechanically and electrically in depth. In this chapter the contact mechanism shall be investigated.

For this purpose a simplified model of the embroidered contact is developed and analyzed in theory. This is followed by a theoretical analysis of the more complex embroidered contact. The developed theory is then applied to anticipate the thermal cycling behavior of both contacts – the simplified one and the real one.

Based on these considerations, chapter 5 will develop experimental setups of the simplified model and the real embroidered contact, and expose these to the exemplary thermal cycling stress proposed in 2.3.3 to verify the theory.

4.1 Simplification

The assembly of an embroidered contact is rather complex as Figure 4.1 shows using the example of a *machine* embroidered contact. Therefore, the contact shall be simplified to model its characteristic behavior.
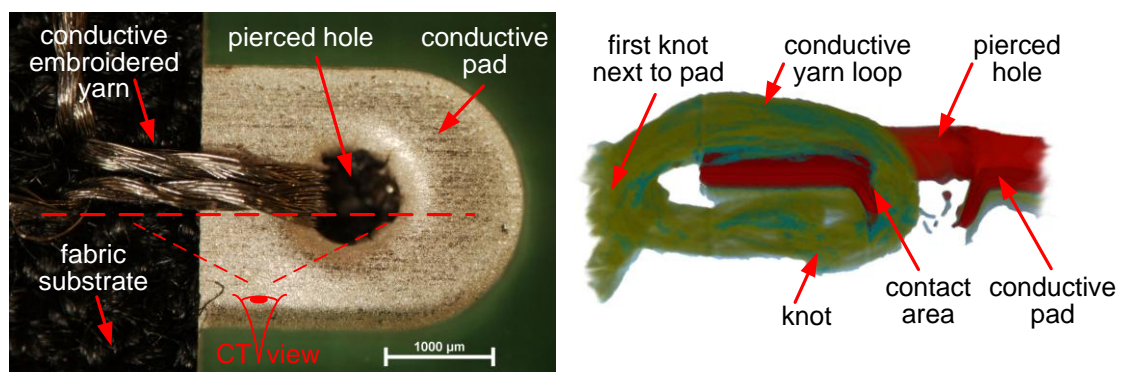
Figure 4.1: Embroidered contact assembly: a conductive pad made from metallized polymer substrate is being pierced by an embroidery needle; the latter lays a conductive yarn over the pad creating an electrical contact between the yarn and the pad (left picture); computed tomography (CT) image of an embroidered contact (right); the tomography is taken perpendicular to the hole axis (hole axis is in the paper plane).

Essentially, the contact consists of a yarn loop around comparably rigid material. In Maggie Orth's knot or in Leah Buechley's hand embroidered contact, one yarn is

tied around a rigid electronic substrate (ref. to Figure 2.4 and Figure 2.6). In machine embroidered contacts the embroidery process forms a loop consisting of needle thread and bobbin thread (both being conductive). These are held by interlacing knots at the bottom side of the fabric substrate. Both threads lay double on top and bottom side as the embroidery seam goes over the pad, then through the pad and back over the pad. This yarn loop encloses a sandwich of a metallized thin polymer substrate glued to a fabric substrate. The computed tomography image in Figure 4.1 shows the cross section of such a contact. In that particular example the substrate was pierced by the needle during the embroidery process. Alternatively, the substrate may be predrilled which will be discussed in 4.2.1.

Hence, simplifying the assembly to a yarn loop around a rigid cylinder, models all three implementations – Maggie Orth's knot, Leah Buechley's hand embroidered contact and the machine embroidered contact. Figure 4.2 illustrates this simplified model (right) and, for better intelligibility, compares it to the machine embroidered contact (left).

In all three implementations the yarn loop may actually consist of a single loop or of multiple loops if sewn multiple times. The effect of this will be discussed in 4.2.2.
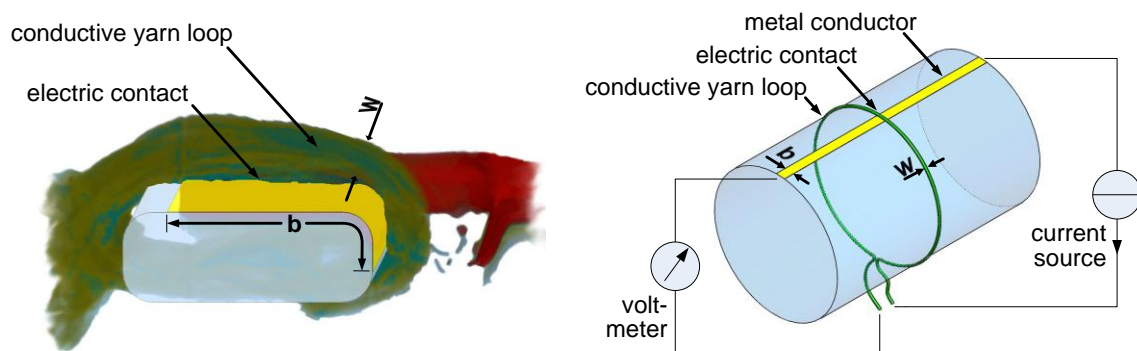
Figure 4.2:   Left: the embroidered contact consists of a yarn loop around rigid material. The shape of this material can be approximated with a cuboid (light blue) with rounded edges. The yarn loop has the width *w*. The conductive pad (yellow) is on the surface of the cuboid and therefore touches the loop. This pad has a width of *b = 2 mm*. Right: the simplified model of the embroidered contact consists of a conductive yarn loop (green) of width *w* that is tied around a rigid cylinder (light blue). The conductive pad is modeled by a metal conductor (yellow) on the surface of the cylinder. Chapter 5 will develop an experimental setup of this simplified model. The radius of the cylinder will be 15 mm and therefore will be much larger than the embroidered contact. The width *b* of the metal conductor will be 2 mm like in the embroidered contact. The yarn loop can be tied (or fixed at the ends) in such a way that the ends do not touch. This will allow a precise measurement of the contact resistance by the four-point probe method also shown in the figure.

The parts, which are enclosed by the different yarn loops, have complex shapes. However, most of these parts have a positive coefficient of thermal expansion (CTE) and – compared to the yarn loop – a high stiffness. Therefore, during heating they

expand and widen the yarn loop around them. Yet, in the case of sandwiched parts[32], bending may occur during temperature alterations. This is difficult to simulate as it is specific to each implementation. Therefore, to not limit the generality of the simplified model, the cylinder shall be assumed to be *stiff* compared to the yarn and to not change with temperature, thus having a *CTE of zero*. This means, *thermo-mechanically* only the forces of the yarn loop are considered in the simplified model.

In Figure 4.2, the part enclosed by the embroidered loop, is approximated as a 2 mm x 0.6 mm cuboid with rounded edges. Maggie Orth's or Leah Buechley's implementation is similar, yet with less rounded edges. Still other shapes and sizes of implementation are thinkable. To keep the model simple and general, the part enclosed by the yarn loop shall be represented by a circular cylinder.

Chapter 5 develops an experimental setup of this simplified model. At this point, it shall already be mentioned that handling problems did not allow making this physical model as small as an embroidered contact. Therefore, the model was built with a glass tube of 15 mm radius. The effect of this enlargement will be discussed in theory in the following subchapters.

The tensioning of the yarn loop around the cylinder should be chosen similar to the one in the embroidered contact. The latter one is mainly defined by the bobbin thread's tension and can be assumed to be smaller than that. In practice, good embroidery results are achieved with bobbin thread tensions generated by 24 to 28 grams [20]. Therefore, the yarn tension around the conductive pad shall be estimated to $F_{yarn}(init) = 0.2\ N$. This is of course an initial tension. As time passes and temperature changes the tension in the yarn changes as well. In fact during the -40 / +20 / +85 °C temperature cycle, the tension is following the curve as shown in the shrinkage force experiment (refer to Figure 3.32). This applies equally to the embroidered contact and to the simplified model. Higher bobbin thread tensions lead to fiber fraying, fiber breakage or even yarn breakage. This explains why it is not necessary to further investigate initial tensions higher than 0.5 N in chapter 3.3.4. Higher tensions cannot be generated with embroidery machines.

The actual electric contact is where the embroidery yarn and the conductive pad touch. This area *A* is defined by the product of the yarn width *w* and width *b* of the conductive pad enclosed by the loop. The yarn width *w* depends of course on the yarn thickness itself and on the number of times the yarn lays on the contact pad. In case of the machine embroidered contact this is at least two times and in the other two implementations at least one time. The width *b* of the conductive pad is about

---

[32] electronic substrates generally have positive CTEs while fabrics have negative CTEs since they are made of fibers; sandwiching these leads to a bending during temperature changes; yet, in the temperature range considered in this thesis bending may be considered negligible

2 mm in the machine embroidered implementation and similar in the other two implementations.

In the simplification the contact pad enclosed by the loop is modeled by a thin metal conductor on the cylinder as shown in Figure 4.2 (right). In the experimental setup described later the width b of this metal stripe is also 2 mm as in the embroidered contact. To keep it simple in theory and experimentally, a single yarn loop shall be considered for the model.

Apart from the mechanical simplification, the model is designed in such a way that it also simplifies the assessment of the electrically relevant quantity, which is the contact resistance. This can be achieved by introducing a non-conductive gap in the mechanically closed loop (in Figure 4.2 shown below the cylinder). In the experimental setup this is effected by fixing the ends of the loop on the cylinder with a drop of glue rather than knotting the ends. This way a four-wire sensing can be carried out as shown in the figure. It measures only the contact resistance and its changes. It excludes resistances and resistance changes of those parts of the yarn loop that are not in contact with the metal stripe. Including these would only blur the data. In the embroidered contact this cannot be avoided entirely. This will be discussed in chapter 4.2.

4.1.1 Electrical Contact Resistance

Before discussing the electric contact in the simplified model the source of contact resistances shall be discussed in short. According to VDE 0660/12.52 an electrical contact is the condition that arises from a current-leading touch between two components. These two components are called contact members. [110]

In a physical sense, solid surfaces of contact members are never absolutely even. At a small scale they are always bumpy. Furthermore, physical surfaces are never absolutely clean. This means the contact members only touch in certain points where they feature micro peaks. This distinguishes three contact areas: the macroscopic apparent contact area A_a, the (mechanical) load-bearing contact area A_b and the true contact area A_t. The load-bearing contact area includes contaminated and clean areas while the true contact area includes only the clean areas. Figure 4.3 (left) illustrates this.
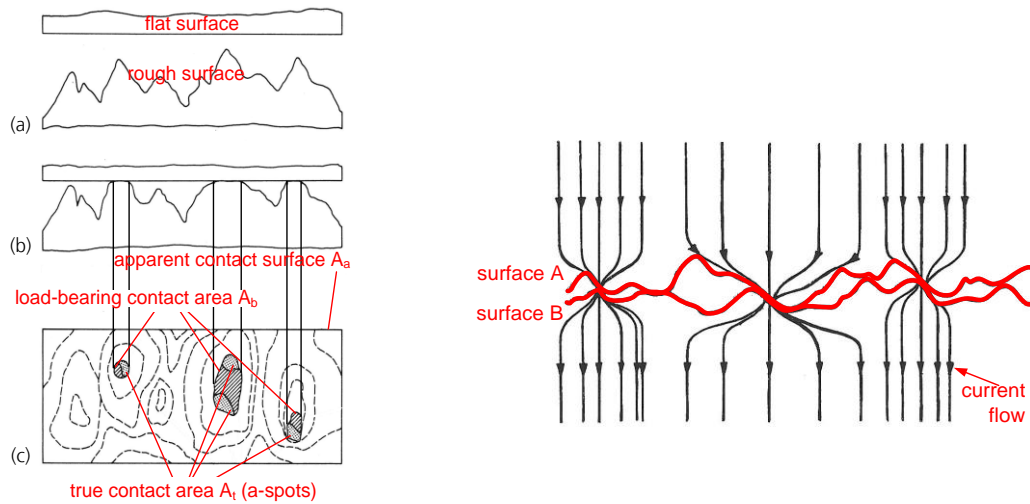
Figure 4.3: Constriction resistance. Modified from [110] and [111].

The individual touching points of the true contact area are often called a-spots. Around these a-spots the current is constricted. This is demonstrated in Figure 4.3 (right). The resistance that is caused by this constriction is called constriction resistance R_C. Surface contamination and tarnish may further increase the resistance. This additional resistance is denoted R_T for tarnish resistance. The sum of these two is the contact resistance:

$$R_{Contact} = R_C + R_T \qquad\qquad 4.1$$

In tarnishing materials, like copper, contact degradation primarily comes from an increase of tarnish resistance (e.g. propagation of tarnish between conductors). In this work the contact materials of the contact pad are gold or silver and the metallization of the yarn is silver. Gold does not tarnish at all. Silver may oxidize to Ag_2O at room temperature. As silver oxide is conductive this does not change the contact resistance. However, silver may also sulfidize to Ag_2S which is an insulator. Both processes are slow and therefore, it is assumed that the influence of R_T is small in this work. Therefore, to simplify the following discussion, it shall be assumed that $R_{Contact}=R_C$. [112]

The constriction resistance R_C depends on the size of the true contact area A_t i.e. on the size and number of a-spots in the contact. These depend of course on the contact materials and their surface finish but also significantly on the mechanical contact load. [113]

Ragnar Holm [112] calculated the constriction resistance of a *single* circular a-spot of diameter d to:

$$R_C = \frac{\rho_1 + \rho_2}{2d} \qquad\qquad 4.2$$

Thereby, ρ_1 and ρ_2 are the specific resistances of the contact members. Typically the contact appears in a number j of a-spots. So, the constriction resistance of such a contact becomes:

$$R_C = \frac{\rho_1 + \rho_2}{2 \sum_j d_j} \qquad\qquad 4.3$$

Note: summing below the fraction line is permitted as can be seen if the formula is developed with the conductance. In this case the various a-spots are providing enhanced conductance as more a-spots are available in a parallel configuration and as larger are their diameters d_j. The formula assumes that the a-spots are distributed in such a way that the current constrictions do not influence each other. In other words, it assumes that the size of the a-spots is small compared to the distance between the a-spots. When this is not the case there are different ways to compensate for this in the calculation but these shall not be considered in this introduction to contact resistance. [110]

The size, number and configuration of a-spots are statistically distributed. Therefore, $R_{Contact}$, which depends on these, is also a statistical quantity. It can only provide a probability distribution of the actual contact resistances measured in many electrical contacts of the same type. [110]

The size and number of a-spots increase with the contact's normal[33] load F_N. This leads to following relationship between R_C and F_N.

$$R_C \sim \left(\frac{1}{F_N}\right)^n \qquad\qquad 4.4$$

Different sources have come up with different values for n ranging from *0.33* to *1*:

- [114] distinguishes between $n = 0.5$ for plastic deformations and $n = 0.33$ for elastic deformations.
- [112] suggests a rule of thumb with $n = 0.33$.
- [110], which is the most recent publication, claims that most contacts are described best with n between *0.9* and *1* and that a value below *0.9* is an indicator for surface contaminations.

---

[33] in this case 'normal' shall mean perpendicular to the contact interface

Common to all is the hyperbolic character of the relation of R_C vs. F_N as shown in Figure 4.4.
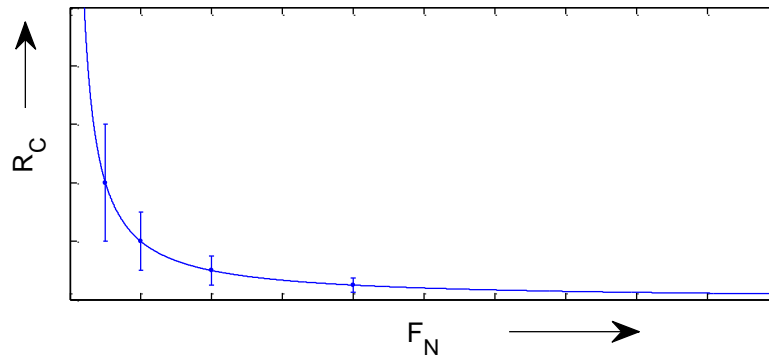
Figure 4.4:   Constriction resistance R_C vs. contact force F_N. A similar graph would be achieved if the constriction resistance R_C vs. the number of a-spots or vs. the diameters d_j would be plotted. Please note, that number and size of a-spots increases with the force F_N.

A consequence of this relation is: at small a-spots and/or at low number of a-spots and/or at low contact loads the *variance* of contact resistances is large. That means, small changes of the load F_N, lead to big changes in the R_C-results. This is also illustrated in Figure 4.4. [110], [115]

A second consequence of this relation is that contact resistance measurements are not useful indicators for changes of contacts at an early stage of contact degradation (the right part of the plotted curve). Rate changes of the contact resistance at this stage are very small. Yet, contact resistance measurements are very useful for detecting changes in the final phase of the degradation and as final failure marker identifying moments of contact disruption (the left part of the plotted curve). In practice this is more interesting anyway, as it reflects the applications' demand that the contact be good. [113]

Another important notion that leads to this relationship 4.4 is pointed out by Roland Timsit [111]: the size of the (mechanical) load-bearing contact area A_b solely depends on the normal force applied to the contact and the hardness of the contact members and is independent of the apparent contact area A_a. Yet, I believe this is true only as long as the load-bearing area A_b is small compared to the apparent area A_a. For metal-to-metal contacts (which are the only type of contacts all literature refers to) this is in practice probably always the case. Therefore, the constriction resistance for these contacts is independent of the apparent contact area A_a.

Accessing the contact resistance experimentally requires the so-called four-point probe method (also: Kelvin sensing) that excludes resistances of the contact members (at least mostly). This is important because a contact resistance is always

in series with both of its contact members – i.e. what is behind each side of the contact. As long as disruption does not occur the resistances of these contact members are often higher than the contact resistance itself. Figure 4.2 illustrates the four-point probe measurement method applied to the simplified model.

4.1.2 Constriction Resistance in Contacts with Conductive Yarn

The constriction resistance inside conductive yarn is essentially more complex than in solid metals. Considering the contact shown in Figure 4.2, it must be remembered that the yarn is not a solid rod but consists of many conductively coated fibers as shown for example in Figure 3.3.

In a contact between conductive yarn and a metal conductor, in the following called yarn-to-metal contact, only a few fibers will actually touch the metal conductor and thereby permit a current flow. More precisely only some points of a few fibers will actually touch the metal conductor. From these a-spots the current will spread over these 'a-fibers'. The 'a-fibers' touch other fibers inside the yarn which again touch other fibers at different a-spots and so on. This current spreading leads to a constriction resistance that should depend on a number of factors:

- fiber resistivity: high fiber resistance leads to high constriction resistance
- density of a-spots amongst fibers and between fibers and metal conductor: higher density leads to lower constriction resistance
- size of a-spots amongst fibers and between fibers and metal conductor: larger a-spots lead to lower constriction resistance
- the distribution of a-spots within the yarn: the more changes a fiber will see with respect to its neighborhood fibers the lower the constriction resistance

The density and size of a-spots between fibers increases with transversal binding between fibers which is influenced by:

- the twist of the fibers and the twist of the fiber strands: the more they are twisted the higher the transversal compression; a higher twist also increases the mixing of fibers which acts positively on the distribution of a-spots in the yarn
- longitudinal tension: more tension brings fibers closer together and increases the transversal compression

The number, density and size of a-spots between a fiber and the metal conductor depend on:

- the contact pressure: higher pressure leads to more, larger and denser a-spots

Until today, these effects have not been quantified or put into an analytical relationship. Yet, it is important to realize, that the result of such a quantification theory would look somewhat similar to the plot in Figure 4.4. This means, the factors that can change the contact resistance most notably are the number and the size of a-spots between the metal conductor and the fibers of the yarn. In fact these are the only factors that can lead to the most dramatic change of all – a contact disruption.

Like in metal-to-metal contacts, these two factors are linked to the contact pressure. Consequently, keeping this pressure up is equally essential for metal-to-metal contacts and for yarn-to-metal contacts.

Yet, unlike in metal-to-metal contacts, the conductive yarn can conform to a convex surface of the other contact member – a metal surface. Therefore, a yarn-to-metal contact is formed by a lengthwise touch between conductive yarn and a metal surface as illustrated in Figure 4.5 on the left.
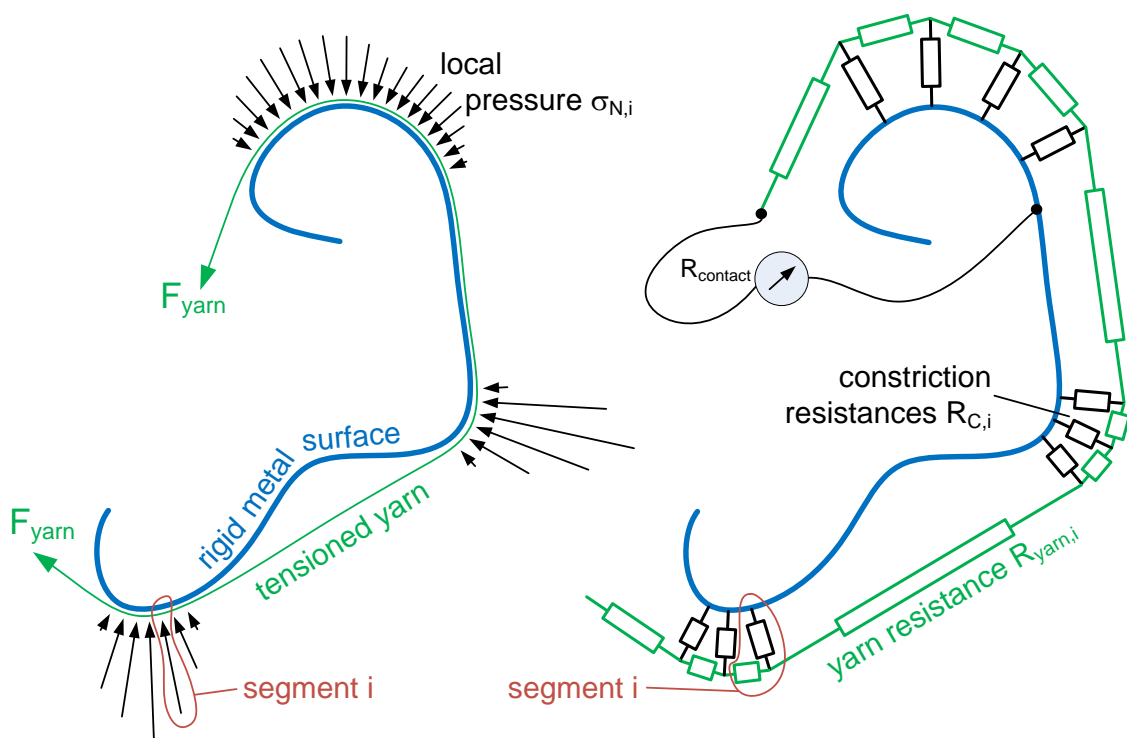
Figure 4.5: Left: local pressures $\sigma_{N,i}$ generated by a yarn (green) tensioned over an arbitrary rigid surface (blue). Right: the contact resistance in yarn-to-metal contacts is actually the result of a network of constriction resistances and yarn resistances. The sketch shows the effect with discrete components.

This has two consequences for the contact resistance. Firstly, the yarn's resistance may become a significant component of the contact resistance as illustrated in Figure 4.5 on the right. In this case, the contact resistance is the result of a complex network of yarn resistances $R_{yarn,i}$ and constriction resistances $R_{C,i}$. This makes

calculations very difficult. As will be shown later, the yarn resistances cannot be neglected in flat or concave sections of the metal surface. As the contact in the simplified model features only a convex surface, it can be assumed that the yarn resistances $R_{yarn,i}$ do not have a significant effect and can be neglected. Yet, in the embroidered contact the yarn's resistance cannot be ignored as the top side of the contact pad is flat.

Secondly, rather than experiencing a single normal force F_N, the contact consists of many parallel constrictions $R_{C,i}$ that each depend on a local force $F_{N,i}$:

$$R_{C_i} \sim \left(\frac{1}{F_{N_i}}\right)^n \qquad\qquad 4.5$$

For a fixed configuration of an apparent contact area, it can be rewritten in a more practical form for yarn-to-metal contacts:

$$R_{C_i} = k_i \left(\frac{1}{\sigma_{N_i}}\right)^n \qquad\qquad 4.6$$

In this relation $\sigma_{N,i}$ is the local pressure the yarn exerts onto the metal conductor at segment i. The factor k_i is a specific constant of segment i. It is dependent for instance on the specific length of the segment. The value of the exponent n may differ from the ones found for metal-to-metal contacts but it is positive making the relationship hyperbolic, too.

If the yarn resistances $R_{yarn,i}$ can be neglected the contact's conductance $G_{contact}$ can be expressed as a sum of all constriction conductances:

$$\frac{1}{R_{contact}} = G_{contact} = \sum \frac{1}{R_{C_i}} = \sum \frac{1}{k_i} \cdot \left(\sigma_{N_i}\right)^n \qquad\qquad 4.7$$

Apparently, the local pressures $\sigma_{N,i}$ are very important for the contact resistance. Therefore, the following subchapters will derive these pressures $\sigma_{N,i}$ generated by the yarn being tensioned over a generic surface.

4.1.3 Contact Pressure σ_N from Yarn Tensioned over a Surface

Let $c(s)$ be a vector function describing an arbitrary convex curve of a surface over which a yarn is tensioned with the force $|F_{yarn}|$[34]. And let s describe the arc length

---

[34] the tension of the yarn can be considered constant over the entire surface curve if the reasonable assumption is made that there are no frictional forces between the yarn and the surface

of that curve. Then the following graph identifies the vector forces of the yarn at the ends of a small element of length Δs of that curve.
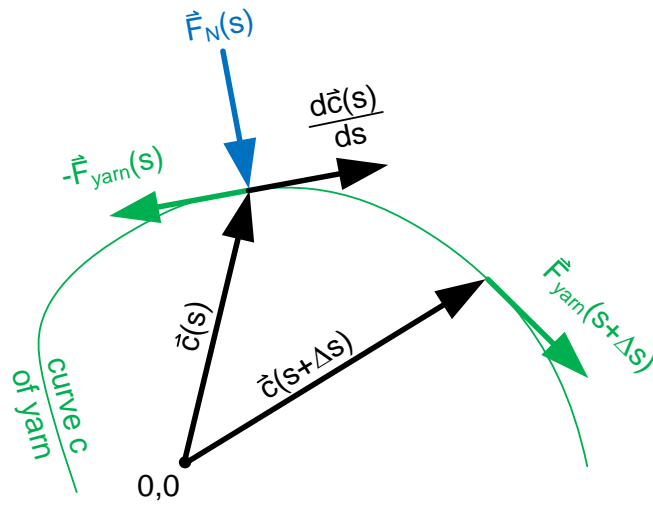
Figure 4.6: Vector forces acting on a surface curve *c(s)* as a result of tensioning a yarn over this surface curve with force $|F_{yarn}|$. F_N is the normal force acting on the surface.

Then the resulting force vector of these two yarn forces is

$$\vec{F}_{res}(s) = \vec{F}_{yarn}(s + \Delta s) - \vec{F}_{yarn}(s)$$

4.8

Thereby, $F_{yarn}(s)$ and $F_{yarn}(s+\Delta s)$ analogous are defined by the normalized tangential vector to the curve and by the magnitude of $|F_{yarn}|$:

$$\vec{F}_{yarn}(s) = \left| F_{yarn} \right| \frac{1}{\left| \frac{d\vec{c}(s)}{ds} \right|} \frac{d\vec{c}(s)}{ds}$$

4.9

It is assumed that $|F_{yarn}|$ is the same at each point of the yarn line based on negligible friction between yarn and metal conductor surface.

By definition of the curve, *s* is the arc length, therefore

$$\left| \frac{d\vec{c}(s)}{ds} \right| = 1$$

4.10

Thus,

$$\vec{F}_{res}(s) = \left| F_{yarn} \right| \left[\frac{d\vec{c}(s + \Delta s)}{ds} - \frac{d\vec{c}(s)}{ds} \right]$$

4.11

The resulting pressure $\sigma_{res}(s)$ generated by the yarn is defined by the fraction of the resulting force F_{res} over the area of the small surface element. This area is defined by the product of the length Δs and the width of the yarn w:

$$\vec{\sigma}_{res} = \lim_{\Delta s \to 0} \frac{\vec{F}_{res}(s)}{\Delta s \cdot w} = \frac{|F_{yarn}|}{w} \left[\lim_{\Delta s \to 0} \frac{\frac{d\vec{c}(s+\Delta s)}{ds} - \frac{d\vec{c}(s)}{ds}}{\Delta s} \right]$$
$$= \frac{|F_{yarn}|}{w} \frac{d^2\vec{c}(s)}{ds^2}$$

(4.12)

Yet, for the constriction resistance the component of $\sigma_{res}(s)$ that is normal to the curve is relevant. This is the local pressure $\sigma_N(s)$. It can be calculated by building the projection of $\sigma_{res}(s)$ onto the unit vector normal to the curve:

$$\vec{\sigma}_N(s) = \frac{\vec{\sigma}_{res}(s) \cdot \vec{e}_N(s)}{|\vec{e}_N(s)|^2} \vec{e}_N(s)$$

(4.13)

Thereby,

$$\vec{e}_N(s) = \begin{bmatrix} 0 & 1 \\ -1 & 0 \end{bmatrix} \frac{d\vec{c}(s)}{ds}$$

(4.14)

So,

$$\vec{\sigma}_N(s) = \frac{|F_{yarn}|}{w} \begin{bmatrix} \frac{d^2 c_x(s)}{ds^2} \left(\frac{dc_y(s)}{ds} \right)^2 - \frac{d^2 c_y(s)}{ds^2} \frac{dc_x(s)}{ds} \frac{dc_y(s)}{ds} \\ \frac{d^2 c_y(s)}{ds^2} \left(\frac{dc_x(s)}{ds} \right)^2 - \frac{d^2 c_x(s)}{ds^2} \frac{dc_x(s)}{ds} \frac{dc_y(s)}{ds} \end{bmatrix}$$

(4.15)

This looks fairly bulky but becomes simple when the curve $c(s)$ is a circle like in the simplified model as will be shown next.

4.1.4 Contact Pressure σ_N from Yarn Tensioned over a Circular Surface

The parametric form of the equation of a circle where the parameter s describes the arc length is

$$\vec{c}_O(s) = \begin{bmatrix} r \cdot \cos \frac{s}{r} \\ r \cdot \sin \frac{s}{r} \end{bmatrix}$$

(4.16)

Hereby, r is the radius of the cylinder around which the conductive yarn is tied. Placing this equation into 4.15 one obtains

$$\vec{\sigma}_N(s) = -\frac{|F_{yarn}|}{r \cdot w} \begin{bmatrix} \cos\frac{s}{r} \\ \sin\frac{s}{r} \end{bmatrix} \qquad 4.17$$

Note the magnitude of the vector is independent of s

$$|\vec{\sigma}_N(s)| = \sigma_N = \frac{|F_{yarn}|}{r \cdot w} \qquad 4.18$$

This means the local pressure σ_N is inversely proportional to radius r of the curve. A (continuously differentiable) convex curve can be split up into small circular segments i. To each of these segments a curvature of radius r_i can be ascribed leading to a segment-wise homogenous pressure $\sigma_{N,i}$. Small radiuses lead to high pressure. Straight lines have an infinite radius leading to zero pressure. Concave surfaces of course also lead to zero pressure.

4.1.5 Contact Resistance of a Yarn-to-Metal Contact

Placing this result into equation 4.6 reveals the constriction resistance for element i:

$$R_{C_i} = k_i \left(\frac{r_i \cdot w}{|F_{yarn}|} \right)^n \qquad 4.19$$

Carefully note: the influence of the yarn's width w is not really w^n (which is why it is grayed out in the equation). This is because k_i depends on the apparent contact area A_a. Yet, the apparent area is the product of the yarn's width and the metal conductor's width: $A_a = w \cdot b$ and therefore contains w. This is also the reason why the influence of b is not present in the equation. To prevent further confusion, w^n will be pulled into the segment specific constant:

$$R_{C_i} = k_i' \left(\frac{r_i}{|F_{yarn}|} \right)^n \qquad 4.20$$

With eq. 4.7 – still neglecting the yarn's resistance – the conductance of a yarn-to-metal contact can be expressed as the sum of segments i with local radiuses r_i:

$$G_{contact} = \sum \frac{1}{k_i'} \left(\frac{|F_{yarn}|}{r_i} \right)^n = |F_{yarn}|^n \cdot \sum \frac{1}{k_i'} \left(\frac{1}{r_i} \right)^n \qquad 4.21$$

The term in the sum depends on the specific configuration of a contact. Considering a segment *i*, it can be assumed that there is an optimum radius for which this term reaches a maximum. This means the optimum yarn-to-metal contact is a circular contact with this optimum radius. Note: the metal conductor's width *b*, which influences k_i', is limited by the radius *r* as it cannot be larger than the circumference of the circular curve (if only one loop of the yarn is assumed).

Also note, this equation 4.21 cannot be applied if local radiuses become infinite – representing a flat (or concave) surface. In this case, the local contact resistances become infinite and the yarn resistances $R_{yarn,i}$ cannot be neglected anymore.

Rewriting equation 4.21 as a resistance for a specific yarn-to-metal contact reveals a familiar relationship:

$$R_{Contact} \sim \left(\frac{1}{|F_{yarn}|} \right)^n \qquad\qquad 4.22$$

This equation is almost identical to 4.4, except that the normal force of the contact has been replaced by the tension of the conductive yarn around the cylinder. Therefore, all considerations in chapter 4.1.1 about the constriction resistance, its variance and its rate changes equally apply to this equation here describing a specific configuration of a yarn-to-metal contact in which neglecting the yarn's resistance is permitted.

Of course, this equation does not yet allow calculating the actual contact resistance as the proportionality factor and the exponent *n* are unknown. Of course, these could be found empirically with a series of experiments that alter the yarn tension for a specific contact. Yet, it has to be kept in mind that especially at very low forces a large number of experiments is required to compensate for the large mean variation.

Using the simplified model and conducting a series of experiments with different cylinder radiuses *r*, different yarns of different widths *w* and different widths *b* of the metal conductor one could also find a complete function for k_i'. With this constant k_i' and exponent *n* one would have a generic equation of the form 4.21 to calculate the contact resistance of any yarn-to-metal contact.

4.1.6 Simplified Model Contact Resistance during Temp. Cycling

Although, the k_i' and *n* are unknown, the above results provide sufficiently profound information to anticipate the simplified contact's behavior during temperature cycling. Yet, one tiny assumption has to be made. From experience with metal-to-metal contacts it is known that very low forces already lead to good contacts [113].

Furthermore, embroidered contacts were used for different design projects and do-it-yourself projects cited in chapter 2, and therefore their contact resistance must be low enough for practical applications to be useful. Yet, these were all handmade and therefore probably have higher initial tensions than are possible with embroidery machines. Anyhow, it may be presumed that also the initial yarn tension of $F_{yarn}(init) = 0.2\,N$ that can be applied with embroidery machines is high enough to generate electrical contacts with low contact resistance and small variance (as long as the manufacturing variances are low). The same should apply for experimental implementations of the simplified model.

The yarn tension F_{yarn} during temperature cycles from Figure 3.32 and the considerations about equation 4.22 allow estimating the simplified model's constriction resistance during temperature cycles. This is sketched in Figure 4.7.
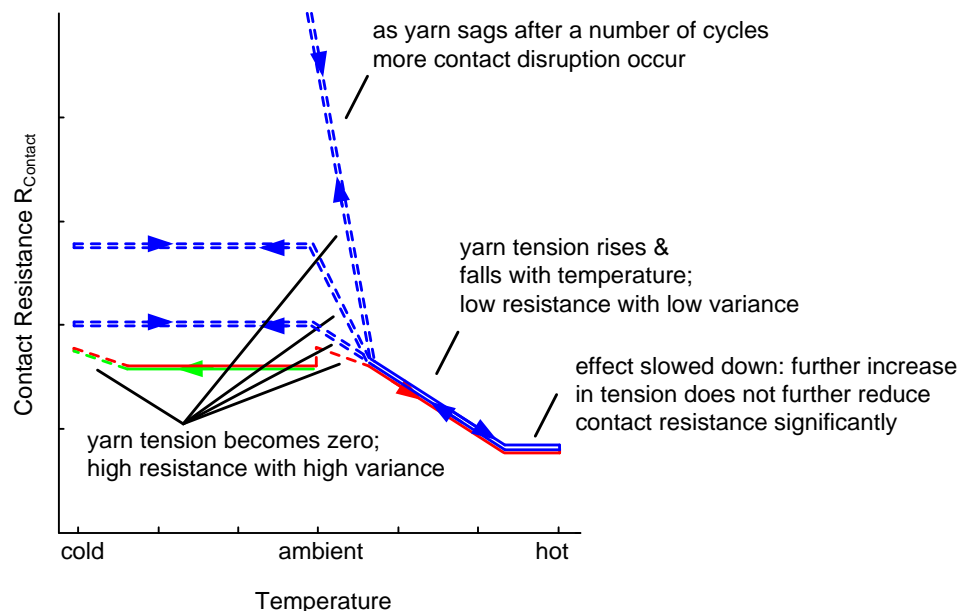
Figure 4.7:   Anticipated contact resistance change in the simplified model during temperature cycling. The green colored curve is the contact resistance during the first cooling phase; the red one is during the first heating phase; and the blue curve is the contact resistance of subsequent cycles. Dotted lines indicate high variance, while continuous lines indicate low variance.

The cycling starts at room temperature with an unknown contact resistance that – according to the assumption above – is low. During the first cooling the force drops to zero as the temperature reaches -20 °C. This is when the contact resistance becomes undefined – mathematically and physically. Neglected factors like the yarn's weight and stiffness become relevant for this unpredictable state. The mean resistance and its variance rise and disruptions could occur.

As the temperature rises during the first heating phase, the yarn tension comes back letting contact resistance and variance drop. At 20 °C there is a dent in the

tension curve. The tension drops to zero, again leading to higher contact resistance and higher variance. At about 55 °C the tension becomes higher than it was initially, reaching 0.5 N at +85 °C. In this phase the constriction resistance and its variance will drop further. Potentially the effect could slow down if the constriction resistance reaches the saturated zone where an increase in tension does not significantly reduce the constriction resistance any further.

During the second and all subsequent cooling phases the tension drops to zero already at +40 °C letting contact resistance and variance rise already at this temperature. Beyond this, as the yarn sags more and more from cycle to cycle (see section 3.3.5), even wind can change the state of the contact. Disruptions become more and more likely. Note, even at room temperature the contact could fail if it has once been heated to +85 °C. Also note that although in average the constriction resistance at low temperatures should rise over time due to yarn sagging, this does not mean that every sample has to rise over time. Individual samples could rise to high resistances at low temperatures and after a number of cycles return to lower resistances at the low temperatures. The state at the low temperature is truly chaotic.

Yet, whenever the temperature returns to the high temperature the tension returns to 0.5 N and therefore the constriction resistance will always return to the same low contact resistance it had reached in the first cycle at the high temperature.

4.2 Embroidered Contact

The embroidered contact is more complex for several reasons. This makes the anticipation of the temperature behavior more cumbersome. However, here the simplified model helps estimating the behavior based on the differences between the embroidered contact and the simplified model.

Firstly, unlike in the simplified model, the embroidered loop is tied around a material that has a non-simple shape. In Figure 4.2, it was approximated as a cuboid with rounded edges. This means in flat areas the contact pressure is zero and in the rounded areas the pressure is like on a circle as described in equation 4.18. Yet, the total resistance cannot be deduced by integration, as the exact influence of the apparent contact area on the constriction resistance is unknown.

Secondly, due to the appearance of flat areas, the contribution of the yarn resistance to the contact resistance can no longer be neglected. This means the contact resistance is actually the result of a network of resistances as sketched in Figure 4.5. In case of the embroidered contact, the total contact resistance consists of the following elements illustrated in Figure 4.8:

- R_{yarn} – the linear resistance of the embroidery yarn on top and bottom: since there are always two yarns next to each other on top and bottom the resistance of the *Shieldex* yarn is 174 mΩ/mm; according to the results presented in Figure 3.6, the yarn's resistance changes during temperature cycling; it rises and falls with temperature; the change is 14% between -40 °C to +85 °C; beyond this, hot phases of the cycle introduce permanent resistance drops that add up to 24 % resistance reduction after 20 temperature cycles

- $R_{constriction}$ – the constriction resistance consisting of $R_{fiber\text{-}to\text{-}fiber}$, which is the constriction inside the yarn, and $R_{fiber\text{-}to\text{-}pad}$, which is the constriction from fibers to the conductive pad: despite the non-simple shape of the material enclosed by the loop it is clear that – like in the simplified model – the constriction resistance must rise and fall inversely with contact pressure and thus inversely with yarn tension F_{yarn} and thus inversely with temperature

- R_{pad} – the resistance of the metallized pad: it is very low and therefore, its contribution to the total contact resistance may be neglected
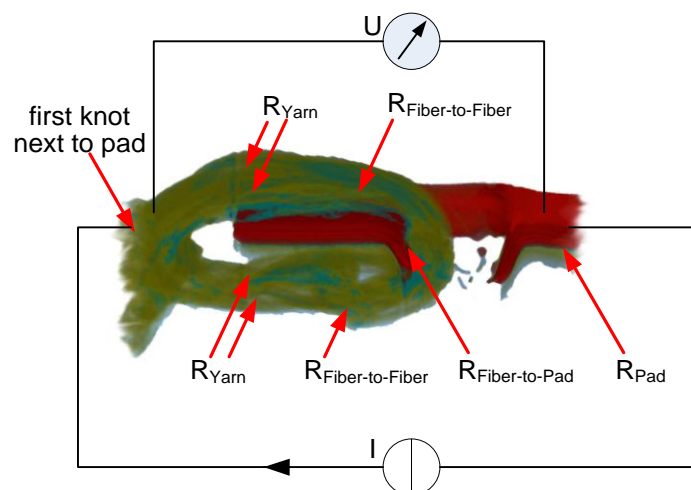
Figure 4.8:   Elements of the contact resistance in the embroidered contact. A four point resistance measurement can only be effected from the first knot next to the pad (left side; greenish) to the embroidery pad (right side; reddish)

Experimentally, these elements are not accessible separately. Touching the yarn loop to measure the constriction resistance would already influence the contact resistance as this would change the contact pressure. Therefore, a four point measurement can only be effected from the embroidery pad to the first knot next to the embroidery pad as also illustrated in Figure 4.8.

The third major difference to the simplified model is that with changing yarn tension not only the a-spot size and density change but possibly also the distribution of a-spots. Figure 4.9 illustrates possible a-spot distributions during the cold phase

and during the hot phase. It becomes clear that with rising temperature not only the constriction resistance will drop but also the resistance of that part of the top thread that contributes to the yarn resistance R_{yarn}. This means, the changes of the constriction resistance $R_{constriction}$ and the changes due to a possible change in the distribution of a-spots show the same trends of temperature behavior. High temperatures lead to low resistances and low temperatures lead to high resistances. The yarn resistance R_{yarn} has the opposite temperature behavior.
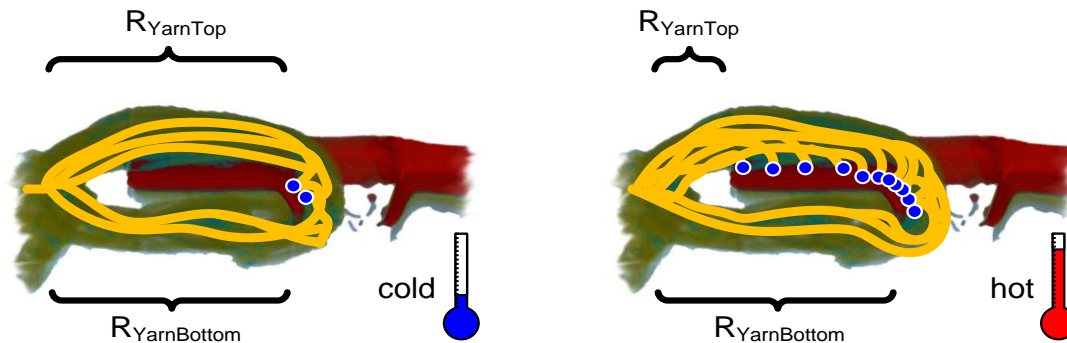
Figure 4.9:   A sketch of current lines (yellow) in the yarn, and a-spots (blue) between contact pad and yarn in cold (left) and hot (right) environment. Note that the temperature not only changes the contact's constriction resistance but also $R_{YarnTop}$.

Fourthly, the dimensions of the embroidered contact are smaller than in the simplified model. This has two effects:

- At smaller radius and unchanged yarn tension, the contact pressure becomes higher and thus, the constriction resistance becomes lower. Certainly, if the yarn tension is zero the contact pressure is also zero – independent of the radius. Therefore, this effect should be relevant only when the tension is non zero.
- However, at zero tension a second effect may appear. The fixing points of the yarn loop are much closer to the contact than in the simplified model. These could hold the yarn in touch with the pad when the yarn tension has dropped to zero. This would lead to fewer failures during the cold phases than in the simplified model. Surely, under these conditions the contact can still not be considered stable.

Lastly, the material enclosed by the yarn loop is not temperature independent. The pad consists of a polymer substrate with a metallization on top and bottom. It expands on heating. The pad is laminated onto a fabric, which consists of fibers and therefore, contracts during heating. Yet, the fibers are meandered inside the fabric and therefore, may not generate a significant contraction force within the envisaged temperature range. Thus, it may be assumed that the material sandwich expands with heating and that bending may be negligible. This means, during heating the contact pressure is further increased with the expansion of the material enclosed by

the yarn loop. Inversely, as the material shrinks during cooling the contact pressure drops to zero more quickly than in the simplified model.

Although these mechanisms partly show opposing temperature behavior, the general character of the contact resistance can still be estimated with some limitation. The sketch in Figure 4.10 illustrates this anticipated behavior.
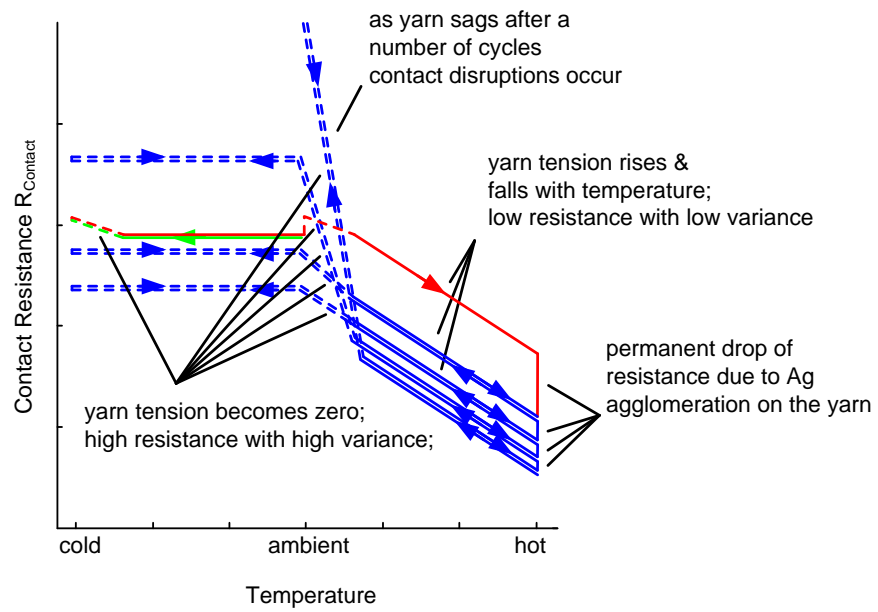
Figure 4.10: Anticipated contact resistance change in embroidered contacts during temperature cycling. The green colored curve is the contact resistance during the first cooling phase; the red one is during the first heating phase; and the blue curve is the contact resistance of subsequent cycles. Dotted lines indicate high variance, while continuous lines indicate low variance.

Without doubt the changes in the constriction resistance $R_{constriction}$ will dominate the changes of the total contact resistance when the contact forces are low. This is the case in the cold phase of the temperature cycle and in the first heating at ambient temperature (i.e. at the dent in the tension curve). Here, the embroidered contact will behave similar to the simplification, i.e. the contact resistance values will be high with high variance. Still, the closer fixing points of the yarn loop may counteract to some extent, and provide some contacts with permanently lower resistances.

During the hot phase the constriction resistance $R_{constriction}$ will always return to the same low values like in the simplification. Therefore, during the hot phase the changes of yarn resistance R_{yarn} probably have a notable influence on the total contact resistance. At least the permanent resistance drop over time as presented in Figure 3.6 should be visible.

The limitation is that the transition temperature at which the pronounced change occurs cannot be estimated due to the different mechanisms contributing to the

total contact resistance. In the simplified model this will occur somewhere around +40 °C as the yarn tension F_{yarn} becomes zero below this temperature. In the embroidered contact this critical temperature has to be determined with measurements on real embroidered contacts. This is described in chapter 6.

4.2.1 Predrilling Holes vs. Piercing the Contact Pad with the Needle

Machine embroidered contacts may be established by embroidering through predrilled contact pads or by piercing contact pads with the embroidery needle. At this point it shall be discussed shortly which variant could proof to be more reliable in the terms of contact resistance stability.

The sketches in Figure 4.11 compare the two variants with their conceivable a-spot distributions for both variants. As already explained, the distribution of pressure generated by the yarn loop is not homogeneous over the surface of the conductive pad. This leads to very few or no a-spots in the flat areas where the contact pressure is zero. At sharp edges (small radiuses) the pressure is locally very high, but the area is so small that there also will not be many a-spots. Only at rounded surfaces the pressure and the area are large so that many a-spots can be established.

Unfortunately, in predrilled contacts the conductive pad features only a flat zone with sharp edges at both ends but no rounded surfaces. Hence, the number of potential a-spots will be small.

However, in the pierced variant the needle bends the substrate downwards and lays the thread around the curved pad. This will leave the pierced variant with more potential a-spots and thus higher contact reliability than the predrilled variant.
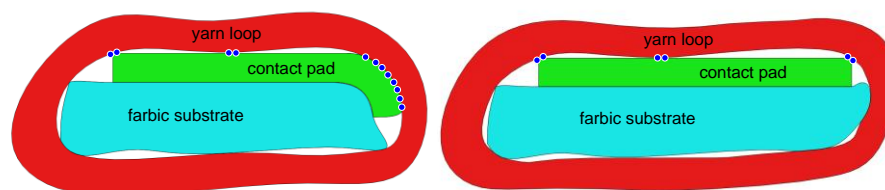
Figure 4.11:   Anticipated a-spot distributions; left: the needle pierced contact pad has a form that lets the yarn touch the pad in an area with high pressure forming many a-spots (blue circles); right: the predrilled contact pad will have less a-spots and therefore be less reliable.

Of course in practice this bending effect could be used a second time (or more) on the other side of the cuboid (in the sketch, this is on the left side). The needle could also pierce the substrate there. Although this is practically useful it does not change the basics of the contact principle considered here – modeling the contact however would become more complex without getting significant advantages.

4.2.2 Multiple Sewing of the Contacts and Redundancy

Until now, it has only been considered that the yarn loop is embroidered once. Embroidering the same contact loop multiple times m will reduce the contact resistance. However, the number and size of a-spots will probably not increase directly proportional to m. The yarns laid second or third do not have the same chance to build a-spots with the contact pad as the first yarn is between them and the pad. Thus, the resistance may drop less than with $1/m$.

Yet, as the tension in the yarn is still crucial for the contact, failures will occur at low temperatures. Of course, if a failure is defined as a resistance rise over a specific resistance value, the failure rate may be lower or the time to failure may be longer than with single stitched contacts at the same failure criterion.

Alternatively, one could obtain redundant contacts by combining several embroidered contacts in parallel (separate loops in separate contact pads). This way the reliability could be adapted to the applications requirements. However, several contacts do need more space which may often not be available. In this work, this will not find further consideration as this can just be applied for practical achievements but does not significantly improve the understanding of basic principles underlying embroidered contacts.

4.3 Other Reliability Issues

The theoretical focus of this thesis is about understanding the contact's behavior during temperature changes. However for practical applications, reliability during other environmental stress is also relevant.

Especially washing is often mentioned when wearable electronics applications are discussed. Yet, making a profound theory that includes all the complex influences of such washing stress on the embroidered contacts is at least hard to achieve. Therefore, washability shall be considered experimentally only.

A second issue is contact resistance during movements. As there are no standard test conditions for electric contacts in textile environment, such need to be defined. At this point a theoretical thought shall be given to the potential impact of movements on the contact resistance. On this basis a test will be developed in the next chapter.

Assuming a rigid module, bending of the fabric at the edge of the module would be the most likely movement. The embroidered conductive yarn is fixed in this fabric at the knot next to the module. So if the fabric bends the conductive yarn moves with it. Especially the a-spots near the edge of the contact pad could be affected by this movement. Figure 4.12 illustrates how. If the fabric is bent upwards it could lift the

yarn loop. The consequence would be a reduction of a-spots near the edge. Vice versa, if the fabric is bent down the yarn loop could be pressed onto the pad and increase a-spots. The far end a-spots are probably less affected by this.
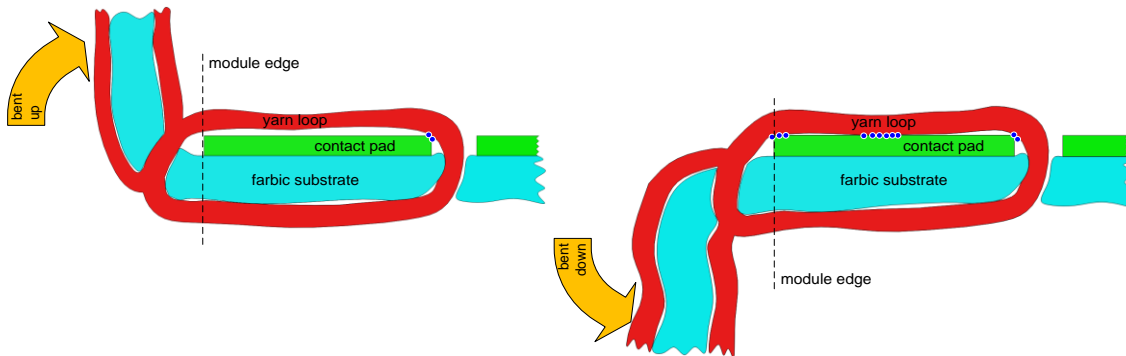
Figure 4.12: Bending stress: bending the fabric at the edge of the module could lead to changes in the contact resistance. A-spots near the edge could be more affected than a-spots near the hole in the contact pad.

This means it can be expected that pierced pads are less sensitive to bending stress than predrilled ones, as they have more a-spots at the far end of the edge to compensate.

Repeated down bending could lead to elongation of the loop which would also negatively affect the contact quality.

4.4 Conclusion

For the first time, this chapter has analyzed the contact mechanisms underlying machine embroidered contacts. A theoretical simplified model of the contact was developed. It was shown that the yarn tension F_{yarn} is crucial for the contact. At low temperatures during temperature cycling, this tension drops to zero and the yarn even sags. This will lead to a loss of contact pressure. The consequence is a chaotic state in which the contact cannot be predicted. Potentially the resistance can become very high or even contact disruption could occur. At high temperatures the yarn tension is high and thus the contact resistance is anticipated to be low.

As it is difficult to predict the exact temperature below which the contact force will become too low for a reliable contact, this will be investigated experimentally.

The following experiments will investigate whether this theoretical analysis – that predicts that embroidered contacts are unreliable at low temperatures – proves to be true. Furthermore, it will be tested whether bending or washing leads to failures, too.

If this is true, additional measures will have to be taken to stabilize the embroidered contact. This however, may reduce the manufacturing efficiency of the technology of embroidered contacts.

5 Development of Tests and Test Vehicles

To verify the theory of the previous chapter, different experiments were developed which are described in this chapter. A physical implementation of the simplified model and different implementations of embroidered contacts were developed. The test structures of both – the simplified model and the embroidered contacts – were designed to measure contact resistance while excluding feeding resistances as far as possible.

The implementations of the simplified model and the embroidered contacts were both exposed to temperature cycling stress while their contact resistances were recorded. This way the contact behavior can be traced. In separate experiments the embroidered contacts were also exposed to bending stress and wash cycling stress. All three stress tests are described in this chapter in detail.

The results of these experiments are presented in chapter 6. This includes a precise description of the numbers of different test vehicles exposed to the different stress tests.

5.1 Assembly of the Simplified Model

The experimental implementation of the simplified model was constructed on a quartz glass tube of 15 mm radius and 2 mm wall thickness. Quartz glass best meets the previously defined requirement of a CTE near zero – its CTE is $0.5 \cdot 10^{-6}$ /K. It is also very stiff compared to the yarn, which was the second requirement defined in chapter 4.1. As already mentioned, handling smaller tubes was difficult, which is why the tube is not implemented with a radius as small as the embroidered contact. A tube was preferred over a full cylinder to provide a quick adaption to the surrounding temperature during temperature cycling.

A 2 mm wide gold stripe representing the metal contact was sputtered onto the surface in longitudinal direction (parallel to the axis) of the tube. To do this, the tube was covered with temperature resistant adhesive tape leaving only a 2 mm wide gap alongside the tube. Then the whole was sputtered and the tape removed. However, to provide a good adhesion of the gold on the glass, it was necessary to heat the whole to 250 °C prior to sputtering. This unfortunately weakened the adhesion of the tape on the glass, allowing gold to slip under the tape's edge, leading to uneven gold edges. This means the width of the gold strip showed some variance (see magnification in Figure 5.2). This has to be kept in mind when interpreting the results of the contact resistance measurements.

According to sputtering tables the applied sputtering parameters lead to a gold stripe thickness of about 100 nm [25]. This means the glass tube with its gold contact can be considered round and without a step at the gold stripe.

For applying the yarn loop the glass tube was fixed in clamping jaws with the gold facing downward as shown in Figure 5.1. The yarn was laid around the tube and suspended with 20 gram weights at the ends to generate the initial tension $F_{yarn}(init) = 0.2\ N$. It was made sure that the loop is really circular, i.e. having the shortest possible circumference around the tube. To eliminate possible frictional forces[35] between the yarn and the tube's surface the whole was turned back and forth around the tube axis a couple of times. Then the loop was fixed with a drop of glue (see magnification in the top right of Figure 5.1). For this purpose glue was selected that adhered well on the glass and on the yarn also during and throughout the temperature cycling. After curing the glue at room temperature, the weights were removed.
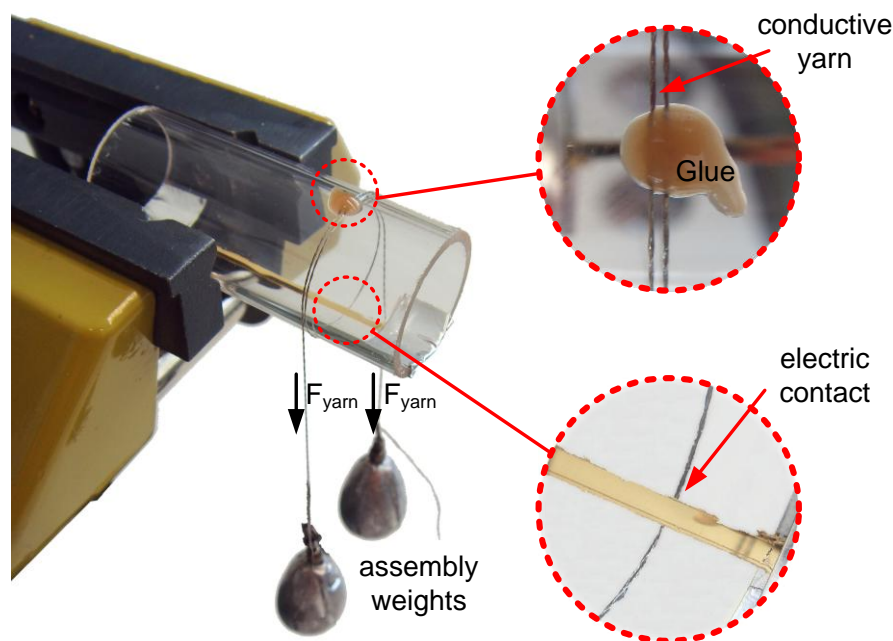
Figure 5.1:   Assembly process of the simplified model. Altered from [25].

The drop of glue serves two purposes. It closes the yarn loop mechanically like a knot, but unlike a knot it electrically insulated the yarn ends. This design allows a precise contact resistance measurement focusing on the constriction resistance and hiding feeding yarn resistances. Figure 5.2 shows how this four-wire sensing was implemented in the simplified model. The current is fed from the left micro clip to the yarn below the glass tube and then through the front half of the yarn loop.

---

[35] remember: the absence of frictional forces between the yarn and the surface over which it is tensioned is the precondition for the assumption that the yarn tension is constant everywhere: $|F_{yarn}(s)| = |F_{yarn}|$ (see chapter 4.1.3)

The current then flows through the contact to the gold stripe and the left alligator clip. The voltage-drop over the contact is measured from the right alligator clip through the gold strip and from the right micro clip through the rear half of the loop.
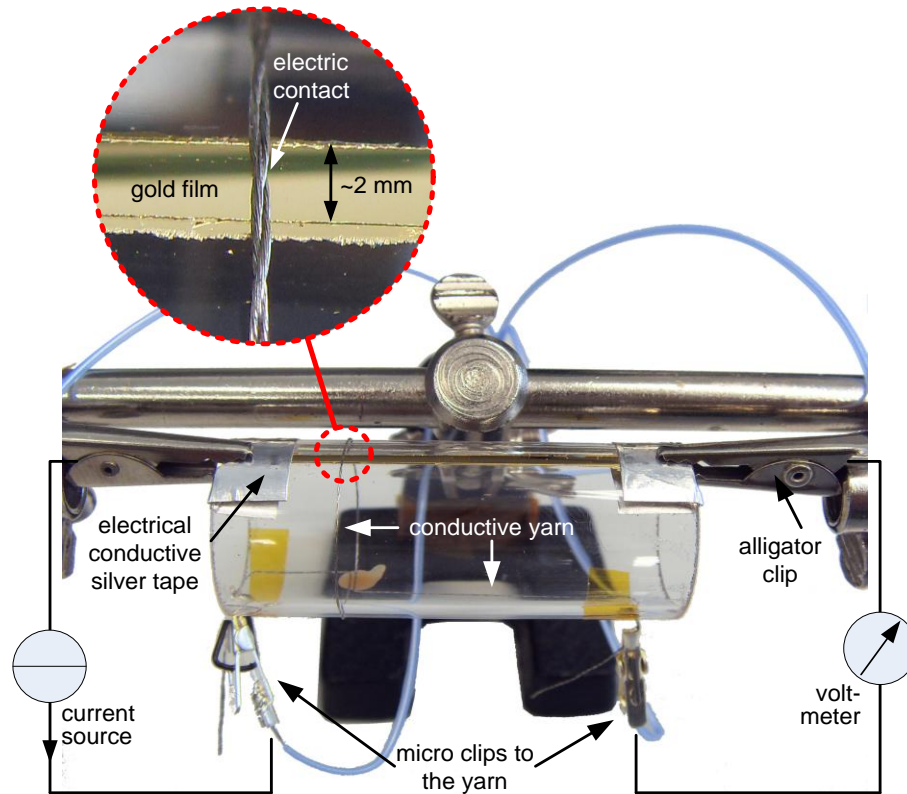
Figure 5.2:   Measurement setup: four-wire sensing of the contact resistance of the simplified model. Altered from [25].

5.2 Assembly Process of the Embroidered Contacts

Following the suggestions of the theoretical work in chapter 4, different variants of embroidered contacts were implemented. The distinguishing attributes are:

- the contact pad finishing: gold or silver;
- the contact type: pad pierced by the needle or predrilled pad; and
- the number of stitches through the pad: one stitch (i.e. standard variant) or four stitches (the latter have only been implemented on needle-pierced silver pads).

Other than these attributes all test vehicles are identical. Figure 5.3 shows an exemplary test vehicle with needle-pierced silver pads. A test vehicle consists of a test module (green, silver and gold colored) laminated to fabric (black) and then contacted with embroidered conductive yarn (silver).

The tests module consists of a rigid substrate (green) with strip wiring and measurement pads and 14 embroidery pads made from metallized thin polymer substrate (silver).

The four-wire contact resistance measurements are effected via measurement pads on the test module and crimped snap fasteners at the ends of the embroidered lines. Strip wires interconnect the measurement pads with the embroidery pads.

The following subchapters describe details of the assembly process. The order of subchapters follows the process sequence.
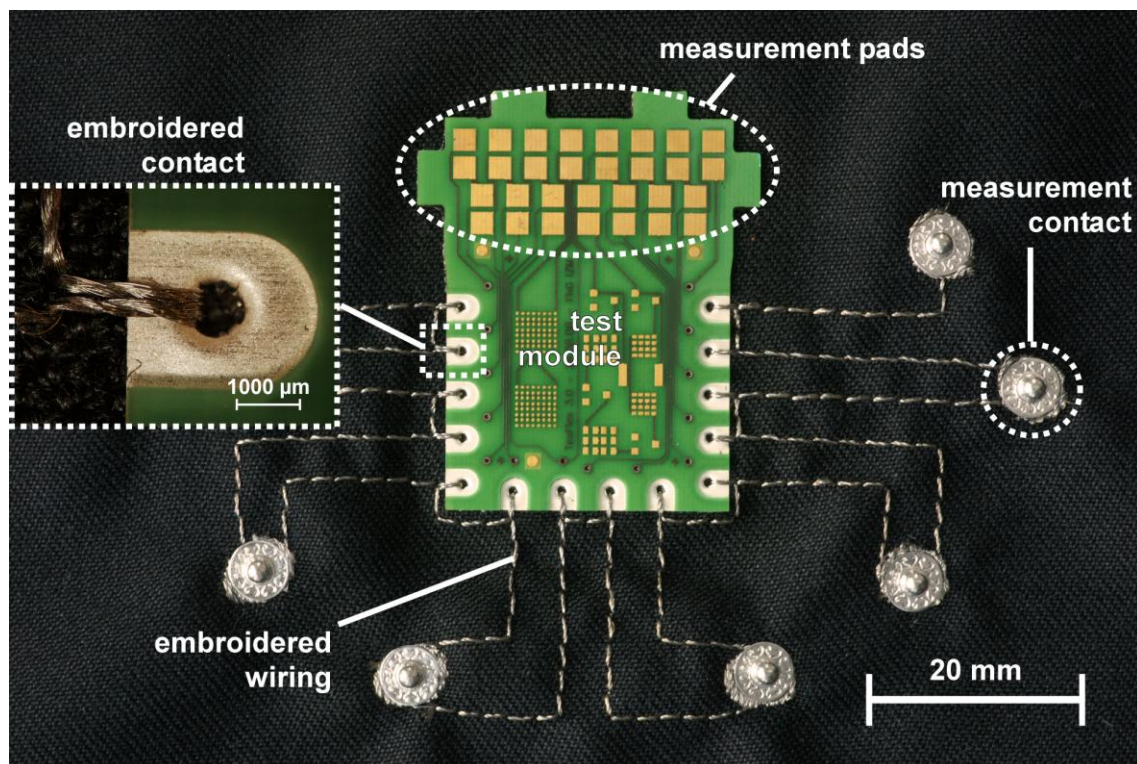
Figure 5.3:   Test vehicle for measuring the contact resistance of embroidered contacts.

5.2.1 Selecting the Embroidery Cloth (Fabric Substrate)

The choice of the embroidery cloth is not a focus of this work. Therefore, the goal was to select a "normal" fabric substrate that also meets the following criteria.

It should be well defined, which is why a brand name manufacturer was selected that provides a datasheet for the product and can guarantee the product's availability for some years. Furthermore, for such a research work it is desirable to keep the assembly simple to not make the interpretation of the results more difficult than necessary. Therefore, a substrate was chosen that does not require

any supporting embroidery backing[36]. Last it is essential that the substrate does not change during processing or testing. Some of the process steps involve temperatures up to 240 °C, while the testing conditions are between -40 °C and +85 °C in air or during washing at 40 °C in water with detergent and mechanical stress.

All these conditions may be met by many different products. The choice fell on a 200 g/m² twill weave fabric made from meta-aramide yarn. Aramide stands for aromatic polyamide fiber. It is resistant to high temperatures (370 °C decomposition temperature), shows good chemical fastness and has a high tenacity [116]. The CTE is expected to be small and negative. Fabrics made from aramide are widely used for protective clothing for firefighters and racing drivers.

5.2.2 The Electronic Test Module

One goal is to compare predrilled and pierced contacts. Another goal is to expose test vehicles to wash cycling. According to 2.2 only thin polymer substrates, that are not fiber reinforced, can be pierced by a needle. However, such thin polymer substrates do not withstand wash cycling (ref. to 2.2). Only rigid, fiber reinforced substrates so called FR4 can resist such stress.

The so called rigid-flex substrate technology provided a solution. It allowed manufacturing test modules that are largely thick and rigid but are thin and pierceable in the locations of the embroidery pads. Figure 5.4 shows a close-up view and a cross section of an embroidery pad and the surrounding FR4 substrate.

The size of the test vehicle is 26 mm x 36 mm (not counting the four small extensions near the measurement pads). The overall thickness is 580 µm. The thickness of the embroidery pads is ~120 µm. They are built from 45 µm polyimide; 45 µm copper-nickel-gold plus 10 µm solder resist[37] on the bottom side and 22 µm copper on the top side. Additionally, depending on the experiment, the copper on the top side is metallized with silver (some nanometers) or with nickel-gold (~5 µm Ni and some nanometers gold). (See Figure 5.4) The bottom side has been metallized to give the pad more stability. The asymmetry between top and bottom metallization is due to the manufacturing process.

The embroidery pads have a size of 2.5 mm by 3.0 mm. The predrilled variant features a laser cut hole of diameter 1.25 mm. This is larger than the embroidery needles thickness, which is 0.8 mm.

---

[36] a non-woven fabric or a paper-like foil sometimes used for supporting the embroidery cloth to keep it from distorting

[37] solder resist is a polymer film applied to printed circuit boards that traditionally serves to prevent solder from bridging conductors; however, it may also be used for electrically insulating conductors on the printed circuit board towards the environment
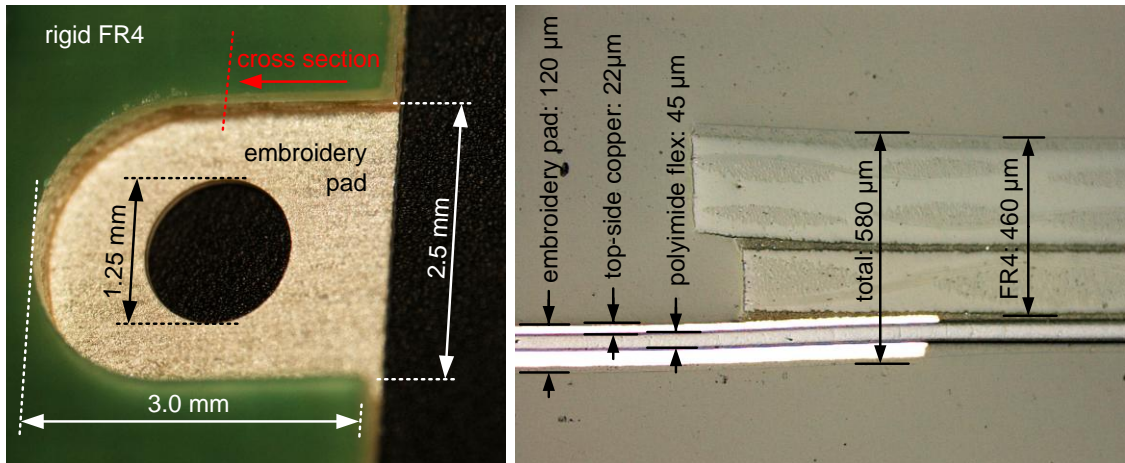
Figure 5.4:   Left: close-up view of a predrilled embroidery pad surrounded by rigid FR4 (green). Right: cross section of the embroidery pad (left) and the rigid FR4 right.

5.2.3 Laminating the Test Module onto the Fabric Substrate

To reduce forces on the embroidered contact during mechanical stress the electronic substrate was laminated to the fabric substrate as suggested in 2.2. For this purpose thermoplastic polyurethane (PU) film was used. This is a common adhesive in the textile industry. However, other adhesives may be used as well.

The lamination process was carried out with an *HP45S* thermo press from *SEFA* shown in Figure 5.5 (right). To assure an equal pressure distribution an embossing tool was developed to account for the topography of the rigid-flex substrate (Figure 5.5 left). For the assembly the embossing tool was placed onto the lower plate; on top the rigid-flex module with the laser cut PU was placed; on top of that the aramide fabric was placed.
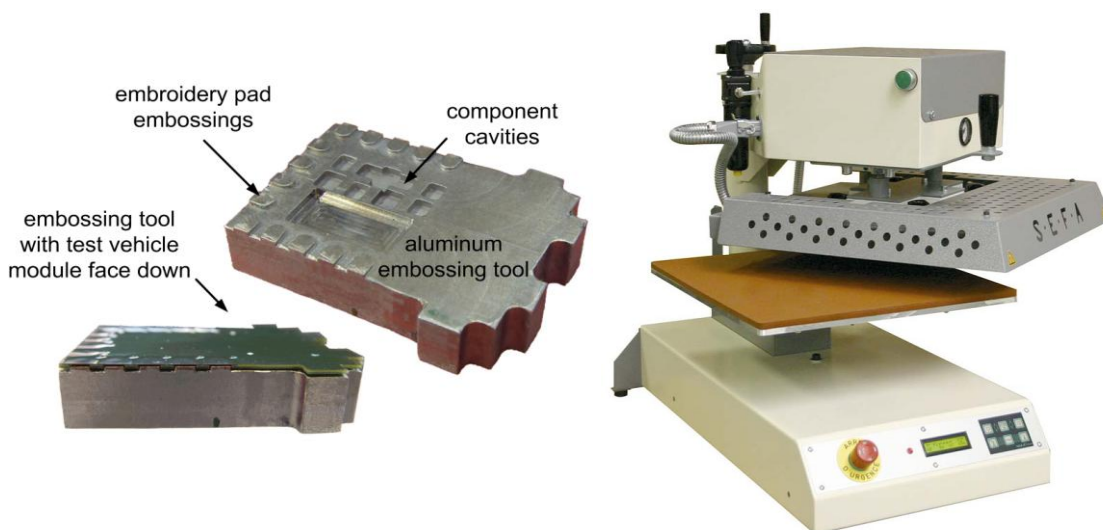
Figure 5.5:   Embossing tool (left) and thermopress HP45S from SEFA (right)

The lamination parameters were optimized for best adhesion which has been verified with peel tests. These parameters are: plate pressure = 3 bars; lower plate temperature = 105 °C; upper plate = 240 °C; lamination time = 180 sec; always two samples have been processed at a time to improve the uniformity of the pressure distribution. The PU film thickness was 100 μm (prior to lamination).

The PU is an elastomer with a CTE around $220 \cdot 10^{-6}$/K. This is large compared to copper for instance. However, its modulus is at least three orders of magnitude smaller than that of copper. This means, the changes of the dimensions of the rigid-flex caused by temperature will dictate the changes of the dimensions of the PU film that is adhered to the rigid-flex.

5.2.4 Embroidery Process

For the embroidery process standard equipment was used without any alteration. The following describes which tools were used to build the test vehicles.

A number of different embroidery design software tools are available on the market. These tools are intended for designing logos, text or graphics. They were neither made for circuit design nor for designing embroidered contacts. However, most of these contain basic design functions which may be used for routing circuits manually, and for defining exact stitch points for embroidering through metallized pads. Examples for such tools are *Bernina Designer Plus*, *Embird* or *GiS*. Since only the basic functions of these tools are required for making embroidered circuits and contacts, the results generated with these tools are very similar. The designs in this work were made with *GiS BasePac 6 v6* – a screen shot is shown in Figure 5.6 on the right.
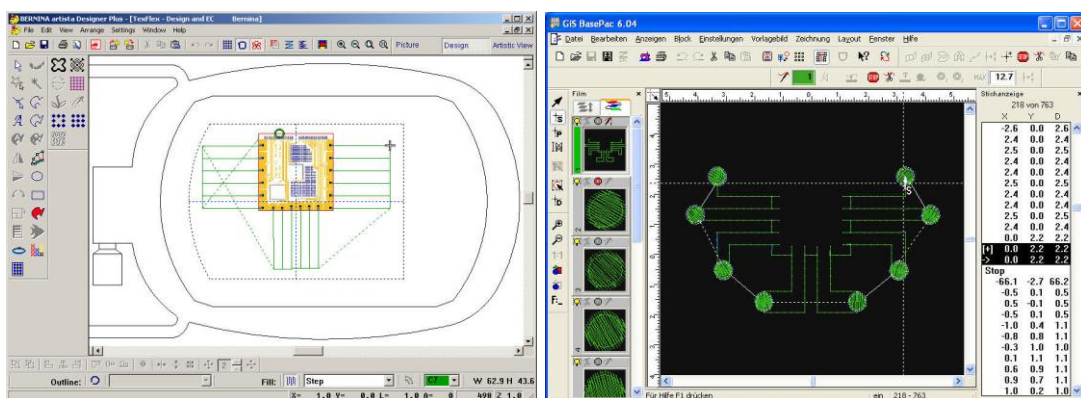
Figure 5.6:   Embroidery Software: *Bernina Designer Plus* (left) and *GiS BasePac 6* (right)

The test vehicles for this research were embroidered with the regular embroidery head on a *ZSK JCZ 01* – a standard industry embroidery machine. It is shown in Figure 5.7. Very similar test vehicles were made with a *Bernina Artista 200* home

embroidery machine which shows that even simpler machines can be used to make embroidered contacts.

Figure 5.7:   Embroidery machine *ZSK JCZ 01* with regular embroidery head.

A medium ball point needle (SUK) was used to reduce the fiber breakage when the needle goes through the same point on the layout twice which is the case next to the embroidered contact. This type of needle point displaces the fibers rather than piercing them [19]. The needle thickness was 80 Nm[38]. This needle is considered a standard needle [117].

Differences in the piercing of the electronic substrate were not observed when comparing this medium ball point needle with other needle types.

As already explained *Shieldex 117/17 Twine* was used in needle and bobbin. The thread tensions for both have been adjusted as described in the ZSK manual [118]. The process of adjusting these tensions on embroidery machines is not very scientific in general. This may lead to variances in the samples' initial yarn tension $F_{yarn}(init)$. It is difficult to estimate these variances. As explained in chapter 4.1, it is expected that the initial yarn tension is about 0.2 N and can definitely not be larger than 0.5 N.

In most test vehicles the needle was stitched *once* through the embroidery pad. Remember: this means that the top thread is laid twice onto the metallized pad: first when going to the stitch point on the metallized pad and second when going back to the point on the fabric next to the pad. However, to test the reliability of multiply sewn contacts as suggested in 4.2.2, some embroidery pads were stitched *four* times.

---

[38] 'Nm' stands for 'numbering metric' and defines the needle diameter in 1/100 mm at the blade, which is above the scarf where the hook passes the needle [19]

5.2.5 Four-Wire Sensing of the Embroidered Contacts

The four-wire sensing of the contact resistances was effected via the embroidered seams and the measurement pads on the test module. An exemplary measurement is shown in Figure 5.8.

Since on the test module there was only space for one strip line per embroidery pad, the strip line resistance was always included in the measured resistance value. In Figure 5.8, this strip line resistance is represented by a white dotted line. To receive the contact resistance (circled yellow) the individual strip line resistance was subtracted from the measured resistance value.

This procedure does not provide a perfect four-wire resistance value of the contact. However, actual measurements showed that the resistance values of these strip lines were always smaller than the contact resistance and exhibit a smaller variance (7 % compared to 34 %). This means, such a subtraction only marginally reduces the accuracy of the contact resistance compared to a perfect four-wire measurement. Note: for the samples exposed to temperature cycles this subtraction was temperature corrected, i.e. it was considered that the resistance of the strip wire changes with temperature.

All the actual contact resistance values presented in the following chapters refer to the result of this subtraction and not to the measured value (i.e. not even if the word 'measurement' is used in that context). These contact resistance values of the embroidered contacts are identical with the definition of the contact resistance considered in the theory chapter in Figure 4.8.
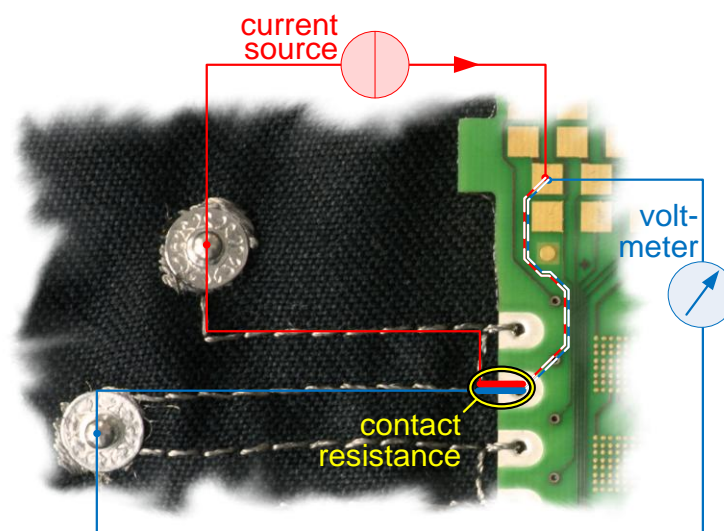
Figure 5.8: Exemplary four-wire resistance measurement of embroidered contact. The white dotted lines represent the strip wire resistance that was subtracted from the measured resistance to receive the contact resistance.

The testing equipment used for the four-wire sensing during thermal cycling was a *Keithley Model 2750 Multimeter/Switch System*. It allows automatically measuring up to 98 contacts at a time. Measurements were effected every 30 seconds, which is the limit for the sample rate when all channels are connected. These so-called insitu measurements provide an insight on the contacts behavior at different temperatures during temperature cycling.

Individual measurements of the contacts before exposure to stress or in-between wash cycles were effected with *Keithley Model 2010 Multimeter*.

Both multimeters were set to a measurement range of 100 Ω. Since this means changes above this value cannot be measured, anything above 100 Ω was considered a disruption of the contact. For practical applications this is reasonable anyway. The accuracy that results from this range setting is 1 mΩ for the *2010 model* and 2 mΩ for the *2750 model*.

Furthermore, dry circuit testing and offset compensation was applied. For more information about this refer to [119] and [120].

For measuring the contact resistance during bending, the sample rate of these two multimeters (~1 Hz) is too small to provide adequate information. Therefore, the four-wire sensing was effected with a current source and a transient recorder (i.e. in principle a storage oscilloscope with a lot of storage for long measurements). The current source supplied 10 mA, while the transient recorder measured the voltage drop over the embroidered contact and over a 10 Ω series resistor. With Ohm's law the contact resistance was calculated. The sample rate was set to 125 Hz. As current source a *Keithley 2420 3A SourceMeter* was applied. The transient recorder was a *TransCom-RackX by MF Instruments*.

5.3 Environmental Stress

Chapter 2.3.3 extracted from literature a long list of potentially useful environmental stress tests for electronics-in-textiles. Furthermore, a temperature cycling and a bending test were selected for analyzing the behavior of embroidered contacts and a wash cycling test was selected for testing the reliability under practically realistic environmental stress. This chapter describes in detail how these tests were applied.

5.3.1 Temperature Cycling

The applied temperature cycling test is very similar to test condition *N* defined in *JEDEC JESD22 A104 C* industry standard for testing consumer electronics [52]. One cycle consists of three isothermal lines at −40 °C, +20 °C and +85 °C. The dwell

times and the transition times are always 15 minutes. In total 25 cycles are run. Figure 5.9 presents the applied temperature profile.

This profile differs from the standard in two ways: the standard does not foresee room temperature isothermal lines, and furthermore applies faster transitions (at least double the speed of the profile here). These changes have been made to receive a more precise picture of the temperature behavior of the contacts. At this slower cycle, more samples can be taken per cycle (remember: the maximum sample rate of the switch system is two samples per minute). Furthermore, at fast temperature changes one cannot be sure that the temperature measured with a temperature sensor is actually the one felt by the contact – there may be delays leading to misinterpretations.
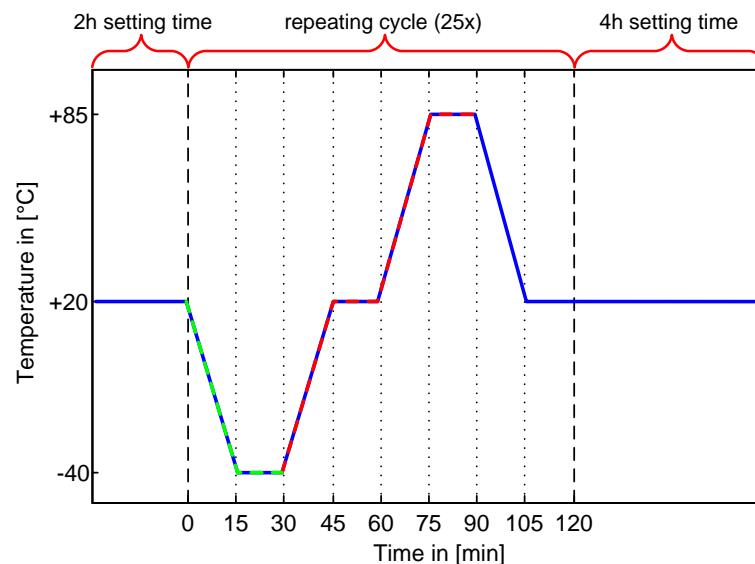
Figure 5.9:   Temperature profile applied in this thesis for analyzing the behavior of the simplified model, the embroidered contact and elements of these, like the yarn resistance. The green dashed line marks the first cooling cycle and the red dashed line marks the first heating cycle, which are often referred to in this thesis. Altered from [25].

The equipment for applying this profile was a *CS-70/300/S* temperature cycling chamber from *CTS GmbH*.

5.3.2 Bending Test

Fabric naturally moves, bends and folds. Any electric contact in fabric environment should support such movements and retain a constant resistance during such movements. Chapter 4.3 has analyzed, which kind of natural movement could be particularly critical for embroidered contacts. This was found to be bending at the edge of the module. Thereby, bending downward could reduce the resistance and bending upward could increase the resistance (assuming the side of the fabric on which the module sits is considered the upper side). This subchapter describes the

experimental setup to test actual the behavior of embroidered contacts during bending.

First, the contact resistance measurement was started as described in 5.2.5. Then a series of bends was performed by hand. Figure 5.10 shows the followed pattern. Hereby, 0° means the fabric was flat, 90° denotes an upward bend at a right angle and -90° denotes a downward bend at a right angle. The fabric was always bent at the edge of the test module (i.e. at the edge of the embroidered contact). Each position was held for 5 seconds. The total test time was 180 seconds.

In total, three samples of each contact type (i.e. pierced and predrilled) were tested. Their pad metallization was always silver. The tests were performed by Christian Böhme during his traineeship at Fraunhofer IZM [121].
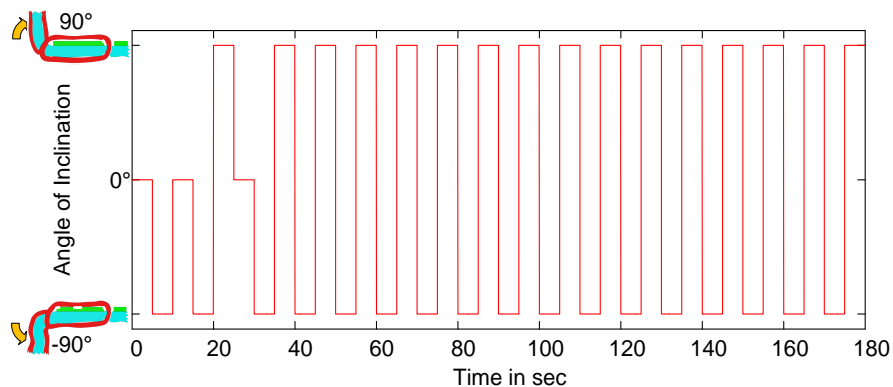
Figure 5.10: Bending test: pattern of manual upward and downward bends at the edge of the embroidered contact.

5.3.3 Wash Cycling Test

A wash cycling test according to *ISO 6330* was applied to test the durability of the embroidered contacts and also of the conductive yarn (see 3.2.3 ff.) This is a norm for domestic washing and drying procedures for textiles [46]. The employed test condition was *6A* which is a normal wash cycle at 40 °C. This selection followed suggestions of sources mentioned in 2.3.3.

The norm offers several different detergent compositions to choose from. A composition was selected that is in line with the cleaning recommendations for the conductive yarn. [122] It is free of phosphate and optical brighteners and in the norm is denoted as *ECE reference detergent A*.

Also according to the norm, sheets of cotton fabric were added to the test vehicles so that the total dry mass always amounted to 2 kg.

The utilized washing machine was a *W465H* by *Electrolux*. This is a front loader compliant with *ISO 6330*.

In all tests (i.e. with embroidered contacts or with conductive yarn), 20 wash cycles were applied. In-between cycles the test vehicles were dried lying flat as described in drying procedure *C* of *ISO 6330*. The resistance measurements were effected in dry state after wash cycles 1, 2, 3, 4, 5, 7, 10, 13, 16 and 20.

6 Experimental Analysis of Contact Behavior in Embroidered Contacts

The previous chapter presented the experimental setups to test the theories of chapter 4. This chapter presents the results of these experiments and compares them to the theory.

As the main focus of this work is on embroidered contact stability during thermal cycling, this is discussed first. After that, the additional experiments on stability during bending and washing are presented.

6.1 Contact Resistances after Manufacturing

After manufacturing and before the samples were exposed to any stress tests their contact resistances were measured. The following table presents the results.

Table 6.1: Contact resistances of samples before stress tests were performed.

Type of Contact	Mean	Std. Deviation	Num. of Samples
simplified model	299 mΩ	99 mΩ	9
embr. cont.: pierced Au pads	395 mΩ	144 mΩ	33
embr. cont.: pierced Ag pads	431 mΩ	136 mΩ	33

The theory could not make any predictions on actual resistance values of these contacts. Yet, it was assumed that the initial tension of F_{yarn} = 0.2 N would generate low contact resistances with low variance. There are no literature values for constriction resistances in contacts with conductive yarn. Yet, the standard deviations of all three contact types feel rather high. This may be explained in two ways. Either the contact force and thus also the number and size of a-spots were small. Or the manufacturing variances were large, e.g. the metal width covered by the yarn (refer to 5.1). Even both could be the case.

The contact resistances of the embroidered contacts with the silver pads were (9 %) higher than of those with gold pads. This may be due to silver sulfidation as suggested in chapter 4.1.1.

6.2 Simplified Model during Temperature Cycling

Nine test vehicles of the simplified model were exposed to temperature cycles while their contact resistances were recorded. They all exhibited a very similar characteristic response. Figure 6.1 shows a typical plot over 25 cycles. In Figure 6.2 this plot is magnified and shows only the first four cycles. More plots are shown in the Appendix A.1. Note: in these plots and all following ones the green part of the curve represents the first cooling phase and the red part of the curve represents the first heating phase. All the following cycles as well as the initial resistance before temperature cycling are plotted blue. For more details on the temperature cycling profile refer to Figure 5.9.
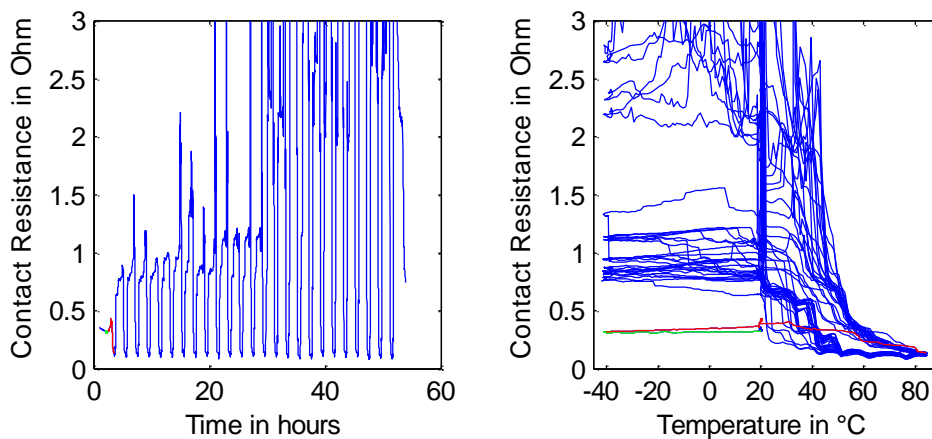
Figure 6.1:   Contact resistance of a simplified model during temperature cycling. At temperatures below 60 °C the contact resistance rises significantly and ultimately disruptions occur. (ID: SM01Au01\558).
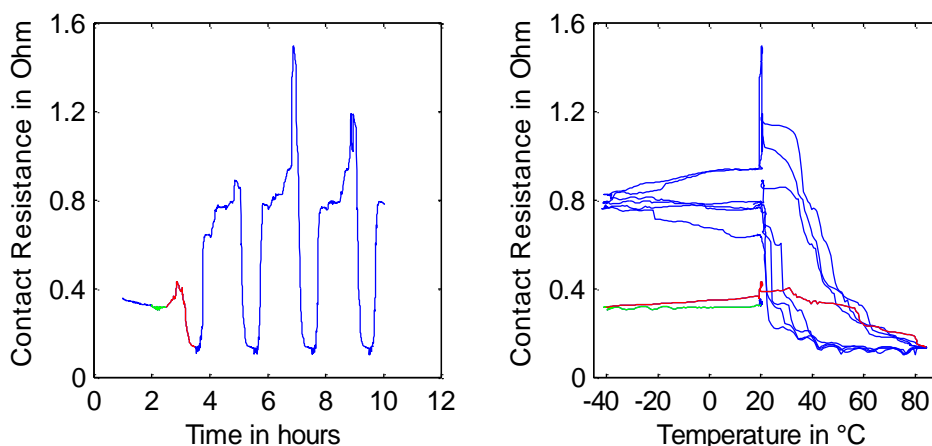
Figure 6.2:   Magnification of the first four cycles of the plot in Figure 6.1. (ID: SM01Au01\686).

The simplified model behaved quite like predicted. During the hot phases, resistance values and variance became low and always returned to similar values

throughout the cycles. It seems that this lowering of resistance with higher temperature was not yet saturated at 85 °C.

In the cold phases, resistance values and variance were high and typically rose from cycle to cycle. Sooner or later, in eight out of nine samples disruptions occurred (meaning the contact resistance rose above the measurement range of 100 Ω). In the remaining one sample, the contact resistance reached a value that was ten times higher than its initial one. Potentially it could also have failed if more cycles had been run.

The temperature below which the contact resistance rose dramatically is between 30 °C and 60 °C, which is in line with theory that suggested that this appears in a range around 40 °C.

After the experiment, it was observed (at room temperature) that the yarn was no longer tight on the glass cylinder, which is a result of the yarn sagging observed in 3.3.5.

Theory suggested that the resistance could rise already during the first cooling as the temperature drops below -20 °C. Below this temperature the yarn tension becomes zero and thus the condition of the contact becomes unpredictable with a potential to rise in resistance. Yet, in none of the nine samples this was observed.

Theory also predicted that during the first heating the tension dent at 20 °C could lead to a rise in contact resistance. In eight out of nine samples this was observed. The sample that did not show this resistance rise is the same that did not disrupt. Figure 6.3 shows an example where this effect is particularly pronounced.
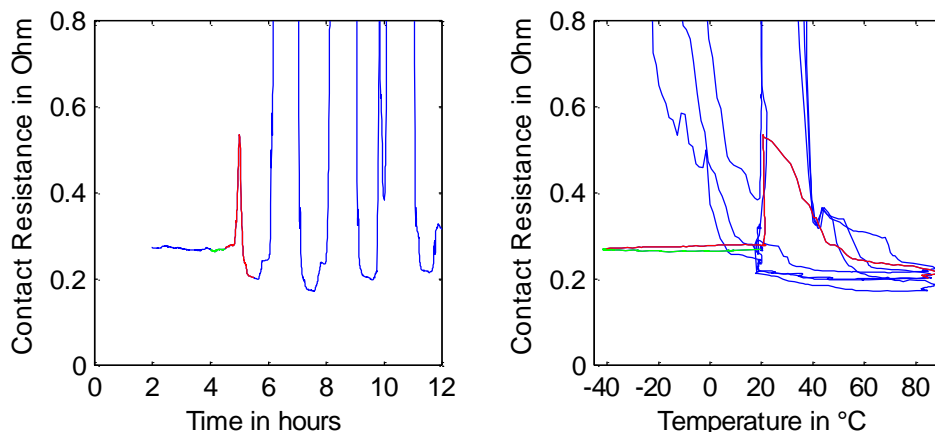
Figure 6.3:   Sample of simplified model during first four cycles. During heating the contact resistance rises significantly at 20 °C (red curve) which is due to the dent in the tension curve at this point (ref. to Figure 3.32). (ID: SM01Au03\778).

Surprisingly, this resistance rise appeared also in subsequent heating cycles at 20 °C as can be seen in Figure 6.2 for instance. At this point there is no change in

the tension curve – the tension is constantly zero from -40 °C to 35 °C (ref. to Figure 3.32). This may imply that the yarn sagging is particularly strong in this temperature range between 20 °C and 35 °C.

6.3 Embroidered Contact during Temperature Cycling

The embroidered contact behaved more heterogeneous during temperature cycling than its simplification. 38 samples[39] with pierced contact pads were exposed to temperature cycles. In general, all contact resistances rose with falling temperatures and inversely fell with rising temperatures. Yet, in 18 % of the samples the contact resistance rose sharply below a certain temperature leading to disruptions. This critical temperature was always below 0 °C. In the remaining samples the resistance rose only slightly at low temperatures. Figure 6.4 and Figure 6.5 show two typical plots for these diverging behaviors. More plots can be found in Appendix A.2.

Nota bene, this is the behavior for 25 temperature cycles. Potentially those contacts that did not fail, could fail if more cycles were run.
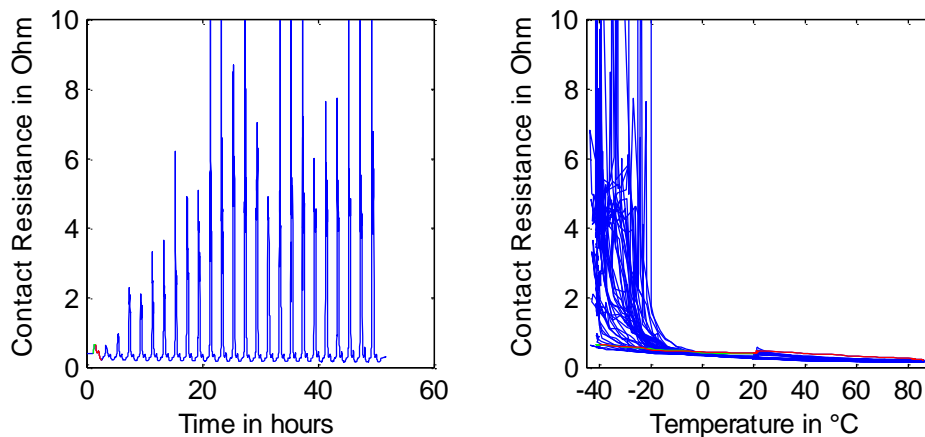
Figure 6.4:   Sample of pierced embroidered contact that fails at the low temperatures. The plot shows 25 temperature cycles. (ID: EC56AuPiercedPad02\196)

---

[39] total sample numbers: 19 samples pierced on gold pad, 19 samples pierced on silver pad
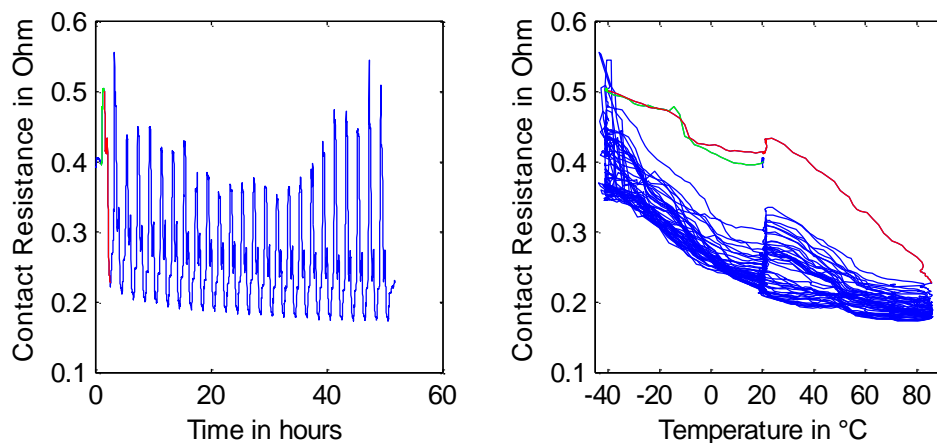
Figure 6.5:   Sample of pierced embroidered contact that rises slightly at low temperatures. The plot shows 25 temperature cycles. (ID: EC54AgPiercedPad01\167)

This behavior is in line with theory. It was argued that the fixing points of the yarn loop are closer to the contact pad and in some samples could hold the yarn in contact with the pad when the yarn tension drops to zero.

Beyond this, also the other features of the plots were predicted well. In all samples the contact resistance rose during the first cooling. Note: In theory this was anticipated also for the simplified model. However, as mentioned above, the simplified model did not feature this contact resistance rise in the first cooling phase.

The majority (74 %) of samples exhibited a resistance rise at 20 °C on rising temperature. Like in the simplified model this was not only observed in the first heating cycle as predicted but also in subsequent heating cycles. In Figure 6.5 this feature is well pronounced. As explained this may be a result of yarn sagging in the temperature domain between 20 °C and 35 °C.

The predicted influence of the dropping yarn resistance (ref. to 3.2.1) was observed in all contacts. The sample in Figure 6.6 demonstrates this very well over the entire temperature range. In the hot phase, silver agglomeration on the fibers leads to a permanent resistance reduction of the yarn leading to a total contact resistance reduction. In the cold phase of other samples (e.g. in Figure 6.5), this effect is covered by the more dramatic change due to tension changes – also as predicted.

Note that Figure 6.6 presents one of the most stable samples. Even here, the negative temperature coefficient of the contact resistance, which is a result of tension changes of the yarn, dominates over the positive temperature coefficient of the yarn resistance - as expected.
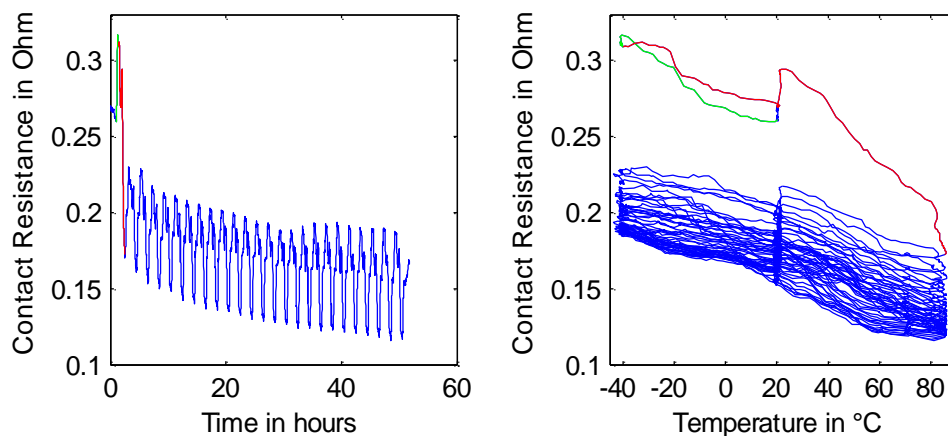
Figure 6.6:   One of the pierced embroidered contacts with the most stable behavior during temperature cycling. The contact resistance drops from cycle to cycle due to dropping yarn resistance at the high temperature. (ID: EC56AuPiercedPad12\206)

Beyond the lower contact resistance of the gold pads, no particular differences were observed between the gold and silver pads during temperature cycling.

6.3.1 Predrilling vs. Piercing the Contact Pad

The theory suggested that piercing the substrate with the needle would result in more reliable embroidered contacts with lower contact resistances than predrilling the contact pad prior to embroidering the contact.

It was reasoned that the bent part of the contact pad, which is a result of the piercing, could produce more and larger a-spots than the rest of the contact pad which is flat. It is not possible to prove this with final certainty as it is not possible to measure or count the actual a-spots.

Yet, the contact resistance measurements presented in the following two tables show, that in deed pierced contacts are generally of lower resistance and are more reliable than predrilled ones.

In total 56 embroidered contacts with predrilled pads were manufactured. Yet of those 56 samples, six samples showed disruptions already after manufacturing. Table 6.2 shows the mean value of the remaining 50 samples and compares it to the pierced contacts of which all 66 samples were faultless after manufacturing. Despite sorting out the worst of the predrilled samples, the contact resistances of pierced contacts were in average five times lower than those of predrilled ones. Also the standard deviation was very high in predrilled contacts, which is an indicator for low number and small size of a-spots.

Table 6.2:   Contact resistances of samples before stress tests were performed.

Type of Contact	Mean	Std. Deviation	Num. of Samples
pierced embr. cont.	413 mΩ	140 mΩ	33 gold, 33 silver
predrilled embr. cont.[40]	2010 mΩ	3669 mΩ	26 gold, 24 silver

Also during temperature cycling, pierced contacts performed better than predrilled ones as suggested by the theory. The failure rates during 25 cycles for different failure criteria are summarized in Table 6.3. Hereby, a contact was being considered to have failed when its resistance rose at least once above the failure criterion of either 1 Ω, 10 Ω or 100 Ω. The percentage values in the table represent the fraction of failed contacts over the total number of contacts.

Table 6.3:   Failures during 25 temperature cycles at three different failure conditions: contact resistance rose at least once above 1 Ω, 10 Ω or 100 Ω.[41]

Type of Contact	1 Ω	10 Ω	100 Ω
pierced embr. cont.	29 %	18 %	18 %
predrilled embr. cont.	100 %	82 %	73 %

Despite their higher resistance and lower reliability, predrilled contacts generally showed the same characteristic temperature behavior as pierced contacts. The only difference is that the critical temperature below which the contact resistance rises dramatically was at a higher temperature. In 59 % of the predrilled samples this temperature was above room temperature, while in the pierced variant this temperature was always below 0 °C. Figure 6.7 shows a typical plot. More plots are presented in Appendix A.3.

---

[40] note that the total number of predrilled contact samples that were manufactured is 56; yet 2 samples with gold pads and 4 samples with silver pads had total disruptions; the mean value includes only those contacts that had not disrupted

[41] total sample numbers: 19 samples pierced gold, 19 samples pierced silver, 12 samples predrilled gold and 10 samples predrilled silver
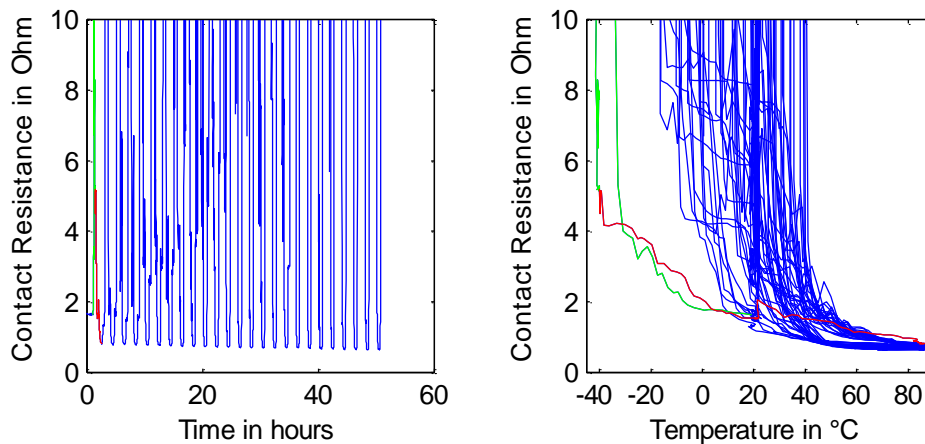
Figure 6.7: Typical sample of an embroidered contact on a predrilled contact pad.
(ID: EC48AgDrilledPad10\239)

6.3.2 Embroidered Contacts Stitched Four Times

As anticipated in chapter 4.2.2 stitching through the contact pad multiple times reduced the contact resistance. Table 6.4 shows contact resistances of four times stitched pads had an almost four times smaller contact resistance than contacts that were stitched only once. The standard deviation drops even more.

Table 6.4:   Contact resistances of samples before stress tests were performed

Type of Contact	Mean	Std. Deviation	Num. of Samples
stitched 1x	431 mΩ	136 mΩ	33 silver pierced
stitched 4x	115 mΩ	15 mΩ	28 silver pierced

Also the performance during temperature cycles improved with multiple stitching as shown in Table 6.5 for the failure criteria 1 Ω and 10 Ω. At first glance it may appear as an accomplishment that there were no failures at the 10 Ω failure criterion. However, it must be remembered that the 25 temperature cycles are merely to prove the theory. After practically relevant 1000 temperature cycles the failure rate at 10 Ω was 14 % for the four times stitched samples.

Additionally, a new failure criterion of 0.27 Ω is introduced that accounts for the lower starting resistance (115 mΩ / 431 mΩ x 1 Ω = 0.27 Ω). It allows comparing the relative changes of the single stitched and the four times stitched contacts. This is done by comparing the failure rate of the single stitched at the 1 Ω failure criterion with the failure rate of the four times stitched at the 0.27 Ω failure criterion. Apparently, the relative change was higher in the four times stitched samples.

Table 6.5:   Failures during 25 temperature cycles at three different failure conditions: contact resistance rose at least once above 0.27 Ω, 1 Ω or 10 Ω.[42]

Type	0.27 Ω	1 Ω	10 Ω
stitch. 1x (pierced)		29 %	18 %
stitch. 4x (pierced)	57 %	7 %	0 %

Note: As suggested by the theory the plots in Appendix A.4 prove that the principle failure mechanism does not change when stitching four times rather than one time.

6.4 Embroidered Contact during Wash Cycling

During the wash cycles at 40 °C many contact disruptions occurred in the embroidered contacts. The pierced contacts performed slightly better, but the overall performance was generally weak as Figure 6.8 shows. Given a failure criterion of 100 Ω all contacts fail after 20 wash cycles. Once a sample exhibited a contact resistance higher than 100 Ω it was considered to have failed from that cycle on, even if it returned to lower values after a later cycle.
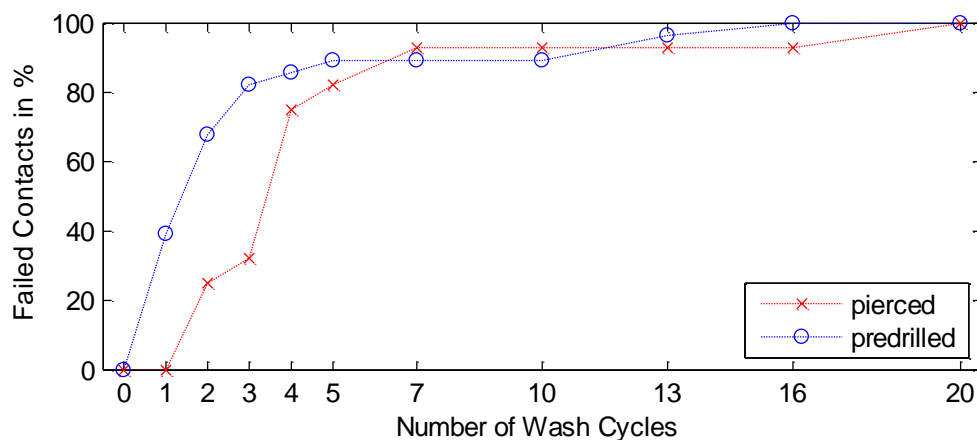
Figure 6.8:   Contact failures in embroidered contacts due to washing. A contact was considered to have failed if it rose above the measurement range of 100 Ω. A contact that had once failed and returned to values below 100 Ω was still counted as a failure. The total sample numbers were 14 pierced silver contacts, 14 pierced gold contacts, 14 predrilled silver contacts and 14 predrilled gold contacts.

Contacts that were stitched four times still rose significantly over 20 wash cycles. Yet, they did not show disruptions (i.e. resistances did not rise above the measurement range of 100 Ω). This enables presenting the change as a change of the mean value of contact resistances as shown in Figure 6.9.

---

[42] total sample numbers: 38 samples stitched one time (19 pierced gold and 19 pierced silver); 14 samples stitched four times (14 pierced silver)
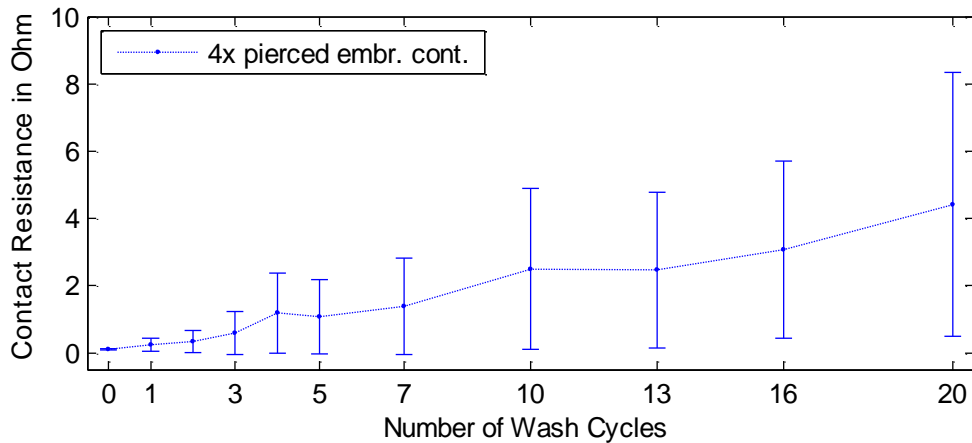
Figure 6.9:   Contact resistance during wash cycles of embroidered contacts stitched four times; the total number of samples was 14. The contact pads had silver metallization and were pierced by the needle. Failure rates after 20 wash cycles at failure conditions 0.27 Ω, 1 Ω, 10 Ω and 100 Ω were 100 %, 86 %; 7 % and 0 % respectively.

6.5 Embroidered Contact during Bending

In chapter 4.3 it was anticipated that the contact resistance of embroidered contacts could rise when the fabric next to the contact pad is bent upwards and that contact resistance could drop again when the fabric is bent downwards. The experiments showed that exactly this is the case. Figure 6.10 shows the resistance change of a typical embroidered contact on a pierced silver pad during the bending test described in 5.3.2. More plots can be found in Appendix C.
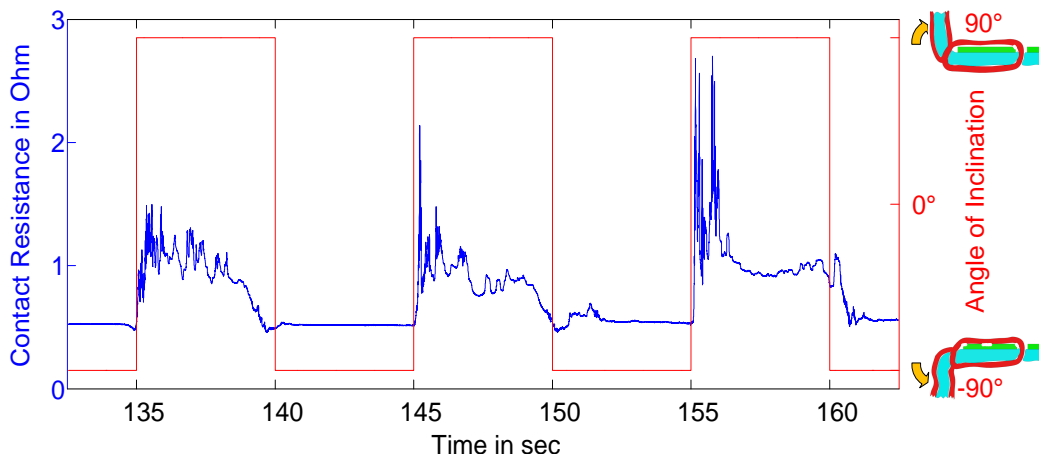
Figure 6.10: Bending test with an embroidered contact on a pierced silver pad. The contact resistance was low when the fabric next to the pad was bent down and significantly rose when bent up.

It was also assumed that pierced contacts would perform better than predrilled ones. It was argued that pierced contacts would build most a-spots near the hole

which is far away from the bending edge and therefore should be less affected by the bending. The experiments showed indeed that pierced contacts perform by far better than predrilled ones. During the bending test all predrilled contacts failed even at the highest failure criterion as Table 6.6 shows.

Table 6.6:   Failures during 180 seconds bending test at three different failure conditions: contact resistance rose at least once above 1 Ω, 10 Ω or 100 Ω[43]

Type	1 Ω	10 Ω	100 Ω
pierced embr. cont.	33 %	0 %	0 %
predrilled embr. cont.	100 %	100 %	100 %

Although the pierced contacts performed much better, they can still not be considered stable contacts as 33 % failed the 1 Ω failure criterion. Remember: the duration of the test is only 180 seconds and only 17 bends are done. For practically relevant applications the contact would need to survive many more bending cycles.

6.6 Conclusions

The experimental results in this chapter strongly support the theoretical fundament established in chapter 4. The yarn tension is crucial to the contact stability during temperature cycling. At low temperatures this tension drops to zero and even yarn sagging occurs leading to contact disruptions. The conclusion that has to be drawn from this is that embroidered contacts (at least machine embroidered ones) are not reliable intrinsically with the high conductive embroidery yarns available today.

Possibly, technical yarns could make a difference once they are available with conductive coating and with machine embroiderability. They have to tend less to tension relaxation and yarn sagging.

Hand embroidered contacts could benefit from the higher initial yarn tension that may be applied. Yet, this was not tested here. However, the simplified model is an excellent test vehicle for analyzing even such contacts which may be embroidered with other conductive yarns or higher pre-tensions. This model mimics very well the essential electrical behavior of the real embroidered contact during thermal changes.

Beyond their weak reliability during thermal cycling, the embroidered contacts also fail basic washing and bending tests. Whether this could improve with technical

---

[43] three samples of each contact type (i.e. pierced and predrilled) were tested; their pad metallization was silver

yarns or higher tensions cannot clearly be predicted at this point as a theoretical analysis on this aspect was not put in place in this thesis.

Unless new yarns are available, a different solution has to be found to overcome the reliability issue of embroidered contacts. This is the objective of the next chapter.

7 Providing Reliability for Embroidered Contacts

In the previous chapters it was shown theoretically and experimentally that embroidered contacts inherently are not reliable during textile typical stress. This is due to the fact that the contact mechanism relies on tension in the yarn which cannot be kept up under these conditions.

Therefore, any solution to make embroidered contacts reliable must focus on extending the contact mechanism, so there is no need to rely on permanent tension in the yarn anymore.

One approach could be to prepare the contact pad in such a way that it catches the yarn and holds it independently of the tension in the yarn. An example design of this idea is shown in Figure 7.1. A trench is cut into the pad prior to embroidery. The width of the trench is smaller than the yarn diameter. During the embroidery process the yarn is pulled into the trench. The trench then clamps the yarn even when tension along the yarn drops.
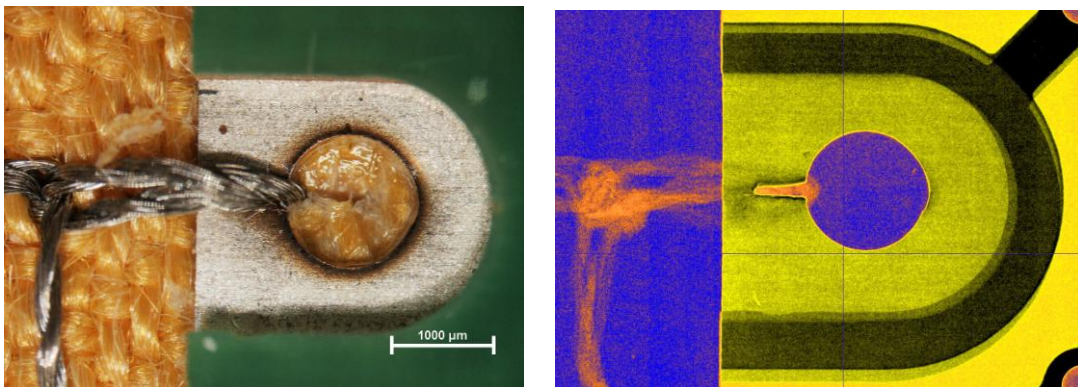
Figure 7.1:   A trenched pad could clamp the thread in the trench rather than relying on the yarn tension to provide the contact force. Optical microscopy image (left). False color X-ray image of the same contact (right).

Developing design rules that successfully catch and permanently clamp the yarn could be the goal of another dissertation on this field.

In this thesis a solution shall be found that fixes the embroidered contact in its initially good state or even better in its best state which is at an elevated temperature when the yarn tension is high. For this purpose different encapsulation technologies shall be investigated in this chapter.

7.1 Theory: Encapsulation Technologies for Embroidered Contacts

Applying encapsulation to protect electric contacts is very common practice. It protects against mechanical stress including temperature induced mechanical stress. It protects against chemicals such as moisture, salts, and atmospheric contaminants like sulfur oxides (SO_2). Sometimes it just holds contact members together. [123], [124]

Embroidered contacts need to be protected from mechanical stress during washing or bending, from thermally induced mechanical stress during temperature cycling, and from moisture during washing. The following subchapters will discuss different encapsulation technologies and their applicability to embroidered contacts. Afterwards, test vehicles will be designed and tests will be carried out to test the different hypotheses.

7.1.1 Transfer Molding

Transfer molding is a particularly reliable encapsulation often used in the automotive industry, and also for encapsulating micro chips. Its main components are epoxy resin and hardener, and a high percentage of SiO_2 filler particles of about 70-90 wt %. These particles adapt the coefficient of thermal expansion (CTE) of the molding compound to the one of electronic components. This reduces the thermal stress during temperature changes which makes a more reliable package. The two-component epoxy raw material is a duromer and is provided in form of pressed powder and has to be stored at -40 °C to prevent early cross linking. In the molding machine it is quickly heated up. As it becomes low viscous it is pressed - transferred - into a mold tool. The mold tool typically has a temperature of around 160-185 °C. This lets the molding compound cure within 1-2 minutes. The mold tool consists of two halves that are pressed together at high pressure to close the form well and prevent low viscous molding compound from spilling out of the form. The process is very common in the electronics industry and used for mass production applications. A drawback is the high cost for the mold tool which makes it expensive for low volume production. [125], [42], [126], [124]

Once encapsulated with transfer molding, embroidered contacts can be expected to stay unchanged even under harsh conditions. The high temperature during the molding process will increase the contact force due to the yarn shrinkage force. This means the embroidered contact will be fixed in a state of excellently low contact resistance. The molding should be applied to top and bottom side to assure a full encapsulation.

Unfortunately, the high temperature of the mold tool and the high pressure at which the mold tool is closed will also act on the conductive yarn coming out of the package. As shown in 3.2.3, *Shieldex* degrades quickly during washing if prior to washing it is heated to temperatures above 190 °C. High pressure will probably worsen the effect.

This means it can be anticipated that the contacts will be well protected by transfer molding but the conductive yarns coming out of the package will be harmed significantly so that during washing they will fail after only a few wash cycles.

7.1.2 Hotmelt Encapsulation

Another molding technology is hotmelt encapsulation. It is much cheaper than transfer molding, due to the lower demands on the tools and due to the lower material costs. These thermoplastic materials become low viscous above their melting temperature (typically 155 °C to 200 °C) and can be molded. At temperatures below the melting point the materials become rigid and keep their shape.

Typically the material is kept in a hot tube in its low viscous state. For application it is pressed into a cold (or slightly warm) form where it solidifies within about 30 seconds.

The viscosity of hotmelts is rather high compared to thermosetting epoxies, which is why the hotmelt materials cannot be filled with particles. The advantage is: without additional filler particles the process is much less abrasive than transfer molding. Therefore, a low cost aluminum tool can be used instead of a hardened steel form. A disadvantage is that it does not provide such a high level of protection as the CTE is not adapted to the one of electronics, and as the chemical resistance of the hotmelt encapsulants is weaker than that of epoxies. [127], [42]

For embroidered contacts it is particularly useful that the form is not hot and does not require a high closing pressure. This means unlike in transfer molding the conductive yarn outside the package will not be harmed.

However, rather than fixing the yarn on the contact pad, the high CTE of the material may lead to new thermo-mechanical instabilities at the embroidered contact especially during thermal cycling.

7.1.3 Local Application of Glob Top

A lower cost option is glob top encapsulation as it does not require a mold tool. A duromer or an elastomer in its initially low viscous state is applied with a syringe

and cured. Typical glob top encapsulants are epoxies and silicones, the latter being an elastomer.

Epoxies have glass transition temperatures above the typical application ranges. They have very high moduli resulting in high shrinkage force during curing and subsequent cooling. This stress can be reduced by adding filler particles and thus reducing the CTE. Yet, with 60-70 wt %, the maximum filler content is lower than in transfer molding compounds. This limitation is necessary to keep the viscosity sufficiently low so it can be dispensed with a syringe. Therefore the reliability of glob top encapsulations does not reach the high level of transfer mold encapsulations. [125] Still, for many applications this is sufficient. For example, to protect a transponder chip in a technical textile application, glob topping with particle-filled epoxy resin has been applied successfully by [48].

The glass transition of silicones is well below typical application temperatures. Therefore their CTEs are very high. Nonetheless this often is not significant because their moduli are so low that they cannot generate any thermal stress. [125]

For fixing the embroidered contacts the glob top material could be applied locally on the contact. Silicones are not suited as they are too soft to hold the yarn and the pad in permanent contact. Instead a particle filled epoxy adhesive should be used. The cure process could be carried out at 85°C when the electric contact is best. So the embroidered contact could be fixed under optimal conditions.

7.1.4 Local Application of Isotropically Conductive Adhesive (ICA)

Applying conductive adhesive is not really an encapsulation technology. Yet, using conductive adhesive instead of non-conductive glob top adhesive (as suggested in 7.1.3) would help to extend the contact mechanism. In that case the conductive adhesive would provide for the current flow from the pad to the conductive yarn. So the embroidered contact would not rely on the yarn tension anymore.

Isotropically conductive adhesives (ICA) are adhesives filled with conductive particles. Commercially most wide spread are epoxy adhesives with silver particles or with silver coated particles. The filler content is typically between 25-30 vol %. [128], [129]

A disadvantage of using conductive adhesive is that it is more brittle than unfilled epoxy adhesives. Especially at the point where the yarn comes out of the ICA glob, it might be prone to cracking during mechanical stress.

7.1.5 Combining Locally Applied ICA or Glob Top with Hotmelt

To overcome the potential shortcomings of hotmelt, glob top or ICA, these technologies may be combined. Glob top or ICA may be applied locally onto the embroidered contacts providing for a good contact. The hotmelt encapsulation may then be applied over the entire module protecting the glob top or ICA from cracking. The hotmelt material is soft and therefore the yarn may be less prone to cracking at the edge of the hotmelt than it may be at the edge of a brittle adhesive.

7.1.6 Adhesive Film Protection

In chapter 3.2.4 it was explained how thermoplastic polyurethane was laminated over the embroidered conductive yarn to successfully protect it during washing. The same lamination film was used to fix the electronic test substrate on the fabric substrate before the contacts are embroidered (refer to chapters 2.2 and 5.2.3).

Laminating this adhesive film over the embroidered contacts may fix the contacts. The pressure of the lamination process may push the yarn onto the contact pads improving the contact in the flat area of the pad. To assure that the yarn does not move after release of pressure, it could be helpful to hold the lamination pressure until the laminate is cooled below its solidification temperature.

A shortcoming of this approach could be that the adhesion of polyurethane is known to be weak on noble metals of which the contact pads are made. This may result in delamination during washing or temperature cycling. In that case it is very likely the electric contact would be lost.

7.2 Experimental Setup

The following subsections will explain the development of the differently protected test vehicles.

7.2.1 Transfer Molding

The transfer mold encapsulation was applied as described in [42] and shall be shortly summarized here.

A number of different transfer mold materials were tested concerning their adhesion to the fabric and to the electronic substrate. The material that performed best was a general purpose overmold epoxy compound with filler particles. It was selected to build the test samples.

A molding tool was developed that allows applying an encapsulation on top and bottom side of the test vehicle. This is achieved in two separate molding steps. The

molding compound was cured at 175 °C during 100 seconds. Post-mold curing[44] was not applied, to not further harm the conductive yarn. The amount of molding compound and the molding pressure were optimized to fill the form well and to minimize wicking into the fabric. Figure 7.2 shows a fully encapsulated test vehicle. The thickness of the encapsulation is 2 mm on top and on bottom. The moldings cover all embroidered contacts, part of the electronic test substrate and part of the fabric substrate. For processing, a FICO Brilliant 100M transfer molding machine was used.
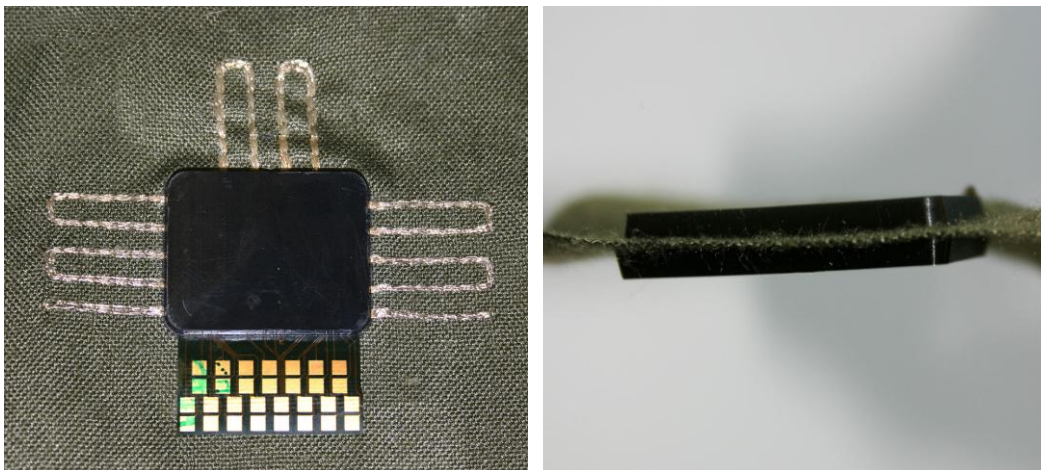
Figure 7.2:   Test module encapsulated with transfer molding on top and bottom. All embroidered contacts, part of the electronic substrate and part of the fabric substrate are encapsulated. Top view (left) and view from the side (right).

The test substrate that was used for the assembly is not identical with the other ones in this thesis. It is not a rigid-flex substrate but a fully flexible substrate. This polyimide substrate has a thickness of 50 μm. The metallization is copper-nickel-gold of 22 μm thickness on top and bottom side. A solder resist passivation of 15 μm is applied on top and bottom – the contact pads are left open. This means the flexible substrate is very similar to the flexible parts of the rigid flex module – which are the contact pads. The shape and size of the contact pads are identical to the ones on the rigid-flex module.

Unlike the other test vehicles in this thesis, this substrate was not adhered to the fabric with thermoplastic polyurethane since this would have melt during transfer molding. However, the bottom side of the substrate is well protected by the transfer mold encapsulation on the bottom side.

The embroidery pad was not predrilled but pierced by the needle. For historical reasons the contacts were embroidered three times rather than only one time like

---

[44] most transfer mold encapsulants need to be cured for several hours to reach their optimized characteristics; this curing process is segmented in a short curing during the molding (up to two minutes) and a long curing after the molding (several hours);

in the other test vehicles in this thesis. This has to be kept in mind, when comparing the contact resistances.

In this assembly the measurement pads stick out from the transfer mold package (shown at the lower end of the left picture in Figure 7.2). These are made from relatively sensitive flexible substrate. To prevent breakage, this part of the substrate was protected with a specially designed clamp that was attached before washing.

7.2.2 Hotmelt Encapsulation

The hotmelt encapsulation – as well as glob top and ICA (see next subchapters) – were applied to the *normal* test vehicles that were manufactured as explained in 5.2.

First a material screening was made. The hotmelt material with the best adhesion to fabric and electronic substrate was selected. The molding parameters were optimized to fill the mold form well and to penetrate the fabric at the sides of the module. These parameters are the temperature of the form, which was set to 55 °C; the temperature of the hotmelt material, which was 220 °C; the molding pressure of 3 bar; the injection time of 12 seconds; and the cool time of 30 seconds.

A molding tool was developed that forms a mold cap of 3.5 mm thickness. The test vehicle was only encapsulated on the top side since the bottom side of the substrate was protected and connected to the fabric via the thermoplastic adhesive film (as explained in 5.2.3). The result is shown in Figure 7.3. The process was carried out with an Optimel OM1100 hotmelt machine.
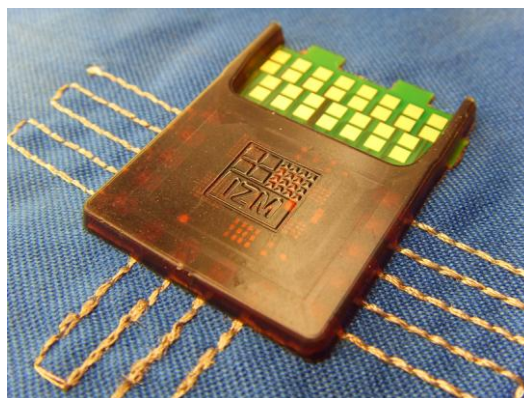
Figure 7.3: Hotmelt encapsulation covers all embroidered contacts, part of the electronic substrate and part of the fabric. The process parameters are optimized so that the hotmelt penetrates the fabric around the three sides of the module where the contacts are.

7.2.3 Local Application of Glob Top

As glob top material a two component standard epoxy adhesive with filler particles was chosen. It was dispensed with a syringe and applied to each embroidered contact of the test vehicles. It was cured at 85 °C for 90 minutes. This means the embroidered yarn loop was in its contracted state as the adhesive hardened. This should provide for a good electrical contact. An example contact is shown in Figure 7.4.
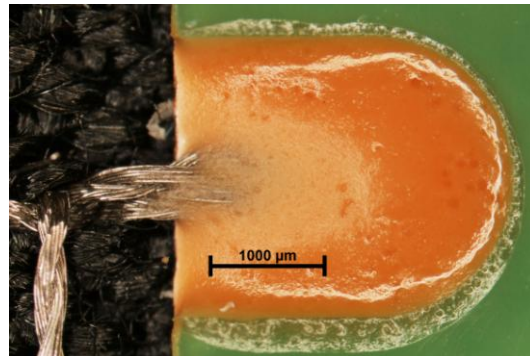
Figure 7.4:   Glob top encapsulated embroidered contact; the encapsulant is a filled epoxy adhesive that was cured at 85 °C for 90 minutes.

7.2.4 Local Application of Isotropically Conductive Adhesive (ICA)

For the ICA protection of the contacts a standard ICA was chosen. It is based on an epoxy matrix filled with silver particles. Like the glob top material, it was applied to each of the contacts with a syringe. The cure conditions were 85 °C for 180 minutes. Figure 7.5 shows an example of the result.
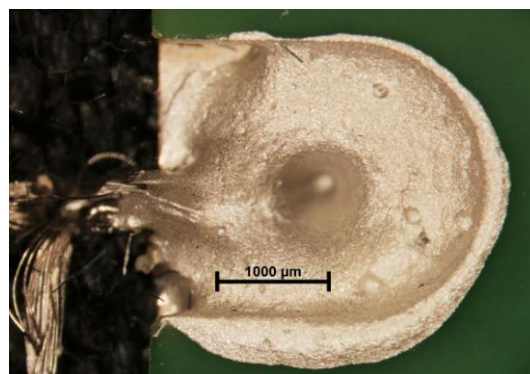
Figure 7.5:   Isotropically conductive adhesive applied to an embroidered contact and cured at 85 °C for 180 minutes.

7.2.5 Combination of Locally Applied ICA or Glob Top and Hotmelt

The test vehicles that combine glob top or ICA with hotmelt encapsulation are manufactured simply by combining the production steps in 7.2.3 or in 7.2.4 with those in 7.2.2 (in that order).

7.2.6 Adhesive Film Protection

A lamination process requires that the parts to be laminated have a flat topography. Yet, the rigid-flex test modules developed in 5.2.2 are not flat. They have cavities where the embroidered contacts are. Therefore, the fully flexible modules introduced in 7.2.1 were used instead of the rigid-flex modules.

These modules were laminated to the fabric substrate similarly to 5.2.3. The difference is that the special lamination tool for the cavities must not be used. Afterwards contacts are embroidered just like in 5.2.4. Finally the thermoplastic polyurethane film is laminated on top. It covers all contacts, a part of the module, and parts of the embroidered yarn as shown in Figure 7.6.

Rather than using a laminator a bonder was used for this last process step. It enables more complex temperature and pressure operations. First pressure was applied to the entire assembly to press the yarn onto the contact pads. Then the assembly was heated to 200 °C so the film melted and adhered to the electronic substrate and the yarn. Then the assembly was cooled to solidify the adhesive film and fix the contacts. Only then pressure was released.
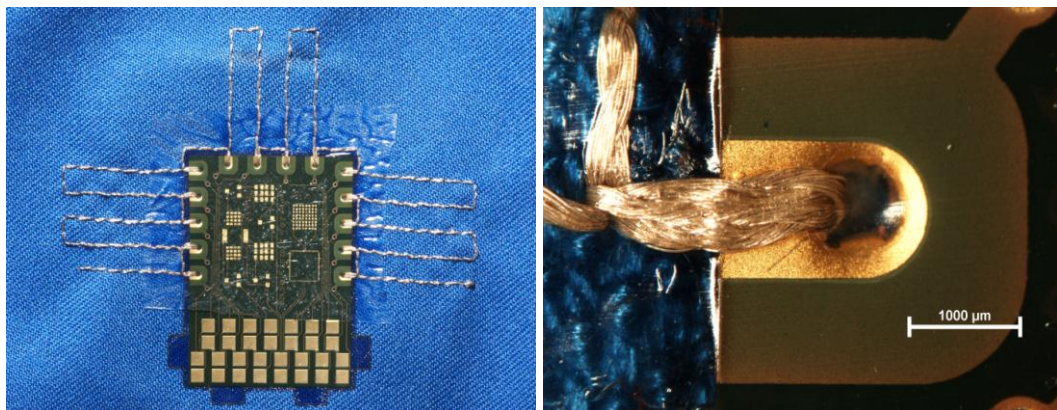
Figure 7.6:   Embroidered contacts on a thin flexible module protected with an adhesive polyurethane film.

Since in this case a thin flexible substrate was used, it needs to be protected from breaking during the wash cycling test. Therefore, a rigid FR4 board with cut-outs at the embroidered contacts was glued to the backside of the fabric after the embroidery process. Essentially, this makes it very similar to the assembly with the rigid-flex modules.

7.3 Results

After manufacturing and before stress testing, the resistances of these protected embroidered contacts were measured. Table 7.1 presents the results.

Table 7.1:   Contact resistances of samples before stress tests were performed.

Encapsulation Type	Mean	Std. Deviation	Num. of Samples
transfer molded[45]	35 mΩ	0.6 mΩ	2 gold[46]
hotmelt encaps.	301 mΩ (gold: 273 mΩ; silver: 314 mΩ)	119 mΩ (gold: 141 mΩ; silver: 106 mΩ)	14 gold, 28 silver
glob top locally	185 mΩ (gold: 169 mΩ; silver: 201 mΩ)	58 mΩ (gold: 52 mΩ; silver: 59 mΩ)	28 gold, 28 silver
ICA locally	135 mΩ (gold: 117 mΩ; silver: 152 mΩ)	68 mΩ (gold: 51 mΩ; silver: 79 mΩ)	11 gold, 11 silver
glob top loc. & hotmelt	233 mΩ	66 mΩ	14 silver
adh. ICA & hotmelt	139 mΩ	35 mΩ	14 silver
adh. film protect.	561 mΩ	521 mΩ	46 gold

During encapsulation all samples were heated to different temperatures as described in the subchapters of 7.2. As anticipated, the embroidered contacts benefited from this heat. Contracting embroidered loops, reduced the contact resistances. In this state the contacts were fixed.

The only type of encapsulation that did not follow this rule is the adhesive film protection. Although the film was applied at 200 °C the contact resistances were higher than the bare embroidered contacts. This circumstance and the very high standard deviation of adhesive film protected contacts indicate that the manufacturing process was still imperfect.

The samples encapsulated with transfer molding benefited most as the molding temperature was as high as at 175 °C. The three times stitched test vehicles encapsulated with transfer molding exhibit a much lower contact resistance than the four times stitched embroidered contacts without encapsulation.

---

[45] remember: the transfer mold encapsulated samples were stitched three times

[46] only two contacts were measured at a sufficiently high accuracy to measure such a low resistance correctly; plots of these two contacts during temperature cycling are shown in appendix A.5; additionally to these two contacts, four more transfer mold samples were exposed to thermal cycling; furthermore 28 samples were measured during washing; however the precision of the measurement of these was only sufficient to tell whether the contact degraded but not to measure precise contact resistances.

The conductive adhesive improves the conductivity further, which is why ICA protected contacts performed better than glob top protected ones.

Some contacts were manufactured in two metallization variants. Again, the gold pads performed better than the silver pads, suggesting there is a resistant film on the silver pads.

These test vehicles either were exposed to 1025 temperature cycles or to 20 wash cycles. The following tables present the results achieved with the differently protected embroidered contacts. Each protection type is discussed separately below these tables. Plots of samples can be found in Appendix A.5 and B.3.

Note: the 1025 cycles were composed of 25 slow cycles as presented in Figure 5.9 followed by 1000 fast cycles. The latter omitted the room temperature isothermal line and therefore each cycle took only an hour rather than two hours.

Table 7.2:   Failures during 1025 temperature cycles at three different failure conditions: contact resistance rose at least once above 1 Ω, 10 Ω or 100 Ω

Type	1 Ω		10 Ω		100 Ω	
transfer molded[47]	0 %		0 %		0 %	
hotmelt encaps.[48]	79 %		36 %		36 %	
glob top locally[49]	0 %		0 %		0 %	
ICA locally[50]	0 %		0 %		0 %	
glob top loc. & hotmelt[51]	0 %		0 %		0 %	
ICA loc. & hotmelt[52]	0 %		0 %		0 %	
adh. film protect.[53]	10 %		10 %		10 %	

---

[47] transfer mold samples: 6 contacts on gold pads; even with a failure criterion of 0.1 Ω no contact failed during 1025 cycles.

[48] hotmelt samples: 14 contacts on pierced silver pads

[49] glob top applied locally to contacts; samples: 13 on pierced gold pads; 14 on pierced silver pads

[50] ICA applied locally to contacts; samples: 5 on pierced gold pads; 5 on pierced silver pads

[51] glob top appl. locally to contacts & then hotmelt appl. to entire module: 7 samples on silver pads

[52] ICA appl. locally to contacts & then hotmelt appl. to entire module: 7 samples on silver pads

[53] adhesive film laminated over the embroidered contacts: 20 samples on pierced gold pads

Table 7.3:   Failures during 20 washing cycles at three different failure conditions: contact resistance rose at least once above 1 Ω, 10 Ω or 100 Ω

Type	1 Ω		10 Ω		100 Ω	
transfer molded[54]	0 %		0 %		0 %	
hotmelt encaps.[55]	0 %		0 %		0 %	
glob top locally[56]	4 %		0 %		0 %	
ICA locally[57]	33 %		0 %		0 %	
glob top loc. & hotmelt[58]	0 %		0 %		0 %	
ICA loc. & hotmelt[59]	0 %		0 %		0 %	
adh. film protect.[60]	96 %		64 %		44 %	

Table 7.4:   Other aspects connected to the technology

Type	Issue	Failure Rate	
transfer molded	embroidered yarn outside the package loses conductivity entirely during the first few washing cycles	100 %	

7.3.1 Transfer Mold Protection

As expected the transfer molding protected the embroidered contacts very well. Even if a failure is defined as a contact resistance rise above 0.1 Ω, no failures occurred during 1025 temperature cycles or during 20 washing cycles. Yet – also as anticipated – the transfer molding process harms the embroidered yarns outside the package. This led to total loss of conductivity after the first few washing cycles. During temperature cycling the yarn did not behave differently than yarn that has not seen these high temperatures and high pressures. So, if the stress condition is temperature cycling, the yarn does not seem to be affected by this process step. This means, transfer molding is not a suited technology for stabilizing embroidered contacts, if wash cycling stress must be considered.

---

[54] transfer molded samples: 28 on pierced gold pads; stitched 3x
[55] hotmelt samples: 14 on pierced gold pads; 14 on pierced silver pads
[56] glob top applied locally to contacts; samples: 14 on pierced gold pads; 14 on pierced silver pads
[57] ICA applied locally to contacts; samples: 6 on pierced gold pads; 6 on pierced silver pads
[58] glob top appl. locally to contacts & then hotmelt appl. to entire module: 7 samples on silver pads
[59] ICA appl. locally to contacts & then hotmelt appl. to entire module: 7 samples on silver pads
[60] adhesive film laminated over the embroidered contacts: 25 samples on pierced gold pads

7.3.2 Hotmelt Encapsulation

During wash cycling hotmelt encapsulation protected the embroidered contacts well – no failures occurred. Yet, it performed weak during temperature cycling. Apparently, the encapsulation seems to have generated a new failure mechanism. The failures were no longer limited to low temperatures as Figure 7.7 shows. Considering the 1 Ω failure condition, seven of 14 contacts failed just at the high temperature. Further four contacts showed failures that were more or less equally distributed over the whole temperature range. Three contacts did not fail over 1025 cycles. The most likely cause for these failures is the high CTE mismatch of the hotmelt material and the electronic substrate. During thermal cycles this probably led to movements at the contact resulting in contact force changes and thus in contact resistance changes. This means hotmelt encapsulation alone is not an appropriate protection for embroidered contacts.
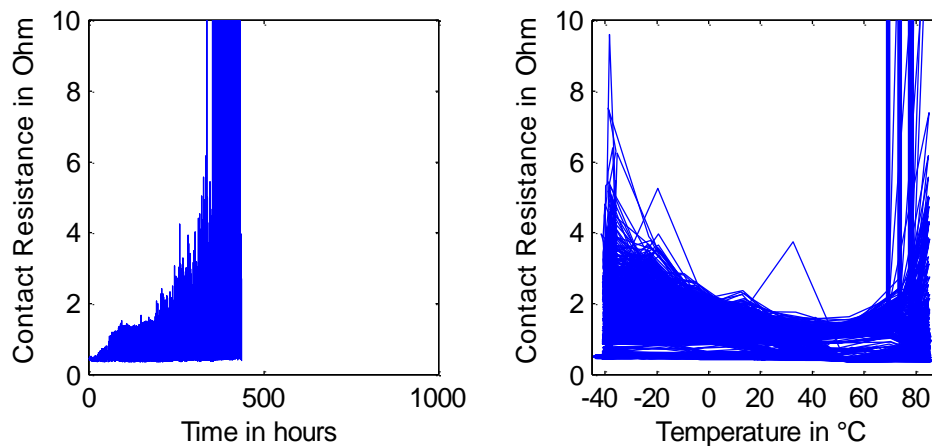
Figure 7.7: Hotmelt encapsulated embroidered contacts tend to fail also at the high temperature. 1025 cycles were run. Yet for better intelligibility only 450 cycles are shown here. The remaining cycles exhibit also failures in the mid temperature range making the right plot an indistinguishable blur of data. The full plot is shown in Appendix A.5. (ID: HM53AgPiercedPad02\474)

7.3.3 Local Application of Glob Top or Local Application of ICA

The local application of ICA or glob top to the embroidered contact both protected the contact well during temperature cycling – no failures occurred. However, during wash cycling some contacts rose above 1 Ω. After 20 wash cycles an optical inspection showed that those samples with conductive adhesive that failed the 1 Ω criterion, in all cases exhibited cracks in the conductive adhesive near the edge of the substrate. Figure 7.8 shows an example. This edge represents the transition from hard substrate to soft fabric. Potentially these cracks may be prevented by redesigning the contact so that the adhesive is not in this transitional area but in the rigid environment of the substrate only. The one glob top sample that failed the 1 Ω criterion looked unchanged after 20 wash cycles.
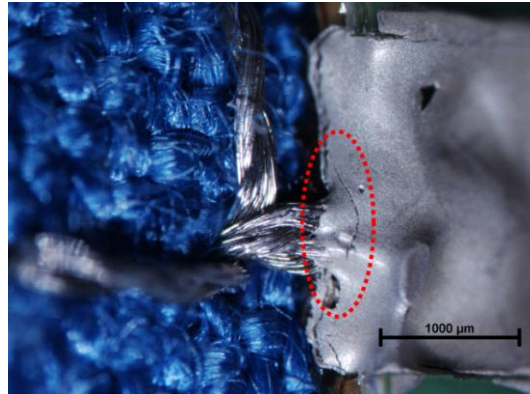
Figure 7.8:   Contacts that failed the 1 Ω criterion during washing exhibited cracks near the edge of the substrate. This picture was taken after 20 wash cycles. This particular contact here rose to 8.5 Ω after 20 wash cycles.

7.3.4 Combination of Locally Applied ICA or Glob Top and Hotmelt

By combining ICA or glob top with hotmelt encapsulation, the reliability issues of each individual technology could be overcome. The local application of adhesive – conductive or non-conductive – protected the contact well. The curing process at elevated temperature of 85 °C reduced the contact resistance and did not harm the yarn itself. The hotmelt then protected the sensitive hard-soft transition area. No failures occurred during 1025 temperature cycles or 20 washing cycles.

7.3.5 Adhesive Film Protection

Embroidered contacts protected with adhesive film did not perform well during both reliability tests, as could be expected from the high initial resistances and the high initial variance. Like the hotmelt encapsulation, the adhesive film developed a new failure mechanism letting the contacts fail also at the high temperature as the example in Figure 7.9 shows.

The cause of this is not sure. Delamination of the adhesive film from the gold pad was suspected but could not be proven with optical or cross sectional analysis.

It may well be that this approach could protect the contact with a different film material.
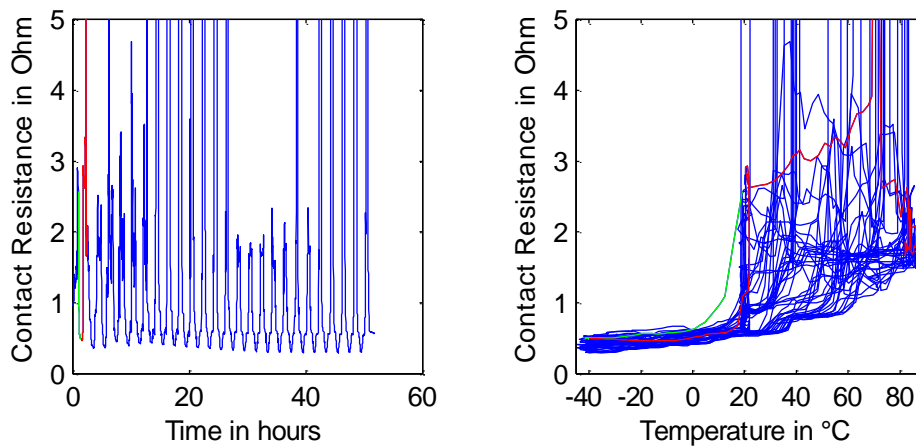
Figure 7.9: The plot shows the adhesive film protected embroidered contact that failed earliest. The failure occurs at the high temperature. During the following thousand cycles the contact will also fail at other temperatures as can be seen in Appendix A.5. (ID: AF51AuPiercedPad09\312)

7.4 Conclusion

It was shown that protecting the embroidered contact can be achieved by combining local application of adhesive – conductive or non-conductive – and hotmelt encapsulation. This way the contact survives realistic textile typical stress. If the contact pad is redesigned, locally applied adhesive could be sufficient for a reliable contact. In this case the hotmelt encapsulation process could be omitted.

However, even if the hotmelt process can be economized, the manufacturing efficiency of embroidered contacts is still lower than initially intended. Therefore, the following chapter shall discuss an alternative approach to contacting embroidered circuits. Instead of embroidering a contact and then enhancing it with adhesive to make it reliable, it just uses adhesive to hold the contact members together. So the contact mechanism is not enhanced but replaced by a new mechanism, which is the adhesive compression.

8 Alternative Approach based on Adhesive Bonding

In microelectronics integration, adhesive technologies have long been used for making contacts. During the so called NCA flip chip bonding process, a bare die chip[61] is glued to a circuit on a substrate. The process is illustrated in Figure 8.1. First, the low viscous adhesive is applied to the substrate with a syringe. Typically a thermosetting adhesive like epoxy is used. Second, the chip is pressed onto the substrate to make the chip-bumps touch the pads on the substrate and create electrical contacts between them. At the same time, temperature is applied to cure the adhesive. Finally, the bond force and temperature are released. NCA stands for non-conductive adhesive. The purpose of this adhesive is to hold the contact members together and this way provide for a permanent contact.
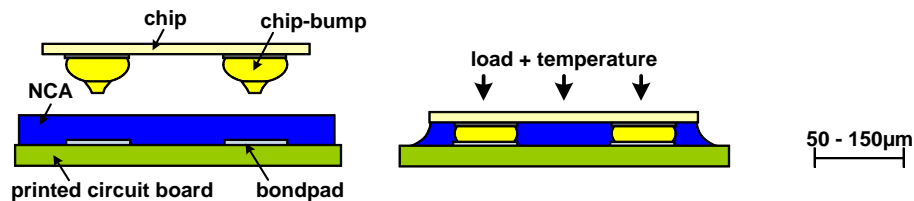
Figure 8.1:   Flip chip bonding process with non-conductive adhesive (NCA) [51]

In the framework of this thesis, it was investigated whether this technology could be adapted to electronics-in-textiles. In this case, an electronic module is bonded to a fabric with embroidered circuits creating electrical contacts between the conductive yarns and the contact pads of the module as shown in Figure 8.2. Also here, the adhesive serves holding the contact members permanently together.
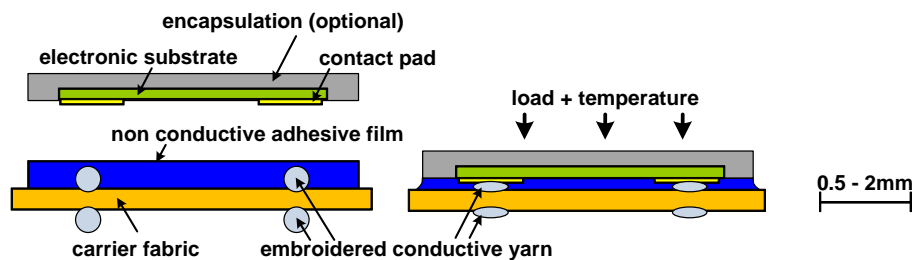
Figure 8.2:   Adhesive bonding applied to electronics-in-textiles: an electronic module is bonded to a fabric circuit with embroidered conductive yarn (with top and bottom thread). [51]

---

[61] a bare die chip is a silicon chip as cut from the wafer without housing

8.1 Fundamental Considerations

In flip chip bonding, the contact mechanism is based on the adhesive compression acting on the contact interfaces and leading to a-spots between the contact members. The compression is introduced by the bonding force and is further enhanced by the curing shrinkage[62] and thermal shrinkage[63] of the adhesive itself. After bonding the compression is kept up by the adhesive, which is why high modulus adhesives with little tendency to relax over time are preferred. A-spots develop particularly well, when at least one contact member is soft, which is why the gold bumps are often annealed at elevated temperature to make them softer. Contact failures primarily derive from adhesive delamination from the interfaces or from cracking of the adhesive.

In electronics-in-textiles assemblies one contact member – the embroidered circuit – is naturally very soft. This reduces the need for a strong compressing force and thus enables the use of all kinds of adhesives, even such with low moduli as long as they do not relax over time. Therefore, in this thesis, different thermosetting and thermoplastic types were considered as NCA adhesive.

Besides their particularly high strength, the advantage of thermosetting adhesives is that they can be processed with fairly simple tools. This allows using such for do-it-yourself projects, which is described in Appendix D.1. The advantage of thermoplastic adhesives is that they are repairable. However, the use of thermoplastic adhesives requires a more complex temperature profile:

- first the mechanical load is applied to the assembly stack consisting of the fabric circuit, the thermoplastic adhesive film and the electronic module
- then the whole assembly is heated above the melting temperature where the adhesive becomes low viscous; the mechanical load squeezes the adhesive to the sides and into the fabric allowing the embroidered yarn and the contact pad on the module to touch and form an electrical contact
- then the whole assembly is cooled below melting temperature, while the mechanical load is kept constant; the adhesive solidifies and holds the contact members together permanently
- finally the mechanical load can be released

A second advantage of thermoplastic adhesives materializes when the application requires that the embroidered yarn in the final system is electrically insulated towards the environment which is often demanded. In this case, rather than using an amorphous or semi-crystalline thermoplastic, a thermoplastic *elastomer* should

---

[62] most thermosetting adhesives tend to shrink when they are cured; in contrast thermoplastic adhesives do not cure and therefore do not exhibit curing shrinkage;

[63] thermal shrinkage occurs when the flip chip assembly cools down from bonding temperature to ambient temperature;

be used. The latter can be applied to play the role of the non-conductive adhesive for bonding the contacts and furthermore can be applied to insulate the yarn even outside of the contacting area. Due to its high elasticity and low modulus such an insulator will not significantly compromise the textile character of the fabric substrate. During the bonding process this insulator will simply be squeezed out of the contacting area like the non-conductive adhesive. Outside of the contacting area, the insulator will stay unchanged and continue to serve its function as insulator of the conductive yarn. [**130**]

This thermoplastic elastomer insulator can be applied as a film over the entire embroidered circuit or can be applied to the yarn prior to the embroidery. The latter, however, requires the use of soutache embroidery (refer to 2.1.4) as these yarns are too thick for top-stitch embroidery.

Of course, one could combine the highly durable thermosetting non-conductive adhesive with the thermoplastic elastomer insulator of the embroidery yarn. The bonding process would melt away the insulator and cure the thermosetting adhesive. However, this would lead to complex interfaces between thermoplastic elastomer and thermosetting adhesive. A golden rule of packaging is to keep the number of interfaces as low as possible to keep the assembly simple and its behavior predictable, so in case of reliability problems one can find the source of failure with reasonable effort. Therefore, combining the two was not considered an option for experiments in this thesis.

Still, being able to contact insulated conductive embroidery in one simple process is very intriguing. Most other contacting technologies require either that the insulator is locally removed prior to contacting or that the conductor is initially not insulated at all but is insulated after contacting. Both require at least one additional process step. Therefore, in this thesis, to benefit of all the advantages that potentially come with the adhesive approach, it was chosen to opt for a thermoplastic elastomer for making the bonded contacts and for also insulating the embroidered circuit prior to bonding.

Besides this in-depth analysis of the approach with a thermoplastic elastomer in this chapter, Appendix D.2 assesses the reliability of adhesively bonded contacts with a thermosetting adhesive. As it turns out the results are similar.

8.1.1 Choosing an Adhesive

As thermoplastic elastomer adhesive (and insulator) a high melting thermoplastic polyurethane (TPU) film was selected. It melts between 155 °C and 170 °C. In fact, this material is the same as was used for gluing the embroidered contact test vehicle to the fabric, and as used for protecting the embroidered contact as explained in chapters 5.2.3 and 7.2.6 respectively.

The objective behind choosing such a high melting adhesive was to provide a good stability in the application range which is below +85 °C as defined by the selected temperature cycling test in 5.3.1. And in fact, this is the case as Figure 8.3 shows. It presents the viscoelastic behavior of this polyurethane adhesive. At 85 °C, over a large time domain the modulus is relatively constant and viscous flow will not appear in significant amount of time. In contrast, at application temperatures as high as 125 °C or 150 °C the modulus quickly drops in the order of hours or seconds respectively.

To make these plots the modulus was measured according to 3.3.1.5 with frequency scans between 0.1 to 25 Hz at temperatures between -60 and +200 °C. Then these modulus curves vs. frequency were shifted parallel to the frequency axis to make the curves fit according to the time-temperature shift as explained in 3.3.1.6. The reference temperature of the master curve was chosen to be 145 °C. This master curve and the resulting time-temperature shift function were used to calculate the moduli at the three temperatures presented in Figure 8.3. A *Tritec 2000B* dynamical mechanical analyzer was used as measurement equipment.
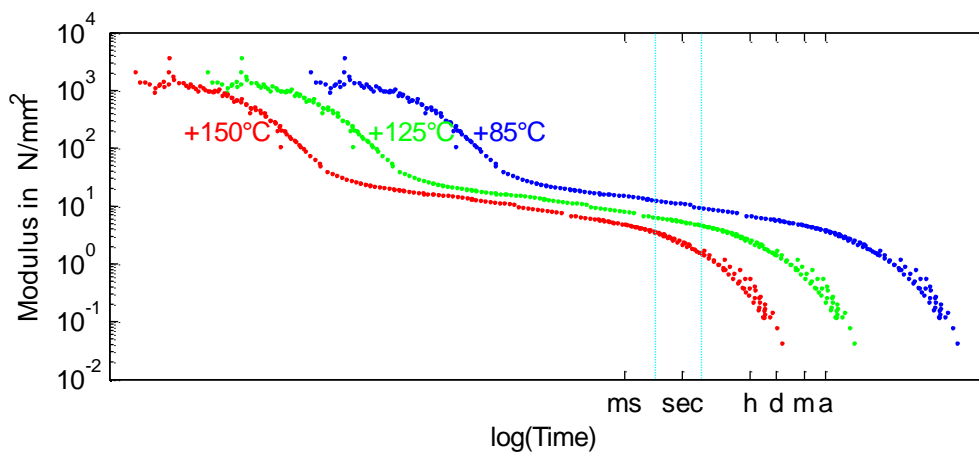
Figure 8.3:   Modulus curves of the thermoplastic polyurethane adhesive (and insulator) at different temperatures. The cyan lines highlight the limits of the experimental window of the DMA frequency scan from 0.1 to 25 Hz.

8.1.2 Providing Adhesion

Besides thermal stability within the application temperature range, a good adhesion of the adhesive to the surfaces of the contact members is important for a reliable contact. These surfaces are the finishing layer and the contact material on the electronic module and the fabric. While the adhesion was known to be good on the fabric, intensive peel tests were performed to find the optimal bonding pressure and temperature for best adhesion on the finishing layer and the contact material. As typical finishing materials, an epoxy solder resist and a polyimide solder resist

was investigated. As typical contact material, copper with a silver coating was investigated, as it is expected that TPU adheres better to silver than to gold. [51]

According to the results of these peel tests the adhesion of the TPU is very good on the polyimide film. At optimal bonding conditions the peel test according to EN 60249 reached an average peel strength of 6.5 N/mm. As comparison: the required minimum value for copper clad on FR4 is 1.4 N/mm. The peel strength of the TPU on the epoxy solder resist was rather weak with only 1 N/mm. [51]

The adhesion of the TPU on silver was so weak that the effort of quantifying this with peel tests was not made. Instead a work around was developed that took advantage of the observation that TPU adhered very well on the FR4 base material. Instead of having a fully metallized contact surface, a contact surface was developed that consisted of a mesh of silver coated copper featuring open areas of FR4 base material as shown in Figure 8.4. Peel tests on such a silver coated copper mesh reached an average value as high as 6.3 N/mm. [51]
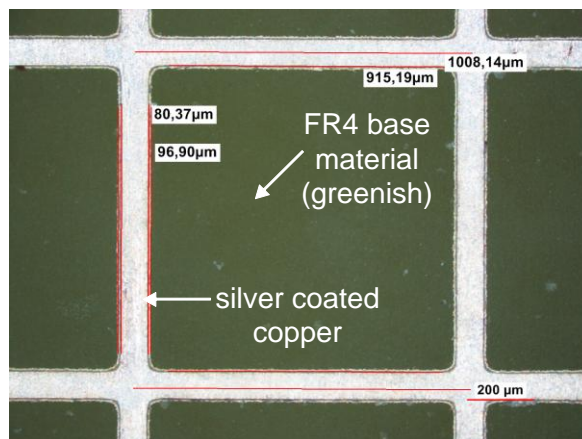
Figure 8.4: Contact surface with meshed silver coated copper on FR4 base material providing that the thermoplastic polyurethane adheres well to the contact surface. [131]

8.2 Development of Test Vehicles

To test the actual reliability of adhesively bonded contacts with the just selected thermoplastic elastomer, I initiated and supervised the diploma thesis of Malte von Krshiwoblozki to develop test vehicles and carry out stress tests. The just mentioned peel tests were also carried out by him. [131]

8.2.1 The Electronic Test Module

The electronic test module was made of standard FR4 base material of 460 µm thickness. Following the results of the peel test, the contact pads were designed as a mesh of silver coated copper. This is important as the adhesion must be very

good in the vicinity of the contacts to prevent contact failures. As finishing layer, polyimide solder resist film was applied over the entire surface except over the meshed contact pads. The test module was made round to prevent peeling at corners; it has a diameter of 30 mm. The test vehicle is shown in Figure 8.5 from the bottom side and in Figure 8.6 (left) from top. Thereby 'bottom' identifies that side that will face the fabric with the embroidery circuit to be contacted. [51]

The test module has five contact pads. Together with the embroidery design on the fabric these contact pads will permit precise four-wire measurements of the contact resistances. The design is such that feeding resistances are excluded.
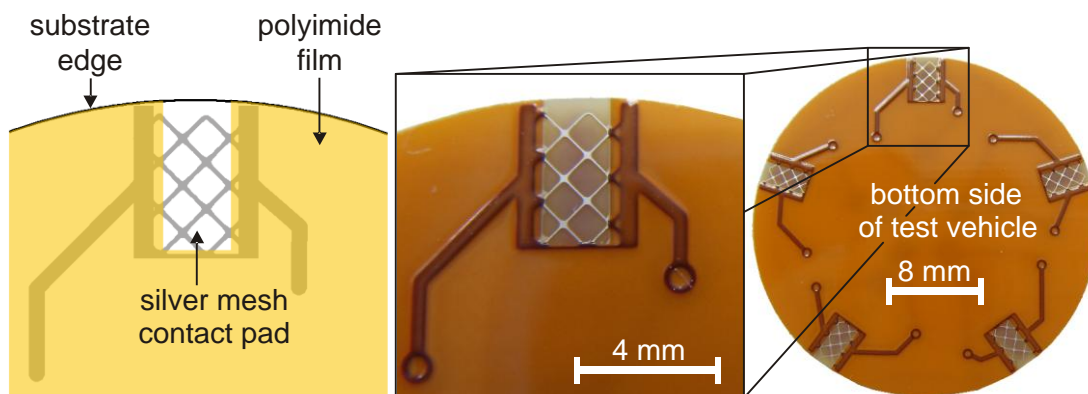
Figure 8.5:   Test vehicle with meshed contact pads of silver coated copper and with polyimide film finishing layer – both providing that the thermoplastic elastomer adheres well on the test vehicle. [51]

8.2.2 The Embroidered Test Circuit

To provide a good comparability to the embroidered contacts, the test circuit was embroidered twice – one over the other. *Shieldex* was applied in the needle and in the bobbin. The embroidery design is shown on the right in Figure 8.6 with an overlay of the bottom side of the electronic test module.

After embroidery, a 100 µm thick film of the TPU was laminated on top and bottom side of the fabric (i.e. the shiny part of the black fabric in Figure 8.6). This serves as electrical insulator and as protection. The later is required as the yarn is heated to 195 °C during the bonding process. According to 3.2.3 and 3.2.4., such heating leads to a significant resistance rise during washing if the yarn is not protected with a polymer film.

The embroidery and the lamination were carried out with the same equipment that was used to make the embroidered contact test vehicles in chapters 5.2.3 and 5.2.4.
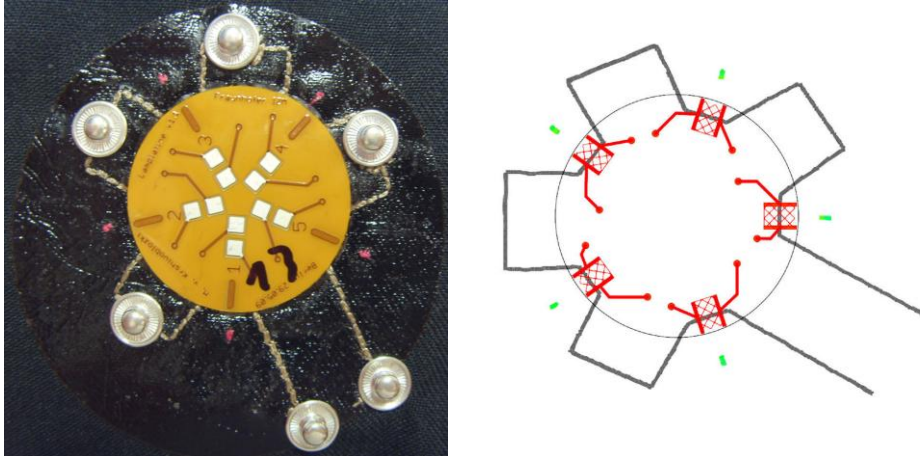
Figure 8.6:   Test vehicle: electronic test module bonded to embroidered test circuit on fabric (left); design of embroidered circuit with an overlay of the bottom side of the test module (right). [51]

8.2.3 The Bonding Process

For the bonding process an additional TPU film of 100 µm thickness was placed between the fabric circuit and the test module. So, together with the insulator film on the fabric circuit the total film thickness was 200 µm. This was done since the peel tests had suggested that adhesion could be better if more polyurethane was available for penetrating the fabric. Then the bond force of 0.7 N/mm² was applied and the assembly was heated to 195 °C. The temperature was held for 30 seconds. Then it was cooled at least until the temperature dropped below 100 °C to be well below the viscous low phase of the adhesive. Then the bond force was released. [51]

For this process relatively expensive equipment was used: a flip chip bonder *FC150* by *SÜSS MicroTec*. The advantage for this research-purpose is that the temperature and the pressure can be controlled very precisely and that the tools are highly coplanar. For manufacturing purpose a lower cost alternative will have to be found.

Figure 8.7 shows a cross section of a resulting contact. The magnification reveals a contact between a *Shieldex* fiber (also sectioned) and a metal strip on the substrate.
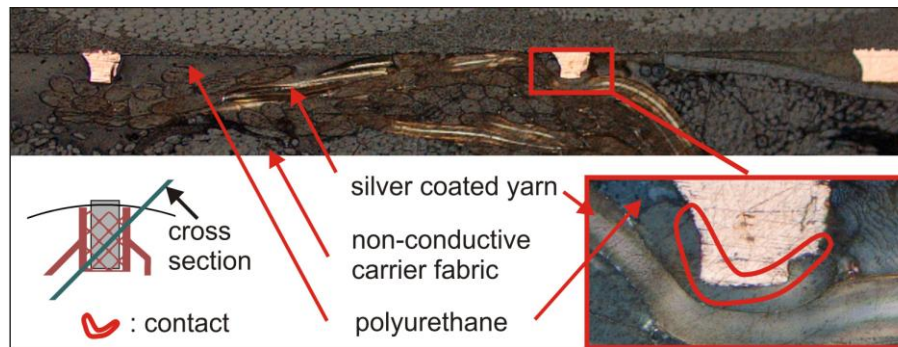
Figure 8.7:   Cross section of adhesively bonded contact showing the electronic substrate with the meshed metal pad contacted to the embroidered yarn on the fabric below. [51]

8.3 Contact Resistance of Adhesively Bonded Contacts

In total, 15 such test vehicles were built, i.e. 75 adhesively bonded contacts. Prior to exposing them to stress their contact resistances were measured. These were much lower than the resistances of all previously discussed embroidered contacts as Table 8.1 reveals. This must be partly due to the fact that these adhesively bonded contacts could be designed in such a way that only the constriction resistance was measured and feeding resistances were excluded. This was not possible in the case of embroidered contacts. Yet, this cannot be the only explanation for such low contact resistances as a comparison to the simplified model shows. The resistance of the simplified model is approximately ten times higher than that of the adhesive contact. Yet, the contact area of adhesive contacts is practically much smaller due to the meshed structure of the contact pad. This means the contact pressure must be much higher with adhesive contacts than with embroidered contacts.

Despite presumably high contact pressure, the standard deviation in Table 8.1 seems high. This can be explained with manufacturing variances. Due to the meshed structure of the pad, small changes in the positioning of the pad versus the embroidered yarn may have a significant impact on the contact resistance.

Table 8.1:   Contact resistances of adhesively bonded samples before stress tests were performed. Calculated from data extracted from [131].

Type of Contact	Mean	Std. Deviation	Num. of Samples
adhesively bonded contact	28.3 mΩ	14.7 mΩ	75

To best appreciate what this contact resistance value of 28.3 mΩ means, chapter 2.3.1 shall be recapitulated. In that chapter, different application scenarios were considered, to identify requirements on contacts for electronics-in-textiles. Power applications set the highest demand on the contact resistance. For the exemplary

10 x 10 LED matrix display the required contact resistance was roughly estimated to 30 mΩ or lower. This means, adhesively bonded contacts are definitely applicable even for power applications.

8.4 Reliability of Adhesively Bonded Contacts

Beyond their low contact resistance adhesively bonded contacts also turned out to be very reliable. Three tests were applied: the temperature cycling test, the wash cycling test and a humidity test.

The humidity test was added here since it is known for being the most harmful condition to adhesive contacts e.g. to NCA bonded flip chips. The applied test conditions followed the recommendation of the *JESD22 A101 B* industry standard for electronics, which foresees applying 85 °C at 85 % rel. humidity for 1000 hours [53]. The test vehicles' four-wire contact resistances were measured regularly outside of the humidity chamber as suggested by the test standard.

Each of the three tests was carried out with 5 test vehicles, i.e. 25 contacts per test. Throughout all three tests the contacts were very stable as Figure 8.8 shows for a typical contact during temperature cycling, and as Figure 8.9 shows for average values and standard deviations measured during the humidity test (left) and during the wash cycling test (right). Furthermore, the summarized result in Table 8.2 shows that even if the failure criterion is set to a value as low as 0.1 Ω, no failures occur.
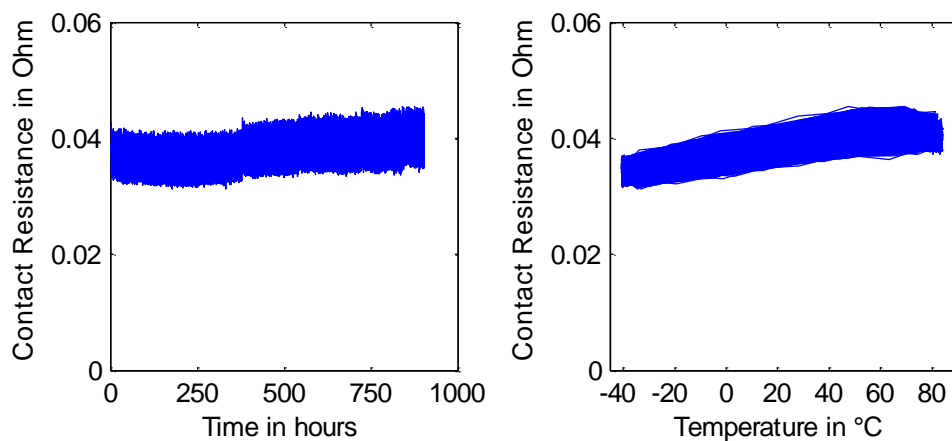
Figure 8.8:   Typical plot of contact resistance of adhesively bonded contact during the temperature cycling test. Test condition: 1000 cycles at -40 °C / +85 °C. (ID: AC05AgMeshedPad05\25) Data from [131].
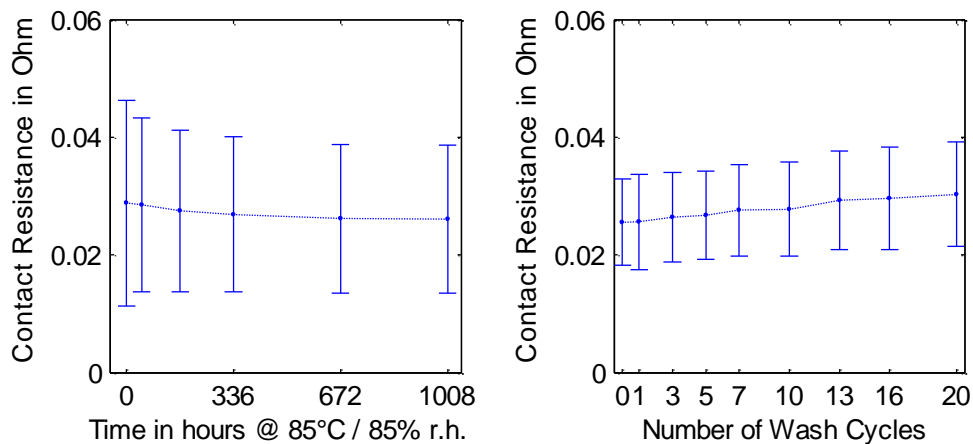
Figure 8.9:   Mean contact resistance and standard deviation of adhesively bonded contacts during reliability tests: humidity test (left) and wash cycling test (right). The total sample number per test was 25 contacts. Data from [131].

Table 8.2:   Failures of adhesively bonded contacts during different stress tests at the following failure condition: contact resistance rose at least once above 0.1 Ω. Calculated from data extracted from [131].

Type	0.1 Ω		Num. of Samples
1000 temp. cycles at -40 °C / +85 °C	0 %		25
20 washing cycles at 40 °C	0 %		25
1000 hours humidity at 85 °C / 85 % rel. hum.	0 %		25

One test vehicle of those exposed to 1000 temperature cycles was exposed to additional temperature cycles of more severe conditions. The objective was to compare the actual reliability to the expectations raised by the considerations about the modulus curves in Figure 8.3. For this purpose additional 1000 cycles at -55 ° / +125 °C and subsequently 500 cycles at -65 °C / +150 °C were run. These tests were run according to *JESD A104 C* test conditions *B* and *C* respectively [52].

Figure 8.10 shows the contact resistance of a typical contact. More plots are shown in Appendix A.5.7. During the test with a maximum temperature of 125 °C, the contact resistance already rises notably. The maximum resistance value attained was 298 mΩ in one of the samples. During the test with a maximum temperature of 150 °C, the resistance rise is faster and much more pronounced reaching a maximum value of 870 mΩ in one of the sample. As explained above, at these temperatures the adhesive becomes soft within short periods of time. This lets the adhesive compression drop which reduces a-spots. If these tests were combined with mechanical stress, the contacts would probably disrupt or the modules would even detach from the fabric.

This result demonstrates the value of the master curve for estimating the stability of an adhesive under different temperature conditions.
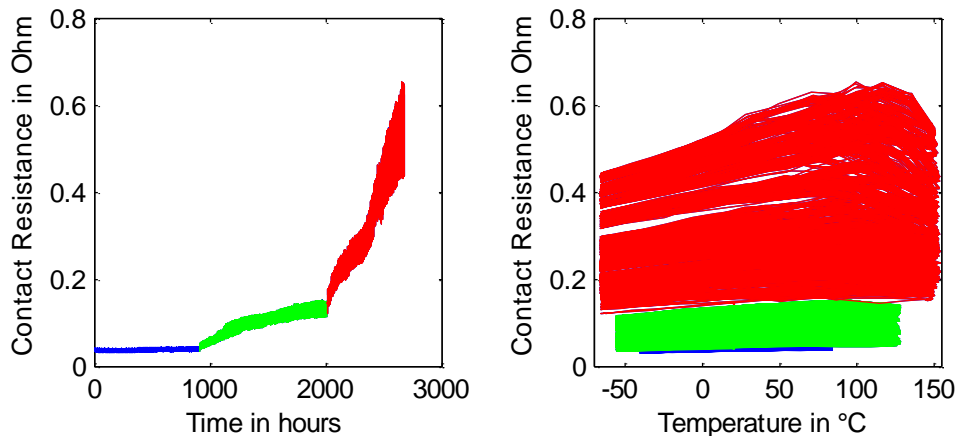
Figure 8.10: Contact resistance during temperature cycling test of a typical sample of an adhesively bonded contact. 1000 cycles at -40 / +85 °C (blue), 1000 cycles at -55 / +125 °C (green), 500 cycles at -65 / +150 °C (red) (ID: AC05AgMeshedPad05\114)

8.5 Applications beyond Embroidered Circuits

Another advantage of this adhesively bonded contact lies beyond the scope of this thesis. The technology is very versatile. It is not limited to contacting printed circuit boards (PCBs) to embroidered conductive yarn, but may also be applied for contacting other electronic components or modules to other fabric circuits. This may eventually solve the contacting issue of many electronics-in-textiles applications. On the electronics side, elements like the following could be applied:

- single components – with or without special housing [130],
- rigid PCBs (like in this chapter),
- flexible PCBs [48], or
- stretchable PCBs [56], [57]

Prior to adhesively bonding these different PCB substrates to fabric circuits, electronic components can be assembled onto these with standard processes and may be encapsulated, if necessary.

On the fabric side, almost any type of fabric circuit may be applied. Such are circuits created:

- by embroidering conductive yarns (like in this chapter),
- by weaving conductive yarns [67], [132], [133],
- by printing conductors [67], [134], [135],
- by laser-cutting conductive fabrics [15], [51], [67], or
- by knitting fabrics with conductive yarns [136], [137], [138]

Of course, like the embroidered yarn, all these fabric circuits may be electrically insulated with a thermoplastic elastomer, prior to the bonding process. The bonding process will melt this insulator locally and squeeze it out of the contacting area, but will leave the insulator intact outside of this area. From a manufacturing point of view this is very simple and efficient – compared to having to remove the insulator in a separate step or having to apply the insulator after the contacting process.

An exemplary application that makes use of the adhesively bonded contact technology is an EMG sensor that was developed in the *EU* project *ConText*. The sensor measures an electromyogram (EMG) which is the electric signal coming from motor neurons controlling muscle activity. There are two features which make this implementation special: firstly, the sensor is integrated into a vest i.e. it is textile integrated, and secondly it measures the EMG capacitively i.e. the sensing does not require a direct body contact. My part in the project was to develop the packaging of the amplifier module, to develop textile sensors and to contact the amplifier to the textile sensor and the textile wiring.

The EMG sensor consists of two capacitive electrode disks connected to amplifiers. Each of these electrodes builds a capacitor with the body of the wearer, thus coupling the bio-potential to the amplifier. However, the capacitance between body and electrodes is very small leading to high input impedances. As such are very sensitive to picking up noise, four provisions were taken to reduce artifacts. Firstly, the amplifiers were placed close to the sensor disks to convert the high impedances to low impedances. Secondly, to prevent that the electrodes capacitively pick up noise from the environment, a guard disk was placed over each electrode side facing away from body i.e. facing to the environment. These guard disks have to be very well insulated from the electrode disk and are kept at the same potential as the electrodes to provide an active shielding. Thirdly, by having two electrodes, a differential amplification can be applied for a further reduction of noise. Fourthly, the amplifiers are entirely shielded from the environment. [139]

The application and the textile integrated system were first presented in 2007 in [11] and [16] respectively. In these publications, the sensor was still implemented with embroidered contacts as shown in Figure 1.2 in the motivation. This implied that also the capacitive electrodes, the guard disks and the wiring to the amplifier for power supply and output signal had to be implemented with embroidered conductive yarn. While this was not an issue for the wiring of the amplifier, it was an issue for the electrodes and the guards. It was not possible to insulate the electrodes from the guards as much as was needed (>50 GΩ). Furthermore, the requirement that the amplifier module had to be shielded made the manufacturing flow relatively complex as the shielding had to be done after embroidering the contacts.

Therefore, a new implementation based on the adhesively bonded contacts was developed. The exploded assembly drawing and an image of this EMG sensor are shown in Figure 8.11. As the bonding process is the last step in the whole process flow, all elements could be manufactured separately – even in separate organizations. The electrode-guard construction was manufactured by laser structuring conductive and insulating fabrics and then laminating them together. The wiring was implemented as a woven ribbon with conductive yarns (although this could also have been implemented with embroidery). Both – the electrode-guard construction and the wiring – were laminated onto a base fabric (i.e. the triangular dark blue fabric patch in the image). The amplifier module consisted of a thin printed circuit board with the amplifier and other components assembled on it. This module was encapsulated by transfer molding and then shielded entirely, except at the contact pads on the bottom side of the module. Then, the amplifier module was bonded with a polyurethane adhesive to the base fabric, thereby creating electrical contacts with the wiring and electrode-guard construction. Finally the sensor patch was integrated into the vest by sewing.
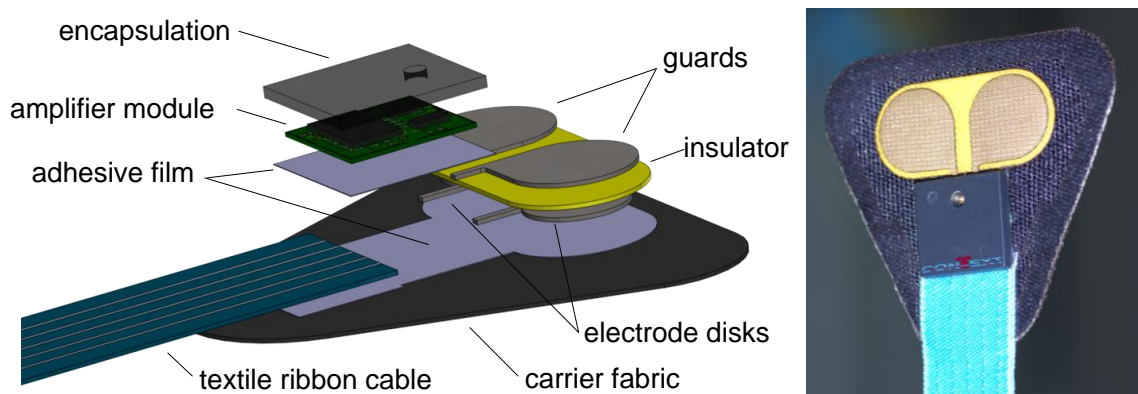
Figure 8.11: EMG Sensor developed in *ConText*: Exploded assembly drawing (left) and picture of sensor (right).

This exemplary application shows well the power of the adhesive bonding technology: it enables the contacting between very different electronics-in-textiles components and puts developers in the position to choose freely the best technology for manufacturing each of these components.

9 Outlook

In this thesis, the contact mechanism of embroidered contacts was analyzed, and it was shown how these contacts can be encapsulated to be reliable in a textile typical environment. The embroidery process and the encapsulation process(es) are potentially suited for volume production. Both processes are widely used in the industry. However, the embroidery process is currently only applied in the textile industry, and the encapsulation process is currently only applied in the electronics industry. For this thesis, the alignment of the contact pads and the embroidery pattern was done manually, and the encapsulation of the test module was done with lab scale processes on a small piece of fabric. In practice, however, this alignment step may have to be automated and the fabrics are large and therefore, tools for the encapsulation need to be adapted. Depending on the production scale and location, some process steps may remain manual.

Another technical aspect that remains to be developed is the electrical insulation of the embroidered tracks to prevent short circuiting. Manual solutions were presented by Leah Buechley in [15], while researchers at *TITV* are currently working on automated processes. A polymer insulation probably provides the best protection. However, for some applications (e.g. circuits on the lining of a jacket [4]) embroidering over the conductive track with a non-conductive thread may be sufficient.

Cost calculations for embroidered circuits and contacts were not part of this thesis. However, this is essential to raise their attractiveness for the business world. The costs depend on many factors such as production volume, number of elements per product, cost of each element, applicable rationalization and production location. The question is also how the cost compares to alternative approaches like the adhesive contact presented in the previous chapter.

The adhesive contact currently receives a lot of attention from industry. The simplicity of the approach seems to be very appealing. A great advantage is that it can contact insulated conductors without having to remove the insulator in a separate process step. Moreover, the technology is very versatile. It is not limited to contacting embroidered conductive yarn with rigid PCBs but may contact all sorts of fabric circuits with all sorts of electronic modules or components. However, the feasibility of the latter still needs to be investigated; and of course, like for the embroidered contact, cost efficient equipment needs to be developed to handle large fabrics during the bond process.

Another promising contacting technology is crimping, which is currently developed by Erik P. Simon at *Fraunhofer IZM*. This research is still in a very early stage. The expected advantages of crimping are that it is very fast and that it does not involve any temperature load. Like the adhesive approach, it may not be limited to embroidered circuits but be very versatile concerning the fabric substrate.

Despite notable improvements in the past, conductive embroidery yarns still need further improvements. The reliability during textile typical stress especially during washing is often not satisfactory especially with highly conductive yarns (i.e. 20 Ω/m or less). This applies equally to conductors for other textile technologies like weaving, knitting or printing. Generally, also the cost of conductive yarns or conductive inks is an issue.

To make embroidered contacts that can keep up the initial yarn loop tension without encapsulation, yarns need to be developed that do not tend to relax but are elastic. For adhesive contacts, yarns with thin thermoplastic insulation should be developed. Currently such insulation films are rather thick, thus compromising the textile character.

Aside from making reliable electrical contacts, for electronics-in-textiles the following of my suggestions made to the *European Commission* in 2008 are still relevant today [140]:

> "...
>
> 2. *Applications for the Technology*
> *The most prominent example for a textile integrated product is a jacket that can play music and controls a mobile. It has received a lot of media attention but has not had great economic success. On the other hand, almost every researcher who works on electronics-in-textiles develops some kind of sensing shirt. (I did that as well.) However both applications do not fully benefit of the textile integration – at least not yet.*
> *Only applications that necessarily require a distributed sensing or a distributed operation of actuators can really benefit of textile integration since they cannot be realized with a single device like a mobile phone.*
> *The above mentioned phone and music jacket can be replaced by a mobile phone that has an integrated mp3 player and hangs around the neck, so it can be controlled directly. Furthermore, this would still work when it is too warm for wearing a jacket.*
> *A single small and hard device cannot sense bio signals on different points of the body instantaneously. Therefore, it cannot compete with a sensing shirt. However, currently the sensing of bio signals with textile integrated sensors is often not reliable enough to extract data that go beyond the data*

that can be extracted with a plastic chest strap. There the benefit of a shirt is not given yet.

It is important to improve the sensing and to learn reducing artifacts. In addition we have to develop applications that require a distributed functionality, only textile integration can provide.

3. *Technical Textiles*

   The enthusiasm about wearable electronics tends to blind the eye for a possibly much bigger business: technical textiles.

   Currently the German government funds a number of research projects that aim at integrating electronics into technical textiles. Technical textiles are a highly innovative industry – much more than the fashion industry. Integrating electronic sensors and actuators into such textiles could be useful for a wide range of applications. Scenarios range from textiles for the logistics industry, to the building industry and to the automobile industry.

   Unfortunately, it is difficult to identify the needs without knowledge on the application in these fields. There is little interaction between the electronics-in-textiles community and respective industries.

4. *Fully Textile Integrated Sensors*

   Some textiles or the coating of some textiles have physical properties that can be used in sensors. Some sensors have already been realized with such textiles. However, a sensor consists of more than just a physical effect. Analog values need to be measured, interpreted and communicated by electronics which is an essential part of the sensor's dedicated functionality. Therefore, a sensor can only be called textile integrated if the electronics are integrated into textiles as well.

   Sensors of different function typically require an individual approach to the integration of electronics.

   Another aspect of sensing, often ignored, is that a sensor development is not completed as soon as the correlation between an environmental parameter and the electrical or logical output of the physical sensor is demonstrated. This correlation is of course necessary but by far not sufficient to make a sensor.

   In practice, the unknown environmental parameter needs to be concluded from the sensor's output. This is far more difficult since the physical sensor is often also sensitive to other environmental changes. This results in artifacts and noise which need to be filtered out.

   Thus, the development of textile integrated sensors should always consist of three equally essential parts: making the physical sensor textile, integrating the sensor electronics into textiles and reducing the noise and artifacts.

5. *Electrodes & Biocompatibility*
   What applies for sensors applies equally for electrodes: textile electrode, textile integrated electronics, and sensing algorithms have to be developed jointly. Artifacts are still a major problem.
   Beyond this, biocompatibility is an important issue especially when it comes to long term monitoring with body contact electrodes.

6. *Textile Integrated Actuators & Displays*
   Textile actuators and textile displays are essential for fully textile integrated systems. Unfortunately, until now little effort has been put into textile actuators and textile displays – mainly because it is a very challenging integration task.
   To overcome these challenges the research agenda should foresee small alternative steps, e.g. start with light emitting textiles rather than matrix capable large area displays.
   ]...[
   Potential actuators are: light emitting fibers for lighting, artificial textile muscles, electrochemical and electromechanical actuators for thermoregulation and micro systems like micro pumps and energy harvesting devices.

   ]...[

9. *Wireless energy & signal transmission*
   It will not always be possible or handy to have a wired connection to every sensor node in different parts of a wearable system (e.g. head-worn device, T-shirt, wrist-worn device, jacket, pants, and shoes). Connectors would be customer unfriendly and highly unreliable.
   Technologies have to be developed to effectively transmit energy, and signals from sensors wirelessly. Of course the antennas and electronics of these transducers have to be integrated into textiles.

   ..."

Glossary

contact / interconnection   in this thesis interconnection shall refer to the conductive textile wiring between two points; while contact shall refer to the electrical contact between an endpoint of this textile conductor and some electronic component or module

drawing   stretching the fiber in length by factors of 3 to 5 to orient the molecules along the fiber axis and to give the fiber its final properties like tenacity, elasticity, etc.

embroidery   decorating technology similar to sewing to apply patterns onto fabric; in this thesis conductive threads are embroidered onto fabric to make fabric circuits

embroidery backing   a non-woven fabric or a paper-like foil sometimes used for supporting the embroidery cloth to keep it from distorting; in this thesis, the use of backing is avoided to keep the assemblies as simple as possible

embroidery cloth   a woven, non-woven or knitted fabric onto which the embroidery is applied [141]; also embroidery ground or in the context of this thesis simply 'fabric substrate'

embroidery ground   see →*embroidery cloth*

fabric substrate   see →*embroidery cloth*

fibers   elements of a →*yarn*; natural fibers and →*man-made fibers* exist; man-made fibers are produced by extruding a polymer solution through a spinning nozzle; man-made fibers are distinguished in staple fibers and →*filaments*; while filaments are continues fibers, staple fibers are chopped after spinning [19], [116];

filament	a man-made continuous (i.e. 'endless') →*fiber*; a monofilament is extruded through a single nozzle spinneret, while a multifilament is drawn through a spinneret with multiple nozzles [19]; if a filament – be it a mono- or multifilament – is a product ready for use in e.g. a sewing machine or a weaving machine, it may be considered to be a →*yarn*; if it needs further treatment like twisting or spinning with other filaments, etc. before being useful for sewing of fabric making it is not considered a yarn.
FR4	a fiber glass reinforced epoxy laminate used as substrate for making printed circuit boards (PCBs)
inorganic man-made fibers	→*fibers* made of the carbon, glass or metal and belong to the group of →*man-made fibers* [19], [116]
man-made fibers	fibers produced by man in contrast to natural fibers like hair, wool, cotton, asbestos etc.; man-made fibers are classified into →*organic man-made fibers* and →*inorganic man-made fibers* [19], [116]; see also →*fibers*
organic man-made fibers	a group of →*man-made fibers* that is classified into fibers made from natural polymers (e.g. viscose, acetate) and fibers made from synthetic polymers, so called →*synthetic fibers* [19], [116]
PCB	printed circuit board
RT	abbreviation for room temperature
Shieldex 117/17 Twine	also called *Shieldex 117/17 2ply* is a conductive embroidery →*yarn* used for all experiments in this thesis; it consists of two twisted →*strands* of 17 silver coated →*filaments*; the filaments are →*synthetic fibers* of polyamide; in this thesis it is referred to as 'Shieldex';
SEM	refers to scanning electron microscopy or to an image from a scanning electron microscope
sewing cloth	see →*embroidery cloth*

solder resist	solder resist is a polymer film applied to printed circuit boards that traditionally serves to prevent solder from bridging conductors; however, it may also be used for electrically insulating conductors on the printed circuit board towards the environment
strand	*"an ordered assemblage of ... fibers ... normally used as unit"* [116]
synthetic fibers	→*fibers* made of synthetic polymers like polyamides (Nylon), polyacrylics, polyester, etc.; synthetic fibers belong to the group of →*organic man-made fibers* [19], [116]
yarn / thread	a continuous string of →*fibers*, →*filaments* or →*strands* in a form suitable for sewing, embroidering, weaving or knitting

Literature

x

[1] Carmen Rapisarda, "Article decorated with light emitting diodes using stranded conductive wire," United States Patent 5366780, November 1990.

[2] Helmut Wilke and Daniel Cervera, "Conveyor belt with carrier tissue in which conductive loops are embedded," United States Patent 6581755, February 2001.

[3] Ernest Rehmatulla Post, *E-broidery: An Infrastructure for Washable Computing*. Thesis for the degree of Master of Science in Media Arts and Sciences, at the Massachusetts Institute of Technology, Cambridge, MA, February 1999.

[4] Henrietta Lipske, *Feminine Wearables - Entwicklung einer Kollektion in Zusammenarbeit mit der HUGO BOSS AG, dem Fraunhofer Institut für Zuverlässigkeit und Mikrointegration und der Infineon Technologies AG*. Diploma thesis supervised by Torsten Linz, at Fachhochschule für Technik und Wirtschaft, Berlin, February 2004.

[5] Gili Weinberg, Maggie Orth, and Peter Russo, "The Embroidered Musical Ball: A Squeezable Instrument for Expressive Performance," in *Proceedings of CHI '00 Conference on Human Factors in Computing Systems*, The Hague, The Netherlands, 2000, pp. 283-284.

[6] Franz Miller, "Mikroelektronik: Wearables - Kleider mit Grips," *Fraunhofer Magazin*, no. 3/4., pp. 32-33, 2003.

[7] Ernest Rehmatulla Post, Margaret A. Orth, P.R. Russo, and Neil Gershenfeld, "E-broidery: Design and fabrication of textile-based computing," *IBM Systems Journal*, vol. 39, 2000.

[8] Margaret A. Orth, *Sculpted Computational Objects with Smart and Active Computing Materials*. Thesis for the Degree of Doctor of Philosophy, at the Massachusetts Institute of Technology, Cambridge, MA, 2001.

[9] Diana Marculescu et al., "Electronic Textiles: A Platform for Pervasive Computing," *Proceedings of the IEEE*, vol. 91, no. 12, December 2003.

[10] Leah Buechley, "A Construction Kit for Electronic Textiles," in *10th IEEE International Symposium on Wearable Computers,* Montreux, Switzerland, October 2006, doi: 10.1109/ISWC.2006.286348.

[11] Joachim Taelman, Tine Adriaensen, Caroline van der Horst, Torsten Linz, and Arthur Spaepen, "Textile Integrated Contactless EMG Sensing for Stress Analysis," in *29th Annual International Conference of the IEEE Engineering in Medicine and Biology Society*, Lyon, France, July 2007.

[12] Diffus Design. (2009, December) Diffus: Climate Dress. [Online]. http://www.diffus.dk/pollutiondress/intro.htm

[13] Torsten Linz, Christine Kallmayer, Rolf Aschenbrenner, and Herbert Reichl, "Fully Integrated EKG Shirt based on Embroidered Electrical Interconnections with Conductive Yarn and Miniaturized Flexible Electronics," in *IEEE BSN International Workshop on Wearable and Implantable Body Sensor Networks*, Cambridge, MA, USA, April 2006.

[14] Leah Buechley. (2007, October) Flickr: leahbuechley's photostream. [Online]. http://www.flickr.com/photos/leahbuechley/with/1480076526/

[15] Leah Buechley and Michael Eisenberg, "Fabric PCBs, Electronic Sequins, and Socket Buttons: Techniques for E-textile Craft," *Journal of Personal and Ubiquitous Computing*, vol. 13, pp. 133-150, August 2007.

[16] Torsten Linz, Lena Gourmelon, and Geert Langereis, "Contactless EMG sensors embroidered onto textile," in *IEEE International Workshop on Wearable and Implantable Body Sensor Networks*, Aachen, Germany, March 2007.

[17] R. Al Mahfudh and C. Rezendes, "Smart Fabrics, Interactive Textiles and Related Enabling Technologies: Market Opportunities and Requirements Analysis," in *Presentation at Intertech Pira smart fabrics Conference*, Charleston, SC, USA, May 2008.

[18] Sabine Gimpel, Frank Thurner, Dirk Zschenderlein, and Uwe Möhring, "Ersetzt das Sticken bald das Löten?," *Eurostitch Magazine*, vol. 87, pp. 32-35, September 2007.

[19] H. Eberle et al., *Clothing Technology.from fibre to fashion*, 5th ed. Haan-Gruiten, Germany: Europa-Lehrmittel, 2008.

[20] Henry Stürmer, "Untergarne: Anmerkungen von Henry Stürmer, TexDesign," *Fachzeitschrift für Textilveredlung und Promotion (TVP Magazin)*, no. 1, p. 57, February 2009.

[21] Margaret Orth, "Defining Flexibility and Sewability in Conductive Yarn," in *Material Research Society Symposium Proceedings*, vol. 736, Warrendale, PA, 2003, pp. 37-48.

[22] Uwe Möhring, "Textile Mikrosysteme im Automobil," in *Technische Textilien*, Petra Knecht, Ed. Frankfurt am Main, Germany: Deutscher Fachverlag, 2006, pp. 317-336.

[23] statex homepage. [Online]. http://www.statex.biz

[24] Yvonne Zimmermann, "ELITEX 235/34 PA/Ag 8/22/30," TITV, technical data sheet, Greiz, Germany, 2008.

[25] Erik Paul Simon, *Analysis of Contact Resistance Change of Embroidered Interconnections*. Diploma thesis supervised by Torsten Linz, at Technical University Berlin, Berlin, Germany, July 2009.

[26] ZSK - Hersteller von Stickmaschinen und Stickerei Software, Einkopf- und Mehrkopf-Stickmaschinen, Punchsoftware. [Online]. http://www.zsk.de

[27] Syscom Advanced Materials, Inc. [Online]. http://amberstrand.com/

[28] Tajima Group Official Site - Multi-Head Automatic Embroidery Machines. [Online]. http://www.tajima.com/

[29] Personal communication with Walter Biegelbauer, Head of Application Technique at ZSK Stickmaschinen GmbH, July 2010.

[30] Torsten Linz, Christine Kallmayer, Rolf Aschenbrenner, and Herbert Reichl, "New Interconnection Technologies for the Integration of Electronics on Textile Substrates," in *Ambience 2005*, Tampere, Finland, September 2005.

[31] Torsten Linz, Christine Kallmayer, Rolf Aschenbrenner, and Herbert Reichl, "Embroidering Electrical Interconnects with Conductive Yarn for the Integration of Flexible Electronic Modules into Fabric," in *IEEE ISWC International Symposium on Wearable Computing*, Osaka, Japan, October 2005.

[32] Oliver Lindner, *Zuverlässigkeitsuntersuchung für mit leitfähigem Faden angenähte flexible Substrate*. Diploma thesis supervised by Torsten Linz, at the Fachhochschule für Technik und Wirtschaft, Berlin, Germany, 2005.

[33] Leah Buechley and Michael Eisenberg, "The LilyPad Arduino: Toward Wearable Engineering for Everyone," in *IEEE Pervasive Computing*, vol. 7, no.2, Apr.-June 2008, pp. 12-15, doi:10.1109/MPRV.2008.38.

[34] Jennifer Darmour. (2010, May) Ping, a social networking garment. [Online]. http://www.electricfoxy.com/ping/

[35] Tony Olsson, David Gaetano, Jonas Odhner, and Samson Wiklund. (2009, July) Open Softwear - Fashionable prototyping and wearable computing using the Arduino. [Online]. http://softwear.cc/

[36] Diana Eng. (2010, July) Fairytale Fashion - Using technology to turn make-believe into reality. [Online]. http://fairytalefashion.org/

[37] Mika Satomi and Hannah Perner-Wilson. (2010, July) KOBAKANT DIY Wearable Technology Documentation. [Online]. http://www.kobakant.at/DIY/

[38] Mark T. Jones and Thomas L. Martin, "Hardware and Software Architectures for Electronic Textiles," in *Smart Clothing - Technology and Applications*, Gilsoo Cho, Ed. Boca Raton, FL, USA: CRC Press, 2010, ch. 6, pp. 135-151.

[39] Li Li et al., "Design of Intelligent Garment with Transcutaneous Electrical Nerve Stimulation Function Based on the Intarsia Knitting Technique," *Textile Research Journal*, vol. 80, no. 3, pp. 279-286, February 2010.

[40] Seungyon Claire Lee and Thad Starner, "Stop burdening your eyes: A wearable electro-tactile display," in *12th IEEE International Symposium on Wearable Computers*, Pittsbrurgh, PA, USA, 2008, pp. 115-116.

[41] Torsten Linz et al., "Abschlussbericht des Fraunhofer IZM zum Projekt TexOLED," Fraunhofer IZM, Berlin, Germany, project final report, August, 2010.

[42] Torsten Linz et al., "Embroidered Interconnections and Encapsulation for Electronics in Textiles for Wearable Electronics Applications," *Advances in Science and Technology*, vol. 60, pp. 85-94, online at http://www.scientific.net, Trans Tech Publications, Switzerland, September 2008.

[43] Josephine B. Lee and Vivek Subramanian, "Weave Patterned Organic Transistors on Fiber for E-Textiles," *IEEE Transactions on Electronic Devices*, vol. 52, no. 2, pp. 269-275, February 2005.

[44] Francine Gemperle, Chris Kasabach, John Stivoric, Malcolm Bauer, and Richard Martin, "Design for Wearability," in *IEEE Second International Symposium on Wearable Computers Digest of Papers*, Pittsburgh, PA , USA , 1998, pp. 116-122.

[45] Claudia Schuster, *Untersuchung des Tragekomforts von Oberbekleidung mit verschiedenen elektronischen Modulen*. Diploma thesis supervised by Torsten Linz, at Fachhochschule für Technik und Wirtschaft, Berlin, September 2006.

[46] "ISO 6330:2000 - Textiles -- Domestic washing and drying procedures for textile testing," International Organization for Standardization, Norm 2000.

[47] J. Rantanen et al., "Smart Clothing for the Arctic Environment," in *IEEE Fourth International Symposium on Wearable Computers (ISWC'00)*, Atlanta, GA, USA, October 2000.

[48] Christine Kallmayer et al., "New Assembly Technologies for Textile Transponder Systems," in *IEEE Electronic Components and Technology Conference*, New Orleans, May 2003.

[49] René Vieroth, Christine Kallmayer, Rolf Aschenbrenner, and Herbert Reichl, "A New Package for Textile Integrated RFID Tags," in *11th IEEE Electronics Packaging Technology Conference (EPTC)*, Singapore, December 2009.

[50] Thomas Vervust, Frederick Bossuyt, Fabrice Axisa, and Jan Vanfletere, "Stretchable and Washable Electronics for Embedding in Textiles," *Mater. Res. Soc. Symp. Proc.*, vol. 1271: JJ04-03, 2010.

[51] Torsten Linz, Malte von Krshiwoblozki, and Hans Walter, "Novel Packaging technology for Body Sensor Networks based on Adhesive bonding," in *IEEE BSN International Workshop on Wearable and Implantable Body Sensor Networks*, Singapore, June 2010.

[52] "JESD22-A104-C Temperature Cycling," JEDEC Solid State Technology Association / Electronic Industry Association, JEDEC Standard 2005.

[53] "JESD22-A101-B - Steady State Tempertare Humidity Bias Life Test - Test Method A101-B," JEDEC Solid State Technology Association / Electronic Industry Association, JEDEC Standard 1997.

[54] "ISO 4892-3:2006 - Plastics -- Methods of exposure to laboratory light sources - Part 3: Fluorescent UV lamps," International Organization for Standardization, Norm 2006.

[55] Personal communication with Jan Vanfleteren of CMST, Ghent University, May 2008.

[56] Thomas Löher, René Vieroth, Manuel Seckel, Andreas Ostmann, and Herbert Reichl, "Stretchable electronic systems for wearable and textile applications," in *IEEE 9th VLSI Packaging Workshop of Japan (VPWJ 2008)*, Kyoto, Japan, 2008, pp. 9-12.

[57] Frederick Bossuyt, Thomas Vervust, Fabrice Axisa, and Jan Vanfletere, "A New Low Cost, Elastic and Conformable Electronics Technology for Soft and Stretchable Electronic Devices by use of a Stretchable Substrate," in *Microelectronics and Packaging Conference, 2009. EMPC 2009. European*, Rimin, Italy, June 2009, pp. 1-6.

[58] Tom Sterken et al., "Lifetime of Stretchable Meander-shaped Copper Conductors in PDMS Subjected to Cyclic Elongation," in *MRS Spring meeting 2010*, San Francisco, CA, USA, April 2010.

[59] "ISO 13934-1:1999 - Textiles -- Tensile properties of fabrics - Part 1: Determination of maximum force and elongation at maximum force using the strip method," International Organization for Standardization, Norm 1999.

[60] Personal communication with Anton Kaasjager from of TNO Science and Industry in Eindhoven, May 2008.

[61] "ISO 7854:1995 - Rubber- or plastics-coated fabrics -- Determination of resistance to damage by flexing," International Organization for Standardization, Norm 1995.

[62] "ISO 12947-2:1998/Cor 1:2002 - Textiles -- Determination of abrasion resistance of fabrics by the Martindale method - Part 2: Determination of specimen breakdown," International Organization for Standardization, Norm 2002.

[63] "ISO 105-E04:2008 - Textiles -- Tests for colour fastness - Part E04: Colour fastness to perspiration," International Organization for Standardization, Norm 2008.

[64] A. Harlin and M. Ferenets, "Introduction to conductive materials," in *Intelligent textiles and clothing*, H.R. Mattila, Ed. Cambridge, UK: Woodhead Publishing, 2006, ch. 13, pp. 217-237.

[65] Franco Marchini, "Advanced Applications of Metallized Fibres for Electrostatic Discharge and Radiation Shielding," *Journal of Industrial Textiles*, vol. 20, no. 3, pp. 153-166, January 1991.

[66] Rointan Framroze Bunshah, "Deposition Technologies: An Overview," in *Handbook for deposition technologies for films and coatings - Science, technology and application*, 2nd ed., Rointan Framroze Bunshah, Ed. New Jersey, USA: Noyes Publications, 1994, ch. 1, pp. 1-28.

[67] Auli Sipilä, Anton Kaasjager, Christian Rotsch, and Torsten Linz, "Integrating sEMG sensors to textile materials," in *AUTEX 2007*, Tampere, Finland, June 2007.

[68] Pu Xue, Xiaoming Tao, Mei-Yi Leung, and Hui Zhang, "Electromechanical properties of conductive fibres, yarns and fabrics," in *Wearable electronics and photonics*, Xiaoming Tao, Ed. Cambridge, UK: Woodhead Publishing, 2005, ch. 5, pp. 81-104.

[69] Emmanuel Gasana et al., "Electroconductive textile structures through electroless deposition of polypyrrole and copper at polyaramide surfaces," *Surface and Coatings Technology*, vol. 201, no. 6, pp. 3547-3551, December 2006, DOI: 10.1016/j.surfcoat.2006.08.128.

[70] Schwarz et al., "Gold coated polyester yarn," *Advances in Science and Technology*, vol. 60, pp. 47-51, online at http://www.scientific.net, Trans Tech Publications, Switzerland, September 2008.

[71] Yvonne Zimmermann, Andreas Neudeck, and Uwe Möhring, "Abscheidung geschlossener Goldschichten auf leitfähigen textilen Materialien," *Galvanotechnik - Älteste Fachzeitschrift für die Praxis der Oberflächenbehandlung*, vol. 100, no. 7, pp. 1496-1498, July 2009.

[72] K. Bertuleit, "Silver Coated Polyamide: A Conductive Fabric," *Journal of Industrial Textiles*, vol. 20, no. 3, pp. 211-215, January 1991.

[73] Statex Produktions und Vertriebs GmbH, "Conductive Yarn: Silver Plated Nylon Yarn 117/17 x 2-ply (PN# PY16125x2)," Bremen, Germany, technical data sheet 2003.

[74] Philipp Foerster, *Untersuchungen zu Eigenschaften von Nano-Silberschichten auf Polyamidfasern*. Student research project supervised by Torsten Linz as part of the degree programm Electrical Engineering, at Technical University Berlin, Berlin, Germany, 2010.

[75] K. Sieradzki, K. Bailey, and T.L. Alford, "Agglomeration and percolation conductivity," *Applied Physics Letters*, vol. 79, no. 21, pp. 3401-3403, November 2001.

[76] R. E. Hummel and H. J. Geier, "Activation Energy for Electrotransport in Thin Silver and Gold Films," *Thin Solid Films*, vol. 25, pp. 335-342, 1975.

[77] Torsten Linz, Erik Simon, and Hans Walter, "Fundamental analysis of embroidered contacts for electronics in textiles," in *3rd Electronic System-Integration Technology Conference (ESTC)*, Berlin, Germany, 2010, pp. 1-5.

[78] Christof Breckenfelder, Christian Dils, and Hans Werner Seliger, "Electrical properties of metal coated polyamide yarns," in *4th International Forum on Applied Wearable Computing (IFAWC)*, Tel Aviv, Israel, March 2007.

[79] Burkhard Stahlmecke, *Elektromigration in Gold und Silber Nanostrukturen*. Thesis for the Degree of Doktor der Naturwissenschaften at Universität Duisburg-Essen, Duisburg, Germany, 2008.

[80] Wolfgang Retting, *Mechanik der Kunststoffe - Die mechanischen Eigenschaften von Polymer-Werkstoffen*. Wien, Austria: Carl Hanser Verlag, 1991.

[81] EN 7724 Polymeric materials: grouping of polymeric materials based on their mechanical behaviour, 1993.

[82] Adolf Franck, *Kunststoff-Kompendium - Herstellung, Aufbau, Verarbeitung, Anwendung, Umweltverhalten und Eigenschaften der Thermoplaste, Polymerlegierungen, Elastomere und Duroplaste*, 6th ed. Würzburg, Germany: Vogel Verlag, 1984.

[83] Friedrich Rudolf Schwarzl, *Polymermechanik: Struktur und mechanisches Verhalten von Polymeren*. Berlin, Germany: Springer, 1990.

[84] Wolfgang Bergmann, *Werkstofftechnik 1: Struktureller Aufbau von Werkstoffen - Metallische Werkstoffe - Polymerwerkstoffe - Nichtmetallisch-anorganische Werkstoffe*, 6th ed. München, Germany: Carl Hanser Verlag, 2008.

[85] Walter Hellerich, Günther Harsch, and Siegfried Haenle, *Werkstoff-führer Kunststoffe: Eigenschaften, Prüfungen, Kennwerte*. München, Germany: Carl Hanser Verlag, 2004.

[86] Maclovio Herrera Salinas, *Untersuchung flüchtiger Verbindungen bei der thermischen Zersetzung von stickstoffhaltigen Polymerwerkstoffen*. Thesis for the Degree of Doktor der Naturwissenschaften, at Technischen Universität München, Germany, 2000.

[87] S. Zaremba, M. Steffens, B. Wulfhorst, P. Hirt, and K.H. Riggert, *Faserstoff-Tabellen nach P.-A. Koch: Polyamidfasern*, 4th ed. Aachen, Germany, 1997.

[88] Wolfgang Grellmann and Sabine Seidler, *Polymer Testing*, Wolfgang Grellmann and Sabine Seidler, Eds. München, Germany: Hanser Verlag, 2007.

[89] David I. Bower, *An Introduction to Polymer Physics*. Cambridge, UK: Cambridge University Press, 2002.

[90] Richard Erwin Taylor et al., *Thermal Expansion of Solids*, Cho Yen Ho, Ed. Materials Park, OH, USA: CINDAS Data Series on Material Properties, ASM International, 1998.

[91] Peter Eyerer, *Polymer engineering: Technologien und Praxis*, Peter Eyerer, Thomas Hirth, and Peter Elsner, Eds. Berlin, Germany: Springer-Verlag, 2008.

[92] W.E. Morton and J.W.S. Hearle, *Physical properties of textile fibers*, 4th ed. Cambridge, UK: Woodhead Publishing, 2008.

[93] Ephraim Catsiff, Turner Alfrey, and M.T. O'Shaughnessy, "Generalized Creep Curves for Nylon," *Textile Research Journal*, pp. 808-820, November 1953.

[94] D.R. Buchanan, "Thermomechanical Responses of Fibres," in *Advances in Fibre Science*, Samir Kumar Mukhopadhyay, Ed. Manchester, United Kingdom: The Textile Institute, 1992, ch. 5, pp. 87-113.

[95] A.T Kalashnik, O.N. Panichkina, G.Ya. Rudinskaya, and A.T. Serkov, "Shrinkage mechanisms in thermooxidative stabilization of acrylic fibers," *Fibre Chemistry*, vol. 33, no. 2, pp. 132-139, 2001.

[96] Toyobo Co., Ltd, PBO Fiber Zylon® - Technical Information (Revised 2001.9), 2001.

[97] M.V. Forward and H.J. Palmer, "The Influence of Heat and of Swelling Agents on 66 Nylon Yarns, Part I: General Experiments on Length Equilibria," *Journal of the Textile Institute*, vol. 45, pp. T510-T538, April 1954.

[98] F. P. Dismore and W.O. Statton, "Chain Folding in Oriented Nylon 66 Fibers," *Journal of Polymer Science: Part C*, vol. 13, pp. 133-148, 1966.

[99] I. M. Fouda, M. M. El-Tonsy, and A. M. Shaban, "Evaluation of the structural behaviour of annealed nylon 6 fibres from density measurements," *Journal of Materials Science*, vol. 26, no. 18, pp. 5085-5092, January 1991.

[100] A Engelter and F.H. Müller, "Thermische Effekte bei mechanischer Deformation, insbesondere von Hochpolymeren," *KOLLOID- ZEITSCHRIFT*, vol. 157, no. 2, pp. 89-111, April 1958.

[101] Brent D. Viers, "Nylon 6,6," in *Polymer Data Handbook*, James E. Mark, Ed. Oxford, United Kingdom: Oxford University Press, Inc., 1999, pp. 189-209.

[102] D.R. Buchanan and J. H. Dumbleton, "Effect of Annealing Conditions on the Structure of Drawn Nylon 66 Yarns," *Journal of Polymer Science*, vol. 7, no. A-2, pp. 113-122, 1969.

[103] J. P. Rath, T. K. Chaki, and D. Khastgir, "Change in Fiber Properties Due to the Heat Treatment of Nylon 6 Tire Cords," *Journal of Applied Polymer Science*, vol. 108, no. 6, pp. 3960-3967, March 2008.

[104] Ch. D. Bechev, "On the characterization by shrinkage forces of as-spun poly(ethylene terephthalate) filaments," *Polymer Testing*, vol. 14, no. 2, pp. 163-172, 1995.

[105] H.-J. Berndt and G. Heidernann, "Beschreibung des inneren Spannungszustandes von Polyester-Faserstoffen durch Messung der Gleichgewichtsschrumpfkraft," *Colloid and Polymer Science*, vol. 258, no. 5, pp. 612-620, 1980.

[106] S.K. Mukhopadhyay and J.W.S. Hearle, "Measurement of the Shrinkage Tension of Melt-spun Fibres with Rapid Heating and Cooling," *Journal of the Textile Institute*, vol. 81, no. 2, pp. 156-166, February 1990.

[107] Personal communication with Wolfgang Scheibner, Andreas Neudeck, Sabine Gimpel of TITV Greiz and Ivo Locher of Sefar AG at 4. öffentliches Status Meeting mst-textil, Berlin, June 2010.

[108] Takayuki Murayama, John H. Dumbleton, and Malcolm L. Williams, "The viscoelastic properties of oriented nylon 66 fibers Part III: Stress relaxation and dynamic mechanical properties," *Journal of Macromolecular Science*, vol. 1, no. 1, pp. 1-14, March 1967.

[109] Tatsuya Yoshitomi, Kazuo Nagamatsu, and Kiiti Kosiyama, "On the Stress Relaxation of Nylon 6," *Journal of Polymer Science*, vol. 27, pp. 335-347, 1958.

[110] Albert Keil, Wilhelm A. Merl, and Vinaricky Eduard, *Elektrische Kontakte und ihre Werkstoffe: Grundlagen, Werkstoffeigenschaften, Technologien, Anwendungen in der elektrischen Nachrichten- und Energietechnik*, Albert Keil, Ed. Berlin, Germany: Springer Verlag, 1984.

[111] Roland S. Timsit, "Electrical Contact Resistance: Fundamental Principles," in *Electrical Contacts: Principles and Applications*, Paul G. Slade, Ed. New York, USA: Marcel Dekker Inc., 1999, ch. 1, pp. 1-88.

[112] Ragnar Holm, *Electric contacts - Theory and application*, 4th ed. Berlin, Germany: Springer Verlag, 1967.

[113] Lewis S. Goldmann, Robert T. Howard, and Dexter A. Jeannotte, "Package Reliability," in *Microelectronics Packaging Handbook – Technology Drivers, Part I*, 2nd ed., R.R. Tummala, E.J. Rymaszewski, and A.G. Klopfenstein, Eds.: Chapman & Hall, 1997, ch. 5, pp. I-404 - I-551.

[114] F. Llewellyn Jones, *The Physics of Electrical Contacts*, Willis Jackson et al., Eds. Oxford, UK: Oxford University Press, 1957.

[115] Jin Jin Gu, Keith Warner, Shu Qin, and Chung Chan, "Constriction Resistance of Microcone-Based Contacts," *IEEE Transactions on Components, Packaging and Manufacturing Technology*, vol. 18, no. 2, pp. 385-389, June 1995.

[116] Hans J. Koslowski, *Dictionary of Man-Made Fibers: terms, figures, trade-marks*, 1st ed. Frankfurt am Main, Germany: International Business Press, 1998.

[117] A. Taylor, "Digital embroidery techniques for smart clothing," in *Smart clothes and wearable technology*, J. McCann and D. Bryson, Eds. Cambridge, UK: Woodhead Publishing, 2009, ch. 14, pp. 279-299.

[118] ZSK Stickmaschinen GmbH, "Betriebsanleitung: F-Kopf," Krefeld-Gartenstadt, operating manual 2006.

[119] Keithley Instruments, Inc., "Model 2750 Multimeter/Switch System," Cleveland, Ohio, USA, user's manual 2003.

[120] Keithley Instruments, Inc., "Model 2010 Multimeter," Cleveland, Ohio, USA, user's manual 2003.

[121] Christian Böhme, "Integration elektronischer Komponenten in Textilien," Fraunhofer IZM, Berlin, report on internship supervised by Torsten Linz, December 2009 - March 2010.

[122] Statex Produktions & Vertriebs GmbH, "Informationen zur Reinigung," Bremen, Germany, application note.

[123] C.P. Wong and Treliant Fang, "Fundamentals of Sealing and Encapsulation," in *Fundamentals of Microsystems Packaging*, Rao R. Tummala, Ed. Atlanta, GA, USA: McGraw-Hill, 2001, ch. 15, pp. 580-610.

[124] Edward R. Salmon, *Encapsulation of electronic devices and components*. New York, NY, USA: Marcel Dekker, 1987.

[125] Louis T. Manzione, *Plastic Packaging of Microelectronic Devices*. New York, NY, USA: Van Nostrand Reinhold, 1990.

[126] T. Braun et al., "Reliability Potential Of Epoxy Based Encapsulants For Automotive Applications," in *Proc. of ESREF*, Arcachon, France, October 2005.

[127] T. Braun et al., "Hotmelt Encapsulation: New Possibilities For Packaging Of Sensitive Components," in *SMT*, Nürnberg, Germany, June 2000.

[128] Ken Gilleo, "Materials," in *Polymer Thick Film*, Ken Gilleo, Ed. New York, NY, USA: Van Nostrand Reinhold, 1996, ch. 2, pp. 21-53.

[129] Yi Li, Daniel Lu, and C.P. Wong, *Electrical Conductive Adhesives with Nanotechnologies*. New York, NY, USA: Springer, 2010.

[130] Torsten Linz, "Method for connecting two parts mechanically and electrically at the same time," Patent Pending WO/2010/037565, September 30, 2009.

[131] Malte von Krshiwoblozki, *Untersuchung von Klebeverbindungen zur Integration von Elektronik in Textilien*. Diploma thesis supervised by Torsten Linz, at Hochschule für Technik und Wirtschaft Berlin, Berlin, August 2009.

[132] Anuj Dhawan, Abdelfattah M. Seyam, Tushar K. Ghosh, and John F. Muth, "Woven Fabric-Based Electrical Circuits - Part I: Evaluating Interconnect Methods," *Textile Research Journal*, vol. 74, no. 10, pp. 913-918, October 2004.

[133] Ivo Locher and Gerhard Tröster, "Fundamental Building Blocks for Circuits on Textiles," *IEEE Transactions on Advanced Packaging*, vol. 30, no. 3, pp. 541-550, August 2007.

[134] Ivo Locher and Gerhard Tröster, "Screen-printed Textile Transmission Lines," *Textile Research Journal*, vol. 77, no. 11, pp. 837-842, 2007.

[135] Yongsang Kim and Hyejung Yoo, Hoi-Jun Kim, "Electrical Characterization of Screen-Printed Circuits on the Fabric," *IEEE Transactions on Advanced Packaging*, vol. 33, no. 1, pp. 196-205, February 2010.

[136] M. Bickerton, "Effects of fibre interactions on conductivity, within a knitted fabric stretch sensor," in *IEE Eurowearable '03* , vol. 67, Birmingham, UK, September 2003, p. 67–72.

[137] Rita Paradiso, Giannicola Loriga, and Nicola Taccini, "A Wearable Health Care System Based on Knitted Integrated Sensors," *IEEE Transactions on Information Technology in Biomedicine*, vol. 9, no. 3, pp. 337-344, September 2005.

[138] Mathieu Belly, Fabrice Pirotte, and Michael Catrysse, "The Development of Intelligent Textiles at Centexbel," *mst news*, vol. 2, p. 44, April 2005.

[139] Lena Gourmelon and Geert Langereis, "Contactless sensors for Surface Electromyography," in *Proceedings of the 28th IEEE EMBS Annual International Conference*, New York City, USA, August 2006, pp. 2514-2517.

[140] Torsten Linz, "Enabling Micro System Technologies for Electronics in Textiles," in *Concertation WS on EC Funded projects on Smart Fabrics & Interactive Textiles (SFIT) and Consultation on Future R&D Challenges and opportunities*, Brussels, Belgium, January 2008.

[141] Lothar Bühring and Nora Grawitter, *Lexicon of Embroidery and Lace*, Textile Research Insitute Thüringen-Vogtland, Ed. Greiz, Germany, 2006.

[142] TITV hompage. [Online]. http://www.titv-greiz.de

x

Appendix A   Temperature Cycling Test

A.1 Simplified Model of the Embroidered Contact
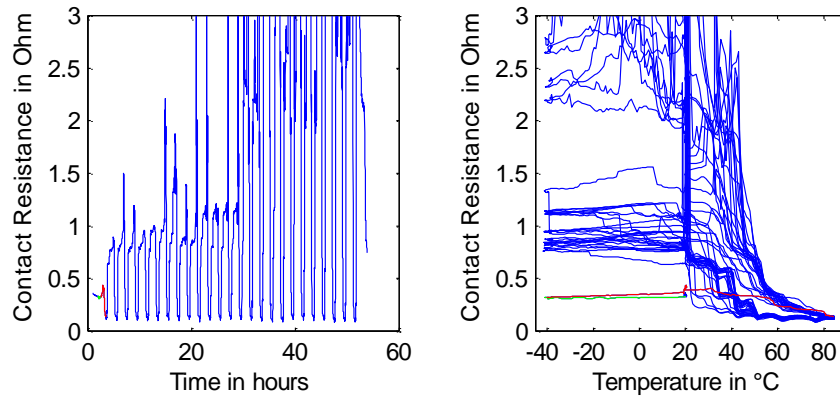
Figure A.1   (ID: SM01Au01\558)
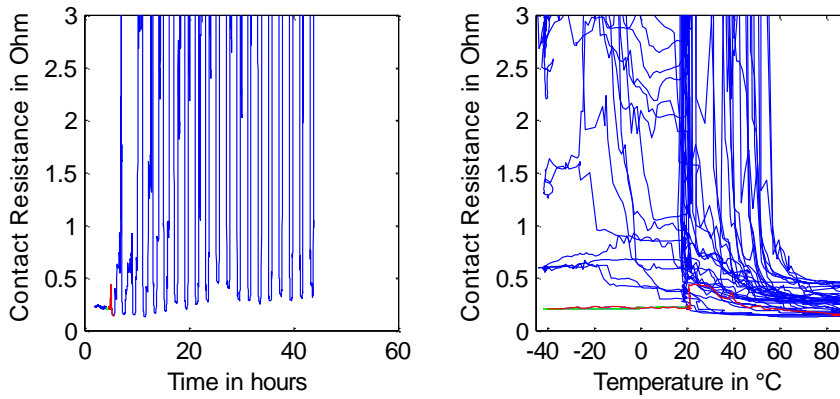
Figure A.2   (ID: SM01Au02\585)
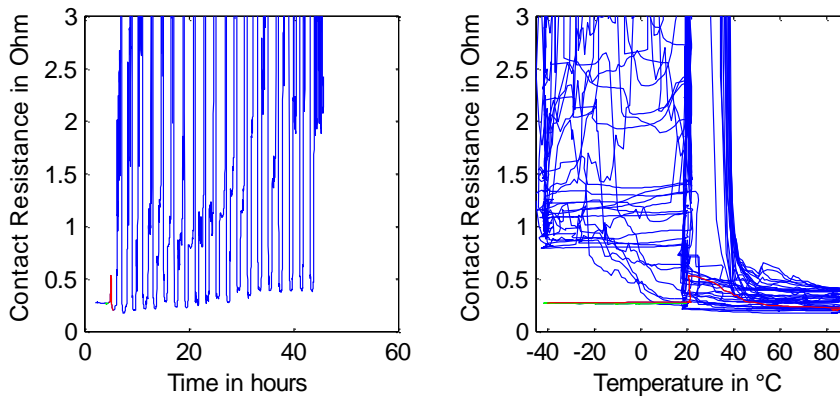
Figure A.3   (ID: SM01Au03\586)
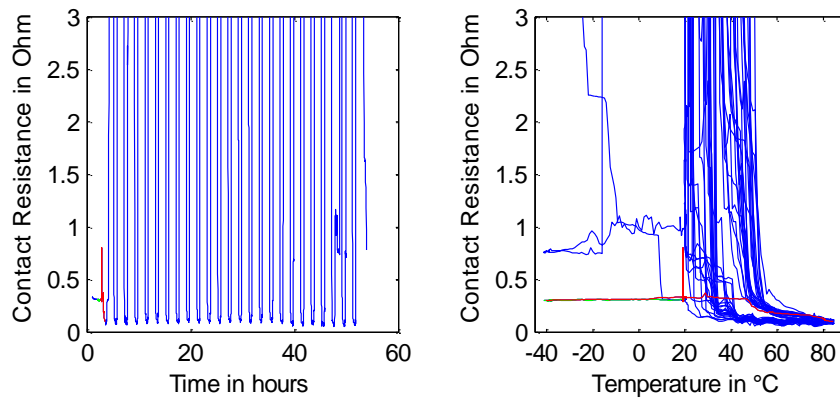
Figure A.4   (ID: SM02Au01\555) Data from [25].
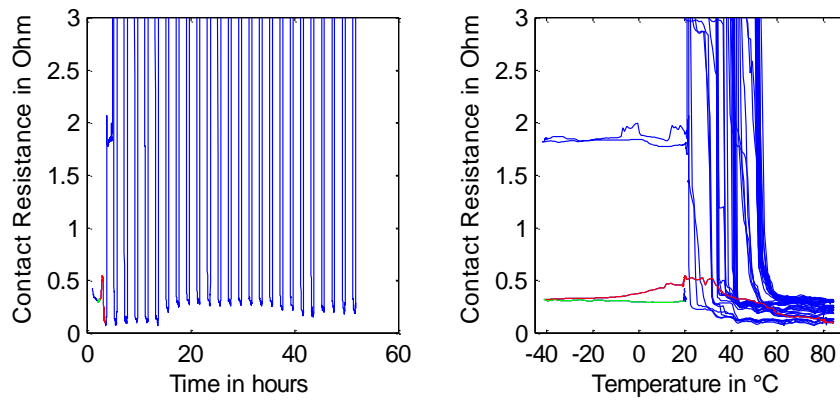
Figure A.5   (ID: SM02Au02\556) Data from [25].
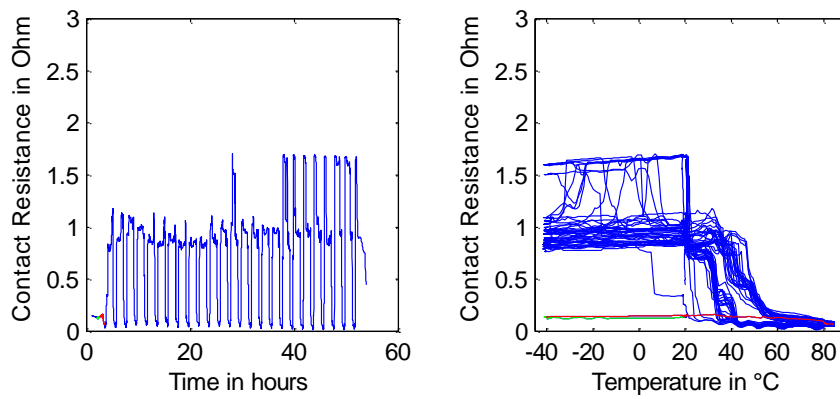
Figure A.6   (ID: SM02Au03\557) Data from [25].

A.2 Embroidered Contacts with Pierced Contact Pads
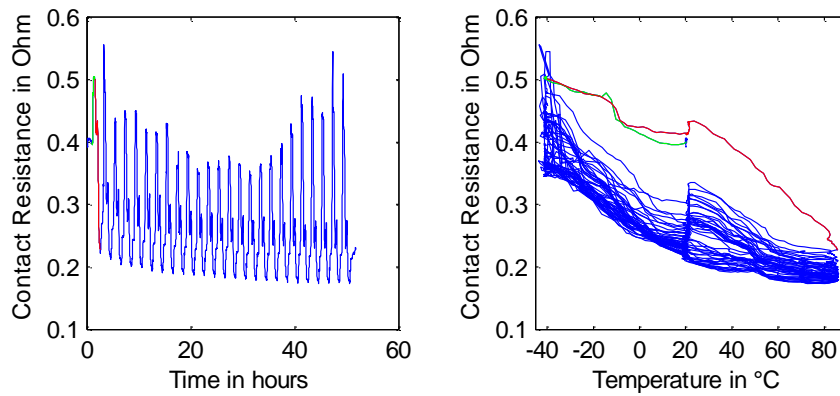
Figure A.7   (ID: EC54AgPiercedPad01\167)
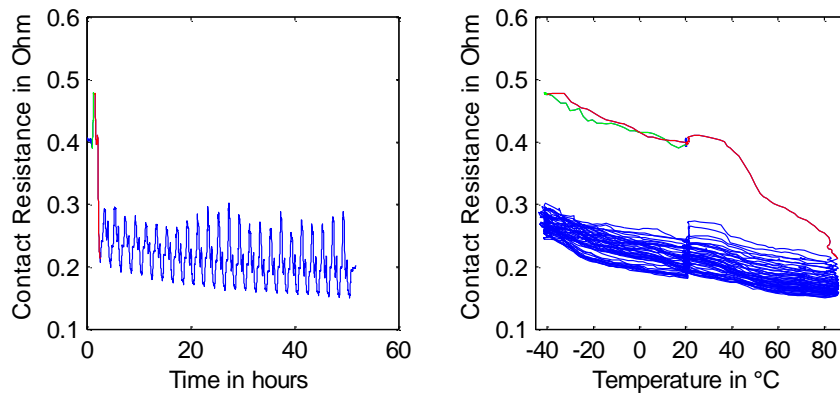
Figure A.8   (ID: EC54AgPiercedPad08\174)
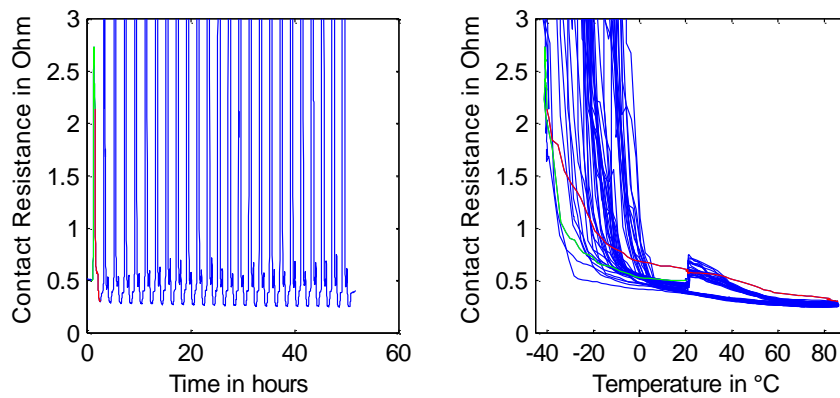
Figure A.9   (ID: EC54AgPiercedPad09\175)
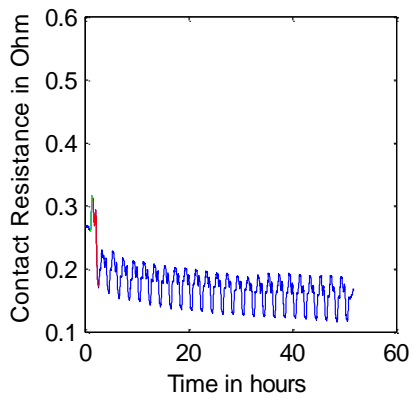
Figure A.10   (ID: EC56AuPiercedPad12\206)
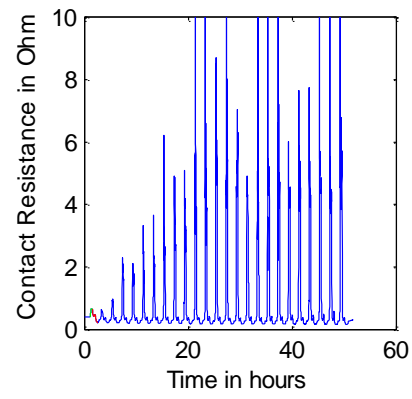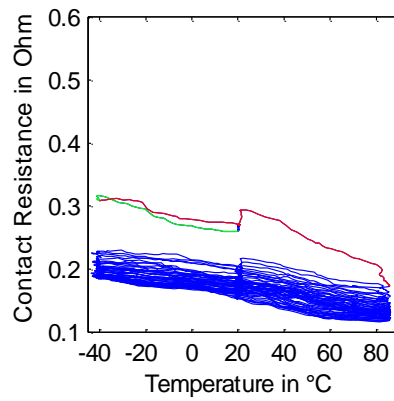
Figure A.11   (ID: EC56AuPiercedPad02\196)
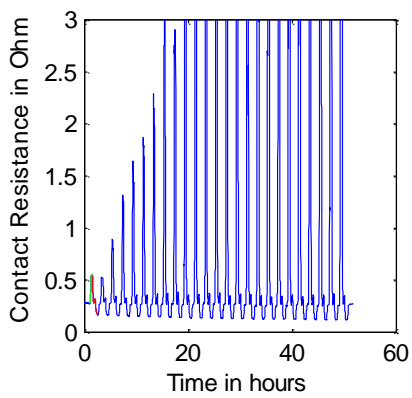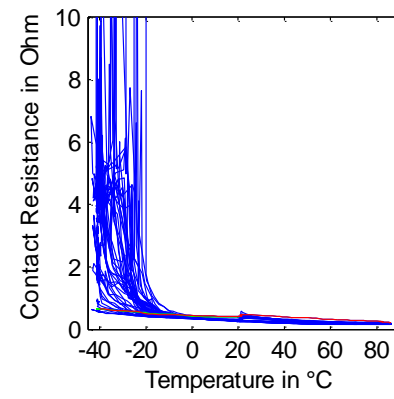
Figure A.12   (ID: EC56AuPiercedPad04\198)
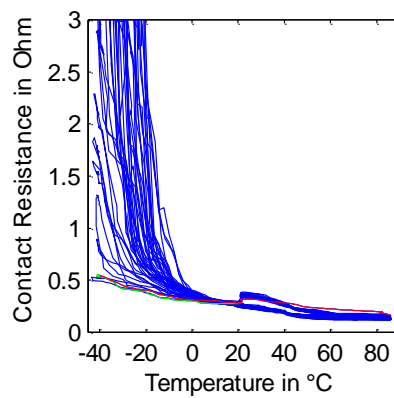
A.3 Embroidered Contacts with Predrilled Contact Pads
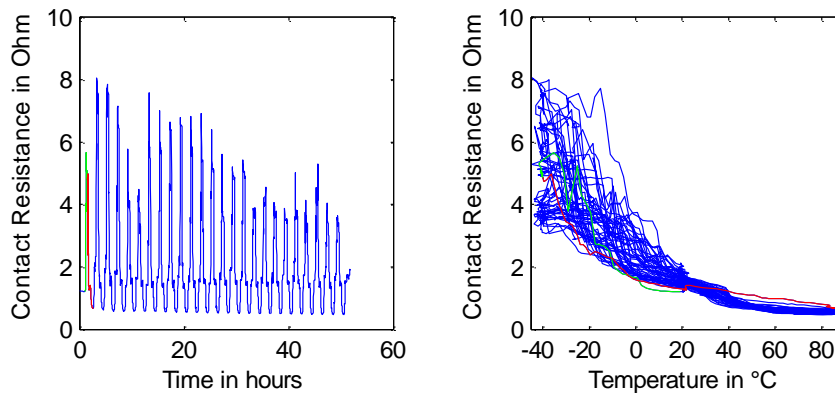
Figure A.13   (ID: EC48AgDrilledPad14\243)
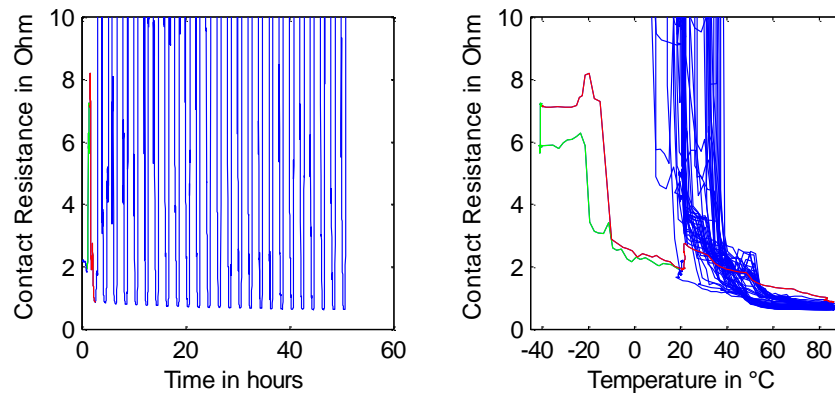
Figure A.14   (ID: EC48AgDrilledPad03\232)
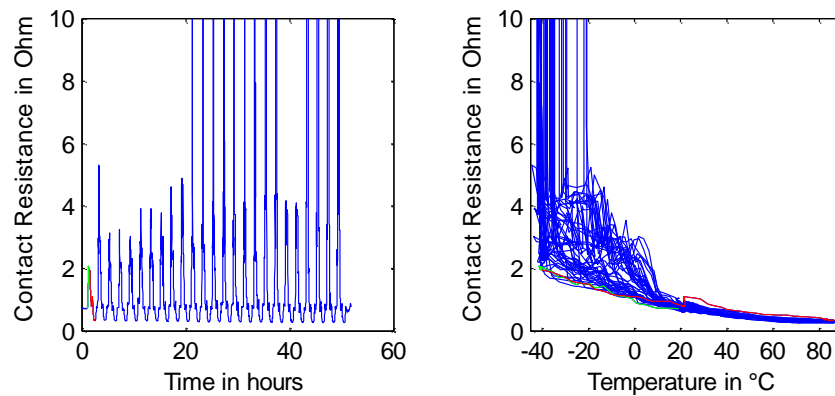
Figure A.15   (ID: EC48AgDrilledPad12\241)
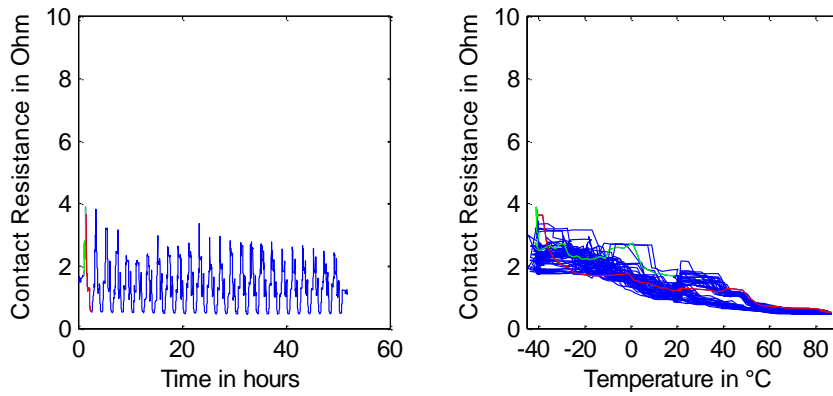
Figure A.16   (ID: EC45AuDrilledPad02\245)
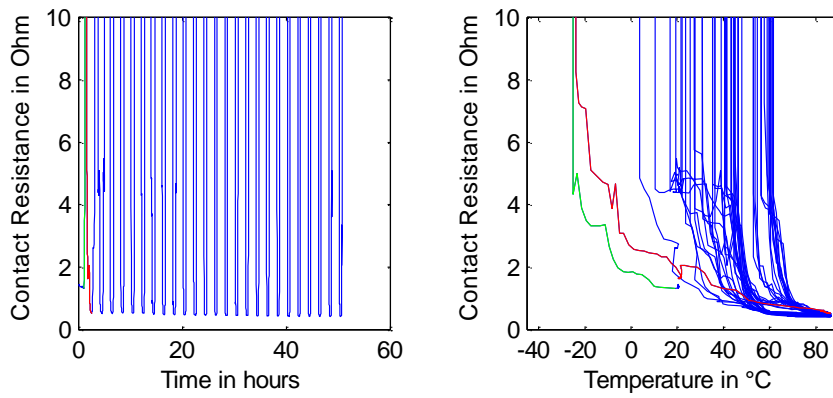
Figure A.17   (ID: EC45AuDrilledPad09\252)
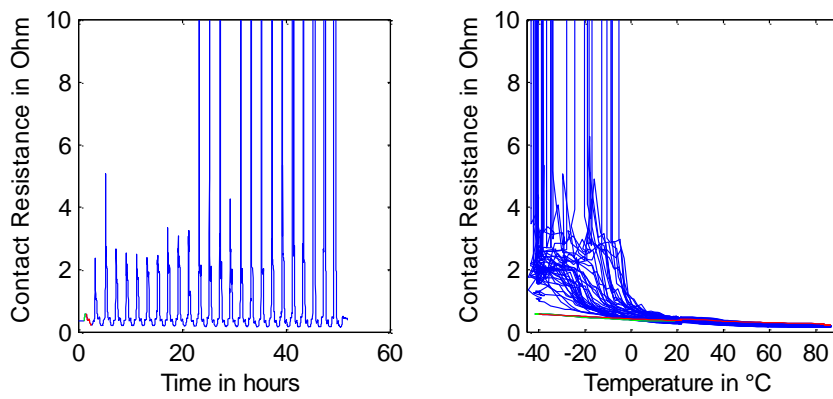
Figure A.18   (ID: EC45AuDrilledPad10\253)

A.4 Embroidered Contacts Stitched Four Times
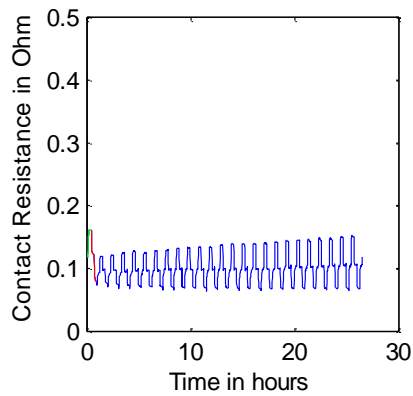
Figure A.19 (ID: EC4xAgPiercedPad05\595)
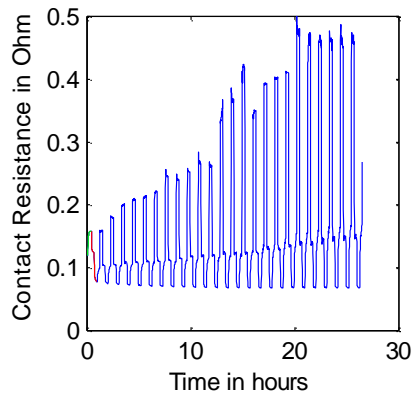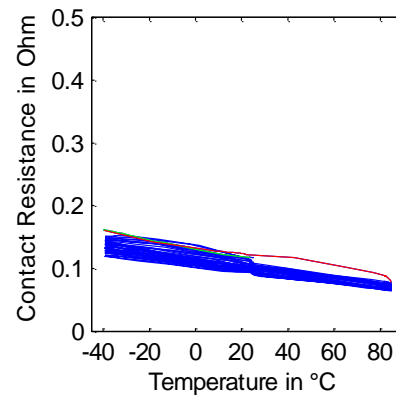
Figure A.20 (ID: EC4xAgPiercedPad07\597)
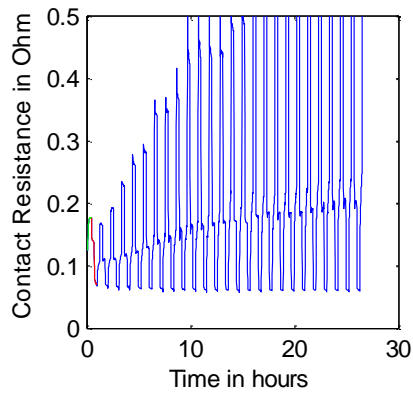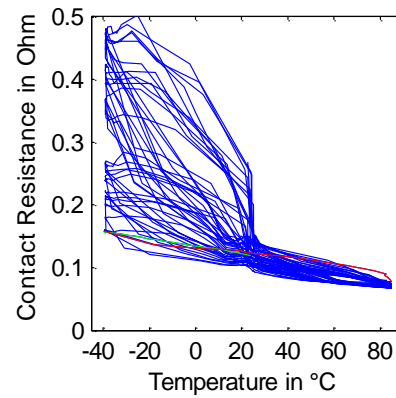
Figure A.21 (ID: EC4xAgPiercedPad12\602)
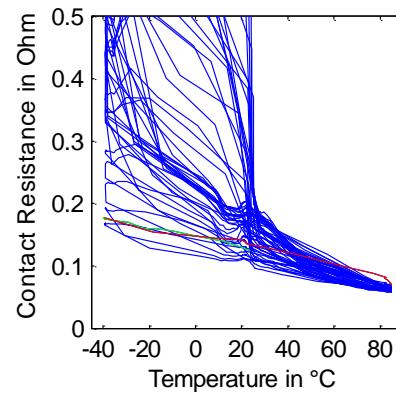
A.5 Embroidered Contacts with Protection

A.5.1 Transfer Mold Encapsulated Embroidered contacts
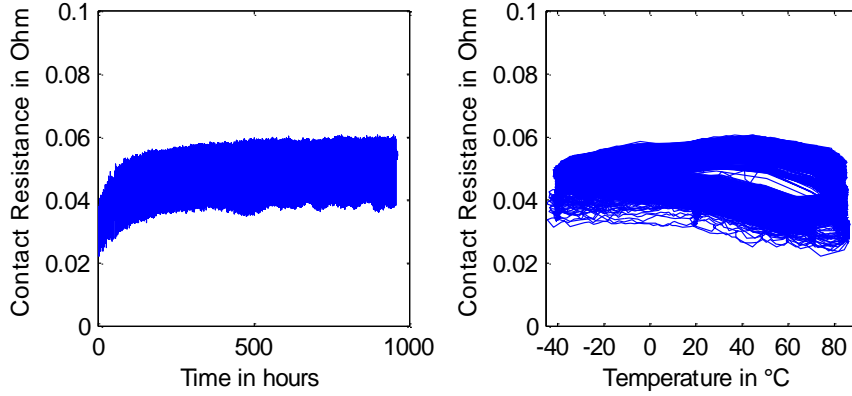
Figure A.22   (ID: TM82AuPiercedPad07\489)
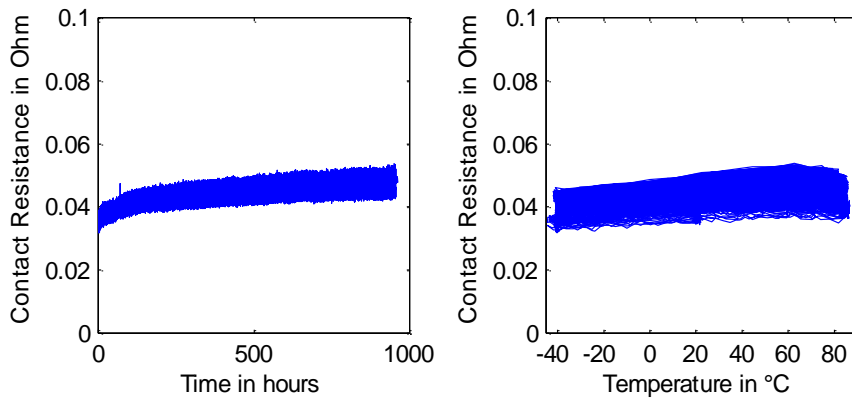
Figure A.23   (ID: TM126AuPiercedPad07\496)
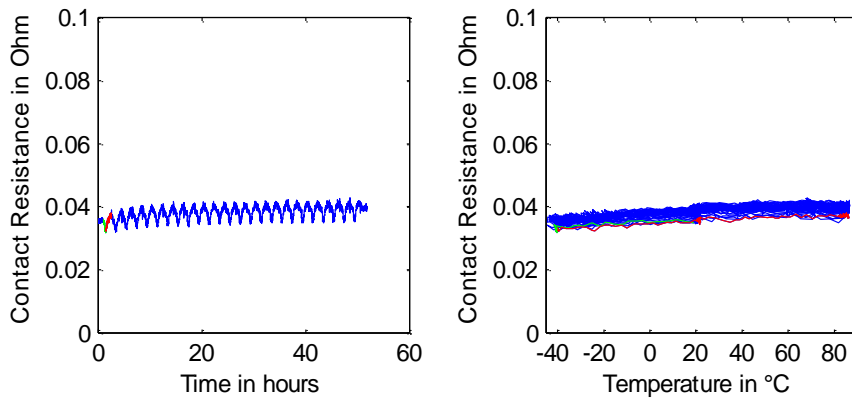
Figure A.24   (ID: TM126AuPiercedPad07\295) First 25 cycles of the plot in Figure A.23.

A.5.2 Hotmelt Encapsulated Embroidered Contacts
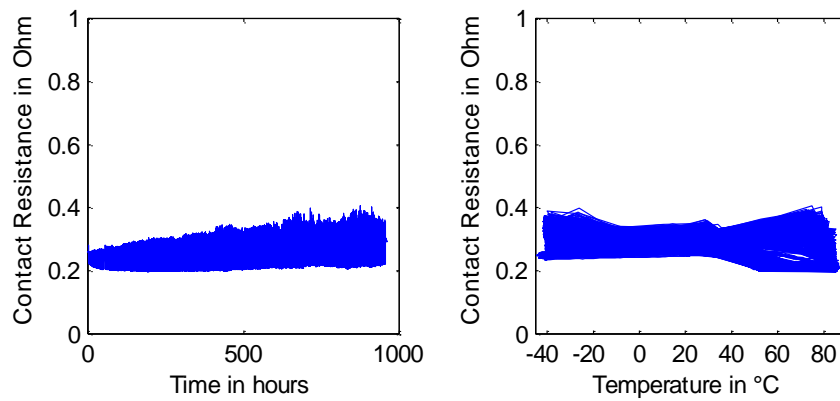
Figure A.25   (ID: HM53AgPiercedPad14\486)
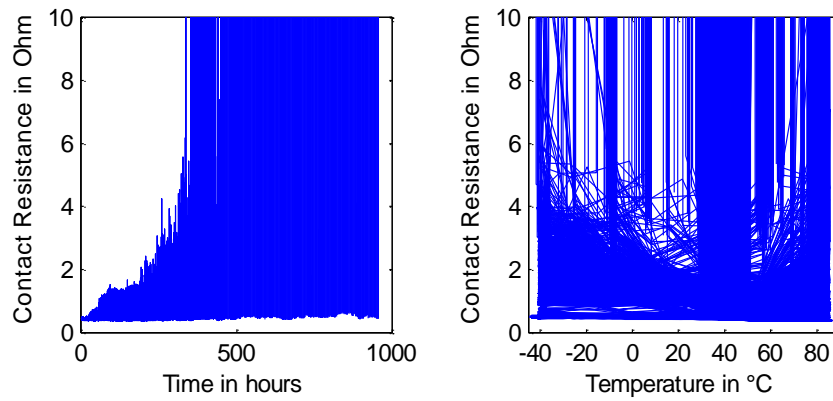
Figure A.26   (ID: HM53AgPiercedPad02\474)
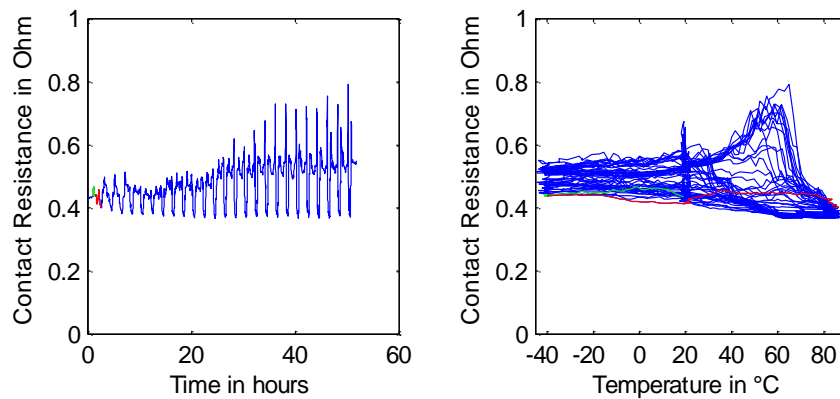
Figure A.27   (ID: HM53AgPiercedPad02\273) First 25 cycles of the plot in Figure A.26.

A.5.3 Embroidered Contacts locally protected with Glob Top (Epoxy)
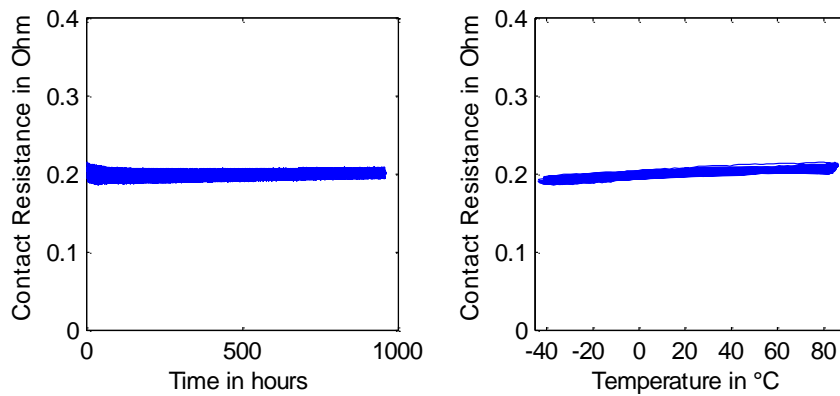
Figure A.28   (ID: GT62AuPiercedPad06\415)
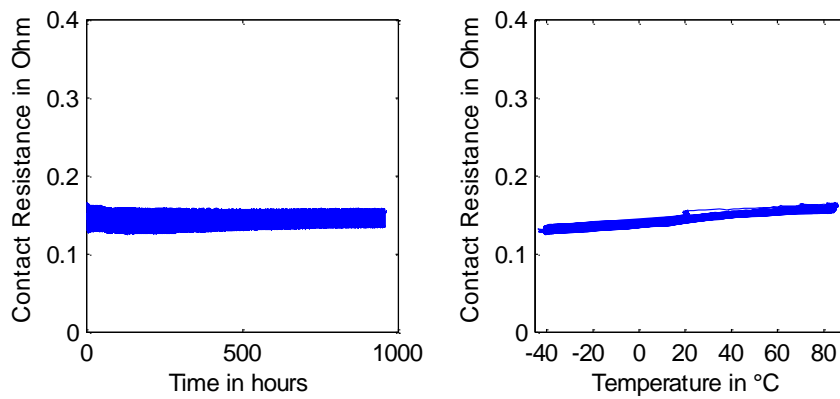
Figure A.29   (ID: GT63AgPiercedPad10\391)

A.5.4 Embroidered Contacts locally protected with ICA (Silver-filled Epoxy)
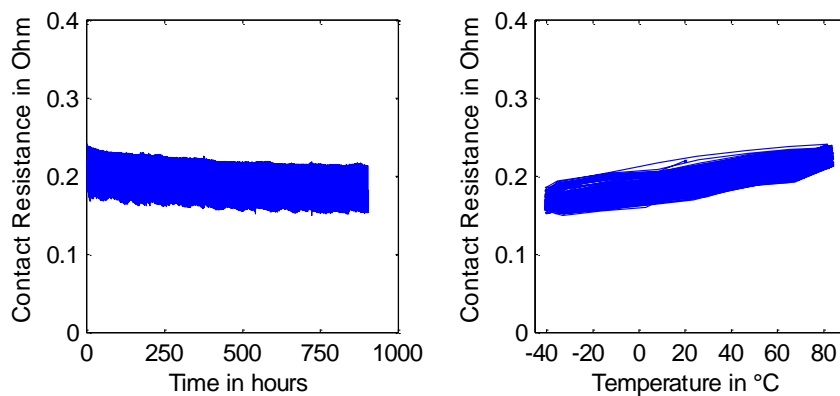
Figure A.30   (ID: ICA98AgPiercedPad06\69)
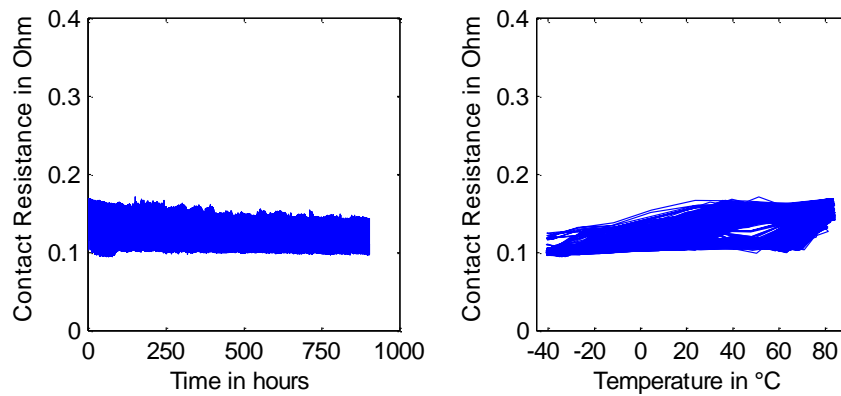
Figure A.31   (ID: ICA99AuPiercedPad03\71)

A.5.5 Embroidered Contacts locally protected with Glob Top or ICA and then Encapsulated with Hotmelt
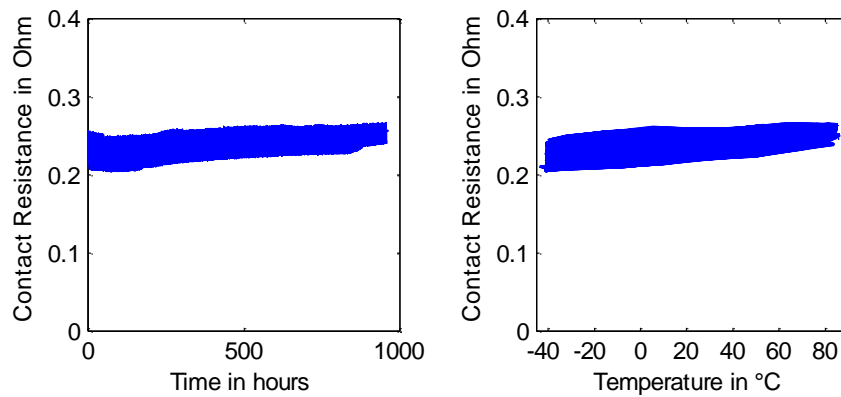
Figure A.32   (ID: GT+HM65AgPiercedPad10\358)
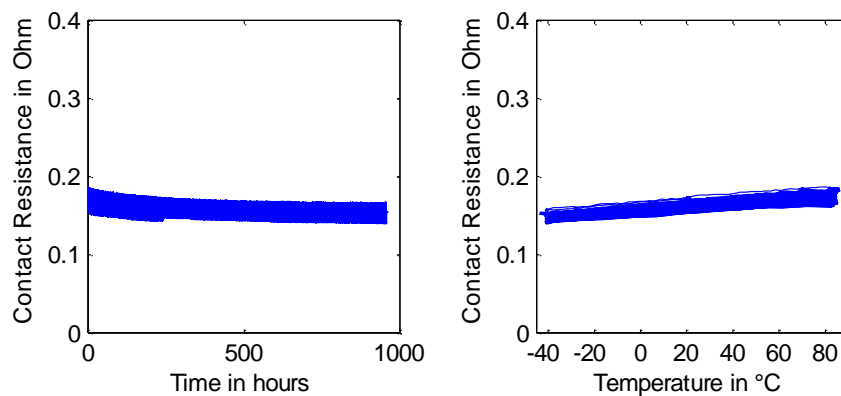
Figure A.33   (ID: ICA+HM65AgPiercedPad02\350)

A.5.6 Embroidered Contacts protected with Laminated Adhesive Film
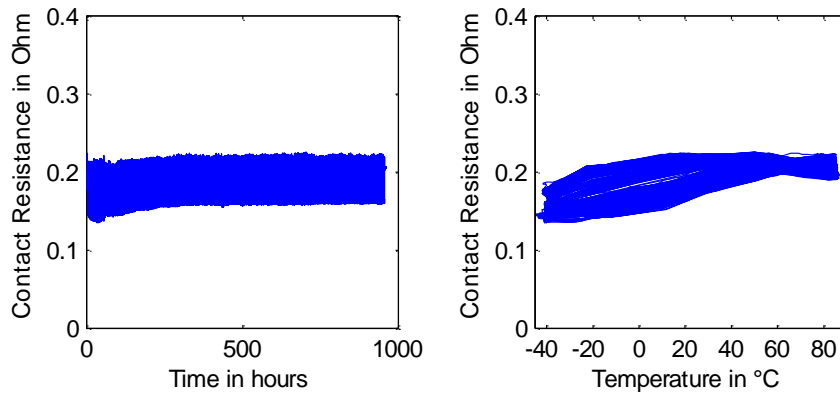
Figure A.34   (ID: AF51AuPiercedPad12\516)
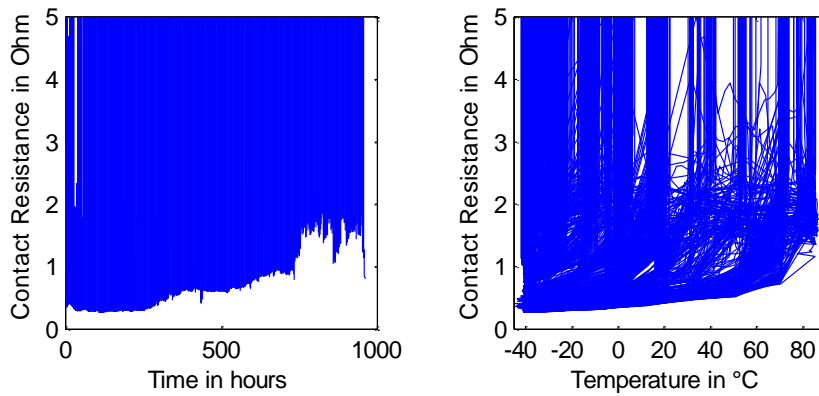
Figure A.35   (ID: AF51AuPiercedPad09\513)
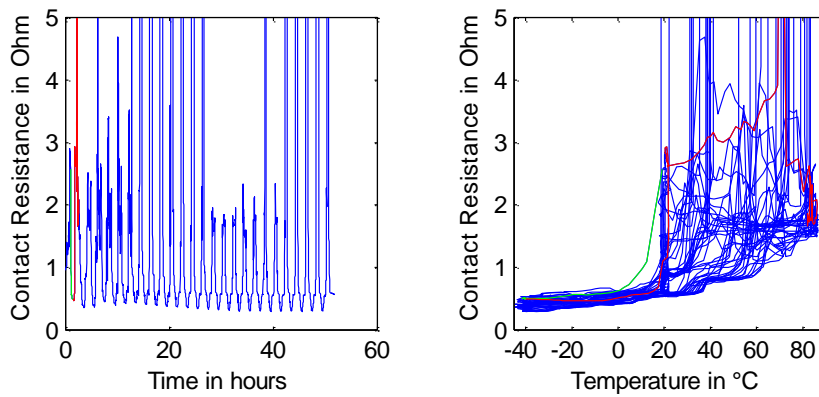
Figure A.36   (ID: AF51AuPiercedPad09\312) First 25 cycles of the plot in Figure A.35.

A.5.7 Adhesively Bonded Contacts
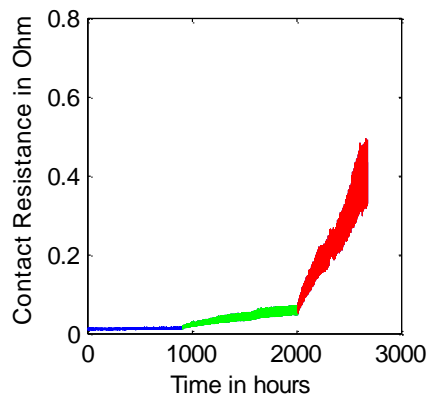
Figure A.37 (ID: AC05AgMeshedPad02\111)
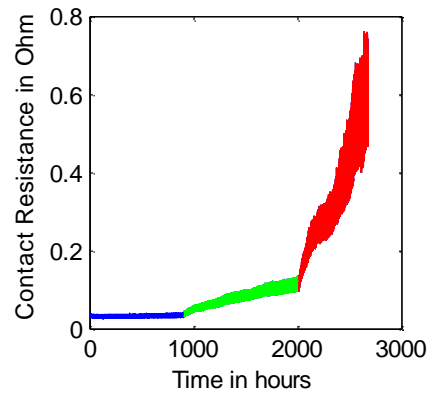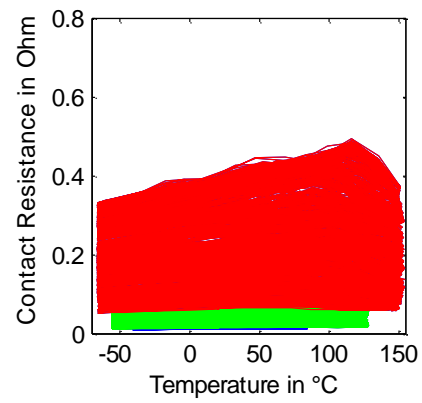
Figure A.38 (ID: AC05AgMeshedPad04\113)
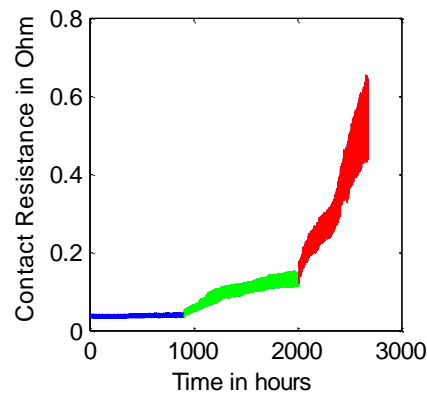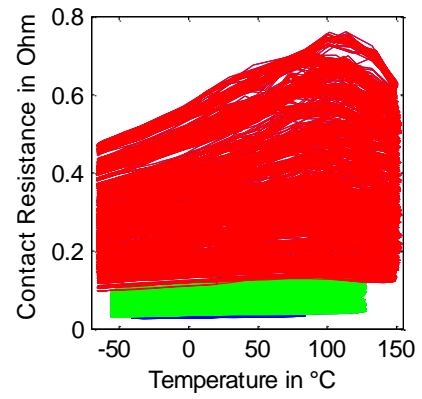
Figure A.39 (ID: AC05AgMeshedPad05\114)
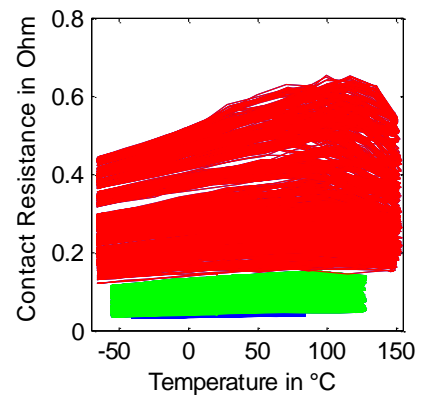
Appendix B   Wash Cycling Test

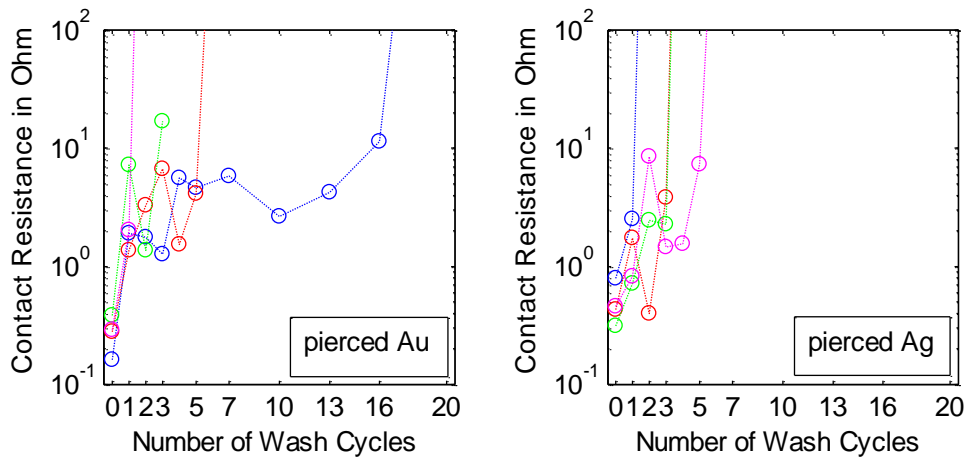## B.1 Embroidered Contacts on Pierced and Predrilled Pads

Figure B.1   Examples of typical resistance changes in pierced embroidered contacts during wash cycling. Each color represents one sample. After a few cycles disruption occurs. Significant differences between gold and silver pads were not observed.
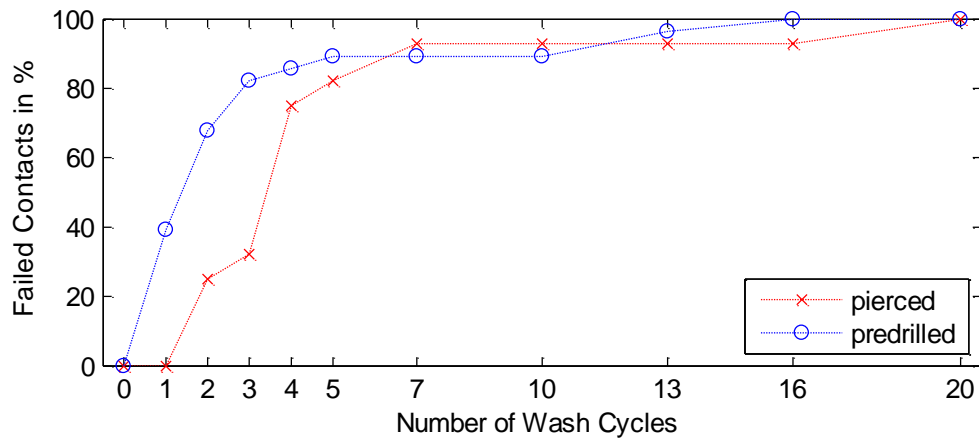

Figure B.2   Contact failures in embroidered contacts due to washing. A contact was considered to have failed if it rose above the measurement range of 100 Ω. A contact that had once failed and returned to values below 100 Ω was still counted as a failure. The total sample numbers were 14 pierced silver contacts, 14 pierced gold contacts, 14 predrilled silver contacts and 14 predrilled gold contacts.

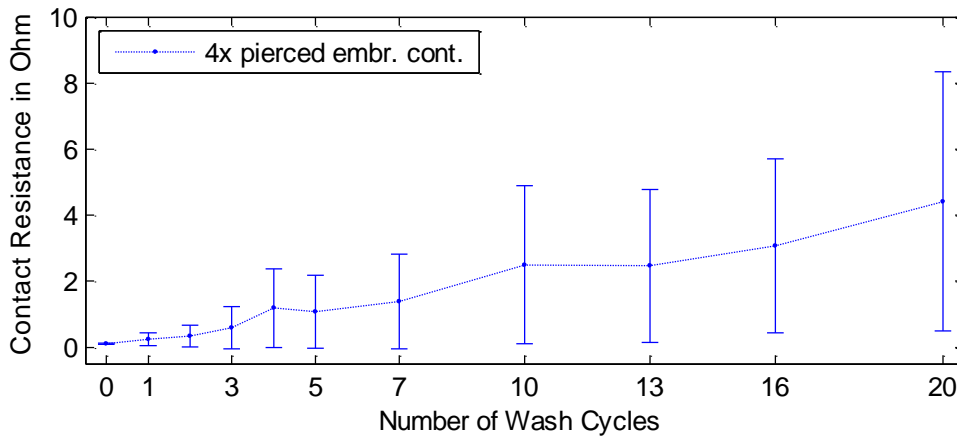## B.2 Embroidered Contacts Stitched Four Times

Figure B.3   Contact resistance during wash cycles of embroidered contacts stitched four times; the total number of samples was 14. The contact pads had silver metallization and were pierced by the needle. Failure rates after 20 wash cycles at failure conditions 0.27 Ω, 1 Ω, 10 Ω and 100 Ω were 100 %, 86 %; 7 % and 0 % respectively.

B.3 Embroidered Contacts with Protection

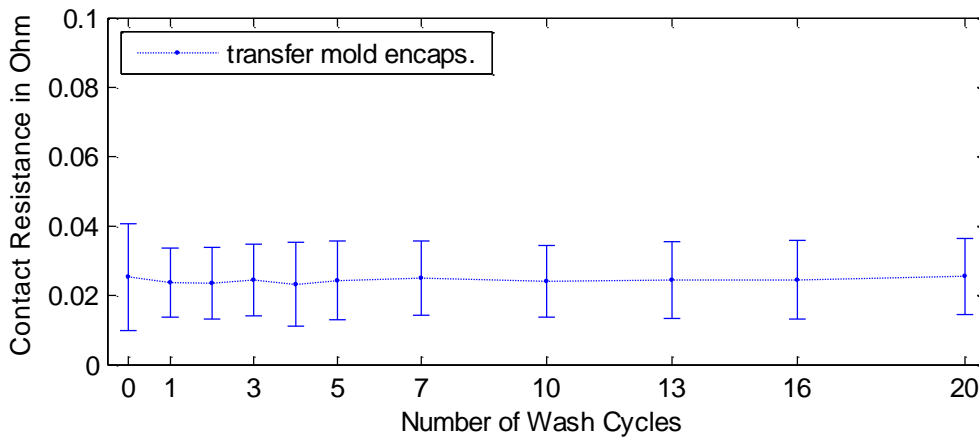### B.3.1 Transfer Mold Encapsulated Embroidered contacts

Figure B.4   Mean and standard deviation of contact resistances in transfer mold encapsulated embroidered contacts over 20 washing cycles. 28 contacts with needle-pierced gold pads were measured.

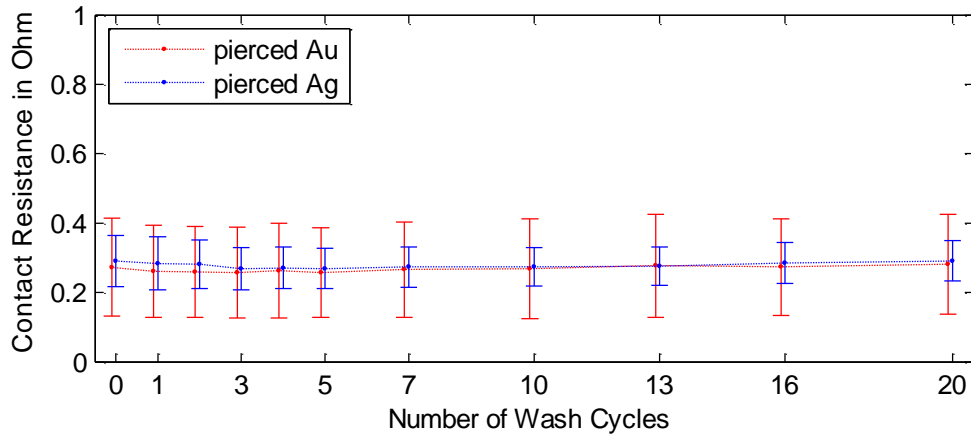## B.3.2 Hotmelt Encapsulated Embroidered Contacts

Figure B.5   Mean and standard deviation of contact resistances in hotmelt encapsulated embroidered contacts over 20 washing cycles. Of each contact metallization 14 needle-pierced samples were tested.

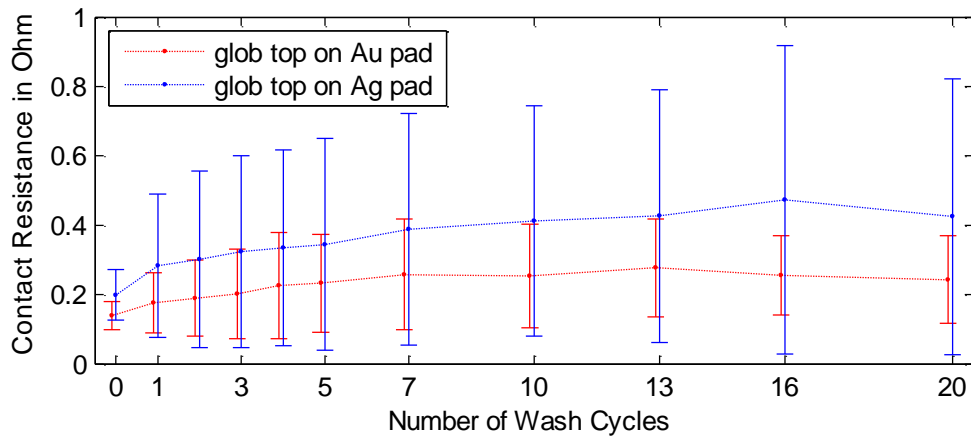## B.3.3 Embroidered Contacts locally protected with Glob Top (Epoxy)

Figure B.6   Mean and standard deviation of contact resistances of embroidered contacts locally protected with glob top (epoxy adhesive). Of each contact metallization 14 needle-pierced samples were tested.

B.3.4 Embroidered Contacts locally protected with ICA (Silver-filled Epoxy)
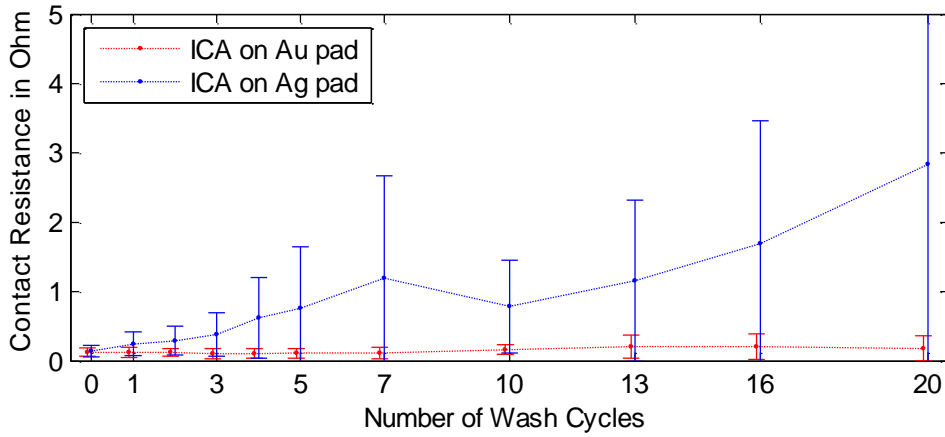

Figure B.7   Mean and standard deviation of contact resistances of embroidered contacts locally protected with conductive adhesive (epoxy filled with silver particles). Of each contact metallization 6 needle-pierced samples were tested.

B.3.5 Embroidered Contacts locally protected with Glob Top or ICA and then Encapsulated with Hotmelt
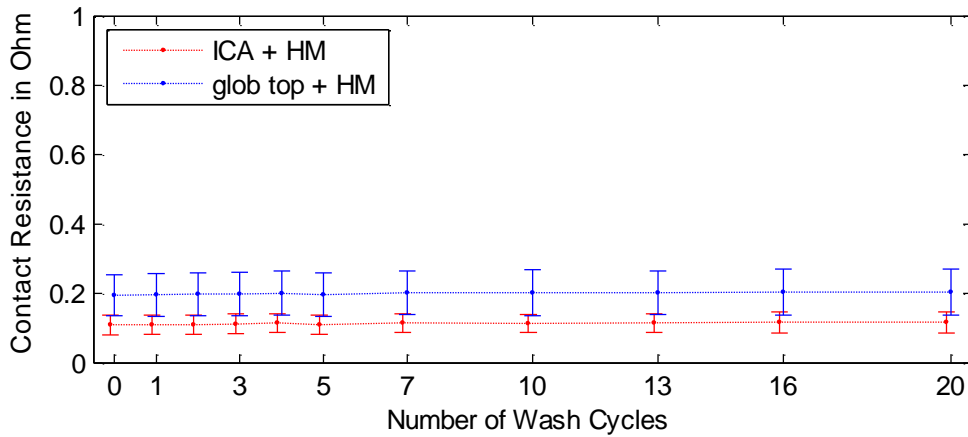

Figure B.8   Mean and standard deviation of contact resistances of embroidered contacts locally protected with conductive adhesive or with glob top (epoxy adhesive) and subsequently encapsulated with hotmelt. Of each type of adhesive 7 needle-pierced samples were tested.

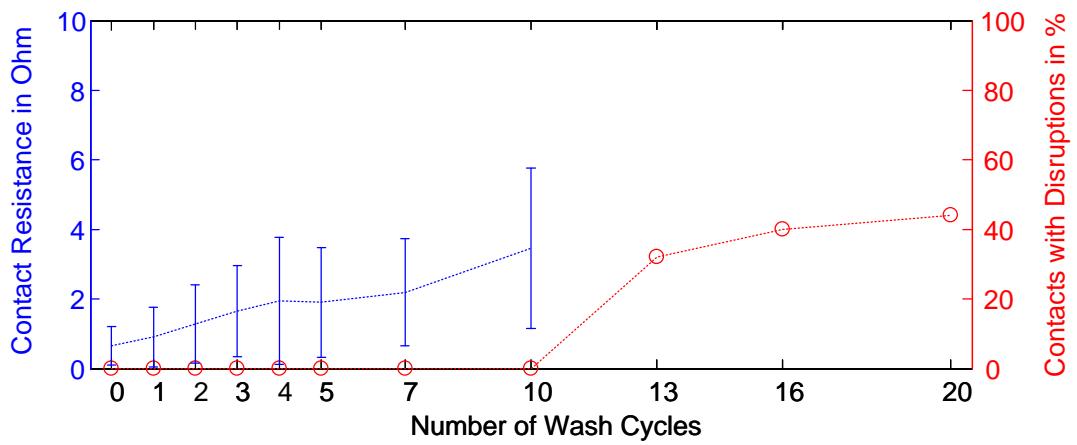## B.3.6 Embroidered Contacts protected with Laminated Adhesive Film

Figure B.9   Mean and standard deviation over 10 wash cycles of contact resistances of embroidered contacts protected with laminated thermoplastic polyurethane film. After 10 washing cycles disruption occurred. Therefore, it was no longer useful to calculate the mean. From 10 to 20 washing cycles the percentage of contacts is plotted that had contact resistances above 100 Ω. 25 contacts with needle-pierced gold pads were tested.
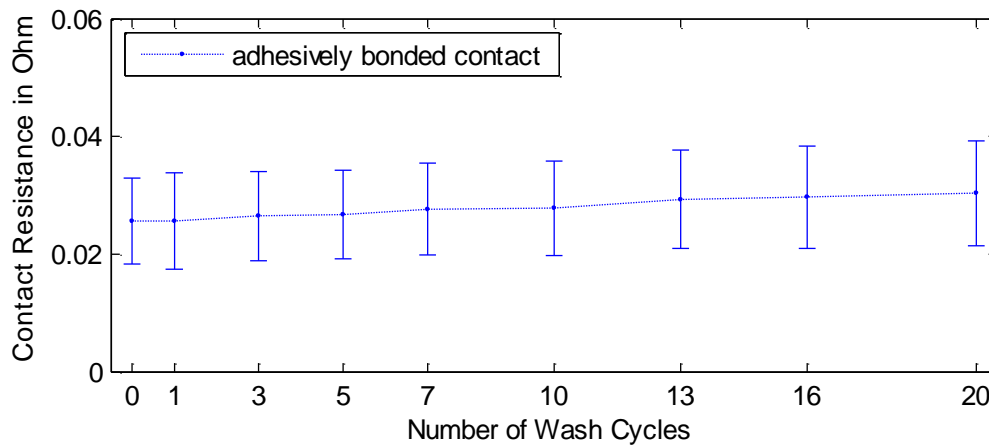
B.4 Adhesively Bonded Contact

Figure B.10   Mean and standard deviation of contact resistances of adhesively bonded contacts. The total sample number was 25 contacts.

Appendix C   Bending Test

C.1 Embroidered Contacts with Pierced Contact Pads
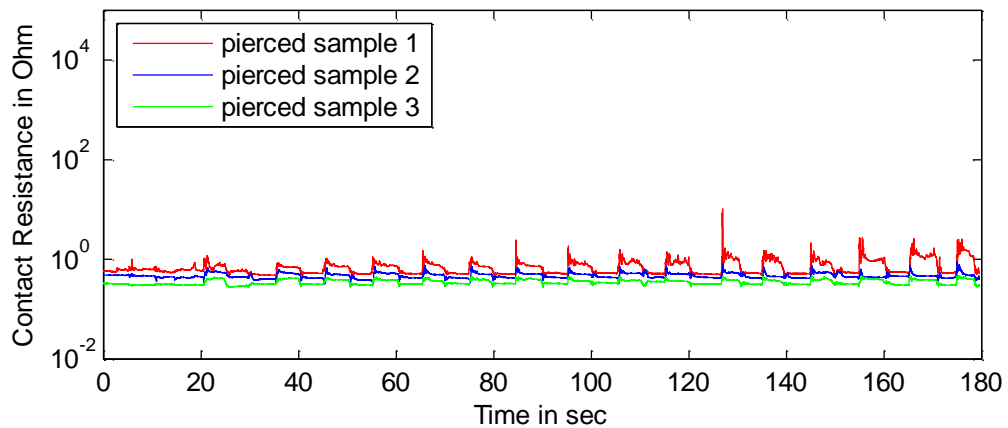
Figure C.1   Bending test with embroidered contacts on pierced silver pads. The contact resistances were low when the fabric next to the pad was bent down and significantly rose when bent up. The highest attained contact resistance appeared in sample 1 and was 10.3 Ω

C.2 Embroidered Contacts with Predrilled Contact Pads
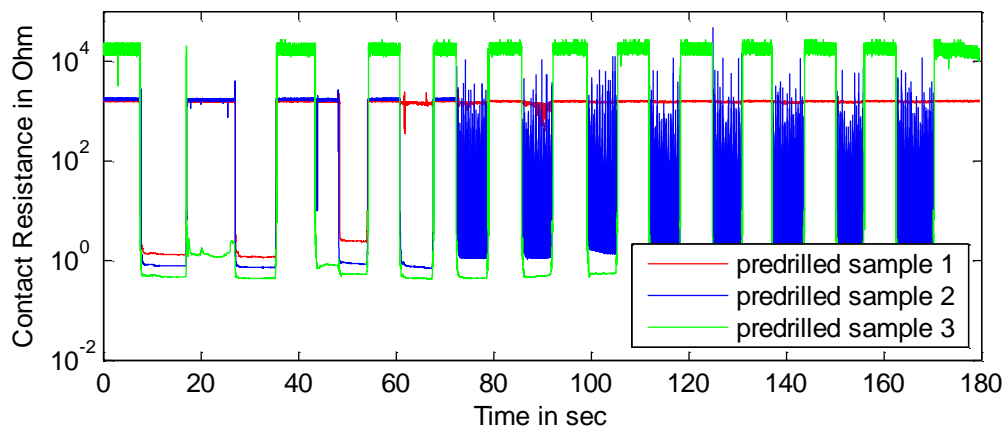

Figure C.2   Bending test with embroidered contacts on predrilled silver pads. When the fabric next to the pad was bent down contact resistances were significantly lower than they were when bent up. Compared to the pierced samples the contact resistances were much higher. In sample 2, disruptions occurred at some instances of time.

Appendix D   Adhesively Bonded Contacts for Do-It-Yourself Projects

In chapter 8, adhesively bonded contacts were introduced, and test vehicles with a thermoplastic elastomer adhesive were built. These proved to be very reliable during relevant stress tests. Unfortunately for designers and artists, the choice of a thermoplastic adhesive – as advantageous as it is for contacting insulated conductors – requires the use of a relatively complicated tool for bonding. The latter can be replaced by much simpler tools, if a thermosetting adhesive is applied instead. However, in this case, the embroidered conductor must not be insulated at all or at least the insulation must be removed locally prior to contacting. The following explains how to make contacts between electronic modules and fabric circuits with a thermosetting adhesive. Furthermore, results of reliability tests are presented. The assembly process here uses the module and the embroidered circuit developed in 8.2.

D.1 How To

As adhesive a standard two component epoxy is used. It is applied to the fabric circuit and to the bottom side of the module as shown by the example setup in Figure D.1 (left). Then, both parts are joined and fixed with a bar clamp. To prevent the assembly from gluing to the bar clamp, a PTFE foil is placed on top and bottom of the assembly stack prior to clamping, as shown in Figure D.1 (right). Then the adhesive is cured (in the clamped state) in accordance with the data sheet of the adhesive. Finally, the clamps are released.
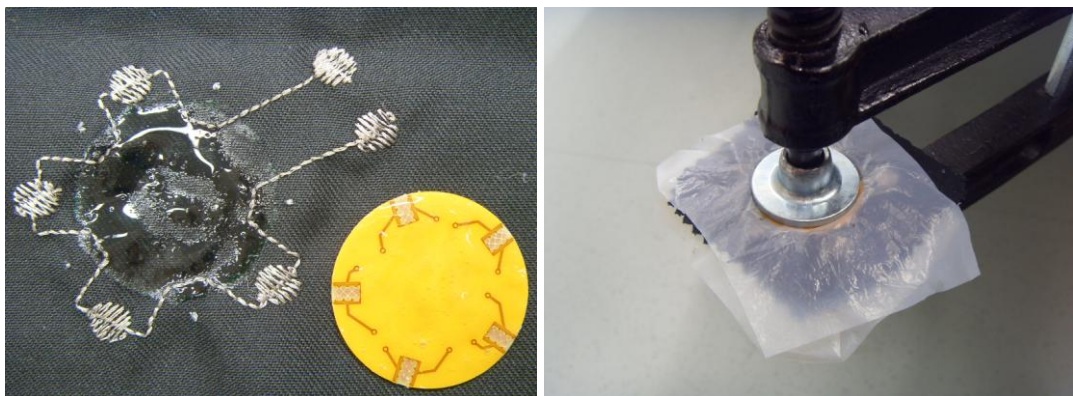

Figure D.1:   Adhesively bonded contacts with thermosetting standard adhesive as applicable for do-it-yourself projects.

D.2 Contact Resistances and Reliability Results

To assess the reliability two test vehicles were built, i.e. 10 contacts. As adhesive *UHU plus 300 kg epoxy* was used. The cure conditions were 45 minutes at 70 °C in accordance with the data sheet. It is also possible to cure at room temperature for 12 hours.

As Table D.1 shows, the mean and standard deviation of the contact resistances were in the same order of magnitude as of those samples bonded with thermoplastic adhesive.

Table D.1:   Contact resistances of samples bonded with *UHU Plus 300 kg* before stress tests were performed.

Type of Contact	Mean	Std. Deviation	Num. of Samples
adhesively bonded contact	19.4 mΩ	7.2 mΩ	10

The following plots and the following table show that also the reliability of these test vehicles proved to be as good as the reliability of the test vehicles bonded with thermoplastic adhesive. One test vehicle, i.e. 5 contacts, was exposed to 1000 temperature cycles at -40 °C / +85 °C and a second test vehicle was exposed to 20 washing cycles at 40 °C.
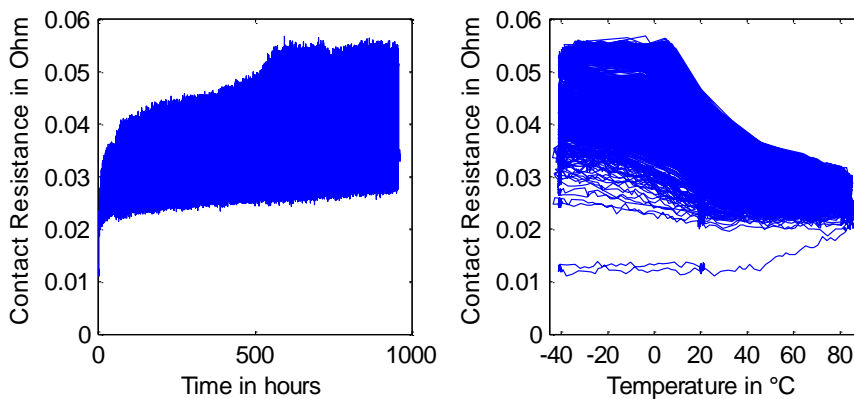
Figure D.2   Typical sample of contact bonded with thermosetting adhesive during 1000 temperature cycles at -40 °C / +85 °C.
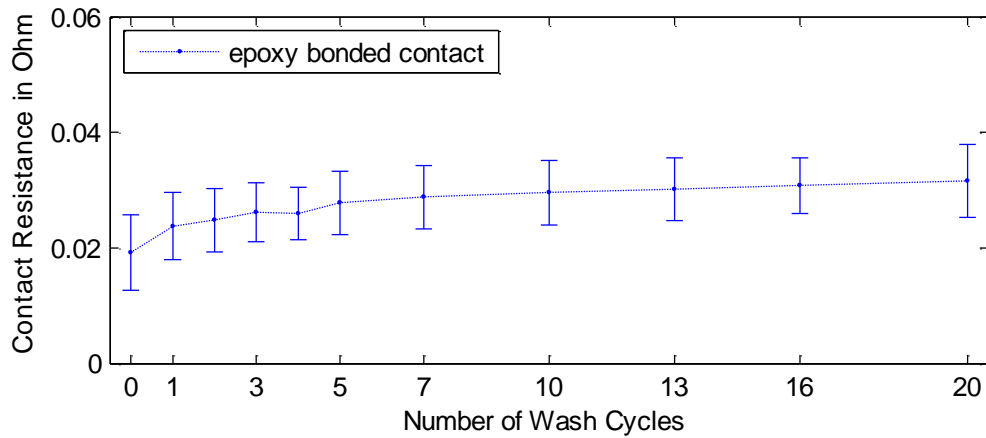
Figure D.3   Mean and standard deviation of contact resistances of contacts bonded with thermosetting adhesive during wash cycling. The total sample number was 5 contacts.

Table D.2:   Failures of contacts bonded with thermosetting adhesive during different stress tests at the following failure condition: contact resistance rose at least once above 0.1 Ω.

Type	0.1 Ω		Num. of Samples
1000 temp. cycles at -40 °C / +85 °C	0 %		5
20 washing cycles at 40 °C	0 %		5

Appendix E   Publications of the Author

E.1 First Authorship Publications

Title of the Publication	Type
Torsten Linz, Erik Paul Simon, and Hans Walter, "Modeling Embroidered Contacts for Electronics in Textiles," *The Journal of the Textile Institute*, pp. 1-10, September 2011.	A1
Torsten Linz, Erik Simon, and Hans Walter, "Fundamental analysis of embroidered contacts for electronics in textiles," in *3rd Electronic System-Integration Technology Conference (ESTC)*, Berlin, Germany, 2010, pp. 1-5.	P1[64]
Torsten Linz, Malte von Krshiwoblozki, and Walter Hans, "Novel Packaging technology for Body Sensor Networks based on Adhesive bonding," in *IEEE BSN International Workshop on Wearable and Implantable Body Sensor Networks*, Singapore, June 2010.	P1[64]
Torsten Linz, "Method for connecting two parts mechanically and electrically at the same time," Patent Pending WO/2010/037565, September 30, 2009.	patent applic.
Torsten Linz et al., "Embroidered Interconnections and Encapsulation for Electronics in Textiles for Wearable Electronics Applications," *Advances in Science and Technology*, vol. 60, pp. 85-94, online at http://www.scientific.net, Trans Tech Publications, Switzerland, September 2008.	P1
Torsten Linz, "Enabling Micro System Technologies for Electronics in Textiles," in *Concertation WS on EC Funded projects on Smart Fabrics & Interactive Textiles (SFIT) and Consultation on Future R&D Challenges and opportunities*, Brussels, Belgium, January 2008.	position paper

---

[64] previous conferences of these two conference-series were listed in the List of Conferences 1990-2011 (April) of the Conference Proceedings Citation Index: although the titel of this document implies to include conferences held in 2010, it appears that these recent conferences are not yet completely listed; therefore, it may be assumed that these to publications are P1 publications.

Torsten Linz, Lena Gourmelon, and Geert Langereis, "Contactless EMG sensors embroidered onto textile," in *IEEE International Workshop on Wearable and Implantable Body Sensor Networks*, Aachen, Germany, March 2007.	P1
Torsten Linz, Christine Kallmayer, Rolf Aschenbrenner, and Herbert Reichl, "Fully Integrated EKG Shirt based on Embroidered Electrical Interconnections with Conductive Yarn and Miniaturized Flexible Electronics," in *IEEE BSN International Workshop on Wearable and Implantable Body Sensor Networks*, Cambridge, MA, USA, April 2006.	P1
Torsten Linz, Christine Kallmayer, Rolf Aschenbrenner, and Herbert Reichl, "Embroidering Electrical Interconnects with Conductive Yarn for the Integration of Flexible Electronic Modules into Fabric," in *IEEE ISWC International Symposium on Wearable Computing*, Osaka, Japan, October 2005.	P1
Torsten Linz, Christine Kallmayer, Rolf Aschenbrenner, and Herbert Reichl, "New Interconnection Technologies for the Integration of Electronics on Textile Substrates," in *Ambience 2005*, Tampere, Finland, September 2005.	conf. paper

E.2 Co-Authorship Publications

Title of the Publication	Type
Philipp Foerster, Torsten Linz, Malte von Krshiwoblozki, Hans Walter, and Christine Kallmayer, "NCA Flip-Chip Bonding with Thermoplastic Elastomer Adhesives," in *IEEE 13th Electronics Packaging Technology Conference (EPTC 2011)*, Singapore, status: accepted for publication; conference scheduled for December 2011.	P1
Joachim Taelman, Tine Adriaensen, Caroline van der Horst, Torsten Linz, and Arthur Spaepen, "Textile Integrated Contactless EMG Sensing for Stress Analysis," in *29th Annual International Conference of the IEEE Engineering in Medicine and Biology Society*, Lyon, France, July 2007.	P1

Auli Sipilä, Anton Kaasjager, Christian Rotsch, and Torsten Linz, "Integrating sEMG sensors to textile materials," in *AUTEX 2007*, Tampere, Finland, June 2007.	P1
Geert Langereis, Auli Sipilä, Lenneke de Voogd-Claessen, Christian Rotsch, Arthur Spaepen, and Torsten Linz, "ConText: Contactless sensors for body monitoring incorporated in textiles," in *2007 IEEE International Conference on Portable information devices*, Orlando, FL, March 2007, pp. 11-15.	P1
Herbert Reichl, Christine Kallmayer, and Torsten Linz, "Electronic Textiles," in *True Visions: The Emergence of Ambient Intelligence*, Emile H. L. Aarts and José L. Encarnação, Eds. Berlin, Germany: Springer Verlag, 2006, ch. 6, pp. 115-132.	book chap.
Sabine Gimpel and Torsten Linz, "Kontaktierung von Mikrobauelementen auf partiell leitfähigen textilen Strukturen," in *Mikrosystemtechnik Kongress 2005*, Freiburg, Germany, Oktober 2005.	conf. paper
Christine Kallmayer, Torsten Linz, Rolf Aschenbrenner, and Herbert Reichl, "System Integration Technologies for Smart Textiles," *mst news*, no. 2, pp. 42-43, 2005.	journal paper

E.3 Supervised Diploma Theses, Master Theses, etc.

Title of the Publication	Type
Philipp Foerster, *NCA Flip-Chip Bonding with Thermoplastic Elastomer Adhesives - Fundamental Failure Mechanisms and Opportunities of Polyurethane bonded NCA-Interconnects*. Diploma thesis, at Technical University Berlin, Berlin, Germany, May 2011.	Diploma thesis
Christian Böhme, *Design and Implementation of a Power-Line Communication for Controlling Individually Addressable RGB-LED Modules*. Bachelor thesis, at Beuth Hochschule für Technik Berlin - University of Applied Sciences, Berlin, Germany, March 2011.	BA thesis
Philipp Foerster, *Untersuchungen zu Eigenschaften von Nano-Silberschichten auf Polyamidfasern*. Student research project as part of the degree programm Electrical Engineering, at Technical University Berlin, Berlin, Germany, 2010.	Student research project

Christian Böhme, "Integration elektronischer Komponenten in Textilien," Fraunhofer IZM, Berlin, internship report December 2009 - March 2010.	Internship
Sebastian Born, "Optimierung der InSitu-Mess-Software," Fraunhofer IZM, Berlin, internship report, August 2009 - October 2009.	Internship
Malte von Krshiwoblozki, *Untersuchung von Klebeverbindungen zur Integration von Elektronik in Textilien*. Diploma thesis, at Hochschule für Technik und Wirtschaft Berlin, Berlin, August 2009.	Diploma thesis
Erik Paul Simon, *Analysis of Contact Resistance Change of Embroidered Interconnections*. Diploma thesis, at Technical University Berlin, Berlin, Germany, July 2009.	Diploma thesis
Lars Paasche, *Entwicklung eines hochintegrierten, tragbaren Low-Power EKG-Systems mit drahtloser Datenübertragung für die Integration in ein T-Shirt*. Diploma thesis, at Technical University Berlin, Berlin, Germany, July 2008	Diploma thesis
Claudia Schuster, *Untersuchung des Tragekomforts von Oberbekleidung mit verschiedenen elektronischen Modulen*. Diploma thesis, at Fachhochschule für Technik und Wirtschaft, Berlin, September 2006.	Diploma thesis
Friedemann Schäfer, *Miniaturisierung eines EKG-Moduls*. Student research project as part of the degree programm Electrical Engineering, at Technical University Berlin, Berlin, Germany, 2006.	Student research project
Oliver Lindner, *Zuverlässigkeitsuntersuchung für mit leitfähigem Faden angenähte flexible Substrate*. Diploma thesis, at the Fachhochschule für Technik und Wirtschaft, Berlin, Germany, 2005.	Diploma thesis
Henrietta Lipske, *Feminine Wearables - Entwicklung einer Kollektion in Zusammenarbeit mit der HUGO BOSS AG, dem Fraunhofer Institut für Zuverlässigkeit und Mikrointegration und der Infineon Technologies AG*. Diploma thesis, at Fachhochschule für Technik und Wirtschaft, Berlin, February 2004.	Diploma thesis